

Mechanical Evaluations of Reinforced-Rehabilitated Bituminous Pavement Layers with Geosynthetic Materials

by

Ehsan SOLATIYAN

MANUSCRIPT-BASED THESIS PRESENTED TO ÉCOLE DE
TECHNOLOGIE SUPÉRIEURE IN PARTIAL FULFILLMENT FOR THE
DEGREE OF DOCTOR OF PHILOSOPHY
Ph.D.

MONTREAL, DECEMBER 20th, 2020

ÉCOLE DE TECHNOLOGIE SUPÉRIEURE
UNIVERSITÉ DU QUÉBEC

© All rights reserved, Ehsan Solatiyan, 2020

© Copyright reserved

It is forbidden to reproduce, save or share the content of this document either in whole or in parts. The reader who wishes to print or save this document on any media must first get the permission of the author.

BOARD OF EXAMINERS

THIS THESIS HAS BEEN EVALUATED

BY THE FOLLOWING BOARD OF EXAMINERS

Mr. Alan Carter, Thesis Supervisor
Department of Construction Engineering, École de technologie supérieure

Mr. Nicolas Bueche, Thesis Co-supervisor
Department of Architecture-Wood-Civil Engineering, Bern University of Applied Sciences

Mr. Éric Wagnac, President of the Board of Examiners
Department of Mechanical Engineering, École de technologie supérieure

Mr. Michel Vaillancourt, Member of the jury
Department of Construction Engineering, École de technologie supérieure

Mr. Francesco Canestrari, External Evaluator
Department of Science Engineering, Marche Polytechnic University, Italy

Mr. Didier Lesueur, External Evaluator
Institut Mines-Telecom Lille Douai, France

THIS THESIS WAS PRESENTED AND DEFENDED

IN THE PRESENCE OF A BOARD OF EXAMINERS AND PUBLIC

DECEMBER 16TH, 2020
AT ÉCOLE DE TECHNOLOGIE SUPÉRIEURE

ACKNOWLEDGMENT

I would like to express my heartfelt gratitude to my family in my home country Iran. They have always encouraged me to remain focused on this journey and provided companionship along the way.

Dr. Alan Carter, my advisor during my graduate program at École de technologie supérieure, merits my deepest and warmest appreciation for helping me grow academically and personally. He also secured financial funding for my research work and supported my ideas and efforts. I also would like to thank my Co-Supervisor Dr. Nicolas Bueche, for providing valuable feedback on my research work and for supporting my professional development. My appreciation also goes to Dr. Michel Vaillancourt for his valuable advice and scientific guidance.

Life in a foreign country is not always easy and therefore I am very grateful to all my friends in Canada. First of all, I have to thank Saeed Badeli, who spent a lot of his time and energy to make my stay in Canada pleasant and enjoyable. Without his support and friendship, I would not have survived the hardship of the first weeks. My special thanks and gratitude go to my friend Seyed Sina Mousavi for his inspiring conversations. Besides, many thanks to Simone Raschia and Theophile Kakpo Edeme for their assistance in the laboratory.

I also wish to thank all the technicians whose assistance was a milestone in the completion of this thesis. Firstly, I would like to express my deepest gratitude to Sylvain Bibeau for his continued advice and inspiring thoughts throughout this research project. Secondly, I am extremely grateful for Johnathan Auger, who has supported me during the large part of my laboratory tests and had to put up with my stresses. Also, my special thanks go to Francis Bilodeau for sharing his expertise and sincere and valuable guidance during my study. Finally, from the bottom of my heart I would like to say big thank all the following participants, which financially support me and enabled this research to be possible:

- Natural Sciences and Engineering Research Council (NSERC)
- TEXEL Corporation
- S&P Clever Reinforcement Company
- Canadian Technical Asphalt Association (CTAA)

Évaluations Mécaniques de Couches de Chaussées Bitumineuses Renforcées Réhabilitées avec des Matériaux Géosynthétiques

Ehsan SOLATIYAN

RÉSUMÉ

Les chaussées bitumineuses couvrent une grande partie du réseau routier canadien. La circulation et les charges environnementales causent des détresses et des dommages à la structure de la chaussée. Une approche traditionnelle pour la réhabilitation des chaussées consiste à mettre en œuvre une couche d'enrobé sur une chaussée bitumineuse détériorée existante à des moments précis de sa durée de vie. Cependant, cette approche est quelque peu coûteuse à long terme et non respectueuse de l'environnement. D'autre part, plusieurs études indiquent que l'inclusion d'une couche géosynthétique sous un revêtement d'enrobé conduit à une durée de vie prolongée de la chaussée. Néanmoins, il existe encore des écarts entre les observations sur sites et les résultats de la modélisation, qui proviennent principalement du fait que le comportement mécanique des chaussées renforcées n'a pas été entièrement compris, ce qui conduit à sous-estimer ou surestimer les solutions de conception. Cette recherche vise à examiner différents aspects de l'interaction mécanique entre le matériau géosynthétique et les couches de chaussées bitumineuses, puis à éclairer les considérations importantes à prendre en compte dans la procédure de conception pour obtenir une structure de chaussée bitumineuse renforcée et réhabilitée de manière optimale.

Mots-clés: Renfort de chaussée bitumineuses, revêtement d'enrobés, matériaux géosynthétiques.

Mechanical Evaluations of Reinforced-Rehabilitated Bituminous Pavement Layers with Geosynthetic Materials

Ehsan SOLATIYAN

ABSTRACT

Bituminous pavements cover a large part of the Canada's roadway network. Traffic and environmental loadings cause distresses and damages in the pavement structure. A traditional approach for pavement rehabilitation is to implement an asphalt overlay on existing deteriorated bituminous pavement at specific times during its service life. However, this approach is somewhat expensive in the long run and not environmentally friendly. On the other hand, several studies indicate that the inclusion of a geosynthetic layer under an asphalt overlay leads to extended pavement service life. Nevertheless, there are still some discrepancies between fields and modeling results, which mainly stems from the fact that the mechanical behavior of reinforced asphalt overlay has not entirely been understood which results in underestimate or overestimate design solutions. This research aims to review different aspects of mechanical interaction between geosynthetic material and bituminous pavement layers and then shed light on the important considerations that need to be considered in the mechanistic-based design approaches to obtain an efficient reinforced-rehabilitated bituminous pavement structure.

Keywords: Bituminous pavement reinforcement, Asphalt overlay, Geosynthetic materials.

TABLE OF CONTENTS

| | Page |
|--|------|
| INTRODUCTION | 1 |
| CHAPTER 1 LITERATURE REVIEW | 5 |
| 1.1 Introduction..... | 5 |
| 1.2 Background on pavement design methods | 8 |
| 1.2.1 Design methods proposed for reinforced bituminous pavements with geosynthetics..... | 10 |
| 1.2.1.1 Response models in the M-E pavement design | 16 |
| 1.2.1.2 Distress prediction models in M-E pavement design | 17 |
| 1.2.1.3 Hierarchical input levels | 21 |
| 1.2.2 Literature review summary | 21 |
| CHAPTER 2 PROBLEM DESCRIPTION AND OBJECTIVES | 23 |
| 2.2 Problem description | 25 |
| 2.3 Objectives | 27 |
| CHAPTER 3 A REVIEW ON MECHANICAL BEHAVIOR AND DESIGN CONSIDERATIONS FOR REINFORCED-REHABILITATED BITUMINOUS PAVEMENTS..... | 31 |
| 3.1 Abstract | 31 |
| 3.2 Introduction..... | 32 |
| 3.3 Mechanical behavior of geosynthetics in asphalt overlays..... | 37 |
| 3.3.1 Reinforcement mechanism of geosynthetic in asphalt layer..... | 38 |
| 3.3.2 Geosynthetic position in asphalt overlay | 45 |
| 3.3.3 Interface condition between geosynthetic and asphalt overlay..... | 47 |
| 3.4 Design considerations for the reinforced asphalt overlay with geosynthetics | 62 |
| 3.4.1 Design methods..... | 62 |
| 3.4.2 Mechanical models | 66 |
| 3.5 Conclusion | 74 |

CHAPTER 4 PERMEABILITY AND MECHANICAL PROPERTY MEASUREMENTS OF REINFORCED ASPHALT OVERLAY WITH PAVING FABRICS USING NOVEL APPROACHES77

4.1 Abstract77

4.2 Introduction.....78

4.3 Research background on thermally driven reflective cracking.....80

4.4 Materials and methods83

 4.4.1 Materials 83

 4.4.2 Methods..... 86

4.5 Results and discussion90

 4.5.1 Crack resistance and formation..... 90

 4.5.2 Load-displacement relationship 92

 4.5.3 Water permeability result..... 94

4.6 Conclusion96

CHAPTER 5 EXPERIMENTAL MEASUREMENTS OF INTERFACIAL MECHANICAL PROPERTIES BETWEEN REHABILITATED BITUMINOUS LAYERS USING INNOVATIVE APPROACHES.....97

5.1 Abstract.....97

5.2 Introduction.....98

5.3 Research background99

5.4 Experimental program101

 5.4.1 Materials and Specimen Preparation 102

 5.4.2 Test Methods..... 105

5.5 Results and discussions.....112

 5.5.1 Results and Discussions on Anti-Reflective Properties at the Interface. 112

 5.5.2 Results and discussions on the shear test..... 115

 5.5.3 Results and Discussions on Complex Modulus Test 116

5.6 Conclusions.....123

CHAPTER 6 MECHANICAL PERFORMANCE OF REHABILITATED BITUMINOUS LAYERS WITH PAVING FABRIC UNDER CYCLIC LOADING125

6.1 Abstract.....125

| | | |
|--|---|-----|
| 6.2 | Introduction..... | 126 |
| 6.3 | Research Background | 129 |
| 6.4 | Material and methods..... | 131 |
| 6.4.1 | Materials | 132 |
| 6.4.2 | Test methods | 134 |
| 6.5 | Results and discussions..... | 136 |
| 6.5.1 | Rutting test..... | 137 |
| 6.5.2 | Fatigue Test..... | 139 |
| 6.6 | Conclusion | 142 |
| CHAPTER 7 LABORATORY EVALUATION OF INTERFACIAL MECHANICAL PROPERTIES IN GRID-REINFORCED BITUMINOUS LAYERS | | 145 |
| 7.1 | Abstract | 145 |
| 7.2 | Introduction..... | 145 |
| 7.3 | Research background..... | 147 |
| 7.4 | Material and Methods | 149 |
| 7.4.1 | Materials | 150 |
| 7.4.2 | Test methods | 154 |
| 7.5 | Results and analysis | 157 |
| 7.5.1 | 3-PBT results and discussions | 158 |
| 7.5.2 | Interface Shear Test Result and Discussion..... | 166 |
| 7.5.3 | Combined Analysis of 3-PBT and Interface Shear Test Results | 169 |
| 7.6 | Conclusion | 173 |
| CHAPTER 8 MECHANICAL CHARACTERIZATION OF GRID-REINFORCED INTERFACES WITHIN BITUMINOUS LAYERS | | 175 |
| 8.1 | Abstract..... | 175 |
| 8.2 | Introduction..... | 176 |
| 8.3 | Research background..... | 177 |
| 8.4 | Experimental program | 180 |
| 8.4.1 | Materials and specimen preparation | 181 |
| 8.4.2 | Test methods | 187 |

| | | |
|-------|---|-----|
| 8.5 | Results and discussions..... | 190 |
| 8.5.1 | Results and discussion on complex modulus test..... | 191 |
| 8.5.2 | Results and discussion on fatigue test..... | 198 |
| 8.6 | Conclusion and recommendations | 202 |
| | CONCLUSION AND RECOMMANDATIONS..... | 205 |
| | BIBLIOGRAPHY..... | 219 |

LIST OF TABLES

| | Page |
|-----------|--|
| Table 2.1 | Environmental effect from traditional pavement renovation methods.....23 |
| Table 2.2 | Long-Term Cost Benefit Analysis of Different Renovation Strategies.....24 |
| Table 3.1 | A review of test methods to measure the interlock capacity provided at the interface between geosynthetic and adjacent materials43 |
| Table 3.2 | Various adhesion theories developed for two involved surfaces.....50 |
| Table 3.3 | Important considerations to include the geosynthetics into design models.....65 |
| Table 3.4 | Models developed for the prediction of damages in reinforced overlay67 |
| Table 3.5 | FEM studies for asphalt overlay reinforced with geosynthetics68 |
| Table 4.1 | Gradation and volumetric characteristics of the mixture.....83 |
| Table 4.2 | The mechanical properties of paving fabric.....84 |
| Table 4.3 | Air void content and specific gravity of specimens.....85 |
| Table 4.4 | T-Test: Two-Sample Assuming Unequal Variances91 |
| Table 5.1 | Experimental design.....103 |
| Table 5.2 | Main Technical Specification of Fabric (Supplied by the Company)104 |

| | | |
|-----------|--|-----|
| Table 5.3 | Dimensional details of mechanical notch and energy dissipation | 114 |
| Table 5.4 | 2S2P1D model parameters..... | 119 |
| Table 6.1 | Technical specifications of hot mixes..... | 132 |
| Table 6.2 | Principal mechanical specification of fabric (provided by the company) | 133 |
| Table 6.3 | Fatigue test specifications at $T= 10\text{ }^{\circ}\text{C}$ and $f= 10\text{ Hz}$ | 140 |
| Table 6.4 | Comparison of fatigue parameters based on NF50% failure criterion | 142 |
| Table 7.1 | Mechanical specifications of asphalt concrete mixtures..... | 151 |
| Table 7.2 | Technical properties of grids (provided by the geogrid supplier)..... | 151 |
| Table 7.3 | J-Integral values for the different systems tested..... | 161 |
| Table 7.4 | Crack Resistance Index (CRI) for each type of structure and interface | 165 |
| Table 7.5 | Average values of Coefficient of Interface Bonding (CIB)..... | 167 |
| Table 7.6 | ANOVA summary results..... | 171 |
| Table 7.7 | ANOVA result for the regression model..... | 172 |
| Table 8.1 | Mechanical specifications of asphalt concrete mixtures..... | 182 |
| Table 8.2 | Technical properties of grids (supplied by the company)..... | 183 |
| Table 8.3 | Mean value of air void content measured by image analysis method..... | 186 |

| | | |
|-----------|--|-----|
| Table 8.4 | 2S2P1D model parameters fitted with the experimental data from Ext. 25 mm | 194 |
| Table 8.5 | 2S2P1D model parameters fitted with the experimental data from Ext. 50 mm | 195 |
| Table 8.6 | Fatigue test specifications at T= 10 °C and f= 10 Hz | 199 |
| Table 8.7 | A Comparison of parameters employed in development of Wöhler curve .. | 201 |

LIST OF FIGURES

| | Page |
|-------------|---|
| Figure 1.1 | Assumed cross section to investigate the effect of geosynthetic6 |
| Figure 1.2 | A comparison of horizontal shear stress distributions6 |
| Figure 1.3 | Changes in shear stress at the interface level with bouning conditions7 |
| Figure 1.4 | Changes in vertical deflection with modulus of bituminous course8 |
| Figure 1.5 | Evolution of design methods for flexible pavements9 |
| Figure 1.6 | Flow chart for Mechanistic-Empirical pavement design method10 |
| Figure 1.7 | Load distribution in a compound method13 |
| Figure 1.8 | A typical form of rutting in the wheel path.....16 |
| Figure 1.9 | Typical form of alligator or map cracking.....18 |
| Figure 1.10 | A typical shape of transverse cracking18 |
| Figure 1.11 | A view of reflective cracking formation19 |
| Figure 2.1 | General and specific objectives26 |
| Figure 2.2 | Layers involved in complex modulus test.....27 |
| Figure 3.1 | Mean service life of an HMA overlay installed on a cracked pavement32 |

| | | |
|-------------|---|----|
| Figure 3.2 | Treatment alternatives regularly employed to control reflective cracking. ... | 33 |
| Figure 3.3 | Steps to evaluate the presence of geosynthetics in the asphalt overlays..... | 34 |
| Fatigue 3.4 | Improved mechanical performance of reinforced asphalt overlay | 35 |
| Figure 3.5 | Improved resistance against reflective cracking. | 35 |
| Figure 3.6 | Enhanced performance of reinforced asphalt overlay against rutting | 36 |
| Figure 3.7 | Maximum rut depth for different subgrade and geogrid stiffness | 37 |
| Figure 3.8 | Tensioned membrane effect due to the concave shape in geogrid..... | 39 |
| Figure 3.9 | Lateral confinement effect in geogrids | 40 |
| Figure 3.10 | Horizontal tensile strain distribution at the interface | 41 |
| Figure 3.11 | The effect of geogrid position in asphalt overlay on fatigue resistance | 45 |
| Figure 3.12 | The effect of geogrid position on rutting | 46 |
| Figure 3.13 | The effect of geogrid position on reflective cracking..... | 46 |
| Figure 3.14 | Design chart to estimate the asphalt overlay thickness | 47 |
| Figure 3.15 | Effect of reduced interlayer bonding on fatigue life..... | 48 |
| Figure 3.16 | Attractive force between dissimilar surfaces..... | 49 |
| Figure 3.17 | Schematic of failure modes at the interface | 49 |
| Figure 3.18 | Different modes of loading imposed to the interface in real condition | 50 |

| | | |
|-------------|---|----|
| Figure 3.19 | Shear device employed to measure bond strength at the interface | 51 |
| Figure 3.20 | Stress distribution under different bonding condition | 52 |
| Figure 3.21 | Mechanical behavior of interface under shear stress | 53 |
| Figure 3.22 | Evolution of shear stiffness at the interface | 54 |
| Figure 3.23 | Effective factors on bond strength at the interface | 54 |
| Figure 3.24 | Correlation between pull-off tensile strength and bitumen stiffness..... | 55 |
| Figure 3.25 | The influence of tack coat dosage in bonding condition..... | 56 |
| Figure 3.26 | The variation of adhesion force and internal friction with loading rate | 57 |
| Figure 3.27 | The shear strength at the interface in a wide range of temperatures | 58 |
| Figure 3.28 | The effect of normal stress on shear strength at the interface | 58 |
| Figure 3.29 | Effect of changes in air voids and moisture content on adhesion strength ... | 59 |
| Figure 3.30 | Effect of surface roughness on shear strength at interface | 60 |
| Figure 3.31 | Variation in interlayer shear strength versus temperature..... | 61 |
| Figure 3.32 | Variation in interlayer shear strength versus dosage of tack coat | 61 |
| Figure 3.33 | Variation in interlayer shear strength versus loading rate | 62 |
| Figure 3.34 | Traffic loading simulation in 2-D plane strain model | 70 |
| Figure 3.35 | Traffic loading for axisymmetric model..... | 71 |

Figure 3.36 Traffic loading for 3-D model71

Figure 3.37 Rheological behavior of asphalt layer72

Figure 3.38 Axial load-axial strain results in the weak and strong directions74

Figure 4.1 Graphical presentation of prepared specimens for each test85

Figure 4.2 3-Ponit Bending Test (a) schematic design (b) test setup.....87

Figure 4.3 Crack Widening Device (CWD) (a) schematic design (b) test setup.....88

Figure 4.4 Water-Vacuum Permeability Device.....90

Figure 4.5 Comparative results for crack generation and crack formation.....92

Figure 4.6 Load-displacement behavior of specimens under shear stresses.....93

Figure 4.7 Typical view of crack at the top surface of the specimen94

Figure 4.8 The result of permeability tests95

Figure 5.1 Gradation curves of mixes103

Figure 5.2 Schematic presentation of the shape and number of specimens.....105

Figure 5.3 Scheme of 3-PBT107

Figure 5.4 Scheme of modified slant shear device109

Figure 5.5 Scheme of adjusted complex modulus test.....111

Figure 5.6 The load-displacement curve for different notch depths114

| | | |
|-------------|--|-----|
| Figure 5.7 | Crack width development below and above the interface..... | 114 |
| Figure 5.8 | Interlayer shear strength versus interlayer shear displacement | 116 |
| Figure 5.9 | The Cole-Cole diagram developed based on the measured data | 117 |
| Figure 5.10 | The Black diagram developed based on the measured data | 118 |
| Figure 5.11 | Difference in the norm of complex modulus..... | 120 |
| Figure 5.12 | Changes in dynamic modulus master curves..... | 122 |
| Figure 5.13 | A comparison of dynamic modulus and phase angle | 123 |
| Figure 6.1 | Mix design sieve curves | 132 |
| Figure 6.2 | A schematic view of specimens prepared for each type of test | 134 |
| Figure 6.3 | A view of rutting test..... | 135 |
| Figure 6.4 | A view of fatigue test: (a) test setup; (b) arrangement of extensometers | 136 |
| Figure 6.5 | Rutting depth evolution by the number of cycles..... | 138 |
| Figure 6.6 | The rut depth after 30000 cycles | 139 |
| Figure 6.7 | The rut depth measured at different locations | 139 |
| Figure 6.8 | Wöhler curve developed for each type of composite structure | 141 |
| Figure 6.9 | Comparison of parameter ϵ_6 for the reference and reinforced structures ... | 142 |
| Figure 7.1 | Gradation curves of the mixes | 150 |

| | | |
|-------------|--|-----|
| Figure 7.2 | Experimental procedure followed for each slab..... | 153 |
| Figure 7.3 | A schematic of size and number of specimens for each type of test | 154 |
| Figure 7.4 | A scheme of 3-PBT setup..... | 156 |
| Figure 7.5 | Scheme of slant shear device..... | 157 |
| Figure 7.6 | Average load-displacement curve in different notches (ESG10/ESG14)..... | 159 |
| Figure 7.7 | Average load-displacement curve in different notches (ESG 14/GB 20)..... | 160 |
| Figure 7.8 | The changes in load-displacement curve for GR 10/14 specimen..... | 161 |
| Figure 7.9 | Crack propagation under and over the interface (ESG10/ESG14)..... | 163 |
| Figure 7.10 | Crack propagation under and over the interface (ESG14/GB 20)..... | 164 |
| Figure 7.11 | Changes in crack development angles below and above the interface..... | 166 |
| Figure 7.12 | Shear displacement at the interface | 167 |
| Figure 7.13 | Average load-shear displacement curves (ESG-10 /ESG 14)..... | 168 |
| Figure 7.14 | Average load-shear displacement curves (ESG-14/GB-20)..... | 169 |
| Figure 7.15 | Radar plot indicating the changes in CRI values to CIB values..... | 173 |
| Figure 7.16 | Sensitivity of the J-integral to mechanical indices at the interface level.... | 170 |
| Figure 7.17 | Interrelationship between CIB and CRI for each type of structure..... | 171 |

| | | |
|-------------|--|-----|
| Figure 8.1 | Gradation curves of each type of hot mixture..... | 181 |
| Figure 8.2 | Experimental procedure followed for each slab | 184 |
| Figure 8.3 | A schematic view of the arrangement and dimensional size | 187 |
| Figure 8.4 | A view of complex modulus test | 189 |
| Figure 8.5 | A view of DGCB test method..... | 190 |
| Figure 8.6 | The Cole-Cole diagram measured with different sizes of extensometers.... | 192 |
| Figure 8.7 | The Black diagram measured with different sizes of extensometers..... | 193 |
| Figure 8.8 | Changes in stiffness modulus between measured and predicted values | 196 |
| Figure 8.9 | Changes in dynamic modulus master curves..... | 198 |
| Figure 8.10 | A comparison of dynamic modulus and phase angle | 198 |
| Figure 8.11 | Wöhler curve for each type of structure | 200 |
| Figure 8.12 | Comparing the ϵ_6 value among different structures..... | 201 |

LIST OF ABBREVIATIONS

| | |
|-----------|--|
| AASHTO | American Association of State Highway Transportation Officials |
| AC | Asphalt Cement |
| ASTRA | Ancon Shear Testing Research and Analysis |
| ATA | Asphalt Interlayer Association |
| AUT - SLT | Amirkabir University of Technology Shear Lab Tester |
| BBR | Bending Beam Rheometer |
| BBS | Bitumen Bind Strength |
| BCR | Base Course Reduction |
| CBR | California Bearing Ratio |
| CIB | Coefficient of Interlayer Bonding |
| CMOD | Crack Mouth Opening Displacement |
| COV | Coefficient of Variation |
| CRI | Crack Resistance Index |
| CWD | Crack Widening Device |

XXVIII

| | |
|------|--|
| CZM | Cohesive Zone Model |
| DC | Dielectrice Value |
| DGCB | Département de Génie Civil et Bâtiment |
| DI | Damage Index |
| DSCT | Disk-Shaped Compact Tension Test |
| DST | Double Shear Test |
| FEM | Finite Element Method |
| FI | Freezing Index |
| FLRT | French Laboratory Rut Tester |
| FPZ | Fracture Process Zone |
| FRC | French Roller Compactor |
| FWD | Falling Weight Deflectometer |
| HMA | Hot Mix Asphalt |
| HV | High Viscosity |
| IDOT | Illinois Department of Transportation |

| | |
|---------|---|
| IDT | Indirect Diametral Test |
| IFSTTAR | Institut Français des Sciences et Technologies des Transports de L'Amenagement et des Reseaux |
| IRI | International Roughness Index |
| ISAC | Interlayer Stress Absorbic Composite |
| ISD | Interlayer Shear Displacement |
| ISS | Interlayer Shear Strength |
| ITS | Indirect Tensile Strength |
| TBR | Traffic Benefit Ratio |
| LCR | Layer Coefficient Ratio |
| LET | Layered Elastic Theory |
| LISST | Louisiana Interlayer Shear Strength Tester |
| LVDT | Linear Variable Deflection Transformer |
| LVE | Linear Viscoelastic |
| MEPDG | Mechanistic Empirical Pavement Design Guide |
| MIF | Modulus Improvement Factor |

XXX

| | |
|---------------------|--|
| MSA | Millions of Standard Axles |
| MS | Medium Setting |
| MTS | Material Testing System |
| NMAS | Nominal Maximum Aggregate Size |
| OT | Overlay Test |
| PET | Polyester Grid |
| PG | Performance Grade |
| PI | Plasticity Index |
| P_{precip} | Average Annual Precipitation of Rainfall |
| PVA | Polyvinyl Alcohol Grid |
| QI | Quality Index |
| QS | Quick Setting |
| RD | Rut Depth |
| RS | Rapid Setting |
| SAMI | Stress Absorbing Membrane Interlayers |

| | |
|---------|--|
| SBS | Styrene-Butadiene-Styrene |
| SCB | Semi-Circular Bend Test |
| SEB | Single-Edge Notched Beam |
| SF | Site Factor |
| SISTM | Sapienza Inclined Shear Test Machine |
| SS | Slow Setting |
| TC | Transverse Cracking |
| TIF | Traffic Improvement Factor |
| TTSP | Time-Temperature Superposition Principle |
| WRC | Wheel Reflective Cracking |
| WVPD | Water Vacuum Permeability Device |
| 2S2P1D | 2 Springs, 2 Parabolic elements, 1 Dashpot |
| 3-PBT | 3 Point Bending Test |
| 4 - PBT | 4 Point Bending Test |

LIST OF SYMBOLS

| | |
|--------------|--|
| $ E^* $ | Dynamic Modulus (Norm of the complex modulus) |
| K | Coefficient of Permeability |
| E_T | Shear Stiffness |
| E_0 | Glassy Modulus |
| E_{00} | Static Modulus |
| a_T | Shift factor |
| f_r | Reduced frequency |
| ϕ | Phase Angle |
| ESG - 10 | Asphalt mixture with nominal maximum aggregate size 10 |
| ESG - 14 | Asphalt mixture with nominal maximum aggregate size 14 |
| GB - 20 | Asphalt mixture with nominal maximum aggregate size 20 |
| ϵ_6 | Strain level at one million cycles |
| S | Slope of the rutting evolution curve |
| J | Non-linear energy release rate |

INTRODUCTION

The pavement is a structural element implemented on top of the natural soil that undergoes traffic and environmental loads and distributes them to a tolerable amount by the natural soil. Based on the stiffness of materials and also the structural performance, pavement is classified into two broad categories: flexible pavements and rigid pavements.

Flexible pavements, sometimes called bituminous pavements, are composed of a mixture of aggregates and bitumen (or asphalt cement) in which the external loads are distributed through an aggregate-to-aggregate contact. On the other hand, rigid pavements, made of cement concrete and in some cases rebars, behave like a rigid plate, and the loads are transferred to underlying layers through the flexural function of the plate.

In comparison, flexible pavements have received more attention in the road engineering community from different aspects, especially due to the low initial costs, the possibility of the stage construction, and easier implementation and repair procedures. Approximately, 80% of all roads in the province of Québec are paved by a bituminous layer (El-Hakim & Tighe, 2014) which is a rather expensive layer and plays an important role in the mechanical performance of the flexible pavement structure (Zapata, 2005). However, because of the application of low stiffness materials, premature failures such as fatigue cracking and permanent deformation (rutting) are frequently observed, which results in shorter service life, and higher required maintenance costs.

A traditional approach to treat the premature failures is to implement an asphalt overlay on existing deteriorated bituminous surface in specific times during its service life. However, this approach is rather expensive and not environmentally friendly due to the appearance of premature failures after a short time, which necessitates another rehabilitation.

Field experience and laboratory results of using geosynthetic material into the bituminous pavement structure, especially in the base and subgrade layers, proved its effectiveness in terms of extending the service life (Haas et al., 1988; Miura et al., 1990; Leng & Gabr, 2002; Moghaddas-Nejad & Small, 2003; Chen et al., 2009; Abu-Farsakh & Chen, 2011; Qian et al., 2011; Ghafoori & Sharbaf, 2016; Abu-Farsakh et al., 2016). Nonetheless, a unanimous design method to incorporate the mechanical effects from geosynthetic materials into the existing or

new HMA overlay has not been yet proposed which results in overdesigned or underdesigned solutions.

Therefore, this thesis has attempted to illuminate the main considerations that are required to be taken into account in response model and performance prediction models embedded in a mechanistic based design approach for a reinforced - rehabilitated pavement structure, through a comprehensive laboratory examination. On this basis, this manuscript is presented in eight chapters. Chapter 1 covers a literature review on design methods developed for bituminous pavements from early days up to now. Chapter 2 describes problems in designing a reinforced or rehabilitated bituminous structure. It continues with the explanation of general and specific objectives. Chapter 3 provides a specific literature review on mechanical behavior and design considerations for reinforced-rehabilitated bituminous pavements in which the mechanical effects coming out of the interface are first discussed and then the main considerations to include them into mechanistic based design methods are explained. The derived paper from this study was published in *Construction and Building Materials*. Different issues are highlighted in chapter 3, and among those issues is the waterproofing capacity of a cracked pavement structure rehabilitated with a paving fabric. Because of this, chapter 4 addresses the permeability and anti-reflective property of double-layer bituminous systems, rehabilitated with a layer of paving at the interface, through novel laboratory approaches. This is specifically important to provide better judgment on selecting proper drainage coefficient of granular layers and retained modulus of both bituminous and granular layers in design methods for systems including paving fabric. The derived paper from this study was published in *Materials and Structures*.

As explained in chapter 3, the presence of paving fabric or geogrids in a bituminous pavement does have an impact on the mechanical response of the pavement structure to loads. There are different problems related to the characterization in the laboratory of the rheological behaviour of a system composed of two asphalt mixes with a geosynthetic embedded in between, to the behaviour of the interface, to the crack propagation resistance, and to the degradation of those pavements in general. Those questions were addressed in this research project and the work done to answer those problems is exposed in the following chapters. Chapter 5 explains how the placement of a layer of paving fabric in a rehabilitated structure could influence the fracture

parameters of the composite system and tangential and axial stiffnesses at the interface level of adjacent materials. In other words, the required changes in mechanistic design approaches with respect to response model and performance prediction model in terms of reflective cracking, in the presence of a rehabilitated interface are explained. Findings from this study were accepted for publication in the *Journal of Materials in Civil Engineering* (ASCE). Chapter 6 reveals the main considerations that need to be taken into account in performance models of a rehabilitated system for better prediction of rutting and fatigue cracking. The findings from this study were submitted for the evaluation in the *Journal of Road Materials and Pavement Design*. Chapters 7 and 8 focus on reinforced bituminous layers with grid products. The fracture toughness of grid-reinforced structures and its effect on delaying reflective cracking is discussed in Chapter 7, accepted for publication in the *Journal of Geotextiles and Geomembranes*, and the changes in response model and structural integrity of reinforced interface are addressed in Chapter 8, submitted in *Construction and Building Materials*.

CHAPTER 1

LITERATURE REVIEW

1.1 Introduction

Bituminous layers constitute the upper part of flexible pavements, which are usually in close contact with applied loads from vehicles and the environment. Therefore, the materials employed in the dressing layer need to be impermeable and resistant enough to maintain its quality throughout the service life so that a smooth, comfortable and safe roadway for the users could be guaranteed. To satisfy this requirement, it is not only essential to supply construction material in accordance with the standards, but also to reduce the possibility of the occurrence of premature failures due to unexpected or ever-increasing traffic loads through new technologies such as interlayer products. Interlayer systems compensate for the absence of tensile strength in hot mixtures and lead to the enhanced structural integrity of the entire system against fatigue cracking, rutting, and reflective cracking.

Various kinds of products are available in the market functioning as a reinforcing material to extend the flexible pavement service life. Some of them are (Helstrom et al., 2007): SAMIs (Stress Absorbing Membrane Interlayers), sand asphalt, geosynthetics (including paving fabrics and geogrids), or a combination of the above materials. In comparison, geosynthetics comprises noticeable assets that make it more interesting than the rest. It is both firm and flexible. Its modulus is considerably higher than any other reinforcing products and any components of the flexible pavement structure. It is also able to undergo high mixing and compacting temperatures during construction operations without any loss in its performance. It receives almost no harm from de-icing salt, petroleum, or bitumen. In addition, under adverse weather conditions or attacks from corrosive chemicals, it resists very well (Al-Qadi et al., 2008). However, there are two main obstacles in its use in asphalt layers, which need to be further studied: mechanical interaction between geosynthetic and surrounding bituminous layers and its recyclability during the maintenance measures.

In this research, the mechanical interaction at the interface of the geosynthetic and adjacent bituminous materials is studied. It is believed that any changes made at the interface of

bituminous layers could affect the distribution of pavement responses to applied loads and then makes the prediction of mechanical performance of the structure more complicated (Wu et al., 2017; Galaviz-González et al., 2019; Romanoschi et al., 2001). To clarify this effect, first a pavement cross section is assumed with the details indicated in Figure 1.1.

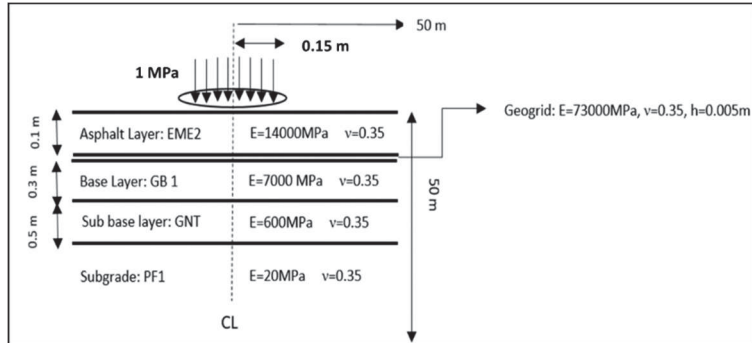


Figure 1.1 Assumed cross section to investigate the effect of a layer of geosynthetic on structural responses of the system

The structural analysis of the assumed configuration with Abaqus software (Abaqus 2019), as can be seen in Figure 1.2, demonstrated that the introduction of a high modulus interlayer between bituminous layers could affect the distribution of horizontal shear stresses at the interface level.

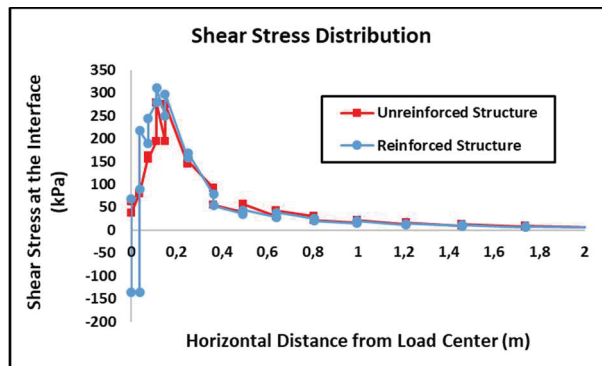


Figure 1.2 A comparison of horizontal shear stress distributions in unreinforced and reinforced structures at the interface level

Furthermore, the bounding condition at the interface is another concern that could complicate further the distribution of structural responses of the system under loading. Figure 1.3

illustrates the distribution of shear stresses between bituminous layers (i.e. between EME2 and GB1 in the assumed cross section) induced by a dual wheel in Y-Y direction. This analysis was made by Alize-Lcpc software.

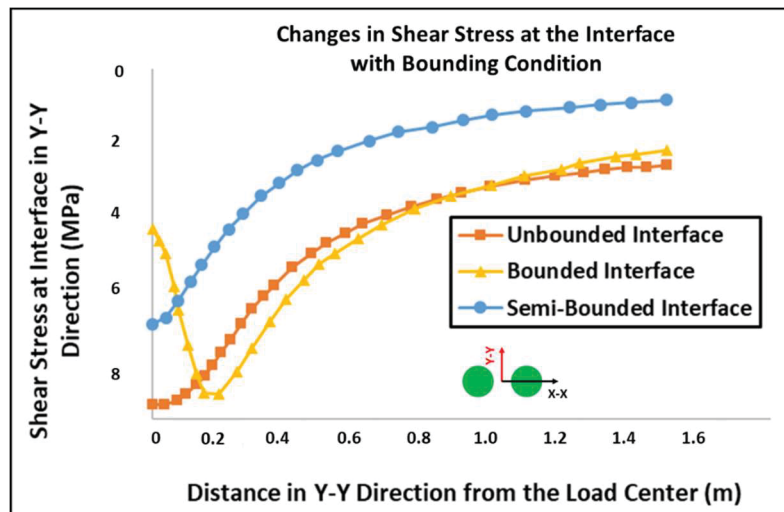


Figure 1.3 Changes in shear stress at the interface level with different bounding conditions

Besides, the presence of a layer of geosynthetic in the form of paving fabric between bituminous layers (between EME2 and GB1 layers in the assumed construction) could limit surface damages and extend the pavement service life by keeping away the binder course from the percolation of water from the surface layer and maintain its initial modulus. Figure 1.4 shows the surface deflection analysis made by Alize-Lcpc for the assumed cross-section under a dual wheel. As can be seen, if the water is allowed to enter into the binder course, its retained modulus, according to the MTQ standard, is allowed to drop to 70% of the initial modulus, which in turn, the surface deflection will increase compared to the reinforced structure.

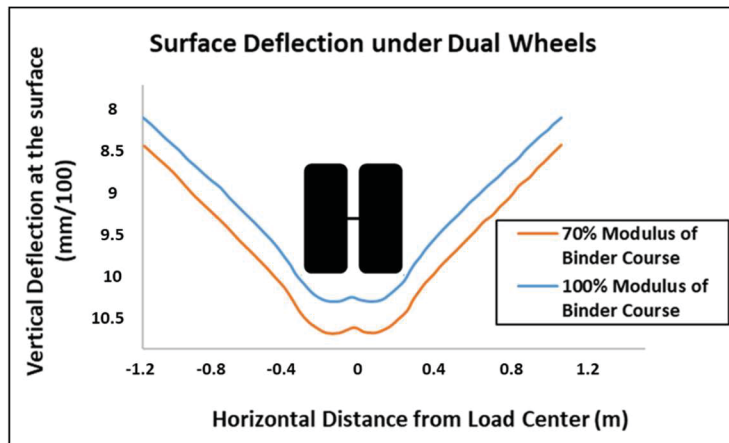


Figure 1.4 Changes in vertical surface deflection with modulus of bituminous binder course

However, because of the lack of a standard test method and apparatus to measure the structural responses in a reinforced structure, design methods can lead to underestimate or overestimate solutions with pertinent economic burdens on authorities. On this basis, for the sustainability of the composite reinforced structure, it is vital to provide authentic and reliable mechanical measurements from a reinforced structure by means of novel approaches in order to ease its analysis procedure. This would also facilitate the application of any mechanistically based design approaches for the reinforced structure.

This thesis will try to provide necessary inputs or modifications required to be considered for the design of a reinforced or rehabilitated structure with geosynthetic materials by the mechanistic-empirical (M-E) design approaches. A review of studies on design methods and their components along with a description of existing problems and the objectives are presented in the following sections. In the end, the framework of this thesis will be introduced.

1.2 Background on pavement design methods

Pavement design has changed considerably since the early 1900s. This continuous trend is due to the growing need for a more accurate correlation between field observation and anticipated performance to consider not only the effect of continual change in speed and configuration of wheel loads but also new material types.

The evolution of design methods is demonstrated in Figure 1.5. In the early stages of development, road designs were based solely on engineering judgment or experience. The concept of having a stiff layer with high-quality material in the top and low-quality material at the bottom was assumed by the Romans, which nowadays forms the main structure of flexible pavements. In the 1930s, after the Great Depression and development in new technologies, cover-based design methods (e.g. CBR method) were initiated. However, these methods were still based on engineering judgment. It was in the 1960s that the AASHO road test was implemented in the field and resulted in the AASHTO design method. In the mid-1970's a new linear elastic mechanistic-empirical design method (M-E method) was proposed, which required more parameters as inputs for the design and corresponding elaborated field and laboratory test methods to obtain these inputs. With the advent of high-speed processing computers, the possibility of doing more accurate analysis by the finite element method was brought up to consider both linear and non-linear behaviors of materials, which formed the basis of currently Mechanistic-Empirical Pavement Design Methods.

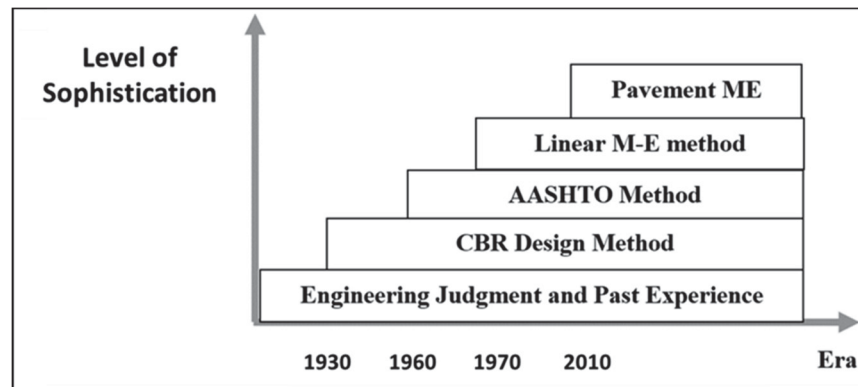


Figure 1.5 Evolution of design methods for flexible pavements

Pavement design based on the M-E method is an iterative process, which gives the pavement distress and smoothness as output instead of the layer thicknesses, normally reported by empirical methods. First based on the site conditions (i.e., traffic, climate, foundation, pavement geometry, and material properties) a trial design is proposed for a new pavement or existing pavement. Then, the structural responses (e.g. stress and strain) are calculated through response models embedded in the M-E Pavement method. This part constitutes the mechanistic part of the design method. After that, the structural critical responses are entered into the

distress prediction models to predict key distresses (i.e. fatigue cracking, rutting, thermal cracking, and reflective cracking) in flexible pavement structures. The trial design is then checked for adequacy against the failure criteria defined in the M-E Pavement design by the user. If the design does not meet the failure criteria at the specified reliability, it is revised and the evaluation process repeated as much as necessary. Thus, the designer is fully involved in the design process and has the flexibility to consider different design features and materials to satisfy the failure criteria for the site conditions. Figure 1.6 shows a flow chart of a typical M-E pavement design procedure (AASHTO, 2008).

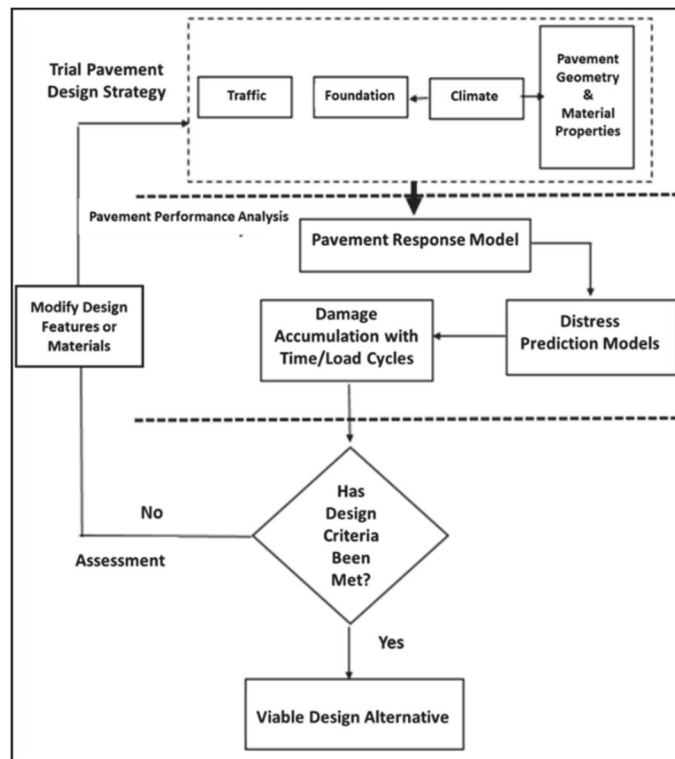


Figure 1.6 Flow chart for Mechanistic-Empirical pavement design method (AASHTO, 2008)

1.2.1 Design methods proposed for reinforced bituminous pavements with geosynthetics

A review of the literature shows that the majority of design methods proposed for a reinforced layer with geosynthetic materials are empirical and solely developed for reinforced layers

made up of granular materials. The use of these methods are also limited in practice due to several factors (Berg et al., 2000):

- Design methods were not part of a nationally recognized pavement design procedure.
- Design methods applied to a limited range of design conditions.
- Most of the design methods are proprietary which is rather difficult to extend the results for other brands of the same kind but different specifications.

For example, an empirical method proposed based on the modification of the original formula (Equation (1.1)) used in AASHTO (1993) to solve SN, by introducing two separate ratios in the equation; one Traffic Benefit Ratio (TBR), and the other Base Course Reduction (BCR) which are defined as below (Murad, 2017).

$$\log w_{18} = Z_R \times S_0 + 9.36 \times \log(SN + 1) - 0.2 + \frac{\log \frac{\Delta PSI}{2.7}}{0.4 + \frac{1094}{(SN+1)^{5.19}}} + 2.32 \log M_R - 8.07 \quad (1.1)$$

Traffic Benefit Ratio (TBR) is specified as the ratio of the number of traffic repetitions on a pavement section reinforced with a grid to attain specific failure criteria (N_r) to the number of traffic repetitions on an unreinforced section, with the same properties, to reach the same criteria (N_u). It is sometimes termed Traffic Improvement Factor (TIF) and calculated according to Equation (1.2).

$$TBR = N_r / N_u \quad (1.2)$$

Base Course Reduction (BCR), is determined by the reduction in the reinforced base course layer thickness (T_r) with respect to the unreinforced thickness (T_u), with the identical material components, to attain the same specific failure level. It is defined as Equation (1.3).

$$BCR = T_r / T_u \quad (1.3)$$

On this basis, TBR is applied to the number of traffic W_{18} in the Equation (1.1) and BCR is applied to the base thickness value according to the Equation (1.4) & Equation (1.5):

$$SN = (a \times d)HMA + BCR \times (a \times d \times m)base + (a \times d \times m)subbase \quad (1.4)$$

Then, the base course thickness in a reinforced structure would be

$$d_{base,(R)} = \frac{SN_u - (a \times d)HMA - (a \times d \times m)subbase}{BCR \cdot (a \times m)base} \quad (1.5)$$

In which SN_u is the structural number for the unreinforced pavement. TBR ranges from 1.5 to 70 and BCR from 20% to 40%.

In an attempt to seek for the performance of geogrids implemented over different types of subgrades, from soft to stiff ones, and then to quantify it into design methods, two empirical factors were introduced: modulus improvement factor (MIF) and layer coefficient ratio (LCR), which are defined according to Equation (1.6) and Equation (1.7) (Goud et al., 2020).

$$LCR = \frac{0.249 \log_{10} \left(\frac{E_B}{0.0069} * MIF \right) - 0.977}{0.249 \log_{10} \left(\frac{E_B}{0.0069} \right) - 0.977} \quad (1.6)$$

where E_B is the modulus of the base course and MIF is the modulus improvement factor, obtained from Equation (1.7).

$$MIF = \frac{E_{B(Rienforced)}}{E_{B(Unrienforced)}} \quad (1.7)$$

The calculated LCR is then applied to the layer coefficient of the base layer to take the reinforcement effect of geogrid into account.

Another method is to assume the distribution of the wheel load as indicated in Figure 1.7. The stiffer the layer, the more load spreads to the bottom layers. Based on the assumption that utilizing geogrids will enhance the stiffness of the layer and consequently will increase the load spreading, the bearing capacity of the granular layer or soil is calculated based on the CBR (California Bearing Ratio) value. Then this value is compared with the applied load on top of the layer. If the bearing capacity is higher than the load, the safety factor will be higher

than 1.0. Similarly, the same method can be used for the asphalt, base, and subbase layers (Elias, 2004).

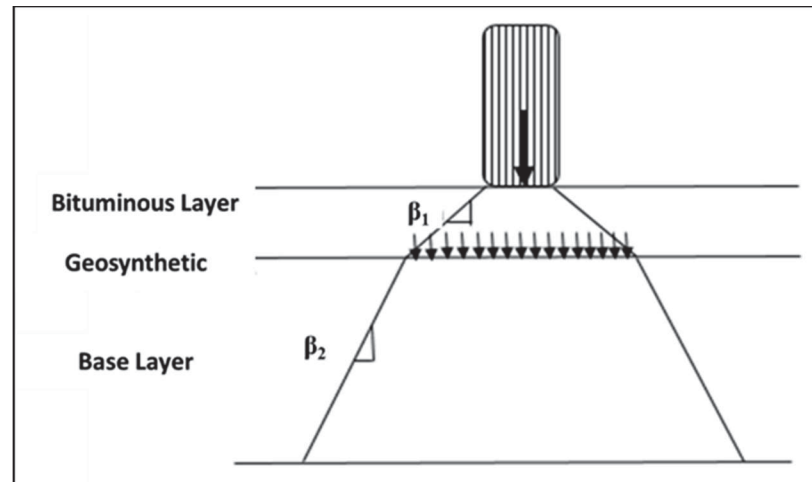


Figure 1.7 Load distribution in a compound method

However, the best way to design a pavement system including an asphalt layer reinforced with geogrid is to use an M-E design approach. Unlike the granular materials, the enhanced mechanical behavior is more complicated to quantify with some factors and also the improved structural performance in terms of fatigue cracking and permanent deformation can be measured and evaluated in the field (Al Qadi et al., 2008). On this basis, It was suggested that in addition to the common input parameters into M-E design approaches, namely traffic, climate, material properties, and pavement geometry, for asphalt layers reinforced with geosynthetics, the following considerations need to be considered (Rathmayer, 2007; Khay and Giraud, 2004; Chen et al., 2009; Palmeira and Antunes, 2010; Perkins, 1999; de Bondt, 2012; Zofka et al., 2017):

- Properties of the reinforced material like complex modulus of the interface and integrated system in order to analyze the structural responses through response models;
- Location of the interlayer in pavement cross-section;
- Mechanical characteristics of each pavement layer and the subgrade;
- Stiffness and thickness of layers in contact with the interlayer;
- Calibration of distress prediction models based on field condition and new materials;

- The interaction between the reinforcement interlayer and adjacent layers or the bonding condition. In this connection, most of the proposed models were focused on defining the geosynthetic material as a membrane element to resemble the frictional effect. However, only a few of these studies tried to consider the lateral confinement effect of the geogrid layer provided by the presence of apertures in its structure. It was suggested that this effect could be simulated by an additional force applied on the sides of the geogrid layer, which was then distributed as uniform stress around the geogrid layer (Yang and Han, 2013). However, this hypothesis is not correct because the reinforcement effect of geogrid on adjacent materials is decreasing as the distance from the geogrid layer is increasing. In another study, the confinement force was taken into account by a triangularly distributed stress applied on the side of the geogrid layer (Gu et al. 2016).

As mentioned earlier, the M-E Pavement Design approaches can take the effect of interlayer products into account. On this basis, various types of interlayers could be classified into two broad categories in terms of their applications in pavement structure. First, rehabilitation-purpose products such as geotextile, paving fabric, paving mats, and stress-absorbing interlayer (SAMI), which are mainly employed to waterproof the pavement system and to retard the propagation of reflective cracks from the bottom layers to the top. Second, reinforcement-purpose products such as grids made of a wide range of raw materials, which are utilized to enhance the structural integrity of the pavement system against shear and tensile stresses induced by external loads.

In this thesis, the required inputs and modifications in the M-E design approaches for both of these reinforcement and rehabilitation strategies were addressed. Like the new pavement design method, the M-E approach for rehabilitation or reinforcement projects is an iterative process, which starts with a trial rehabilitation or reinforcement strategy proposed by initial inputs. Then the trial strategy is analyzed by response models and distress prediction models to ensure that it meets the user's performance expectations.

1.2.1.1 Response models in the M-E pavement design

The response model aims to determine the structural responses of the pavement system due to traffic loads and environmental effects. In most cases, numerical analyses such as finite element methods using the ABAQUS software have been employed to obtain the pavement responses (e.g., stresses, strains, and deformations), and thereby to predict the pavement performance. Of particular interest are the critical responses required as inputs into the pavement distress models, which include (AASHTO 2008):

- Tensile horizontal strain at the bottom or top of the HMA layer (for HMA fatigue cracking).
- Compressive vertical stresses or strains within the HMA layer (for HMA rutting).
- Compressive vertical stresses or strains within the base\subbase layers (for rutting of unbound layers).
- Compressive vertical stresses or strains at the top of the subgrade (for subgrade rutting).

Each of these variables should be assessed at the critical location within the pavement system where the variable has the maximum value.

Two material behaviors apply to the M-E design method. For cases in which all the materials in the pavement structure can realistically be treated as linearly elastic, multilayer elastic theory is used to determine the pavement responses. In cases where the nonlinear behavior of materials is considered, a nonlinear finite element procedure is applied instead of determining the pavement responses. In this case, it is necessary that the finite element method be validated by the laboratory data to confirm its accuracy.

1.2.1.2 Distress prediction models in M-E pavement design

After calculation of the critical responses by the mechanistic unit, the output is entered into the distress prediction models, which has been developed based on the laboratory measurements and adjustment with the field results. The design life of the pavement is first divided into some intervals and then damages are computed for each interval. An analysis interval of one month is defined as the minimum unit for estimating incremental damage in order to account for the possible changes in the traffic and environmental conditions. Distresses are then accumulated

for each interval and reported as the predicted value. The followings are the types of distresses, which are considered in the M-E Pavement Design for hot mixture overlays.

Rut Depth

A surface lateral distortion in the wheel path, which is mainly caused by the plastic or permanent vertical deformation in the HMA, unbound layers, and subgrade (Yinfei et al., 2018), is called rutting as indicated in Figure 1.8. For all HMA mixtures, the field-calibrated form of the laboratory-derived relationship from repeated load permanent deformation tests is as Equation (1.8) (AASHTO, 2008).

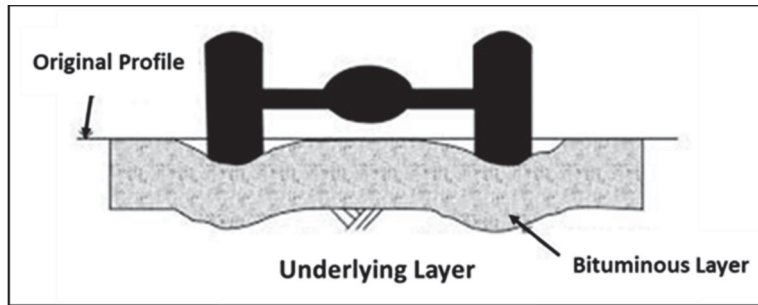


Figure 1.8 A typical form of rutting in the wheel path (adapted from Mashaan et al., 2014)

$$\Delta_{p(HMA)} = \varepsilon_{p(HMA)} \cdot h_{HMA} \beta_{1r} \cdot k_z \cdot \varepsilon_r(HMA) \cdot 10^{k_{1r}} \cdot n^{k_{2r}} \cdot \beta_{2r} \cdot T^{k_{3r}} \cdot \beta_{3r} \quad (1.8)$$

where $\Delta_{p(HMA)}$ is accumulated permanent vertical deformation in the HMA layer/sublayer, $\varepsilon_{p(HMA)}$ is accumulated permanent or plastic axial strain in the HMA layer/sublayer, $\varepsilon_r(HMA)$ is resilient or elastic strain calculated by the structural response model at the mid-depth of each HMA sublayer, $h(HMA)$ is the thickness of the HMA layer/sublayer, n is the number of axle-load repetitions, T is mix or pavement temperature, k_z is depth confinement factor, $k_{1r,2r,3r}$ is global field calibration parameters (from the NCHRP 1-40D recalibration; $k_{1r} = -3.35412$, $k_{2r} = 0.4791$, $k_{3r} = 1.5606$), and β_{1r} , β_{2r} , β_{3r} , are local or mixture field calibration constants; for the global calibration, these constants were all set to 1.0.

Fatigue Cracking

The M-E Pavement Design Method assumes that alligator or fatigue cracking initiates at the bottom of the HMA layer and then propagates to the surface with the continued effect of truck traffic as indicated in Figure 1.9. The allowable number of axle-load applications needed for the incremental damage index approach to predict fatigue cracking is calculated through Equation (1.9) (AASHTO, 2008).

$$N_{f-HMA} = k_{f1}(C)(C_H) \cdot \beta_{f1} \cdot (\varepsilon_t)^{k_{f2} \cdot \beta_{f2}} \cdot (E_{HMA})^{k_{f3} \cdot \beta_{f3}} \quad (1.9)$$

where N_{f-HMA} is the allowable number of axle-load applications for HMA overlays, ε_t is the tensile strain at critical locations and calculated by the structural response model, E_{HMA} is the dynamic modulus of the HMA, k_{f1} , k_{f2} , k_{f3} are global field calibration parameters (from the NCHRP 1-40D re-calibration; $k_{f1} = 0.007566$, $k_{f2} = -3.9492$, and $k_{f3} = -1.281$), and β_{f1} , β_{f2} , β_{f3} are local or mixture specific field calibration constants; for the global calibration effort, these constants were set to 1.0.

Then the M-E method calculates the incremental damage indices on a grid pattern throughout the HMA layers at critical depths. The incremental damage index (ΔDI) is calculated by dividing the actual number of axle loads by the allowable number of axle loads (Known as Miner's method) within a specific time increment and axle-load interval for each axle type. The cumulative damage index (DI) for each critical location is determined by summing the incremental damage indices over time as Equation (1.10) (AASHTO, 2008).

$$DI = \sum (\Delta DI)_{j,m,i,p,T} = \sum \left(\frac{n}{N_{f-HMA}} \right)_{j,m,i,p,T} \quad (1.10)$$

where n is the actual number of axle-load applications within a specific time period, j is the axle-load interval, m is the axle-load type (single, tandem, tridem, quad, or special axle configuration), i is truck type using the truck classification groups included in the MEPDG, p is the month, and T is median temperature.

The area of alligator cracking is calculated from the total damage over time by using the transfer functions as Equation (1.11) (AASHTO, 2008).

$$FC_{Bottom} = \left(\frac{1}{60}\right) \left(\frac{1}{1 + e^{(C_1 C_1'' + C_2 C_2'' \text{Log } DI_{Bottom} * 100)}} \right) \quad (1.11)$$

where FC_{Bottom} is the area of alligator cracking that initiates at the bottom of the HMA layers, % of total lane area, DI_{Bottom} is the cumulative damage index at the bottom of the HMA layers, and C_1 and C_2 are transfer function regression constants.

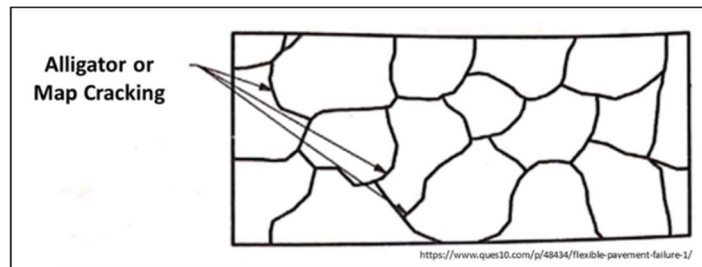


Figure 1.9 Typical form of alligator or map cracking

Transverse Cracking

Low-temperature cracking occurs when tensile stresses develop in an HMA as the temperature drops to an extremely low value. At that moment, if the tensile stress equals the strength of the hot mixture at that temperature, a micro-crack appears at the surface. At colder temperatures or repeated temperature cycles, the crack propagates and penetrates the full depth and width of the hot mixture. The primary pattern of low-temperature cracking is transverse to the direction of traffic as shown in Figure 1.10.

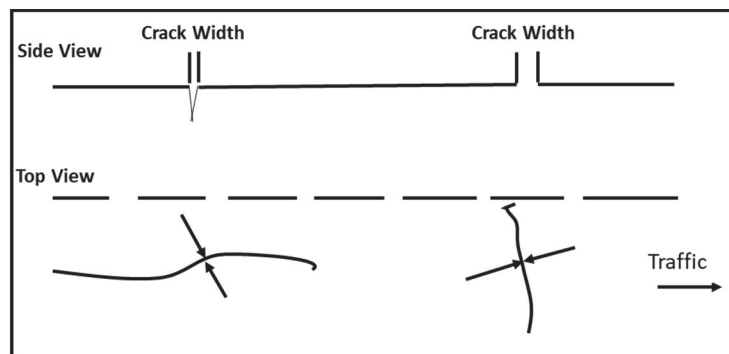


Figure 1.10 A typical shape of transverse cracking

The degree of cracking is predicted by the M-E method using an assumed relationship between the probability distribution of the log of the crack depth to the HMA-layer thickness ratio and the percent of cracking according to the Equation (1.12).

$$TC = \beta_{t1} \cdot N \left[\frac{1}{\sigma_d} \log \left(\frac{C_d}{H_{HMA}} \right) \right] \quad (1.12)$$

where TC is observed amount of thermal cracking, ft/mi, β_{t1} is regression coefficient determined through global calibration, $N [z]$ is standard normal distribution evaluated at $[z]$, σ_d is the standard deviation of the log of the depth of cracks in the pavement (0.769), C_d is crack depth, and H_{HMA} is the thickness of HMA layers.

Reflective Cracking

Reflective cracking frequently appears on the surface of bituminous pavement shortly after the rehabilitation of an existing deteriorated structure. The stress concentration at the crack tip, caused by traffic loads, passing over existing cracks, or temperature fluctuations is the main contributor to this type of crack (Pais, 2013) as shown in Figure 1.11.

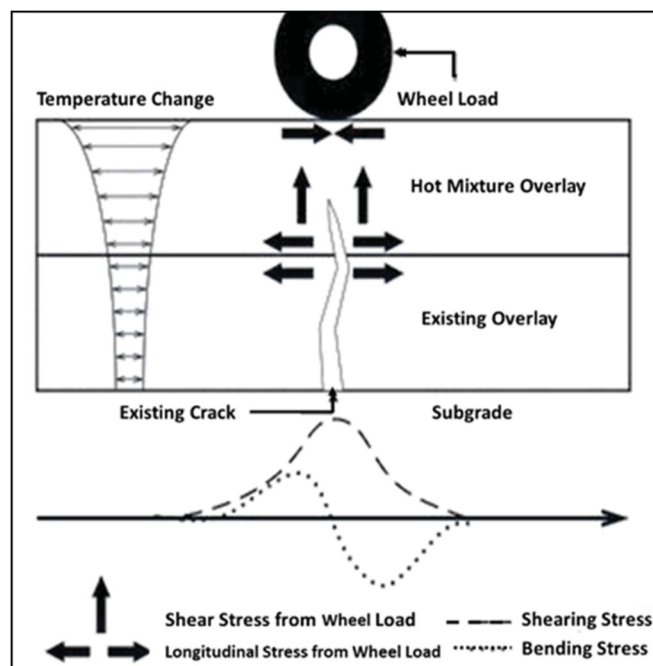


Figure 1.11 A view of reflective cracking formation

The amount of reflective cracking stricken a bituminous overlay in terms of the percentage of the total area is estimated empirically by a sigmoid function as indicated in Equation (1.13).

$$RC = \frac{100}{1 + e^{a(c)+bt(d)}} \quad (1.13)$$

where RC is the percentage of the area stricken by reflective cracking; t is the time in year; a, b are regression fitting parameters; and c, d are user-defined parameters, in which d reflects the crack delaying ability of the layer.

Altogether, based on the distresses predicted by distress prediction models, the M-E method assumes that smoothness degradation is due to the occurrence of surface distresses which will result in increased roughness (increasing IRI value), or in other words, a reduction in smoothness. On this basis, all the distresses computed by distress prediction models are transferred to a single value, as IRI through the Equation (1.14). This value is then employed to control the adequacy of the proposed trial design against the allowable amount defined by the user.

$$IRI = IRI_0 + 0.0150(SF) + 0.4(FC_{(Total)}) + 0.008(TC) + 40(RD) \quad (1.14)$$

where IRI_0 is initial IRI after construction, SF is site factor, according to Equation (1.15); $FC_{(Total)}$ is the area of fatigue cracking, percent of the total lane area. All load-related cracks are combined on an area basis, TC is the length of transverse cracking (including the reflection of transverse cracks in existing HMA pavements), and RD is average rut depth.

$$SF = Age [0.02003(PI + 1) + 0.007947 (Precip + 1) + 0.000636(FI + 1)] \quad (1.15)$$

where Age is pavement age in yr., PI is percent plasticity index of the soil, FI is average annual freezing index, and $Precip$ is the average annual precipitation or rainfall.

1.2.1.3 Hierarchical input levels

In the M-E design approach, the input values for material, traffic, and climate for a specific pavement section could be determined through one or mix of three levels:

Level I: This level presents greatest knowledge about the input parameter by directly measuring it in the laboratory or in the field.

Level II: The value for input parameter is estimated based on empirical relationships or regression equations developed based on material properties.

Level III: The input parameter is specified based on default values, which has the least knowledge and in turn lowest laboratorial testing effort.

The selection of each level for input data depends on the importance of the project and the availability of resources (AASHTO 2008). On this ground, more reliability on the level of input data leads to more accurate design solutions for a given project.

1.2.2 Literature review summary

According to the review mentioned above, the M-E pavement design method is currently a worldwide acceptable design method for flexible pavements because of its following advantages over purely empirical methods:

- It can be employed for both existing pavement and also new pavement structures;
- It incorporates the changes in traffic loadings and environmental conditions;
- It can better describe material specifications, which in turn allows for taking advantage of available materials and new products;
- It gives better and reliable performance predictions.

It is composed of two separate parts: the mechanistic unit to analyze the pavement responses to external loadings and the empirical unit to predict pavement performance during its service life in terms of fatigue cracking, rutting, and transverse cracking based on the critical responses calculated in the mechanistic unit.

However, the effect of geosynthetics into the M-E pavement design method has not yet been incorporated. In order to introduce the interlayer effects into the M-E design method, a comprehensive laboratory study needs to be performed in order to provide level I input data to accurately justify the interface response to external loadings and predict the reinforced or rehabilitated pavement performance during the service life.

CHAPTER 2

PROBLEM DESCRIPTION AND OBJECTIVES

2.1 Introduction

Traditional techniques, which are employed to treat a distressed pavement surface could bring life extension in the service life to varying degrees. Table 2.1 provides a fair comparison in terms of service life among different pavement renovation methods. As can be seen, despite the life extension that they bring into the existing pavement, they require large amounts of energy to obtain and process raw materials, transport, mix and apply the final product that impacts greenhouse gas emissions on different levels.

Table 2.1 Environmental effect from different traditional pavement renovation methods
(Chehovits & Galehouse, 2010)

| Treatment | Life Extension (Years) | Energy Use per Year (MJ/m ²) | GHG Emission per Year (kg/m ²) |
|---|---------------------------|---|---|
| Hot Mix Asphalt Overlaying (5 cm) | 5-10 | 7.7-15.4 | 0.7-1.3 |
| Hot In-place Recycling (5 cm; 50/50 Recycle/New) | 5-10 | 6.5-13 | 0.5-1 |
| Chip Seal (Emulsion 1.6 L/m ² & Aggregate 15kg/m ²) | 2-5 | 1.3-3.3 | 0.08-0.2 |
| Micro-Surfacing (Type II, 14% Emulsion, 8.7 kg/m ²) | 2-4 | 1.2-2.4 | 0.05-0.1 |
| Crack Seal (0.37 kg/m) | 1-3 | 0.4-1.1 | 0.03-0.08 |
| Crack Fill (0.74 kg/m) | 1-2 | 1-2 | 0.07-0.14 |
| Fog Seal (0.69 L/m ² , 50/50 Diluted Emulsion) | 1 | 1.2 | 0.07 |

On the other hand, previous studies demonstrated that by using interlayer systems between an existing deteriorated asphaltic surface and a new bituminous overlay, the service life could be even more extended than only hot mix overlaying.

In addition, a long-term cost benefit analysis of different renovation strategies for a 10 cm thick overlay for a high volume road shows that a significant cost advantage around 20 to 40% depending upon local design conditions and material costs, would be expected in case of using interlayer systems instead of traditional mill and fill technique, as indicated in Table 2.2.

Table 2.2 Long-Term Cost Benefit Analysis of Different Renovation Strategies for a 10 cm thick overlay for a high volume road (Tensar International Corporation (2015))

| Type of Strategy | New Asphalt Overlay after 5 Years | Crack Sealing operation after 5 Years + Extra 2.5 cm Overlay | Introducing a Layer of Geosynthetic before New Asphalt Overlay |
|------------------|--------------------------------------|--|--|
| Total Cost | 32 \$/m ² | 25 \$/m ² | 18 \$/m ² |

2.2 Problem description

The mechanical effects of interlayers between bituminous layers has not been included in the mechanistic based design approaches. This is mainly due to a lack of theoretical basis and reliable data to develop a model to calculate the critical responses in any points of the structure and also to predict the pavement performance through the distress prediction models, which could be regarded as a key reason for low rate of interlayer usage compared to traditional techniques. In this connection, improper and inadequate design methods lead to appearance of premature failures in the form of fatigue failure, rutting, or reflective cracking, which causes reduced structural capacity, increased roughness, and poor riding quality.

To solve this problem, it is essential that the new mechanical effects coming from the interlayer systems be properly determined. To this end, two methodologies could be adopted: laboratorial examination and field data collection. In this study, the laboratorial approach was selected for different reasons: first, there is no need to invest too much money for site preparation or close the road for the traffic. Second, data acquisition in the field is very difficult because of the harsh condition. Third, to control the effects from other sources is so challenging. In other words, it is very difficult to know what causes what. Last, the experiment in the field is so lengthy. It may take several years of site preparation to gather data. On this basis, doing laboratory tests seem quite reasonable. However, a few challenges are associated with the laboratorial approach. Firstly, traffic and environmental loads should be simulated as is the case in the real condition, in order to obtain reliable design inputs. Secondly, the available test

devices and standards, specialized for structures including geosynthetics are so limited and new test methods or adjustments on existing test devices are required. Thirdly, the specimen preparation should follow the steps that actually happen in the field and lastly, small-scale laboratorial specimens should reflect the mechanical behavior in a full-scale situation. Therefore, in response to these challenges, simplifications and assumptions are imminent, which will be presented for each type of test in the research methodology section.

2.3 Objectives

The principal objective of this research was to provide new methodologies that presented level I laboratorial input data into the M-E design method for reinforced-rehabilitated pavement structure. It should be emphasized that the scope of this study was not to have directly applicable information/inputs for Pavement ME or Alize, but to have information that could be used in ME pavement design methods. In other words, the methodologies presented in this study, are applicable to characterize the mechanical effects from the interface, treated with different interlayers and made up of various raw material and mechanical specifications. On this basis, the specific objectives, shown in Figure 2.1, were addressed throughout this thesis. An important feature of this research was its inclusiveness in study of two types of interlayer products from the application standpoint (i.e. rehabilitation and reinforcement purposes), embedded in different types of hot mixtures, in terms of nominal maximum aggregate size (NMAS). This provided a fair comparison of changes in the mechanical behavior of reinforced and rehabilitated structures in various interfacial conditions with corresponding unreinforced structures. It also helped to illuminate the location of interlayer products within the bituminous pavement cross-section to properly address each type of distress by keeping its negative effect on the bonding condition as low as possible.

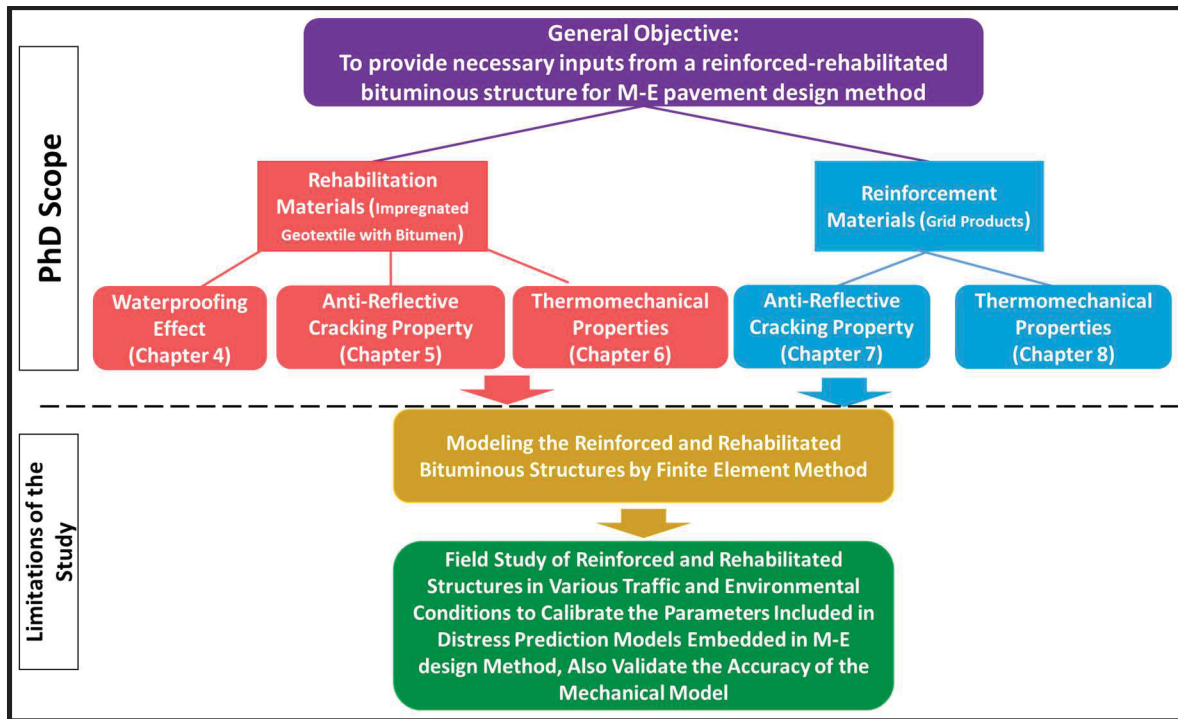


Figure 2.1 General and specific objectives to attain the M-E Pavement Design Method for rehabilitated and reinforced pavements

All the specific objectives indicated in Figure 2.1 were based on experimental investigations on small-scale laboratory specimens of different sizes and shapes. Two types of interlayer from the application perspective were studied: paving fabric was selected as a rehabilitation technique, which is normally employed between a cracked bituminous layer and the wearing course to fight against the rise of cracks and maintain the waterproofing of the coating in the long term. It consists of a non-woven polypropylene geotextile membrane (GEOPAVE geotextile) impregnated with a modified bitumen (MAXE). The geotextile essentially plays the role of a bitumen reservoir. As for bitumen, thanks to its low viscosity, it ensures partial decoupling of the asphalt layers. On the other side, various types of grids with dissimilar raw materials and tensile strengths were employed between bituminous layers as a reinforcement solution to strengthen the structural capacity of the pavement system. The mechanical characteristics of rehabilitated and reinforced composite systems were studied under different loading conditions, both static and cyclic, to resemble thermal and traffic load effects respectively. To capture new mechanical properties of the composite structure, which emerges by the presence of an interlayer product between different hot mixtures, novel laboratory

equipment or modifications on the setup or configuration of existing test methods were required. This research dealt with introducing new laboratory approaches to provide reliable mechanical inputs required in mechanistic-based design methods, which is introduced in the following section.

2.4 Methodologies

As explained earlier, any mechanistic-empirical design approach has two arms: mechanistic arm to predict structural responses in critical locations and empirical arm to predict the pavement performance in terms of rutting, fatigue failure, and reflective cracking based on the critical responses determined in the mechanistic arm.

To understand the mechanical changes in structural responses of composite reinforced or rehabilitated systems, tension-compression complex modulus test was conducted as suggested by the University of Lyon/ENTPE laboratory to study bituminous materials (Di Benedetto et al., 2007a; Nguyen et al., 2009). It is of great importance to note that since the test method is applicable on homogeneous specimens, the system composed of three different layers, as shown in Figure 2.2, was simplified in order to ease the analysis of data. A similar assumption was made previously to identify the rheological behavior of a bituminous interface (Freire et al., 2018). Given that, Equations (2.1) and (2.2) among the deflections in each layer of a cylindrical shape specimen was considered.

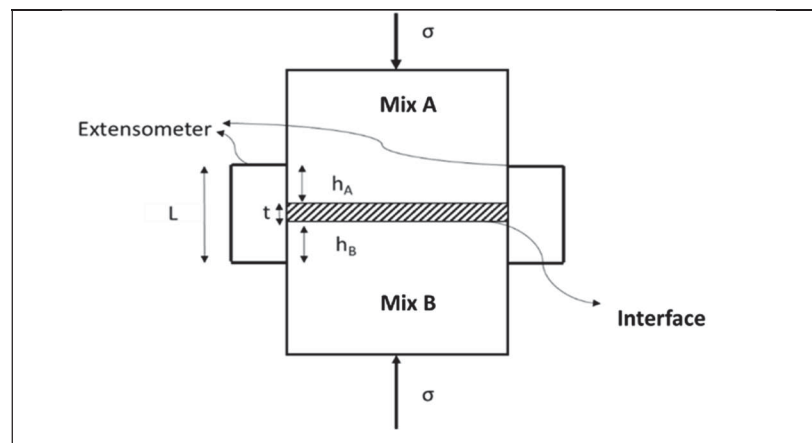


Figure 2.2 The position of the interface in a typical composite system employed in the complex modulus test

$$\Delta L = \Delta t + \Delta h_A + \Delta h_B \quad (2.1)$$

or

$$\frac{\sigma^*.L}{E^*} = \frac{\sigma^*_G.t}{E^*_G} + \frac{\sigma^*_A.h_A}{E^*_A} + \frac{\sigma^*_B.h_B}{E^*_B} \quad (2.2)$$

where ΔL is deflection in extensometer; Δt is deflection in the interface; Δh_A is deflection in mixture type A; Δh_B is deflection in mixture type B; E^* is complex modulus measured by extensometer; E^*_G is interface complex modulus; E^*_A is complex modulus of mixture type A; E^*_B is complex modulus of mixture type B.

Since the applied stress is the same in all parts, it can be removed from Equation (2.2). On the other hand, E^*_A , E^*_B and E^*_G can be obtained by solving simultaneously a set of equations in the general form of Equation (2.3), based on three sets of extensometers.

$$\frac{L_i}{E^*_i} = \frac{t}{E^*_G} + \frac{h_i}{E^*_A} + \frac{h_i}{E^*_B} \quad (i = 1, 2, 3) \quad (2.3)$$

For further simplification, it can be assumed that $h_A=h_B=h$. Therefore, Equation (2.4) can be derived:

$$L = t + 2h \quad \text{or} \quad h = \frac{(L-t)}{2} \quad (2.4)$$

To shed light on the interlayer effect on distress prediction models, three different test setups were adopted in connection with three key pavement distresses namely reflective cracking, fatigue failure and rutting.

A new configuration of 3-point bending test was developed to evaluate the fracture toughness in terms of the J-integral and to measure crack resistance index (CRI) at the interface level of a composite bituminous system, which could reflect the anti-reflective property of treated interfaces. In this regard, it was stated that at least three meshes of geogrid are required at the interface to interpret correctly the response of a reinforced system to cracking (Romeo et al. 2014). Given this and in order to obtain as many specimens as possible from each double-layer slab, cubic shape specimens with the size of 80×80×80 mm was considered acceptable to study

the crack retardation ability of the system. Also, given the fact that the bonding condition at the interface has substantial effect on crack retardation ability of interface, a new shear test device was developed to quantify the bonding condition into analysis. It is necessary to note that in the analysis of the results, great care should be taken because of the variability of normal load applied at the interface.

The structural integrity of the composite system that may be jeopardized by low bonding condition at the interface in the presence of an interlayer, was studied by the uniaxial tension-compression test according to the DGCB method (Département de Génie Civil et Bâtiment) developed at the ENTPE (École Nationale de Travaux Publics de l'État, (Lyon, France)). In case of low bonding between successive bituminous layers in a pavement structure, the maximum tensile strain will appear at the bottom of each layer independently, which endanger the performance of the system against fatigue failure.

To study the rutting resistance of systems under cyclic loading, the French Laboratory Rut Tester (FLRT) developed by France's Laboratoire Central des Ponts et Chaussées (LCPC) was utilized complying with Transport Quebec's standard. It was assumed that under cyclic loading, the bitumen applied as a tack coat layer at the interface could migrate to the top hot mixture and compromise the rutting resistance of the top layer.

Also, in order to characterize the water permeability of rehabilitated systems in design methods, a piece of equipment named crack widening device (CWD) was built, which is able to resemble the crack opening phenomena from an existing discontinuity at the bottom to the top surface under thermal effect. Thereafter, the permeability of cracked specimens in different crack widths was studied through a water-vacuum permeability device (WVPD) designed for this purpose, which is basically an accelerated version of the traditional falling head permeability test. The result from these devices could provide a more realistic view into selecting a proper drainage coefficient for granular layers and a reasonable retained modulus for bituminous layers located underneath.

It is worth mentioning that the M-E method has a unique feature that allows the designer to adjust the distress prediction models based on the mechanical behavior of new material and local data sets.

CHAPTER 3

A REVIEW ON MECHANICAL BEHAVIOR AND DESIGN CONSIDERATIONS FOR REINFORCED-REHABILITATED BITUMINOUS PAVEMENTS

Ehsan Solatiyan ^a, Nicolas Bueche ^b, Alan Carter ^c

^{a,c} Department of Construction Engineering, Université du Québec, École de Technologie Supérieure (ÉTS), 1100 Rue Notre-Dame O, Montréal, QC H3C1K3, Canada

^b Department of Architecture-Wood-Civil Engineering, Bern University of Applied Sciences (BFH), Pestalozzistrasse 20, CH-3401 Burgdorf, Switzerland

Paper published in *Construction and Building Materials*, October 2020

3.1 Abstract

Bituminous pavements cover a large part of Canada's roadway network. Traffic and environmental loadings cause distresses and damages in the pavement structure. A traditional approach for pavement rehabilitation is to implement an asphalt overlay on existing deteriorated bituminous pavement at specific times during its service life. However, this approach is somewhat expensive in the long run and not environmentally friendly. On the other hand, several studies indicate that the inclusion of a geosynthetic layer under an asphalt overlay leads to extended pavement service life. Nevertheless, there are still some discrepancies between fields and modeling results, which mainly stems from the fact that the mechanical behavior of reinforced asphalt overlay has not entirely been understood which results in underestimate or overestimate design solutions. This paper first aims to review different aspects of mechanical interaction between geosynthetic material and asphalt overlay and then shed light on the important considerations that need to be considered in the design procedure to obtain an efficient reinforced-rehabilitated bituminous pavement structure.

3.2 Introduction

Bituminous pavements deteriorate under loadings as it ages and makes the pavement surface uneven for drivers and passengers. In general, there are two fundamental approaches to soothe this issue: one is to frequently mill and apply a new asphalt overlay (mill and fill) at certain intervals of the pavement's service life. This approach is rather expensive due to a need for renewal in a short period of time, which in turn requires additional financial and material resources and does not correspond with the environmental concerns arising from releasing large amounts of emissions in the air along with high-energy consumption. Figure 3.1 indicates the mean service life of a 40-50 mm thick HMA overlay installed on a cracked pavement in the United States. As evident, for most states, the mean service life is in the range of 1 to 6 years, which is in fact considered very short (Kwon, et al., 2005).



Figure 3.1 Mean service life of a 40-50 mm HMA overlay installed on a cracked pavement in the United States (adapted from (Kwon, et al., 2005))

In place of mill and fill, alternatives have been recommended to extend the service life such as increasing overlay thickness (Sherman, 1982), using interlayer systems (Dhakal et al., 2016) and open-graded HMA mixtures (Hensley, 1980). Taking advantage of interlayer systems into asphalt overlay has proven its effectiveness in terms of enhancing the capability of HMA materials against fracture. They consist of steel reinforcement (Elseifi & Al-Qadi 2005), stress-relief interlayer systems such as Interlayer Stress Absorbing Composite (ISAC) and Stress Absorbing Membrane Interlayer system (SAMI) to absorb destructive deformations in the

cracking realm (Bozkurt & Buttlar, 2002), and fracture tolerant interlayer systems such as sand - mix (Baek, 2010). Another option, which in recent years has drawn many attentions from engineering community, is to reinforce the bituminous pavement system by embedding geosynthetics in the asphalt layers (Brown, 1985; Nithin et al., 2015; Brown, 2009), which brings additional advantages in terms of low deformations and cracking (Correia & Zornberg, 2016; Siriwardane et al., 2010; Graziani et al., 2014; Khodaii, 2009; Yu & Yang, 2013; Virgili, 2009; Mounes et al., 2015; Laurinavičius & Oginskas, 2006; Gonzalez-Torre et al., 2015; Fallah & Khodaii, 2015; Correia, 2014; Al-Qadi et al., 2008; Al-Qadi et al., 2009; De Bondt, 2000; Lytton, 1989). However, it should be taken into account that the positive effects of any interlayer system are limited only to mitigate the occurrence rather than to stop the formation and propagation of reflective cracking (Button & Lytton 2007).

Figure 3.2 demonstrates a review of treatments that are frequently employed to control reflective cracking in rehabilitation activities of deteriorated existing pavement in the United States.

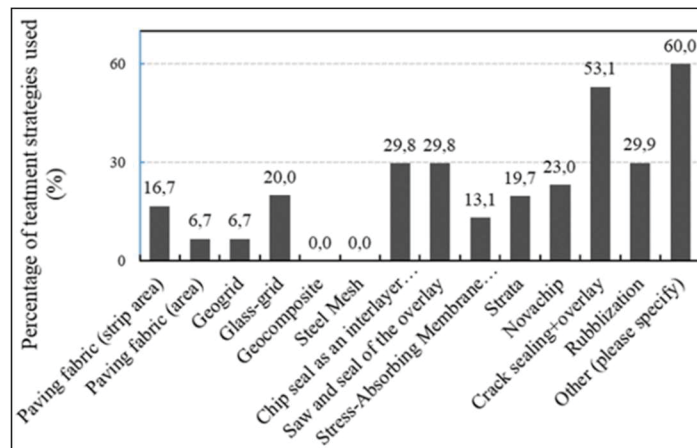


Figure 3.2 Treatment alternatives regularly employed to control reflective cracking in the United States (adapted from (Kwon et al., 2005))

Among all these alternatives, crack sealing along with an asphalt overlay are the most common methods to minimize reflective cracking while using geosynthetic materials is the least. One important consideration that prevents the widespread usage of geosynthetic-related materials is the lack of a proper design method to accurately reflect the mechanical effects of these materials (Perkins et al., 2004). This could be covered through predicting the mechanical

behavior of the reinforced pavement system under traffic and environmental loadings (Gupta & Mishra, 2016).

On this basis, this paper aims first to review the possible reinforcement benefits that using geosynthetics induces in the asphalt overlay. Then, the reinforcement mechanisms pertaining to geosynthetics are discussed in detail followed by identification of the influencing factors on mechanical properties at the interface between geosynthetic and adjacent asphalt layers. At the end, the mechanical models proposed for reinforced pavement structures are presented and the important features that should be incorporated into design methods are studied. The flowchart presented in Figure 3.3 demonstrates the framework of this paper.

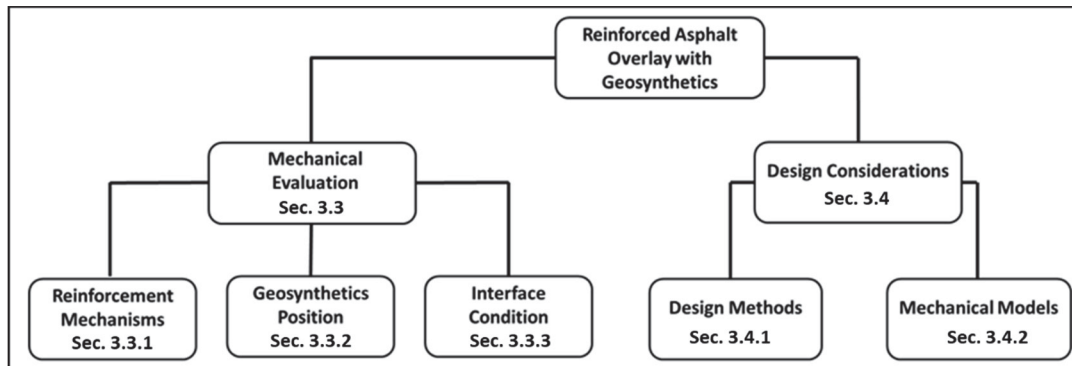
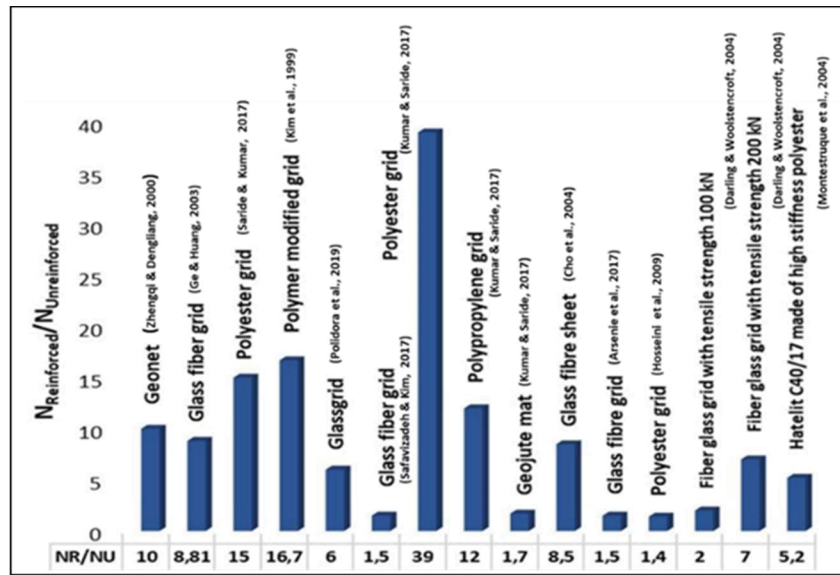


Figure 3.3 A framework of the steps taken to evaluate the presence of geosynthetics in the asphalt overlays

Reinforcement benefits of geosynthetics in bituminous pavements

Geosynthetics are categorized into different types according to their applications. For the pavement reinforcement purposes, geogrid, geotextiles and geocomposite (which is in fact a combination of geotextile and geogrid) are the ones usually employed due to their potential advantage in extending the pavement service life (Hosseini et al., 2009; Bueno et al., 2005; Benjamin et al., 2007). However, experimental results demonstrate that geogrids compared to geotextiles have nearly 2.5 times higher reinforcing capacity (Barksdale et al., 1989). Geosynthetics can be employed to extend pavement service life by mitigating fatigue cracking, reducing rut depth and delaying reflective cracking (Saraf, et al., 1996; Austin & Gilchrist, 1996; Pasquini et al., 2013). The Tables 3.1 to 3.3 (see Appendix I, Table –A I-1 to Table-A I-3) list previous findings on the application of geosynthetics in the asphalt overlays. In

addition, Figures 3.4 to 3.6 indicate the improvement level of asphalt overlay reinforced with various kinds of geosynthetics compared to unreinforced ones.



Fatigue 3.4 Improved mechanical performance of reinforced asphalt overlay in terms of fatigue life

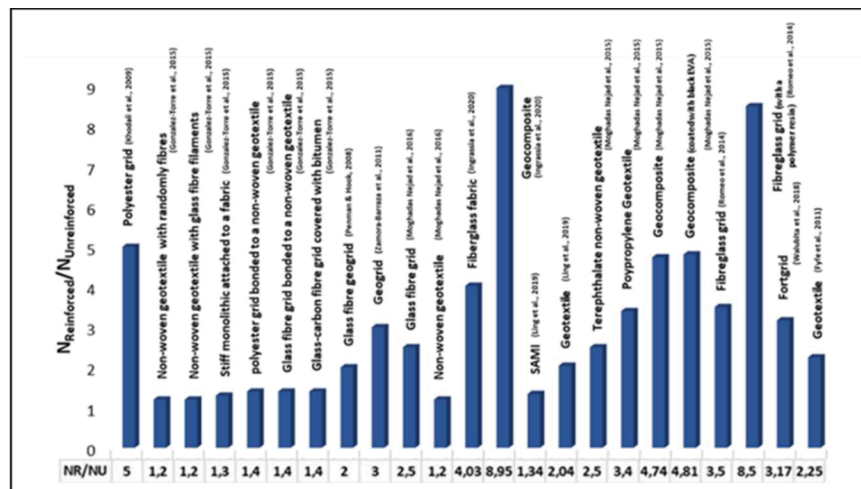


Figure 3.5 Improved resistance of reinforced asphalt overlay against reflective cracking

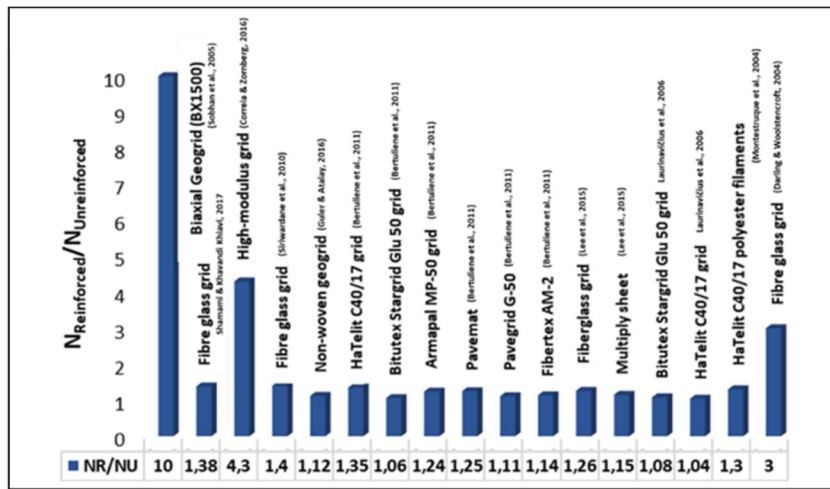


Figure 3.6 Enhanced performance of reinforced asphalt overlay against rutting

Based on Figures 3.4 to 3.6, the reinforcement effect of interlayers in the asphalt overlay is highlighted on fatigue life followed by reflective cracking and rutting. In addition, a significant difference in level of reinforcement is observed among different kinds of raw materials employed in grids, which mainly comes from a heterogeneity in test methods and mechanical behavior of composite reinforced structure.

The enhanced fatigue life associated with the reinforced asphalt overlay is owing to the fact that geosynthetic retains its stiffness even after losing the structural capacity of the asphalt overlay under the effect of repeated traffic loading (Austin & Gilchrist, 1996). When a crack initiates and propagates in the asphalt overlay, the geosynthetic will mobilize tensile stresses as a result of the opening of the crack surface and absorbs the energy of the crack by its elongation (Chang et al., 1998). Moreover, it is worth mentioning that the reduced rut depth is predominant for geogrids than geotextiles because of the presence of apertures in the geogrid structure, which provides interlocking with surrounding materials. Nevertheless, according to Figure 3.7, the changes in maximum rut depth on the pavement surface for a variety of geogrids with different stiffness (indicted with J), placed between asphalt layers, depends on the stiffness of the subgrade layer (Correia & Zornberg, 2018). On average, the rut depth is decreased by up to 40% for the subgrades with higher stiffness.

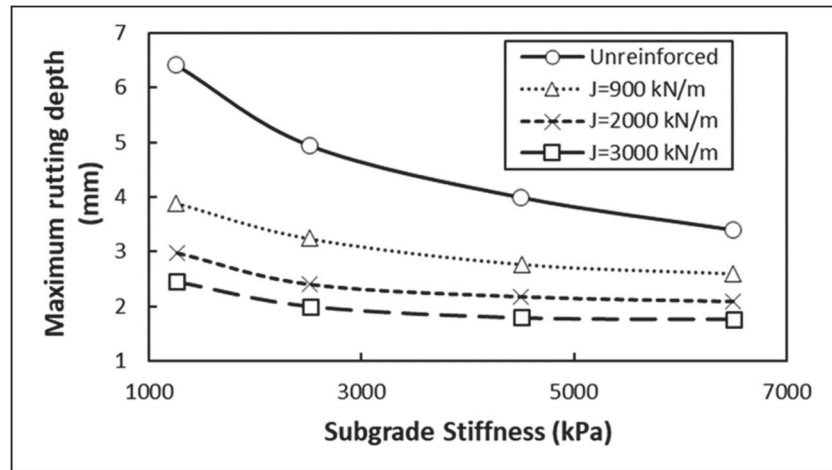


Figure 3.7 Maximum rut depth on pavement surface for different subgrade and geogrid stiffness (adapted from (Correia & Zornberg, 2018))

3.3 Mechanical behavior of geosynthetics in asphalt overlays

The necessity of studying the mechanical behavior of geosynthetics in asphalt overlays comes from the fact that still there are some discrepancies in terms of distress intensity between field observations and mechanical models developed to capture the behavior of geosynthetic in asphalt layers (Perkins & Ismeik, 1997). A root cause of this difference is that past numerical models did not include interface condition and its evolution over time in their models, while the response of the reinforced structure is largely affected by the interface properties (Gupta & Mishra, 2016). Accordingly, realistic consideration of the interface behavior between geosynthetic and adjacent asphalt layers, under different circumstances (e.g. temperature, loading rate, moisture content) is essential to enhance the accuracy of corresponding models. Furthermore, it is worth noting that the previous findings on asphalt overlay reinforcement are rather contradicting. On one hand, the reinforcement effect of the geosynthetic has been assumed negligible in terms of its effect on the stresses and strains within the pavement structure since bituminous pavements can tolerate only small levels of permanent deformation while significant deformation is required by the geosynthetic to mobilize its reinforcement effect. Therefore, the surface deformation and also transient stresses and strains within the pavement structure are slightly reduced by the inclusion of geosynthetic (Barksdale et al., 1989). On the other hand, it has been found that placing a reinforcement interlayer, under

proper conditions, yields to meaningful extended life (Zornberg, 2011; Brown, et al. 1983; Halimm et al., 1983). To clarify these conflicting results, more studies are required to define the mechanisms and level of improvement associated with geosynthetic-reinforced bituminous pavements.

3.3.1 Reinforcement mechanism of geosynthetic in asphalt layer

The first vital step to predict the performance of a bituminous pavement with a reinforced asphalt overlay is to know the mechanisms that enable and govern the reinforcement function. These mechanisms, which are at best unclear, as they have remained mostly unmeasured, differ between geogrids and geotextiles.

Geotextiles are mainly employed to absorb excessive stresses induced at the tip of a crack, and to waterproof the pavement system (Button & Lytton, 2007). A recent study was performed on permeability of the reinforced asphalt overlays with paving fabrics (a system composed of geotextile and asphalt cement as tack coat) by taking advantage of a newly developed water-vacuum permeability device (Solatiyan et al., 2020). The result revealed the high resistance of these interlayer systems against water infiltration in a broad range of crack widths. Nonetheless, the reinforcement effect is only expected for geotextiles with higher stiffness than that of asphalt overlay (de Souza Correia & de Souza Bueno, 2011; Vanelstraete & de Bondt, 1997). In fact, several researchers (Brown et al., 2001; Zamora-Barraza et al., 2010) showed that in case of using geotextiles between asphalt layers, shear resistance is considerably reduced at the interface leading to a poor contribution of these materials in structural capacity of the pavement system. However, the reduced bonding at the interface may bring an additional benefit into the pavement system in terms of dissipation of energy required for crack propagation due to deviated crack path from its initial one, which needs to be further studied. The reinforcement effect of geotextiles can be described and modeled by a membrane layer with appropriate friction coefficient at the top and the bottom (Bohagr, 2013). In this context, the effect of water trapped by the geotextile on stiffness modulus of adjacent asphalt materials and proper side slope to drain free water need to be specified.

For geogrids, the reinforcement mechanism is quite different and more analytical and experimental research is required to explain the improvement associated with geogrids (Zhang & Hurta, 2008). In general, the two following mechanisms have been reported by the researchers for the geogrids in asphalt overlays (Giroud & Noiray, 1981; Holtz et al., 1998; U.S. Army Corps of Engineers, 2003):

1. Tensioned membrane effect, which is activated only when the geogrid receives a concave shape due to permanent deformation or rutting on the surface. However, a considerable rutting depth, which normally exceeds the serviceability requirement of bituminous pavement, is required. This mechanism is depicted in Figure 3.8.

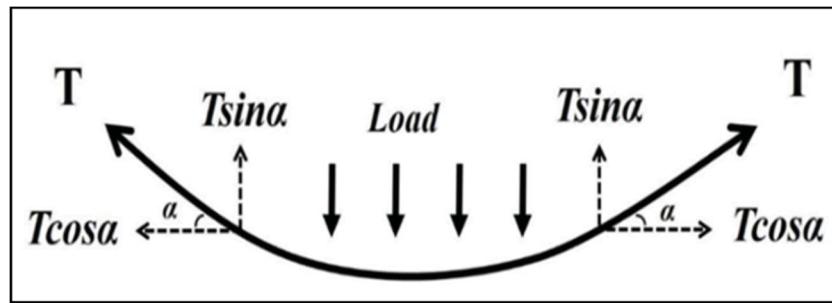


Figure 3.8 Tensioned membrane effect due to the concave shape developed in geogrid (adapted from (Medved et al., 2018))

The increase in capacity is calculated by the Equation (3.1).

$$\Delta p = \frac{2 \cdot T \cdot \sin \alpha}{B} \quad (3.1)$$

where the tension force T is calculated by Equation (3.2).

$$T = E_{CEL} \cdot \varepsilon_{CEL} \cdot h_{CEL} \quad (3.2)$$

where Δp is the increase in structural capacity in N/mm^2 , B is the load width in mm, E_{CEL} is the modulus of elasticity of the geosynthetic under tensile condition in N/mm^2 ; ε_{CEL} is the tensile strain of the geosynthetic, h_{CEL} is the geosynthetic thickness in mm and α is the angle of the tensional force T with the horizon (Ling et al., 2009).

2. Lateral confinement effect, which results from interfacial friction and interlocking between the geogrid and the aggregate present in the asphalt layer. Under this mechanism, the shear stresses imposed by external loads are efficiently transformed from the asphalt layer to the tension in the geogrid layer. Figure 3.9 illustrates a cross-sectional view of this mechanism.

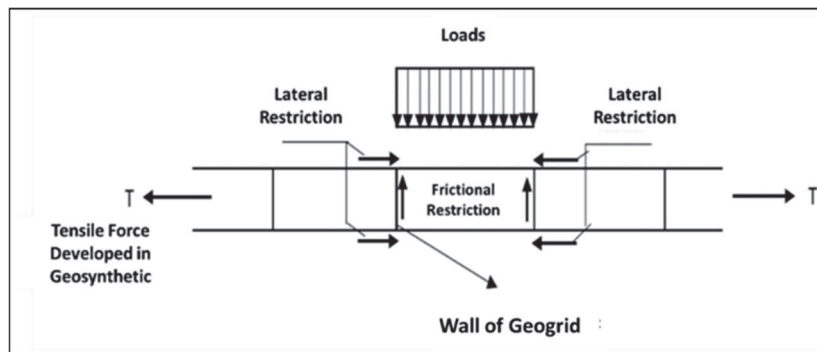


Figure 3.9 Lateral confinement effect in geogrids (adapted from (Ling et al., 2009))

As it can be observed, the confinement effect is the sum of the shear force components in each opening, obtained by multiplying the number of openings under load by the shear force component, according to Equation (3.3) (Avesani Neto et al., 2013).

$$\Delta F_{\tau} = 4 \cdot \frac{h}{d} \cdot k_0 \cdot p \cdot B \cdot L \cdot \tan \delta \quad (3.3)$$

where: ΔF_{τ} is the accumulation of shear stresses developed under load (reinforcement effect) in N, $\frac{h}{d}$ is the aspect ratio of the apertures in geogrid, k_0 is the lateral earth pressure at the rest condition ($k_0 = 1 - \sin \phi'$) in N/mm^2 , L and B are the load length and width in mm, δ is the friction angle at the interface between the asphalt layer and the geogrid surfaces, and p is the load transmitted to the geogrid layer.

A third improvement mechanism, to which not enough attention is paid, is the enhanced structural capacity in terms of stress and strain distributions. Empirical studies have been realized to study the distribution of stress and strain in reinforced structures, but because of the

complexity of the parameters involved, there is still a need for better understanding of their distribution in reinforced structure, and it needs to be verified with field results. It is assumed that the dimension of the load, the stress applied on the upper level of the geogrid, the type of geogrid, the thickness of the geogrid and the internal friction at the interface between geogrid and asphalt layer are some of the effective factors on the stress and strain distribution (Medved, et al., 2018; Mirzapour et al., 2011). A comparative analysis performed on structural responses of reinforced and unreinforced sections implemented on accelerated pavement testing facilities of the IFSTTAR showed that in the early ages of traffic applications, no meaningful differences were expected (Nguyen et al., 2013). However, more research on aged sections and the way of distribution of structural responses, right below and above the geogrid layer are required. Another useful tool to study the responses of a reinforced system under loading is through numerical modeling. Figure 3.10 indicates the effect of geogrid on horizontal tensile strain at the bottom of the asphalt layer for a variety of geogrid and subgrade stiffness values (K_s) (Correia, et al., 2018).

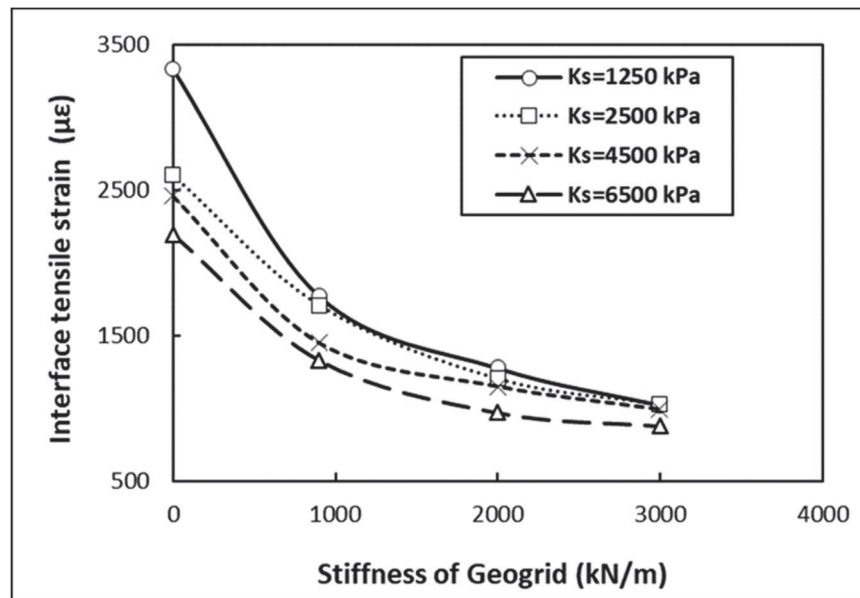


Figure 3.10 Horizontal tensile strain distribution at the interface of unreinforced and reinforced sections for various subgrade stiffness (K_s) values at the center of the wheel load (adapted from (Correia, et al., 2018), zero stiffness on x-axis corresponds to unreinforced asphalt overlay)

It is eminent that horizontal tensile strain at the interface between two asphalt layers decreases due to the presence of geogrid layer and this effect is more obvious in geogrids with higher stiffness. In addition, the tensile strain, in terms of magnitude and distribution pattern, follows a rather similar trend in different subgrade stiffness. It is also interesting to point out that for a pavement structure over a weak subgrade, geogrid stiffness plays an important role to reduce the horizontal tensile strain at the interface, which supports this fact that higher deflection in pavement structure can mobilize the full reinforcement effect of geogrids against tensile forces. In general, lateral confinement and enhanced structural capacity are regarded as the primary and reliable sources of reinforcement provided by geogrids because the tensioned membrane effect necessitates a large amount of deflection before being activated while this would be almost impossible because of serviceability requirements (Austin & Gilchrist, 1996). Lateral confinement and enhanced structural capacity are mostly supplied by the friction and the interlock between the geosynthetic and the adjacent asphalt layer. Table 3.1 shows a brief review of test methods developed to measure the interlocking capacity at the interface.

As can be seen from Table 3.1, the majority of the devices were developed for the case of geogrid embedded in granular materials while for reinforced asphalt layers, very rare effort has been made which it stems from following difficulties:

- The proper incorporation of strain gauges between asphalt layers, which not only resist against compaction pressure but also undergoes high temperature during the construction process;
- The insertion of wires of strain gauges and its attachment to the ribs of geogrid, which may influence the real mechanical behavior of the system;
- The adequate rate of displacement applied on the ribs to resemble field situation;
- Suitable shape of gripping system to provide uniform tension on the ribs while avoiding its rupture;
- The ability of making difference between the displacements of asphalt layer and geogrid because of adhesion provided by tack coat at the interface.

Table 3.1 A review of test methods to measure the interlock capacity provided at the interface between geosynthetic and adjacent materials

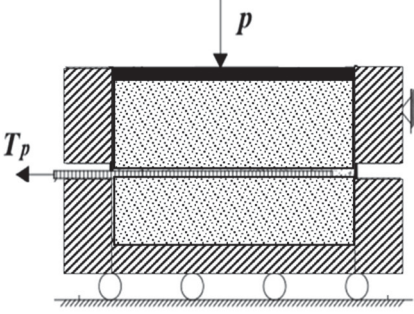
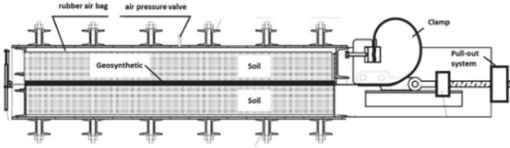
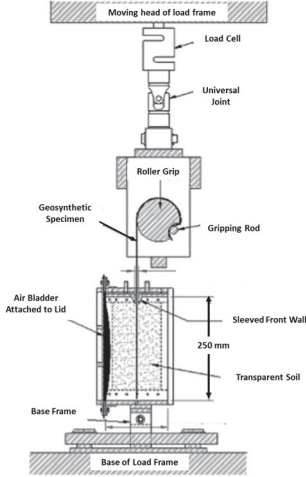
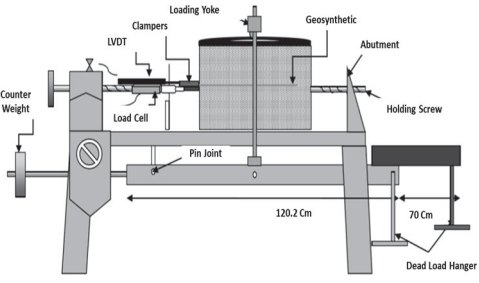
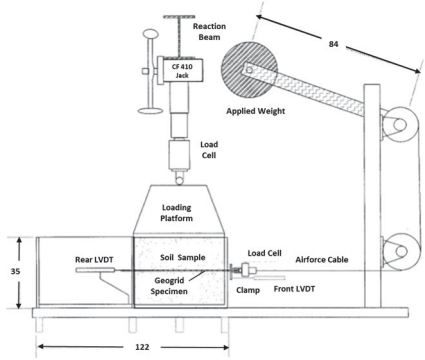
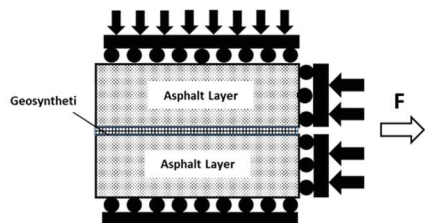
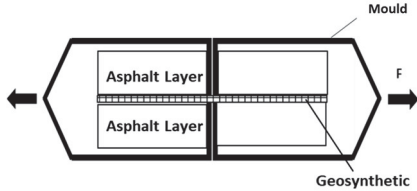
| Type of Interface | Test Method | | Test Specification |
|---------------------------------|---|--|---|
| | <p>TZY-1 typed tester (Shi & Wang, 2013)</p> |  | <ul style="list-style-type: none"> - Displacement-controlled mode (from 0.07 to 8.67 mm/min) - Vertical pressure via closed-loop feedback and pressure stability system |
| | <p>Pull-Out Device (Bolt & Duszynska, 2000)</p> |  | <ul style="list-style-type: none"> - Displacement controlled mode (2 and 3 mm/min) - Vertical pressure by rubber air bag |
| <p>Geosynthetic-Soil</p> | <p>Transparent Pull-Out Device (Ferreira & Zornberg, (2015)</p> |  | <ul style="list-style-type: none"> - Displacement-controlled mode of 25mm/min - Vertical pressure by air bag |

Table 3.1 (Continued)

| Type of Interface | | Test Method | Test Specification |
|--------------------------|--|--|--|
| Geosynthetic-Soil | Modified Pull-Out Device (Prashanth, et al., 2016) |  | <p>- Displacement-controlled mode of 4.57mm/min</p> <p>- Vertical pressure by lever arm system</p> |
| Geosynthetic-Soil | Load-Controlled Pull-Out Device (Fuller, 1997) |  | <p>Displacement-controlled mode of 0.1 mm/min</p> <p>Vertical pressure by a loading jack</p> |
| Geosynthetic-Asphalt Mix | Single-End Device (De Bondt,2000) |  | <p>Displacement-controlled mode of 0.0019mm/s</p> <p>Vertical pressure by loading jack</p> |
| Geosynthetic-Asphalt Mix | Pull-out Device (De Bondt,2000) |  | <p>Proposed Method (no detail on displacement rate)</p> |

On this basis, a novel approach by taking following considerations into account need to develop:

- Simplicity of the implementation of sensors embedded in asphalt layers;

- Repeatability of the results based on the COV value (Coefficient of Variation) less than 25%;
- Sensitivity to displacement rate, type of geogrid, temperature and vertical pressure
- Connectivity to the field conditions;
- Possibility of having changes in temperature and displacement rate;
- Rationality of the cost of test equipment.

3.3.2 Geosynthetic position in asphalt overlay

To perform effectively, the geosynthetic should be placed in the pavement structure in accordance with the type of distress, which it intends to mitigate. As for fatigue cracking, Figure 3.11 shows load ratio (cyclic load divided by 1.11 kN) versus number of cycles to failure for different position of geogrid in asphalt overlay. It can be recognized that reinforced asphalt overlay performs better than the unreinforced one and that the placement of geogrid at the mid-height of the layer results in highest resistance against failure.

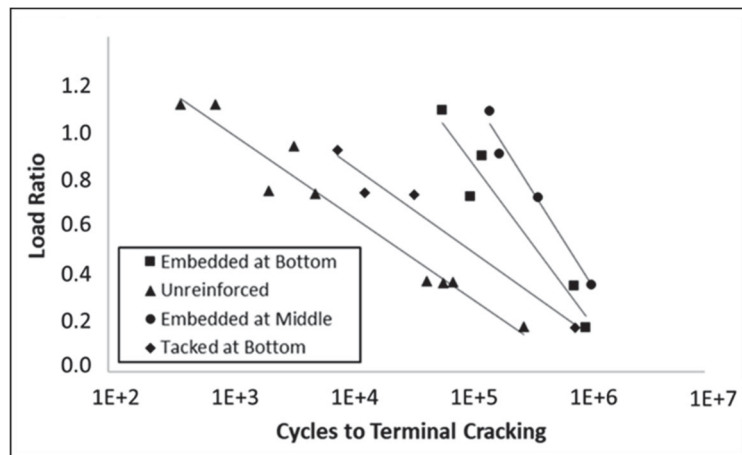


Figure 3.11 The effect of geogrid position in asphalt overlay on fatigue resistance (adapted from (Sobhan et al., 2004))

With regard to the rutting, as depicted in Figure 3.12, the one-third of the overlay thickness has been suggested as the best location of reinforcement, followed by the middle one. Placement of geogrid at the bottom side has almost no effect on rutting, especially at higher numbers of cycles.

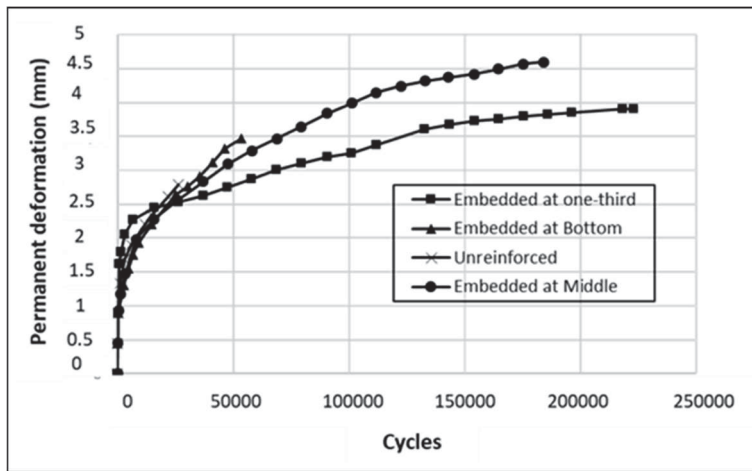


Figure 3.12 The effect of geogrid position on rutting (adapted from (Flutcher & Wu, 2013))

As for the reflective cracking, referring to Figure 3.13, the reinforced overlay with geogrid embedded at a one-third height of the layer has the lowest amount of bottom-up crack extension at any cycle (Khodaii et al., 2009).

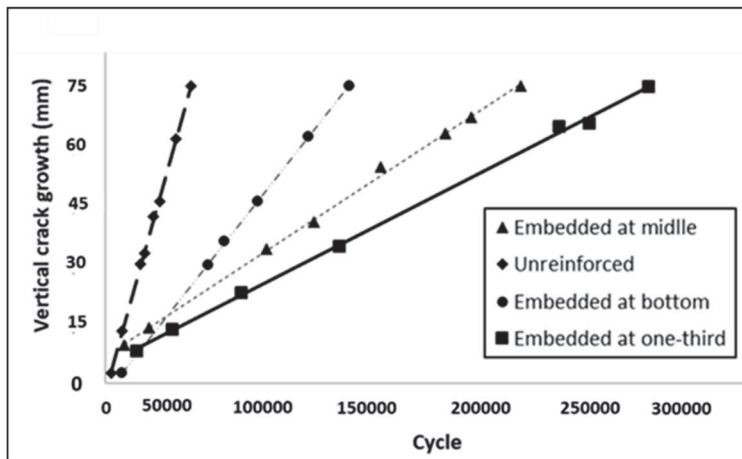


Figure 3.13 The effect of geogrid position on reflective cracking (adapted from (Khodaii et al., 2009))

Figure 3.14 presents the required thickness of asphalt overlay for a given design life in millions of standard axles (MSA) for two locations of grids in asphalt layers in the UK and US. Three cases were assumed: unreinforced, one-layer reinforced structure and two-layer reinforced structure. It is evident that by employing geogrids in two layers, the thickness of the asphalt

overlay, which is obtained from estimated traffic during the service life in millions of standard axles, significantly decreases. It is worth pointing out that the mechanical characteristics of geogrids such as stiffness modulus, tensile strength and creep behavior under loading dictate the design life of the reinforced asphalt overlay and the growth rate of the crack (Correia & Bueno, 2011; Vanelstraete & de Bondt, 1997; Brown et al., 2001; Zamora-Barraza et al., 2010).

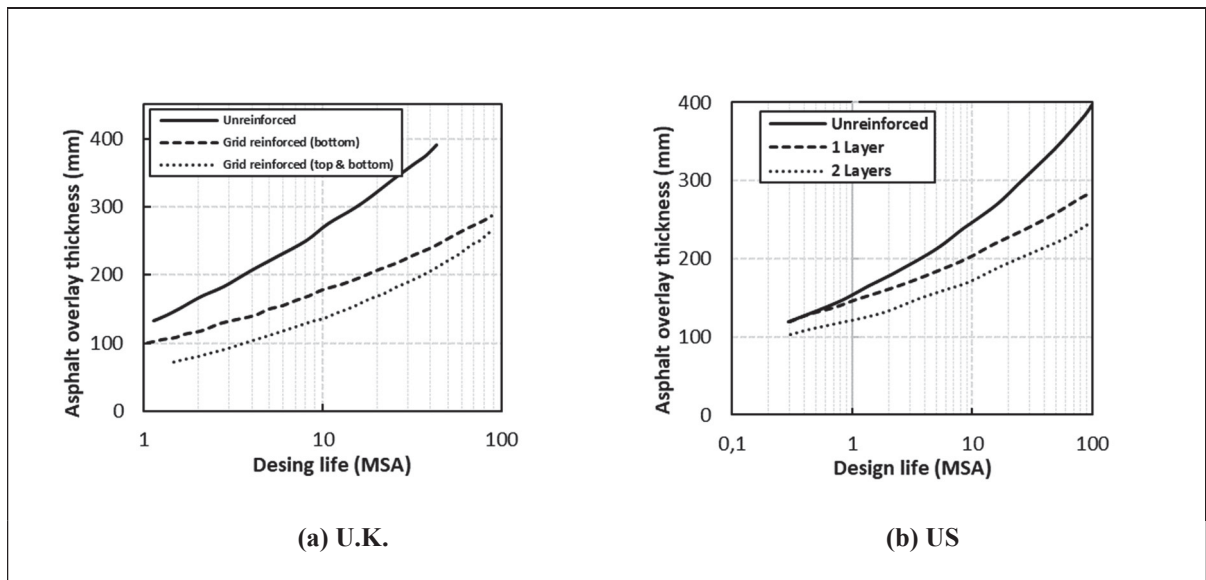


Figure 3.14 Design chart to estimate the asphalt overlay thickness based on the design life in millions of standard axles (MSA) for two different locations of grid in the asphalt overlay: (a) UK; (b) US (adapted from (Yu, et al., 2013))

3.3.3 Interface condition between geosynthetic and asphalt overlay

The mechanical behavior of reinforced structures is to a great extent dependent on the adhesion provided at the interface. On one hand, the inclusion of a geosynthetic layer under an asphalt overlay can enhance the mechanical properties of the pavement structure (Hartadi Sutanto, 2009). On the other hand, it can adversely influence the shear bonding between layers, which is significant for geotextiles, geogrids with higher thickness and torsional stiffness and geogrids with improper size of apertures compared to nominal maximum aggregate size (NMAS) of aggregates employed in asphalt mixture (Canestrari et al., 2018). The weak bonding between asphalt layers may lead to the occurrence of premature failures in the form of shoving, parabolic and crescent-shaped cracks on the surface which in turn result in decreased structural integrity and shortened service life of the pavement structure, poor driving quality,

and increased maintenance costs (Canestrari et al., 2015; Mohammad et al., 2009; Vaitkus et al., 2011). In addition, a decline in interlayer bonding yields to a considerable reduction in fatigue life. This effect is meaningful for thicker asphalt layers as shown in Figure 3.15 (Jaskula & Rys, 2017).

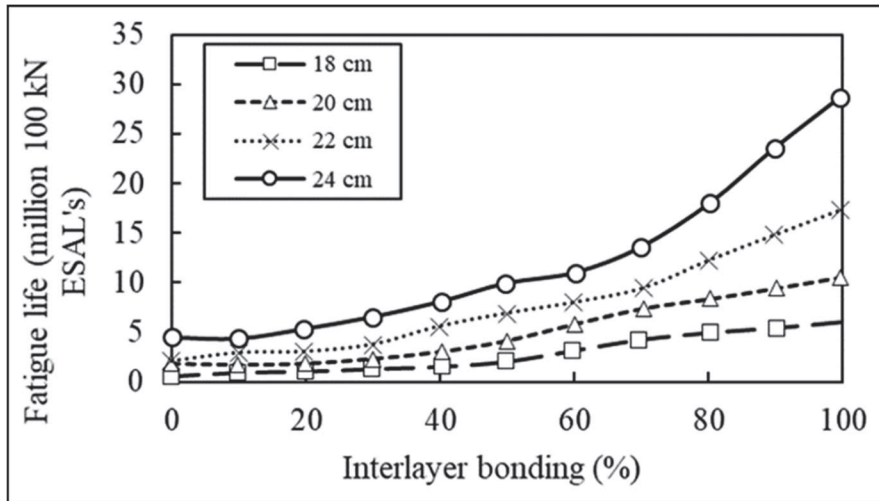


Figure 3.15 Effect of reduced interlayer bonding and total thickness of asphalt layers on fatigue life of pavement structure (adapted from (Jaskula & Rys, 2017))

For instance, in case of an asphalt layer with a total thickness equals to 24 cm, a little decrease in bonding condition from 100% to 70% leads to a remarkable decrease in fatigue life of as much as 50%. Therefore, a balance between the reinforcement effect of geosynthetic and the adequacy of shear strength at the interface is a necessity that must be respected during the design and installation process. The following sections provide a review of theories developed to describe mechanisms of adhesion and influencing factors on bonding failure between two asphaltic layers in a bituminous pavement structure.

3.3.3.1 Adhesion evaluation at the interface

Adhesion between consecutive layers in bituminous pavement structure provides the continuity of the system, which plays a critical role in the pavement performance under external loads (Negeswaran, 2016). Adhesion can be explained as the force developed between molecules on each side of two dissimilar materials in contact with each other (i.e. adhesive and

substrates) that holds the bodies together (Copeland, 2007). An adhesive material is a substance which, when putting on the surface, provides resistance against detachment. On the other hand, substrates are the layers that require an attachment, as demonstrated in Figure 3.16.

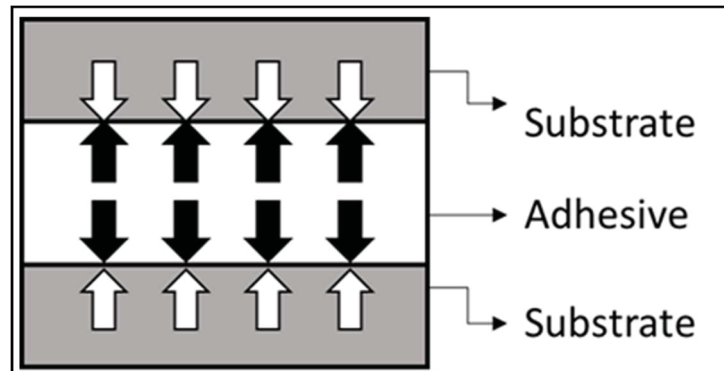


Figure 3.16 Attractive force between dissimilar surfaces

Generally, the adhesion provided at the interface can be explained through four different theories as summarized in Table 2.2. The main source of adhesion is through mechanical interlock, which may be failed in two possible ways as shown in Figure 3.17. The intrusion of water at the interface and pertaining pore pressure, improper thickness of adhesive material and the presence of impurities such as dust or air bubbles, are key factors to cause a weak boundary layer at the interface (White, 2017).

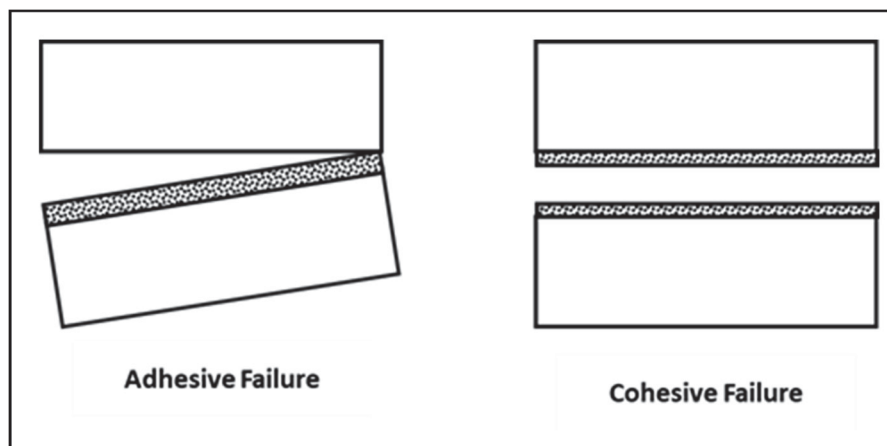


Figure 3.17 Schematic of failure modes at the interface

Table 3.2 Various adhesion theories developed for two involved surfaces

| Theories | Source of Adhesion | Mechanism |
|---|--|-----------|
| Adsorption Theory (Negeswaran, 2016) | Wetting effect between involved faces | |
| Mechanical Theory (Geminger & Jarka, 2016) | Mechanical force between two irregular surfaces | |
| Electrostatic Theory (Ebnesajjad, 2011) | Free electrical charge at the surface of involved surfaces | |
| Diffusion Theory (Packham, D.E. 2005) | Interdiffusion of contacted surfaces over the time | |

In practice, the interface is exposed to four different modes of loadings from traffic and temperature changes, according to Figure 3.18. Modes 1 and 3 are usually resulted from traffic or environmental loadings at the interface of two asphalt layers without any discontinuity. However, mode 2 of loading frequently occurs at the interfaces comprising a jointed concrete pavement underlying an asphalt overlay. Lastly, the shear-tension mode of loading is rarely a matter of interest in a real field condition (Sutanto, 2009; Al-Qadi et al., 2009).

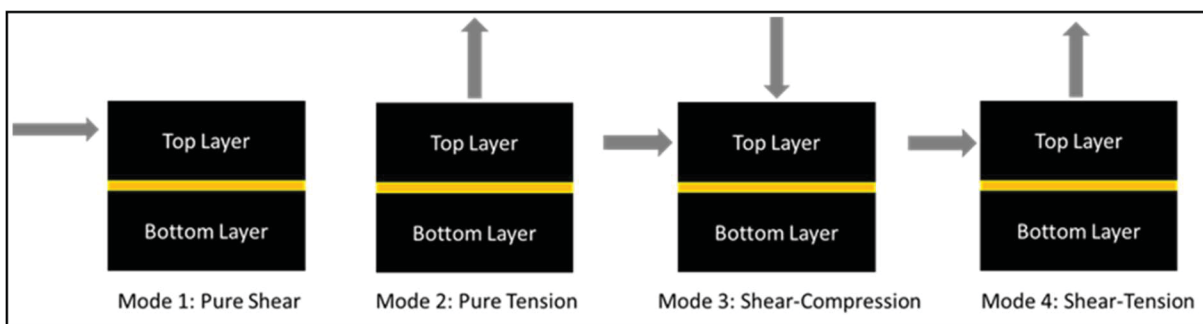


Figure 3.18 Different modes of loading imposed to the interface in real condition (adapted from (Rahman et al., 2017))

Plenty of test methods and equipment, which work under the effect of static or dynamic loading condition, have been proposed by many countries and institutions in order to measure the bonding condition at the interface of an interlayer and adjacent asphalt layer. Marshall stability loading press (Molenaar, 1993), Ancon Shear Testing Research and Analysis (ASTRA) (Canestrari, 2005), Swiss LPDS Tester (Roffe & Chaignon, 2002), Sapienza Inclined Shear Test Machine (SISTM) (D'Andrea & Tozzo, 2012), FDOT Bond Strength Device (Sholar, 2004), ATACKER™ Device (Mohammad, 2009), Tschegg Device (Tschegg, 1995), Krakow Technological University test device (Grzybowska, et al., 1993), Amirkabir University of Technology Shear Lab Tester (AUT-SLT) (Noory, et al., 2018) Louisiana Interlayer Shear Strength Tester (LISST) (Collop, 2003), have been developed by the researchers, which some of them are illustrated in Figure 3.19.

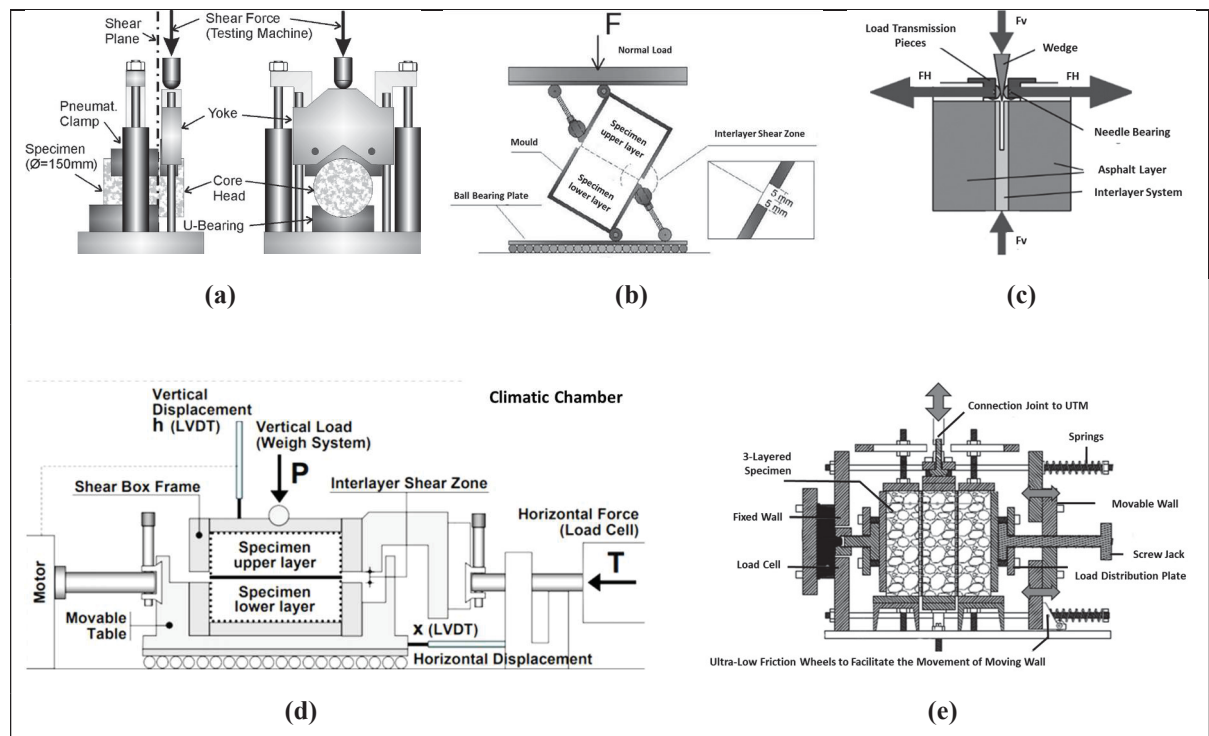


Figure 3.19 Shear device employed to measure bond strength at the interface of the asphalt layer and the geosynthetic a) Swiss LPDS Tester (Roffe & Chaignon, 2002), b) Sapeinza Inclined Shear Test Machine (SISTM) (D'Andrea & Tozzo, 2012), c) Tschegg Device (Tschegg, 1995), d) Ancona Shear Testing Research and Analysis (ASTRA) (Canestrari, 2005), e) Amirkabir University of Technology Shear Lab Tester (AUT-SLT) (Noory, et al., 2018)

3.3.3.2 Influencing factors on bond strength at the interface

The quality of the reinforced structure depends not only on the quality of the materials employed in the composite structure but also on the quality of bonding provided at the interface. In a layered system, when the layers are fully bonded, the most considerable tensile stress occurs at the bottom of the bounded layer, as demonstrated in Figure 3.20. However, if the bonding is weak, the largest tensile stress occurs at the bottom of each layer independently. At that point, the tensile stress at the bottom of the upper layer causes compressive stress at the top of the lower layer, which results in a relative displacement at the interface, causing the shear stresses, which may exceed the interlayer shear strength leading to the slippage between two successive layers (Collop et al., 2003).

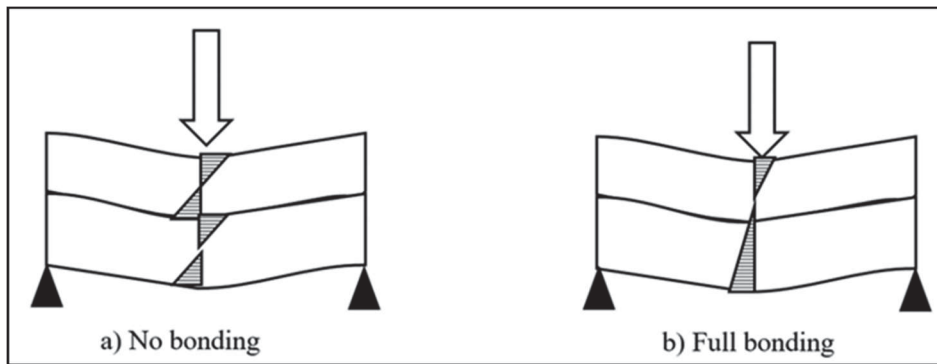


Figure 3.20 Stress distribution under different bonding condition (a) No bonding, (b) Full bonding

Likewise, when a geosynthetic layer is located over an existing pavement, the same problem called debonding effect may occur due to inadequate adhesion and compromise the positive reinforcement effect. This will lead to a reduction in the pavement service life due to the appearance of premature cracking on the surface. According to a statistical analysis on the results obtained from shear collar device, adhesion strength lower than 345 kPa is considered as inadequate and higher than 690 kPa as adequate. However, the maximum limit of shear strength before de-bonding at the interface is still unknown (West et al., 2005). The results obtained from a large-scale shear test on cylindrical asphalt specimens reinforced with different types of geosynthetics made of: glass fiber grid (G), polyvinyl alcohol grid (PVA)

and polyester grid (PET) and unreinforced specimens (UN) are depicted in Figure 3.21 (Roodi et al., 2017).

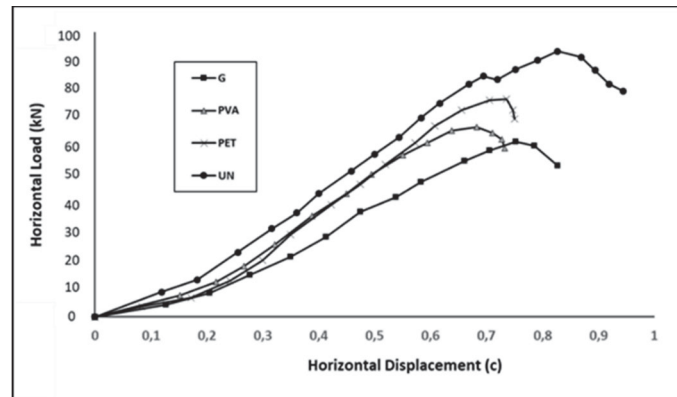


Figure 3.21 Mechanical behavior of interface under shear stress in reinforced and unreinforced specimens (adapted from (Roodi et al., 2017))

As shown in Figure 3.21, the maximum bond strength is attributed to unreinforced specimens, while on average, for reinforced specimens, the bond strength is decreased between 15 to 35%. This result verifies that the presence of a reinforcement layer between asphalt layers may adversely affect the bond strength at the interface.

The evolution of shear stiffness during service life is another aspect that needs to be specified. If K_s is defined as shear stiffness modulus, its value can be estimated by Equation (3.4) (Diakhaté, M. 2007).

$$K_s = \frac{L \times \Delta F_k}{A \times \Delta d_k} \quad (3.4)$$

where L is the thickness of geosynthetic, ΔF_k is the amplitude of shear force at cycle N , Δd_k is the amplitude of shear deformation at cycle N (in mm), and A is the total area from both sides of geosynthetic exposed to shear stress.

The evolution of shear stiffness at the interface occurs in three stages (Figure 3.22). At first stage, the shear stiffness is characterized solely by the adhesion of tack coat to the interlayer. After that, the shear stiffness decreases linearly as the number of cycles increases due to the

interaction between tack coat and geosynthetic. At a higher number of cycles, the shear stiffness decreases sharply owing to a loss of connection between layers.

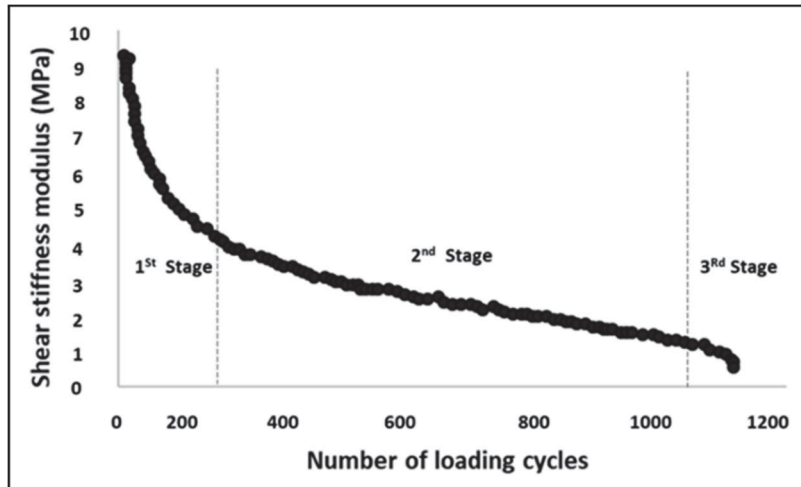


Figure 3.22 Evolution of shear stiffness at the interface with the increase in number of cycles (adapted from (Noory et al., 2018))

Based on the review of pertinent literature, the influencing parameters on adhesion evolution between geosynthetics and asphalt overlay are summarized in Figure 3.23.

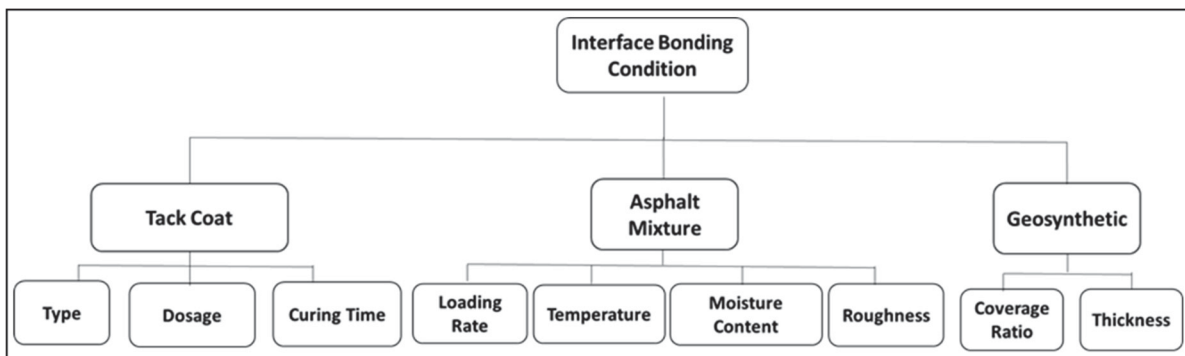


Figure 3.23 Effective factors on bond strength at the interface

From the tack coat perspective, one of the significant factors affecting the bond strength at the interface is the type of tack coat. Emulsified asphalt (such as Rapid setting (RS), medium setting (MS), slow setting (SS), and quick setting (QS), polymer modified emulsions and crumb rubber modified emulsions) is normally employed as an adhesive agent between asphalt layers in bituminous pavements (Roffe & Chaignon, 2002). However, in case of geosynthetic application, hot asphalt binder is usually suggested as a tack coat material since in comparison

with emulsified binder, less amount of binder is required, and due to higher viscosity, better stability in sloped surfaces is expected (Button & Lytton, 2007; Kanitpong & Bahia, 2003). Figure 3.24 shows the adhesion strength results obtained from Bitumen Bond Strength Test (BBS), which is a type of pull-off tensile strength test, conducted on eight different types of asphalt binder with different stiffness (Moraes et al., 2011). It is clear that as the stiffness of bitumen (ΔG^*) increases, the bond strength goes proportionally up.

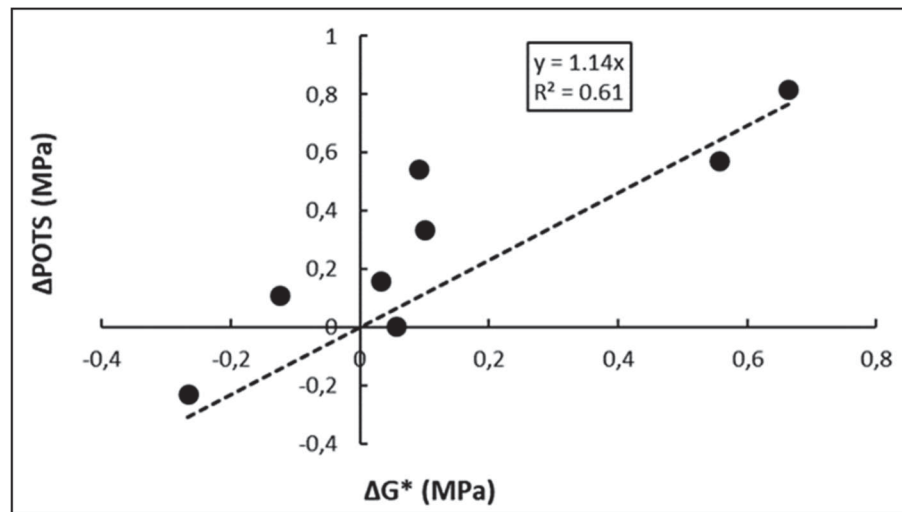


Figure 3.24 Correlation between change in pull-off tensile strength ($\Delta POTS$) and change in bitumen stiffness (ΔG^*) at dry conditioning (adapted from (Moraes et al., 2011))

However, it is of paramount importance to note that, to obtain better results of adhesion quality, the type of tack coat should be the same as that employed in the asphalt mixture (Moraes et al., 2011).

Proper application rate of tack coat is another effective factor on adhesion strength at the interface. Inadequate rate of tack coat is the root cause of poor performance of interlayer systems (Asphalt Interlayer Association (AIA), 1999) since distresses such as slippage cracking or debonding at the interface result from unsaturated geosynthetic. Studies show that by the increasing in the dosage of tack coat, the shear strength enhances (Hu et al., 2017). Nevertheless, excessive tack coat may also cause slippage between layers or appear as bleeding in the wheel path on the pavement surface (Asphalt Interlayer Association (AIA), 1999). Figure 3.25 illustrates the result of a Double Shear Test (DST) performed at the interface between the

geosynthetic and the asphalt layer to investigate the effect of the dosage of tack coat on shear strength (Loui & Satyakumar, 2013).

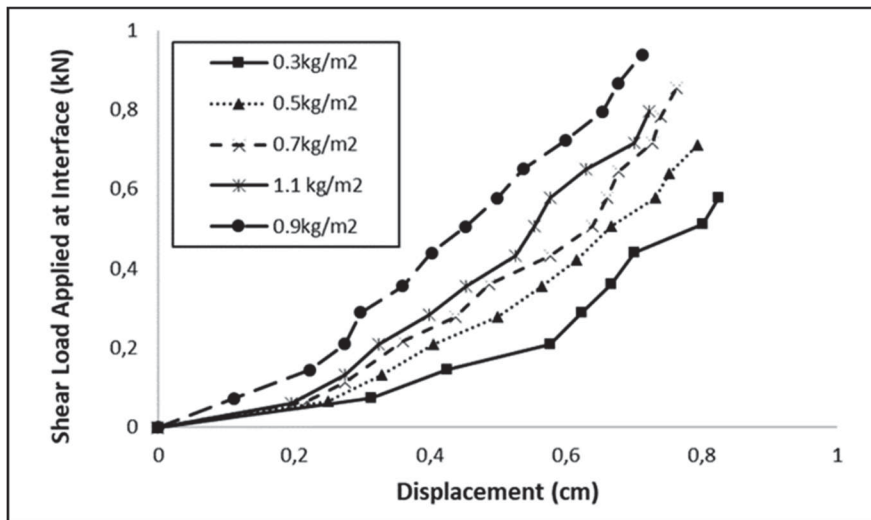


Figure 3.25 The influence of tack coat dosage in bonding condition between geosynthetic and asphalt layer (adapted from (Loui & Satyakumar, 2013))

The results indicate that by increasing the dosage up to 0.9 kg/m^2 the adhesion bond improves but after that, because of the excessive tack coat material, the adhesive force diminishes. It is worth mentioning that the right amount of tack coat in grid products relies upon empirical results. However, the capacity of asphalt retention governs the proper amount of tack coat for fabric application between asphalt layers (ASTM D6140).

The role of curing time on adhesion quality has not yet been clear. Some laboratory studies (Sholar et al., 2004; Hachiya & Sato, 1997) showed a strong connection between curing time and the shear strength developed at the interface, but others (Chen & Huang, 2010; Tashman, et al., 2006) reported a negligible effect. The need for further research on this subject is quite tangible.

On the asphalt mixture scale, the first important consideration is the loading rate. Asphalt mixtures at low loading rates behave more like a viscous material and at high rates exhibit elasticity property (Thi Bui, 2018). The adhesive force is described by both cohesive force and internal friction angle developed between layers (Biglari et al., 2019). Figure 3.26 presents the variation in friction angle and cohesive force at the interface with different rate of loadings

(Xia et al., 2019). It can be understood that by increasing the loading rate, the cohesive force increases at a decreasing rate. However, internal friction angle follows a different trajectory, which is not as definite as the adhesion force. At first, in the low loading rate zone, the friction angle is decreased and then tends to increase at a high level of loading rates.

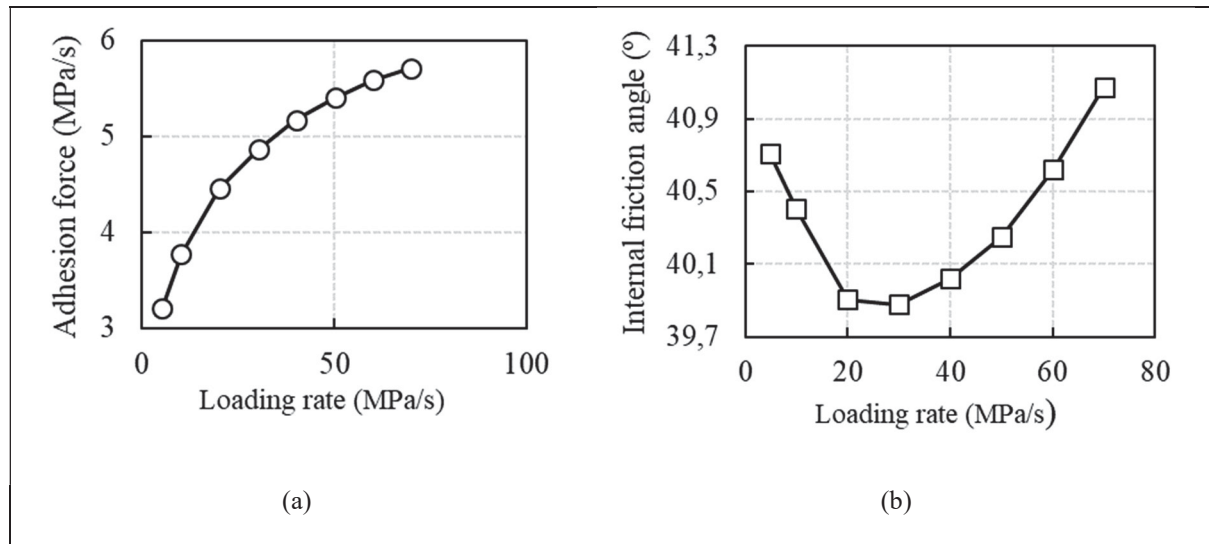


Figure 3.26 The variation of (a) adhesion force and (b) internal friction angle with loading rate (adapted from (Xia et al., 2019))

Moreover, laboratory studies indicate that temperature plays a critical role on the shear bonding strength. As the temperature increases, the shear strength at the interface decreases due to a loss in the stiffness of the tack coat material (Thi Bui, 2018). Figure 3.27 displays the result of a shear test conducted on two types of tack coat: spray-cationic emulsified asphalt (PC) and rapid setting emulsified asphalt with high viscosity (HV), in three different dosages (0.25 kg/m², 0.5 kg/m² and 0.75 kg/m² of residual binder) applied at the interface in a wide range of temperatures (Xia et al., 2019). The shear strength at the interface is less affected at high temperatures, regardless of type and dosage of tack coat. Another valuable point to mention is that, at low temperatures, an alternative way to enhance the interface shear strength is to increase the dosage of the tack coat.

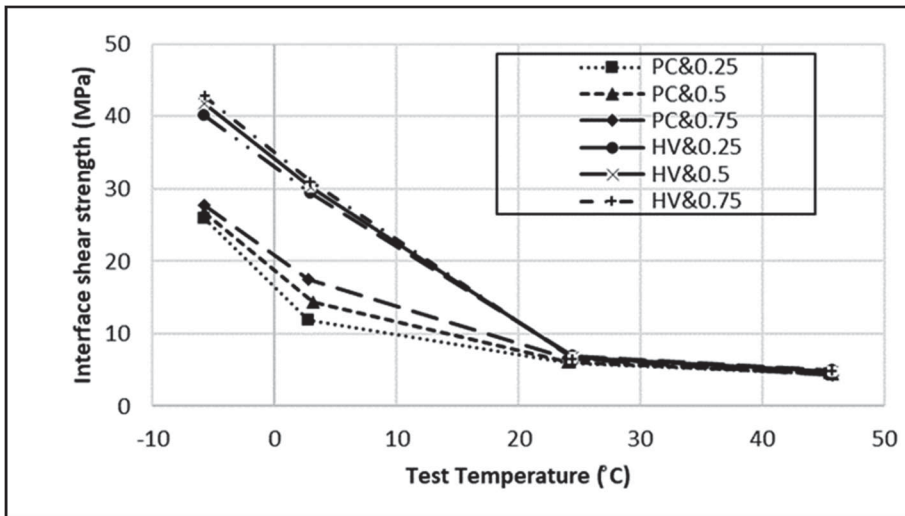


Figure 3.27 The shear strength at the interface in a wide range of temperatures (adapted from (Xia et al., 2019))

Furthermore, the normal load functioning at the interface has a meaningful effect on the variation of shear strength with temperature. Laboratory studies (Canestrari et al., 2005; West, et al., 2005) support this fact that when the normal force applied on the pavement surface increases, the shear strength developed at the interface will enhance at any temperature, as indicated in Figure 3.28 (Kim et al., 2015). Reason for this is that the effect of mean depth of texture, and accordingly, friction on the interlayer shear strength is more appreciable at higher normal stress.

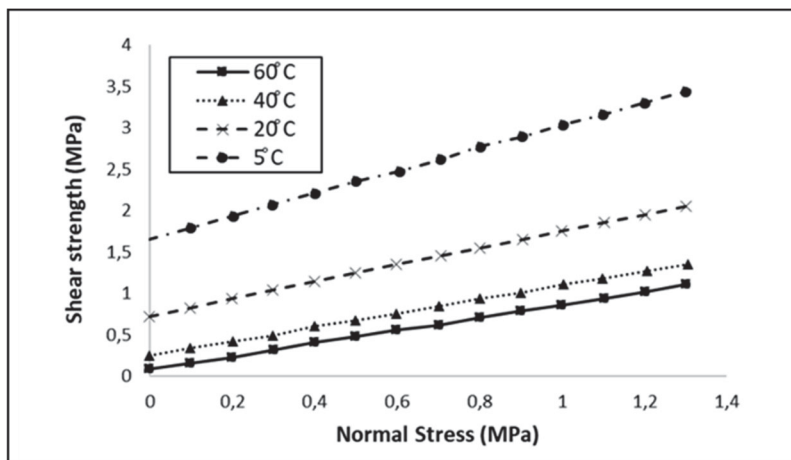


Figure 3.28 The effect of normal stress on shear strength at the interface for cationic emulsion type of tack coat at various temperatures (adapted from (Kim et al., 2015))

Moisture content is another crucial factor that adversely affects the adhesive strength at the interface (St Martin et al., 2003). Water, in the form of liquid or vapour, penetrates into the pavement structure in various ways, such as water seeping through cracks or porous pavements and water rising from the subgrade. In the presence of moisture, the strength of the bond between bitumen and aggregates is compromised and cause moisture-related distresses such as stripping (Tarrer & Wagh, 1991) and reduction in the shear bond strength as much as 15-27% (Raab et al., 2009). This effect is quantified by means of the reduction in indirect tensile strength (ITS), as stated by AASHTO T283. The result of a laboratory study to determine the effect of exposure time to moisture and air void on adhesion strength at the interface, in terms of the indirect tensile strength (ITS), is illustrated in Figure 3.29 (Abu El-Maaty Behiry, 2013).

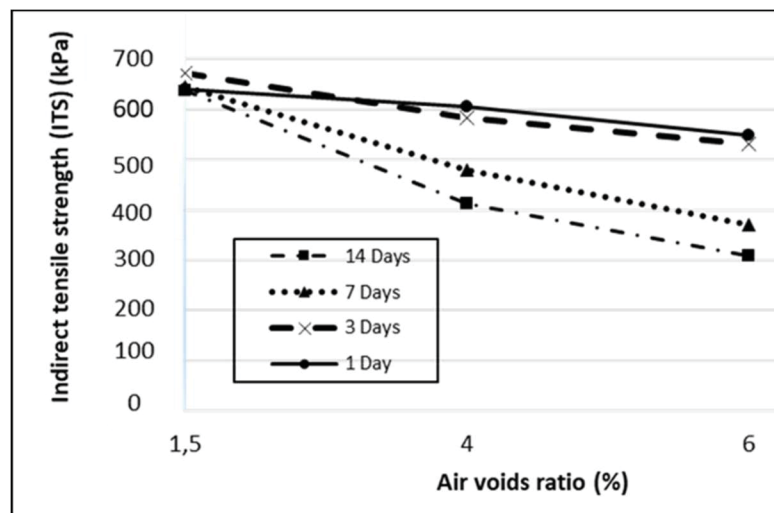


Figure 3.29 Effect of changes in air voids and condition period of moisture on adhesion strength at the interface (adapted from (Abu El-Maaty Behiry, 2013))

It can be understood that in all the cases, as the exposure time to the moisture increases, the specimens with higher air void content experience significant reduction in tensile strength with a considerably higher rate compared to the early days. Nonetheless, for specimens with low air void content, irrespective of the exposure time, the moisture has negligible effect on the adhesive strength.

The last influential factor from asphalt mixture perspective is the roughness of the bottom layer, which is defined through surface texture (Ebnesajjad, 2011; Masad et al., 2005). The

statistical analysis of the results obtained from a direct shear test conducted on three different types of texture cored from the existing surface, e.g. milled and aged surface, unmilled aged non-trafficked surface, and unmilled aged trafficked surface, is depicted in Figure 3.30 (Hasiba, 2012). The bottom layer was covered with a thin film of slow setting asphalt emulsion as the tack coat material and a new asphalt mix layer as top layer. It is possible to conceive that the milled surface has noticeably improved shear strength as compared the two unmilled surfaces, mainly on account of higher surface area and deeper surface texture, which gives rise to better bonding condition at the interface. In addition, within two unmilled surfaces, the cores subjected to traffic indicated higher shear strength as a consequence of an uneven surface even though the difference is not highlighted. This result was further confirmed by a comprehensive study of effective parameters on shear strength of a reinforced interface. In that framework, mean texture depth plays an important role in case of having a normal load applied at the surface due to increased friction between in contact faces (Noory, et al., 2019).

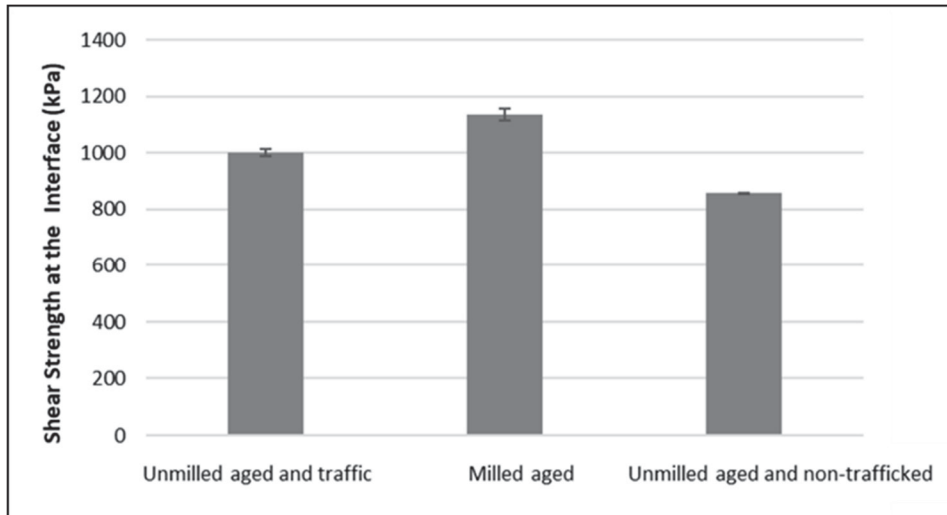


Figure 3.30 Effect of surface roughness on shear strength at interface (adapted from (Hasiba, 2012))

Concerning the geosynthetic, coverage ratio and thickness are two influential factors on adhesion quality. The coverage ratio is explained by the area of the surface covered by the geosynthetic to the total surface area subjected to the shear stress. By increasing this ratio, the contact area of two asphalt layers is substituted by the contact surface of asphalt-geosynthetic, which in turn leads to the lower bond strength. In addition, when thicker geosynthetic is used,

the bond strength at the interface is adversely affected due to lower inter-reinforcement shear strength (Roodi et al., 2017).

In conclusion, among above-mentioned parameters, three of them are identified in the literature as the dominant factors on shear stiffness at the interface, which are temperature, the dosage of tack coat, and the rate of loading. Figures 3.31 to 3.33 illustrate the variation in interlayer shear strength (ISS) by changing in temperature, dosage of tack coat and loading rate reported by various researchers. As temperature and rate of tack coat increase, the shear strength decreases while this trend is conversely followed for the shear strength versus loading rate.

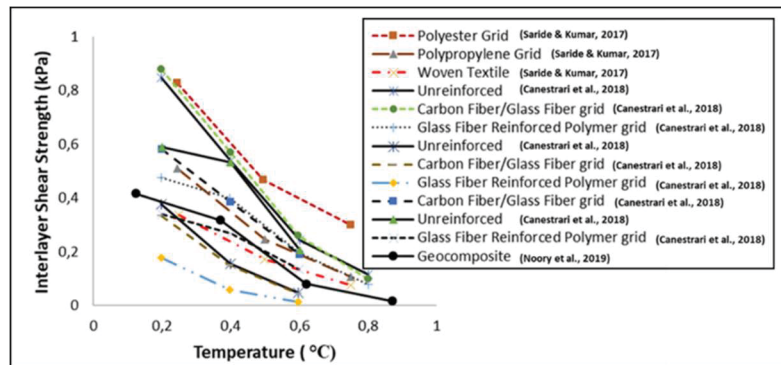


Figure 3.31 Variation in interlayer shear strength versus temperature in constant loading rate

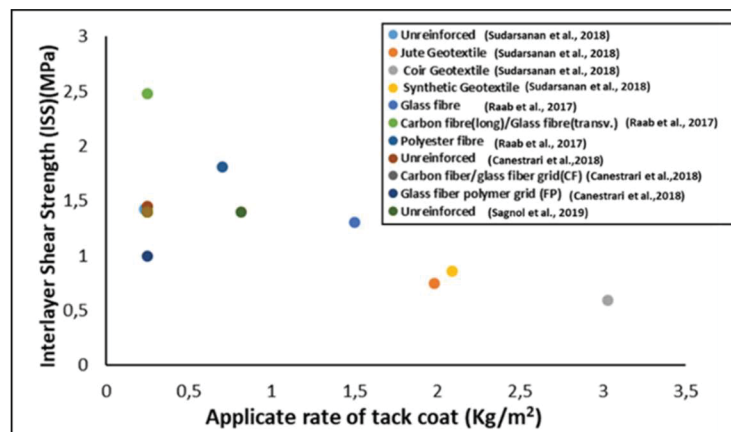


Figure 3.32 Variation in interlayer shear strength versus dosage of tack coat in constant temperature and loading rate

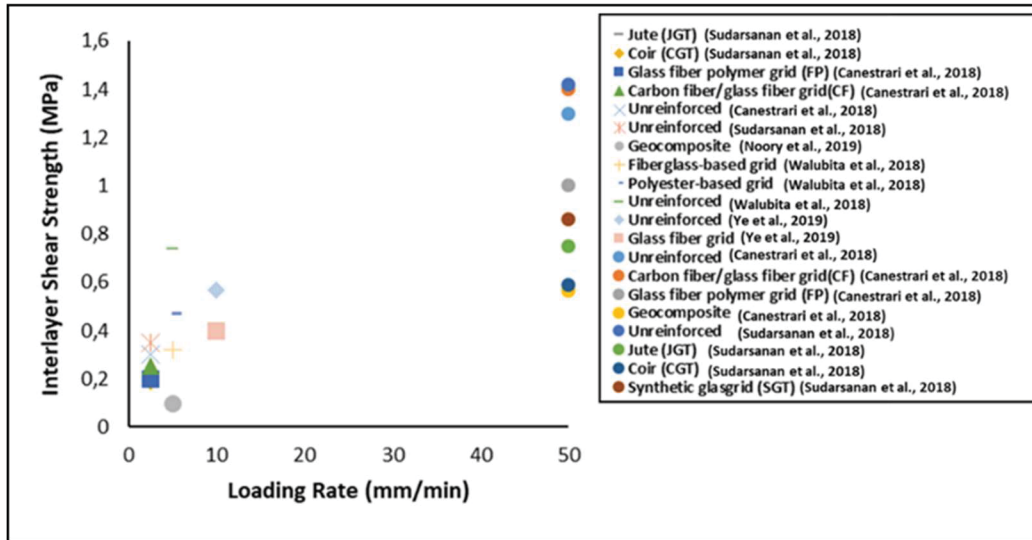


Figure 3.33 Variation in interlayer shear strength versus loading rate in constant temperature and dosage

3.4 Design considerations for the reinforced asphalt overlay with geosynthetics

3.4.1 Design methods

Attempts have been made to incorporate the mechanical effects of geosynthetics into AASHTO (American Association of State Highway and Transportation Officials) and Mechanistic-Empirical (M-E) design methods. The TBR (Traffic Benefit Ratio) and BCR (Base Course Reduction) are two coefficients, which generally have been employed in the AASHTO design approach to take the reinforcement effect of geosynthetic layers into account (Zornberg, 2011). Despite that, this approach is empirical in nature and is specific to the products and test conditions under which these ratios have been calibrated. In addition, these factors do not directly consider the mechanics of the pavement structure, climatic effects, changes in traffic loads, material properties as well as non-traditional layer configurations such as pavement systems constructed with geosynthetic reinforcements (Zornberg & Gupta, 2010). On the other hand, Mechanistic-Empirical (M-E) pavement design method, which in fact is a road performance prediction method, developed under NCHRP project 1-37A, provides a framework to incorporate the use of geosynthetics into bituminous pavements by better characterizing the mechanical effects of geosynthetic and helping to predict the feasible failure

modes (Olidid & Hein, 2004). This method has two key components, mechanistic and empirical parts, which act interdependent. The mechanistic part includes some calculation models to compute critical responses at any desired point in the pavement structure. To this end, it requires input parameters in terms of pavement layers, traffic conditions, climatic conditions and material characteristics. The output of the mechanistic part is then entered into the empirical part in order to predict the pavement performance during its service life at a certain reliability level. If the predicted performance surpasses the desired level of performance, the initial design parameters are modified, and the process is repeated from the first stage as much as necessary (AASHTO, 2008).

Nonetheless, prediction of the behavior of flexible pavements is not a simple subject, since the overall performance is dictated by a myriad of factors, including subgrade strength, load magnitude, layer thickness, material degradation process and oscillations of seasonal and climatic conditions (Al-Qadi, 2006; Dougan, 2007). In addition, the use of geosynthetic reinforcement adds more complexity to the system understanding by introducing a new set of variables, comprising of the reinforcement mechanism, geosynthetic types and stiffness, tensile strength, aperture size and installation location (Zornberg & Gupta, 2010). Therefore, due to uncertainty in quantifying the mechanisms of geosynthetic-reinforcement, neither the AASHTO (1993) nor the M-E approaches are able to incorporate the real geosynthetic properties in their design method and further research is still underway. The following list summarizes the existence insufficiencies identified in the current pavement design methods to incorporate interlayer systems between asphalt layers:

- Design methods proposed for reinforced asphalt overlay were mostly proprietary and they were not generally applicable for various interlayer products.
- The mechanical behavior at the interface and its evolution were not properly defined.
- There is a lack of uniform test method to characterize mechanical specifications of the product.
- Globally acceptable criteria for the sufficiency of the reinforced overlay in terms of rutting and cracking are missing.
- The majority of the proposed test methods to capture the reinforcement effect of interlayer systems were designed based upon comparison with the unreinforced

structure. Very rare reliable test methods were recommended in the literature for the reinforced structure itself.

- Up to now, the effort to include the effect of a geosynthetic layer in the mechanistic model has resulted in developing an equivalent resilient modulus and Poissons' ratio for the system as a whole. Consequently, the benefits of geosynthetic have not been consistently defined in the M-E design.
- The selection of geosynthetic materials in any reinforcement project is still an open question. Geotextiles, geogrids and geocomposites can all be employed as the reinforcement materials if they realize the relevant physical and mechanical specifications. However, there is no methodology to differentiate among them based on material specification such as tensile strength.
- Design softwares based on FEM models in combination with empirical approach such as ARCADESO (De Bondt, 2005), BITUFOR (Vanelstraete et al., 2000), OLCRACK (Thom, 2000), TxACOL and TxME (Brusa, et al., 2016) consider the geosynthetics as a structural element embedded within the materials without considering the redistribution effects in structural responses at the reinforced interface. This will entrain the inhomogeneity into the results.
- The real benefit of introducing an interlayer system into asphalt overlay is neglected in the current design methods and in most of the cases, the reinforcement effect is taken into account by a safety factor or empirical factors derived from experience not through long-term field performance.
- The presence of any discontinuities in the existing deteriorated surface structure, which impresses the severity of reflective cracking, was not taken into consideration in the proposed design models.

On this basis, the design process of reinforced asphalt overlay is not a straightforward task. Table 3.3 introduces the important considerations that need to be taken into account in order to achieve a robust and reliable design tool for reinforced structures:

Table 3.3 Important considerations identified to include the geosynthetics into design models

| Design Consideration | Comment |
|--|---|
| Type of geosynthetic (Brusa et al., 2016) | Stress and strain distribution in reinforced asphalt overlay is dictated by the type of raw materials used in geosynthetic structure. The stiffer the material, the more distribution in structural response. |
| Overlay Thickness (Button & Lytton, 2007) | The minimum reinforced overlay thickness should not be less than the least of 4 times the nominal maximum aggregate size (NMAS) or 4 Cm, to meet compaction requirement |
| Overlay Type (Button & Lytton, 2007) | Only Hot Mix Asphalt (HMA) is allowed to use as overlay with paving fabrics because the trapped water over the interlayer can lead to premature failure due to freeze-thaw cycle effect in combination with traffic loads |
| Design life (Jenner & Uijting, 2004) | Real design life of interlayer system can only be evaluated through long-term field investigation. The design life of the reinforced overlay is the minimum value of two components, i.e. asphalt layer and geosynthetic. |
| Recyclability (Jenner & Uijting, 2004) | Field experience revealed that recyclability of stiff geosynthetics are distinguished than polymer- or steel-based grids. This criterion affects the life-cycle cost of the design strategy. |
| Long-term field calibration (Jenner & Uijting, 2004) | The validation of design method based on long-run pavement performance in the field in different traffic and climatic conditions adds more reliability to the final results. |
| Geosynthetic Specifications (De Bondt, 2000) | Axial stiffness (EA), the resistance to pullout test and anchorage length are important specifications to consider for reinforcing products. On the other hand, for stress absorbing interlayers to mitigate reflective cracking, shear strength, shear stiffness, slippage at the interface and water permeability are more important consideration, which the latter is of great importance for paving fabrics. |

Table 3.3 (Continued)

| Design Consideration | Comment |
|----------------------------------|--|
| Type of distress | As discussed earlier in the mechanical section, the location and type of geosynthetic employed in the asphalt overlay is highly dependent on type of distress such as fatigue cracking, reflective cracking and rutting. In case of rutting, the interlocking effect is much more important than adhesion property. |
| Type of Load (De Bondt, 2009) | In terms of fatigue cracking and shear deflection (rutting), the grid is mostly activated under traffic loads during crack propagation stage. While, thermally induced loads (daily/seasonally fluctuation in temperature) are the main reasons of the occurrence of reflective cracking and activates the reinforcement effect of the grid during crack generation stage. |
| Mechanical behavior at interface | The real mechanical behavior at the interface according to different types of tack coats and its evolution over the time based on validated test methods is necessary to consider in proposed design method. |
| Cost (Zofka & Maliszewski, 2019) | The type of material and installation process are two main additional sources of costs pertaining to geosynthetics which need to be considered along with other factors during evaluation of viable design method for each project. |

3.4.2 Mechanical models

Modelling the damage induced in the reinforced structure would reduce the number of tests required to determine the characteristic of the material. This characterization is essential for better understanding the mechanical behavior and prediction of service life. Table 3.4 provides a review of mechanical models developed to predict the behavior of reinforced asphalt overlay for each type of the damage.

In comparison, numerical models such as finite element method (FEM) has proved its efficiency and adequacy in analysis of reinforced structures, to provide authentic and reliable results especially in modeling a variety of important design and practical considerations

including a slip between the geosynthetic and the surrounding material, slack in the geosynthetic, thermomechanical properties of the reinforced bituminous pavement and the reinforcement mechanisms pertaining to the geosynthetic. It is also capable of handling complex geometry, material properties and different boundary conditions with no difficulty. Two different approaches, namely "linear elastic, cross-anisotropic model" and "non-linear viscoelastic model" have been applied in the FEM to model the reinforced pavement structures with geosynthetics (Ghadimi, 2015). The main reason for using a simplified linear elastic model is that bituminous pavements are generally designed in a linear elastic mode so that only a limited range of permanent deformations can be tolerated. Therefore, almost all the geosynthetics involved in the bituminous pavements can also be postulated to work in a linear range, which in turn results in a simplicity of analyzing the structure. Nonetheless, where a higher degree of accuracy is demanded, non-linear finite element methods can be employed, which is rather a complicated and time-consuming method (Ghadimi & Nikraz, 2017). On this basis, various finite element codes have been applied by researchers to resemble reinforced pavement structures in order to study their mechanical behavior under different conditions in terms of material properties and traffic loadings. ABAQUS (viscoelastic behavior), CAPA-2D (viscoelastic behavior), and Supersap (elastic behavior) are only a few to name (Bohagr, 2013). A review of finite element studies conducted by researchers to simulate the behavior of geosynthetics in asphalt overlay is summarized in Table 3.5.

Table 3.4 Models developed for the prediction of damages in reinforced overlay

| No. | Researcher | Model Name | Model Type | Usage | Comment |
|-----|-----------------------------|-------------|---|---|--|
| 1 | Canestrari et al., 2018 | LET model | Common homogeneous layered elastic theory | Prediction the structural response (stress and strain) of a reinforced asphalt overlay. | The method has been validated through a trial and error way by adjusting the simulated and measured strains in the field |
| 2 | Zofka and Maliszewski, 2019 | RC model | Stochastic reflective cracking model | Prediction of service life in terms of reflective cracking based on MEPDG method | The model has been validated by the result obtained from deflection-based design method |
| 3 | Arseniea et al., 2017 | Bodin Model | Elastic isotropic continuum damage model | Prediction of fatigue damage | The model expresses the decrease in dynamic modulus with cyclic loading |

Table 3.4 (Continued)

| No. | Researcher | Model Name | Model Type | Usage | Comment |
|-----|-----------------------------|---|---|---|--|
| 4 | Gajewska and Jemiołob, 2014 | Composite model | Energetically equivalent isotropic model | A useful tool to incorporate the reinforced composite structure into mechanistic based design methods | Consider the orthotropic nature of grid |
| 5 | Freire et al., 2018 | Linear Viscoelastic Model | 2S2P1D model | Define the mechanical behavior at the interface between geogrid and asphalt layer | |
| 6 | Choi and Kim, 2014 | Shift model | Permanent deformation model | Prediction of rut depth | The model has been validated by triaxial stress sweep (TSS) test |
| 7 | Al-Qadi and Elseifi, 2004 | Fitted design model for reinforced overlay with steel | Regression model | Prediction of service life in terms of reflective cracking | The model was adjusted based on field results by introducing shift factors |
| 8 | N H Thom, 2000 | OLCRACK | A finite element model based on an incremental approach in tensile stains produced in the crack tip | Prediction of top-down and bottom-up crack propagation based on tensile strain in the crack tip | The result of the model was adjusted against the result from pilot scale pavement test and beam test |
| 9 | Scarpas et al., 1996 | CAPA | A finite element model | Prediction of reflective cracking | The model works based on a crack propagation increment |

Table 3.5 FEM studies for asphalt overlay reinforced with geosynthetics

| Researcher | Geometry | Asphalt Layer Model | | Geosynthetic Layer Model | | Interface Element Type | Load Type | Validation |
|---------------------------|------------------------------|---------------------|----------------------|--------------------------|--------------------|------------------------|-----------------|-------------------|
| | | Linear elastic | 4-node plate element | Linear elastic | 4-node bar element | | | |
| Montestruque et al., 2004 | Two-dimensional axisymmetric | Linear elastic | 4-node plate element | Linear elastic | 4-node bar element | Fully bonded | Dynamic loading | Experimental work |

Table 3.5 (Continued)

| Researcher | Geometry | Asphalt Layer Model | | Geosynthetic Layer Model | | Interface Element Type | Load Type | Validation |
|---------------------------------|------------------------------|---------------------|-----------------------------|--------------------------|---------------------------|------------------------|--------------------------|-------------------|
| | | | | | | | | |
| Correia et al., 2018 | Two-dimensional axisymmetric | Linear elastic | 15-noded solid elements | Linear elastic | 15-noded structural solid | Fully bonded | Static loading | Experimental work |
| Coni and Bianco, 2000 | Three dimensions | Elastoplastic | 8-node linear brick element | Linear elastic | Beam element | Fully bonded | Static and dynamic loads | None |
| Bounsanti and Leonardi, 2012 | Three dimensions | Linear elastic | 8-node linear brick element | Linear elastic | 4-node membrane element | Fully bonded | Impulsive loading | None |
| Abdessemed et al., 2015 | Three dimensions | Linear elastic | 8-node brick element | Linear elastic | 4-node block element | Fully bonded | Static loading | Experimental work |
| Taherkhani & Jalali, 2016 | Three dimensions | Viscoelastic | 8-node linear brick element | Linear elastic | 4-node shell element | Fully bonded | Dynamic loading | Experimental work |
| Calvarano et al., 2017 | Three dimensions | Viscoelastic | 8-node linear brick element | Linear elastic | 4-node membrane elements | Semi-bonded | Impulsive loading | None |
| Shamami & Khavandi Khiavi, 2017 | Three dimensions | Linear elastic | 8-point solid element | Linear elastic | 4-point linear membrane | embedded | Cyclic loading | Experimental work |

A critical issue in taking advantage of finite element methods is to accurately define the boundary condition, which is highly related to the geometry of the model, material properties,

loading conditions and constitutive models for each individual layer. In the following subsections, these concerns are discussed in detail.

3.4.2.1 The geometry of model

There are three different types of formulation to model pavement structure: axisymmetric, two-dimensional (or plane strain), and three-dimensional (Cho et al., 2000). Each formulation has its own advantages and disadvantages. For instance, in the case of axisymmetric and two-dimensional plane strain models, the required time for analysis and memory space are quite beneficial. On the contrary, in a three-dimensional model, more memory space and computational time are required, even though the model has a higher accuracy (Bohagr, 2013). Nevertheless, the major shortcoming of using axisymmetric and two-dimensional models for pavement structure is to simulate the traffic loads. In-plane strain model, traffic load is modeled as a line load, according to Figure 3.34. On the other hand, in an axisymmetric model, traffic load is presented by a circular load as depicted in Figure 3.35. However, as specified by Figure 3.36, in a three-dimensional model, traffic load is simulated by a rectangle in the center and two semicircles at two ends, which gives a close representation to real situation (Cho et al., 2000).

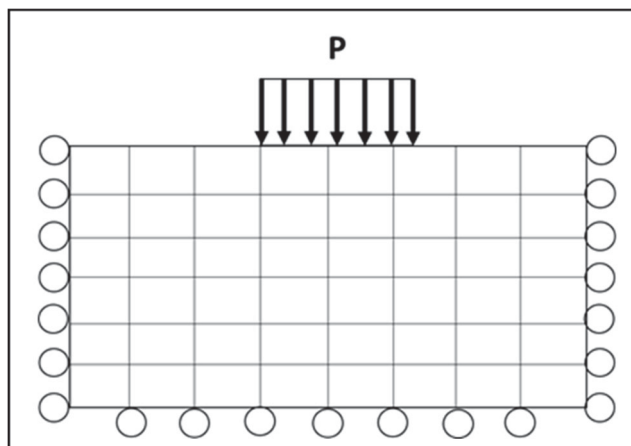


Figure 3.34 Traffic loading simulation in 2-D plane strain model (adapted from (Cho et al., 2000))

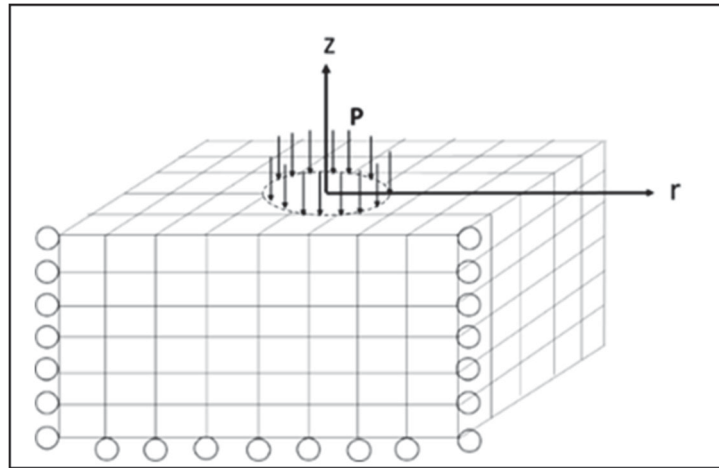


Figure 3.35 Traffic loading for axisymmetric model
(Adapted from (Cho et al., 2000))

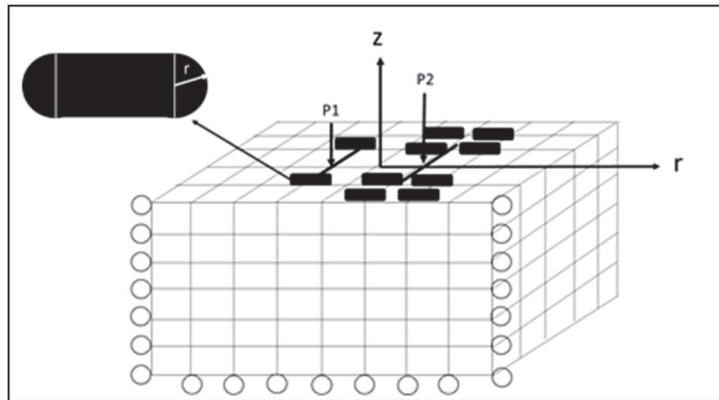


Figure 3.36 Traffic loading for 3-D model (adapted
from (Cho et al., 2000))

It should be recognized that the axisymmetric model is not able to simulate the shoulder conditions or any discontinuity that exists in the pavement structure (Ghadimi, B., 2015). Following advantages were reported in 3-D analysis (Calvarano et al., 2017): 1) It accurately demonstrates the complex mechanical behavior of the pavement system with different materials subjected to different traffic loads; 2) it is a preferable way to validate the results obtained from numerical models with field or laboratory results; 3) it better simulates the real footprint of loaded wheels.

3.4.2.2 Constitutive models

As to the constitutive model for asphalt layer, it has been well documented that HMA materials exhibit frequency and temperature dependent behavior. However, several researchers have tried to use the elastic theory into their models to resemble HMA behavior. The elastic theory, compared with linear viscoelastic (LVE) theory, estimates the pavement responses lower than expected. As a result, it justifies the need for a viscoelastic constitutive model (Abu El-Maaty Behiry, 2013). In this respect, 2S2P1D (2 springs, 2 parabolic elements and one dashpot) model can be utilized to mechanically describe the viscoelastic behavior of the asphalt overlay (Olard & Di Benedetto, 2003). Additionally, a new methodology for the mechanical description of the reinforced interface behavior has been proposed (Freire et al., 2018), which took advantage of laboratory thermomechanical complex modulus tests. The test was performed by applying an axial tension-compression sinusoidal loading in strain-control mode in a broad range of frequencies and temperatures on reinforced asphalt samples with geogrid placed at the interface in two different positions (i.e. vertically and horizontally). By comparing the Cole-Cole diagram obtained from the developed methodology on reinforced and unreinforced asphalt specimens, as shown in Figure 3.37, the interface behavior was considered as linear viscoelastic and mechanically described with 2S2P1D model.

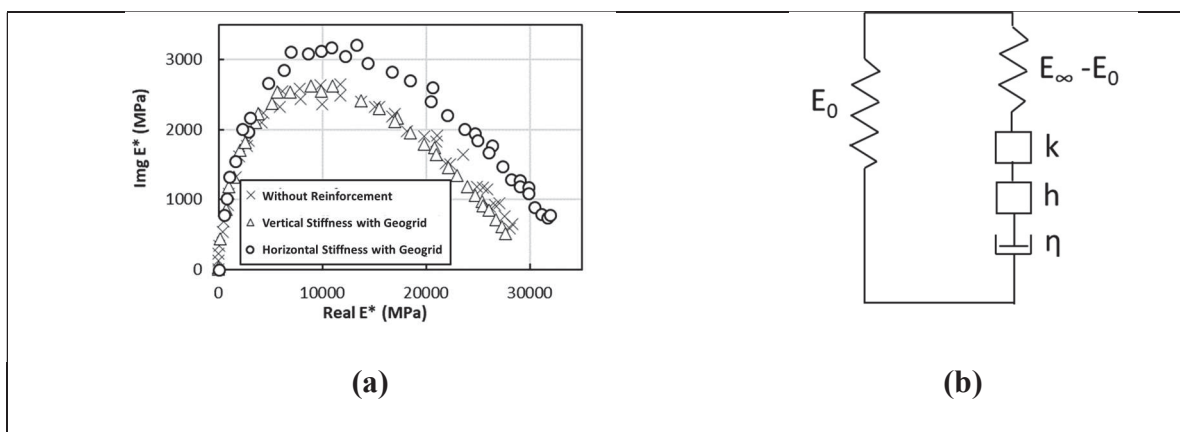


Figure 3.37 Rheological behavior of asphalt layer including geogrid a) Cole-Cole diagram of specimens with and without geogrids b) representation of the 2S2P1D model for bituminous mixes (adapted from (Freire et al., 2018))

To define viscoelastic behavior of asphaltic materials in terms of the stress-strain relationship into Abaqus software, Prony series in the form of shear modulus defined by Equation (3.5) can be employed (Hussein & Meguid, 2015):

$$g(t) = 1 - \sum_{i=1}^N g_i \left(1 - e^{\left(\frac{-t}{\tau_i}\right)} \right), \quad g(t) = (G(t))/(G(t = 0)) \quad (3.5)$$

where $g(t)$ is the shear modulus ratio, defined by the ratio of shear modulus at any time like t , $G(t)$, to the shear modulus at the first stage ($t = 0$, $G(t = 0)$); τ_i and g_i are Prony constants, which are determined based on the material properties; and N is considered as the number of terms used in Prony series, which is normally assumed $N = 5$ (Liao & Sargand, 2010).

Several methods have been proposed to calculate the Prony series constants. One way is to perform complex modulus test and then to convert the dynamic modulus $|E^*|$ in the frequency domain to the relaxation modulus ($E(t)$) in the time domain by an approximation method (Perkins & Edens, 2003).

As far as the constitutive model of geogrid is concerned, almost all the researchers assume mechanical behavior as linear elastic. However, laboratory results, as shown in Figure 3.38, indicate that the geogrids behaves like a nonlinear elasto-plastic hardening material and to simplify this behavior with linear elastic may result in misleading solutions (Liu et al., 2007; Abdi & Zandieh, 2014). An elasto-plastic model can account for the creep behavior and directional dependency of the material (Perkins, 2000; Perkins, 2001). In addition, laboratory results indicate that plasticity has a meaningful effect on the load-displacement relationship, especially, when it approaches the failure point (Perkins & Edens, 2003).

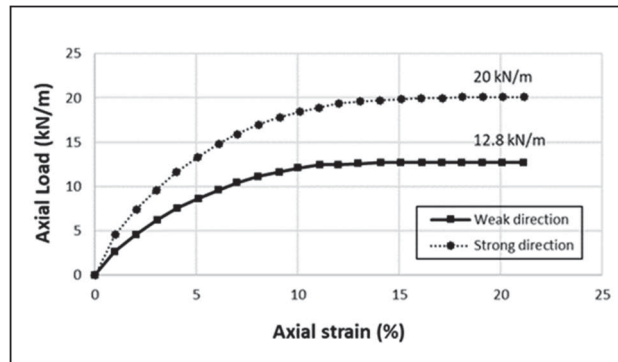


Figure 3.38 Experimental axial load-axial strain results in the weak and strong directions (adapted from (Hussein & Meguid, 2016))

3.4.2.3 Loading condition

The final parameter is the effect of the traffic load, which affects the pavement performance through configuration of axles, tire contact pressure, vehicle speed, and axial load and number of repetitions (Calvarano et al., 2017). The researchers have adopted two different approaches to face traffic loads. One is to apply a static load on a circular shape contact area with uniform pressure (Abdessemed et al., 2015), and the other is to employ a triangular shape pulse load with 0.1 sec loading time and 0.9 sec rest period, which is repeated for a certain number of cycles (Taherkhani & Jalali, 2016). Several studies have tried to compare the numerical results obtained from static loading through laboratory or field tests (Siriwardane et al., 2010; Abdessemed et al., 2015; Ling & Liu, 2003). Nevertheless, it was found that only for high-amplitude loads the dynamic loading plays an important role on geosynthetic-reinforced layers (Faheem & Hassan, 2014).

3.5 Conclusion

This paper presented an overview of the mechanical interaction between geosynthetics and asphalt overlay in bituminous pavements. As it appears, the reinforcement effect is mainly recognized by the lateral confinement and enhanced structural capacity in which the interface property is the dominant factor. Moreover, the study of influencing factors on interlayer shear

strength shows that temperature, dosage of tack coat and loading rate are chief factors, which are required to consider in design models.

From the design point of view, the mechanistic-empirical pavement design method seems to be more appropriate method to take the properties of geosynthetics into account. To this end, a finite element method has been suggested to incorporate into the design method to calculate the responses of reinforced systems in critical locations of the pavement system. The geometry of model, constitutive models of asphalt mix and geosynthetic and type of loading are identified as the influencing factors, which controls the accuracy of the design method.

Based on this review, following gap research are recognized for reinforced bituminous pavements:

Mechanical part:

- To develop a standard test method to capture the interlocking capacity of geosynthetic materials embedded in the asphalt overlay.
- To clarify the influence zone of geosynthetic materials based on the field data in order to define the accurate size of reinforced specimens in the laboratory.
- To verify the positive effect of using two layers of geogrids in asphalt overlay (one near the top and one near the bottom) based on field data.
- To establish criteria based on mechanical performance and serviceability of the reinforced sections.
- To develop standard and reliable laboratory test methods, specifically designed for reinforced specimens (not based on comparison with control specimens), to determine material properties required as inputs into design models.
- To set solid and measurable mechanical requirement to facilitate the selection of the proper type of geosynthetic in each reinforcement project.
- To specify the redistribution effect of reinforcement interlayer on structural responses caused by traffic or environmental loads.

Design part:

- To develop a validated finite element model based on real mechanical behavior at the interface between geosynthetic and adjacent asphalt layers.
- To include the presence of any discontinuities in the existing asphalt layer according to its level of severity.
- To distinguish the stiffness property of the asphalt overlay and the interface in the design models.
- To consider the heterogeneity of the reinforced structure in mechanical models to describe the crack initiation and propagation stages.
- To validate the design methods based on long-term field performance of reinforced sections.

CHAPTER 4

PERMEABILITY AND MECHANICAL PROPERTY MEASUREMENTS OF REINFORCED ASPHALT OVERLAY WITH PAVING FABRICS USING NOVEL APPROACHES

Ehsan Solatiyan^a, Nicolas Bueche^b, Michel Vaillancourt^c, Alan Carter^d

^{a, c, d} Construction Engineering Department École de technologie supérieure (ETS), Montréal, Canada, QC H3C 1K3

^b Department of Architecture, Wood and Civil Engineering Bern University of Applied Sciences (BFH), Bern, Switzerland, CH-3012

Paper published in *Materials and Structures*, January 2020
and presented in 99th *Transportation Research Board annual conference*

4.1 Abstract

In order to study the mechanical behavior of asphalt overlay reinforced with paving fabrics (a system composed of non-woven geotextile and asphalt cement) a new methodology was developed based on three new pieces of laboratory equipment including 3-Point Bending Test (3-PBT) method on cylindrical specimens, Crack Widening Device (CWD) and Water-Vacuum Permeability Device (WVPD). The 3-PBT and CWD were designed to simulate generation and propagation of thermally driven cracking from an existing discontinuity in the pavement system into a new asphalt overlay. In addition, the WVPD was assembled to accelerate the movement of water through a low porosity medium. On such basis, representative parameters have been suggested by the authors as: Crack Resistance Index (CRI) of the system to determine the reinforcement effect and Coefficient of Permeability (K) to evaluate the waterproofing benefit of the paving fabrics. The experimental results of two different rehabilitation strategies of bituminous pavements were compared during this research: a traditional strategy, as a reference case, in which asphalt overlay is directly attached to the existing surface with an asphalt emulsion and a new strategy with the inclusion of paving fabric as an interlayer system between two asphalt layers, as the reinforced case. The results

indicate that the reinforced case has enhanced mechanical properties, in terms of lower crack width manifested at the surface and higher crack resistance index and reduced water permeability. In addition, the proposed methodology appears to be suitable to evaluate the mechanical performance of reinforced asphalt overlays.

4.2 Introduction

Overlaying a deteriorated surface of bituminous pavements with asphalt materials is a common maintenance activity to restore the operational and structural capacity of the pavement system. However, the main issue with an asphalt overlay is the propagation of cracks from a discontinuity in the existing surface into and through the new asphalt overlay (reflective cracking), which yields an accelerated deterioration process of the asphalt surface under the effect of traffic and thermally induced stresses. In addition, it imposes significant strain from economical and constructional points of view on pavement authorities. To address this issue, different approaches such as modified asphalt mixtures, application of stress-absorbing interlayer systems and taking advantage of reinforcement materials at the interface of new and old asphalt layers have been proposed by previous studies, so that reflective cracking can be effectively delayed (Baek et al., 2008; Dhakal et al., 2016; Hajj et al., 2008; Sherman, 1982; Von Quintus et al., 2010; Williams, 2015). In this connection, interlayer systems such as paving fabrics have been suggested to enhance the resistance against reflective cracking (Alvarez, 2008; Amini & Wen, 2016; Buttlar et al., 2000; Button & Lytton, 2007; Rahman et al., 1989; Shukla & Yin, 2004; Steen, 2004) and to reduce the permeability of the integrated system (De Souza Correia & De Souza Bueno, 2011; Marienfeld & Baker, 1999; Zornberg et al., 2017) in order to extend the service life of the asphalt overlay. However, characterization of the reinforcement and waterproofing effects is a key step towards widespread usage of paving fabrics as a rehabilitation strategy.

The reinforcement effect of paving fabrics is mainly attributed to the friction mobilized at the interface as a result of imposed shear stresses from traffic or environmental loads (Fannin, 2007). Many researchers have applied various test methods, such as Wheel Reflective Cracking (WRC) and four-point bending test devices, to measure and quantify the reinforcement property of paving fabrics (Bhattacharjee et al., 2008; Dempsey, 2002; Gallego

& Prieto, 2006; Wu et al., 2008; Yu et al., 2013; Joseph & Haas, 1989) and these are considerably time-consuming and not cost-effective. In addition, none of them gives an indication of reinforcement effect in terms of crack width, which is more tangible in practical usage. To gain knowledge of the crack resistance of the reinforced system is an important consideration to assure satisfactory performance in the field. In general, the crack forms in asphalt-bounded layers in two major ways: traffic induced cracking (fatigue cracking) and thermal driven cracking (reflective cracking). Fatigue cracking is caused by the repetitive action of traffic loads that reduces the structural integrity of the pavement system by the appearance of microcracks and their growing over time. However, thermal cracking occurs when the thermal stress exceeds the tensile strength of the asphalt mix. Cracked structure allows moisture to infiltrate into the pavement system, which can result in further weakening of sublayer materials (Rastegar et al., 2018). The focus of this study would be on thermally induced cracking, which has been recognized as a prevalent issue in North America (Marasteanu et al., 2004). This is because of the fact that when thermal cracks appear early in the pavement surface, it is followed by other forms of distresses including frost heave or localized potholes at the crack location, which could significantly contribute to the loss of serviceability long before the fatigue life of the pavement (Buttlar et al., 2018).

Furthermore, paving fabrics could bring an additional advantage in terms of waterproofing the entire pavement structure, and this, in turn, could maintain the resilient modulus of lower layers in the pavement structure and bring the pavement service life to the anticipated age. Limited studies have been conducted so far to develop laboratory equipment or a methodology to measure the water permeability of asphalt mixtures in small-scale laboratory size specimens. Pezzaniti et al. (Pezzaniti et al., 2009) used a falling head permeability test to investigate the water permeability of permeable asphalt specimens. Fwa et al. (Fwa et al., 1999) employed the constant head permeability test to evaluate the permeability of porous asphalt mixtures. Ahn et al. (Ahn et al., 2017) developed a device to measure the permeability of both soils and asphalt mixture specimens. The main feature of this device was its flexibility to adjust with constant and falling head permeability tests. Texas Department of Transportation (TxDOT) (Yeo et al., 2012) has also developed a non-destructive device called Tube Suction Test (TST),

which works based on measuring the dielectric value (DV) of the asphalt mixture as a representation of the moisture content.

Nevertheless, a suitable device or a methodology that could efficiently measure the permeability of asphalt mixtures or asphalt system (mix-paving fabric-mix) with low air void content and in a cracked condition is still a necessity in order to practically evaluate the performance of rehabilitated asphalt mixtures in small-scale laboratory size specimens.

Therefore, this paper first aims to understand the mechanical behavior of asphalt overlay reinforced with paving fabrics by introducing a novel approach to simulate the crack initiation and propagation. Afterwards, a comparative evaluation is performed on water permeability of asphalt mixtures with and without paving fabrics in a variety of widths of crack through an accelerated method to have an insight into the waterproofing effects of paving fabrics.

4.3 Research background on thermally driven reflective cracking

When an asphalt overlay is implemented on an existing asphalt surface, any movement induced by temperature or traffic at present discontinuities could build up stresses at the bottom of the overlay, which can accelerate the propagation of reflective cracks and finally tearing of the overlay (Dave et al., 2007). The reflective cracking mechanism has been studied through a three-dimensional finite element method by taking the variations in traffic and temperature during a year into account. This study revealed that the changes in temperature contributes more to the occurrence of premature failures in terms of reflective cracking in asphalt overlay. According to this study, reflective cracking is first initiated by the temperature changes and the traffic helps more to accelerate the pavement damages (Sheng, 2016).

Hitherto, low temperature performance of mix design has been taken into account by performing Frass Breaking Point test or Bending Beam Rheometer (BBR) test on bituminous binder. However, previous researches indicated that, because of the complexity of the behavior, this effect needs to be studied on asphalt mix scale (Dave et al., 2008; Marasteanu et al., 2007; Marasteanu et al., 2012; Zofka & Braham, 2009). Accordingly, the focus needs to be directed to define appropriate parameters to demonstrate crack susceptibility of the mixture. Thermally driven reflective cracking in asphalt mixture initiates when temperature drops in a short period of time. It can be caused by expansion, contraction or bending from horizontal

movement of the layers due to significant drop below $-20\text{ }^{\circ}\text{C}$ or high daily fluctuation in temperature, i.e. at least $-10\text{ }^{\circ}\text{C}$ drop per one day, of cooling event (Marasteanu et al., 2007; Marasteanu et al., 2012). It is worth mentioning that because of the relaxation effect under slow moving conditions, daily fluctuation in temperature plays an important role than seasonal temperature changes (Sheng, 2016). This point needs to be considered in selecting the proper rate of loading in the laboratory. When induced tensile stresses at the bottom of the overlay exceed the tensile strength of the material, the thermally driven cracks start to appear (Apeagyei et al., 2008). Once emerging in an asphalt mixture structure, the crack will propagate in width and height by the repeated effect of shear stresses induced by traffic (mode II of cracking) (Sheng, 2016). It is also indicated that the rate and severity of crack propagation is higher for mixes with a high air void and low resistance to cracking (Alvarez, 2008).

Many studies have been performed to characterize the mechanism of generation of thermally driven cracking in asphalt mixtures using laboratory testing and field examination. The studies on the laboratory scale can be divided into two main groups: static cracking test such as Disk-Shaped Compact Tension Test (DSCT) (Wagnoner et al., 2005), and Semi-Circular Bend Test (SCB) (Li & Marasteanu, 2004) and cyclic cracking test including Thermal Stress Restrained Specimen Test (Monismith et al., 1965), Asphalt Concrete Cracking Device (Kim et al., 2009). These tests have been used to resemble the evolution of thermal cracking with time and temperature fluctuation. Although some of these proposed methods are applicable to accommodate asphalt mixtures reinforced with paving fabrics, they are complicated to perform, requiring huge effort in terms of specimen preparation and rigorous procedure to interpret the result.

Furthermore, full-scale studies to directly evaluate the mechanism of thermal cracks in asphalt mixtures including paving fabrics are very rare. The Mississippi Department of Transportation has studied the effectiveness of paving fabrics to retard reflective cracking. The field data showed that the reinforced asphalt overlay thicker than 5 cm or more increases the enhancement effect against reflective cracking (Amini, 2005). Texas Transportation Institute also worked on geosynthetics to see how the reinforced cross sections can reduce the severity or retard thermally induced reflective cracking over 5 to 6 years of this study. Their results indicated that up to 3.5 years the rate of reflected cracks was very slow (Chowdhury et al.,

2009), which can be treated as a static environmental load. Furthermore, it was concluded that application of paving fabrics in asphalt overlay could restrict thermally driven cracks better in locations with hot and moderate temperatures compared to cold ones (Amini, 2005). In another study performed for Airfield Asphalt Pavement Technology Program different mechanisms of reflective cracking in asphalt overlay implemented on both rigid and bituminous pavements have been investigated (Von Quintus et al., 2010). It was concluded that using paving fabrics in thin asphalt overlay (less than 5 cm) has negligible benefits, but its performance in thick overlays is highlighted.

To resemble crack propagation stage in asphalt mixture, fracture-mechanic-based tests have been frequently employed in the crack mouth displacement controlled mode. In this sense, applied force is regulated based on the opening rate of the crack mouth. The conventional methods are the overlay test (OT), developed by the Texas Transportation Institute and the Indirect Diametral Test (IDT) and Single-Edge notched Beam (SEB) test in which the concept of Cohesive Zone Model (CZM) is applied and cohesive energy and strength of the mixture is obtained (Sheng, 2016). The CZM concept has been suggested as a proper way to simulate the crack propagation ahead of a crack tip (Jenq & Perng, 1991). In addition, based on the application of the CZM to evaluate the propagation behavior, it was indicated that propagation process acts independently from the rate of temperature and loading changes (Soares et al., 2003). This result was also confirmed by Paulino et al. (Paulino et al., 2004).

Another point that needs to be considered is to define a laboratory-measured parameter, which can be able to differentiate between good-and poor- performance reinforced mixtures in terms of mechanical behavior. Until now, several indices have been suggested by the researchers for pavement cracking (Zhou et al., 2017). However, to develop a performance based index from a fracture test has received much attention (Al-Qadi et al., 2015; Dave et al., 2015; VanDeusen et al., 2015). These indices are mostly obtained from notched specimens by measuring the required force to receive a predetermined amount of displacement (Zhu et al., 2017). Moreover, two approaches were frequently adopted to obtain fracture indices: energy-based approach and strength-based approach (Wagnoner et al., 2005; Roque et al., 2004). Although energy based approach in most cases results in a better visualization of the crack propagation process, it

cannot differentiate between the materials with high peak load and sharp slope and the ones with low peak load and slight slope.

4.4 Materials and methods

4.4.1 Materials

A single 0-10 mm dense graded hot mix asphalt made with a PG 64-34 bitumen was used for both top and bottom layer of the tested system, according to Table 4.1.

Table 4.1 Gradation and volumetric characteristics of the mixture

| Sieve Size (mm) | Passing (Percent) |
|---|-------------------|
| 14 | 100 |
| 10 | 96 |
| 5 | 63 |
| 2.5 | 36 |
| 1.25 | 18 |
| 0.63 | 10 |
| 0.315 | 8.0 |
| 0.160 | 6.7 |
| 0.080 | 5.7 |
| Volumetric characteristic of asphalt mix | |
| Gmm ¹ | 2.525 |
| Vb ² | 5.9 |
| ¹ Maximum theoretical specific gravity | |
| ² Bitumen content (percent) | |

The paving fabric comprised two important elements: a needle-punched nonwoven geotextile and PG 64-34 bitumen as tack coat material. The physical and mechanical characteristics of the geotextile are presented in Table 4.2.

Table 4.2 The mechanical properties of paving fabric

| Properties | Test Method | Units | Value |
|-------------------------|------------------|------------------|---------|
| Grab Tensile Strength | CAN 148.1 No.7.3 | N | 550 |
| Grab Tensile Elongation | CAN 148.1 No.7.3 | % | 45-105% |
| Mullen Burst | CAN 4.2 No.11.1 | kPa | 1585 |
| Bitumen Retention | ASTM D6140 | L/m ² | 1.15 |

In total, eight slabs with dimension indicated in Figure 4.1 (four slabs for the reference case and four slabs for the reinforced case) were prepared. A typical construction method was followed: the bottom layer was first fabricated and compacted, followed by the implementation of tack coat (and/or paving fabric) and the top layer and then compaction of the whole system. The compaction temperature was selected as 160 ± 2 °C according to the Ministère des transports du Québec standard (MTQ 2018-LC 26-003) based on the performance grade of the bitumen employed in this study (i.e. PG 64-34). The compaction method was based on the French Roller Compactor, which complies with European Standard EN 12697-33.

It should be noted that for the reference case, 5 hours curing time was needed for the asphalt emulsion, type SS-1h used in this study, to completely break before the placement of the top layer. While for the reinforced case, the overlayment process including the implementation of tack coat, geotextile and the top asphalt layer was performed in a sequence, with no delay.

In addition, for the reinforced system, asphalt cement (AC) is normally employed as tack coat instead of asphalt emulsion. Since it is better to use the same AC as tack coat and in the HMA (Button & Lytton, 2007), a PG 64-34 was applied in this study as tack coat when the geotextile was used.

The application rate of the tack coat is another important factor that needs to be respected during the specimen preparation. This is due to the fact that too much can cause slippage, whereas a lower amount may lead to debonding at the interface. The application rate of the tack coat was recommended between 1.2 to 1.4 L/m² for geosynthetics depending on the

surface condition of the existing surface (Shukla & Yin, 2004; Donovan, 2014). Since the surface of the bottom layer was sound and dense, the lower limit (i.e. 1.2 L/ m²) was selected.

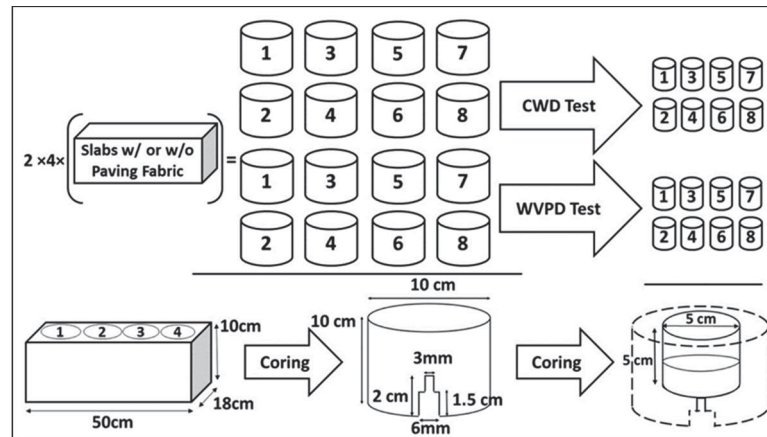


Figure 4.1 Graphical presentation of prepared specimens for each test

After preparation of the slabs, first, cylindrical specimens (100mm diameter and 100mm height) were cored in the perpendicular direction to the compaction after 2 weeks curing time at room temperature according to the Quebec Standard (MTQ, 2018). Four specimens were obtained from each slab. The first two slabs were cored for crack resistance tests and the second two slabs were cored for permeability test (Figure 4.1).

The bulk specific gravity and air voids of the cored specimens were determined according to ASTM D2716M by measuring three weights as W_{ssd} , W_{dry} , and W_{sub} of samples in grams. The results are summarized in Table 4.3.

Table 4.3 Air void content and specific gravity of specimens

| Properties | Test Method | Units | Value |
|-------------------------|------------------|------------------|---------|
| Grab Tensile Strength | CAN 148.1 No.7.3 | N | 550 |
| Grab Tensile Elongation | CAN 148.1 No.7.3 | % | 45-105% |
| Mullen Burst | CAN 4.2 No.11.1 | kPa | 1585 |
| Bitumen Retention | ASTM D6140 | L/m ² | 1.15 |

Prior to performing 3-Point Bending Tests (3-PBT) on specimens, a 2 cm notch, which plays the role of a discontinuity in the existing asphalt surface, was sawed at the midpoint on the bottom side of each specimen in two steps. Firstly, by using a cutting machine, a 1.5 cm deep and 6 mm wide notch was worked out and ended with 3mm wide notch at the top, as shown in Figure 4.1. This configuration induces the generation of a crack on a rather straight plane from the tip of the notch to the surface (Nguyen et al., 2012).

After the generation of the crack with the 3-PBT, the specimens were cut right above the notch and cored from the center to receive 5 cm size specimens in diameter in order first to maintain the proportionality between the diameter and depth of the specimen and second due to laboratory considerations pertaining to the application of the Crack Widening Device (CWD) and Water-Vacuum Permeability Device (WVPD).

4.4.2 Methods

In this paper, the mechanical behavior of paving fabric employed at the interface of two asphalt layers is studied, in terms of reinforcement and waterproofing benefits, by using novel approaches.

In order to identify the reinforcement effects in terms of crack generation and propagation, two types of tests were carried out on specimens. First, a 3-PBT on cylindrical specimens was employed to see how the introduction of the paving fabric into asphalt overlay affects the crack generation from an existing discontinuity in the pavement system to the surface in terms of required force and path of crack. Then, the resistance of the system against crack propagation was evaluated by taking advantage of the CWD. Furthermore, from the waterproofing perspective, the WVPD was designed to compare the water permeability of the reference and reinforced cases in a variety of crack widths, which were generated during earlier stages.

To compare the two different types of strategy, crack resistance index (CRI) defined as the slope of the load-displacement curve, and coefficient of permeability, which is the quotient of the flow rate and hydraulic gradient between two constant points in a particular medium were considered as comparative indications. It was postulated that the proposed test methods would lead to distinct results in defined indices. The following subsections present the new

approaches taken into account in this project to quantify how the presence of paving fabrics can enhance the mechanical performance of asphalt overlays.

4.4.2.1 3-Point Bending Test (3-PBT)

The 3-PBT was designed to simulate the generation of a crack in Mode I of cracking, which is mainly due to excessive tensile stresses caused by flexural effect (Ponniah & Haas, 1989). For this purpose, the 10 cm notched-cylindrical specimens, with and without paving fabrics, were placed on two roller supports at the sides and loaded from the top by a straight narrow plate with the rate of 0.1 kN/sec, as shown in Figure 4.2. This configuration allows specimens to bend as the rollers tend to move away under the compression force applied from the top. For each specimen, the crack width at the bottom and top surfaces, the required force for the crack to reach the top surface and the pattern of crack formation were recorded throughout the 3-PBT at 25 ± 1 °C.

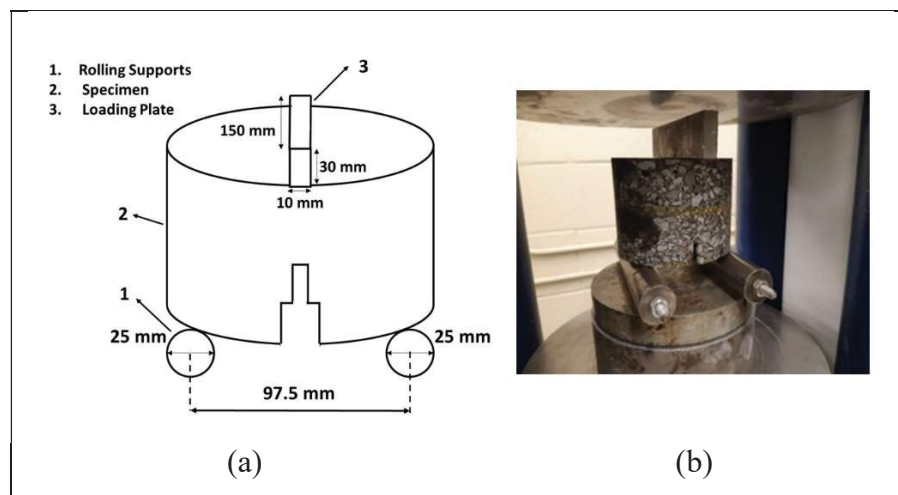


Figure 4.2 3-Point Bending Test (a) schematic design (b) test setup

4.4.2.2 Crack Widening Device (CWD)

This stage was designed to represent the crack widening process in Mode II of cracking in which the initial crack made in the first stage becomes wider under the effect of shear stresses (Ponniah & Haas, 1989). To this end, the CWD was developed and built in order to investigate the resistance against crack propagation in the reinforced asphalt overlay through comparison with the reference case.

The device is composed of a base, two sliding parts on which the specimen is located and a spring to keep the sliding parts fixed in their positions before the onset of the test (Figure 4.3). Compressive load, perpendicular to the interface of specimen and the device, is applied through a Material Testing System (MTS) press that allows the displacement and temperature to be controlled during the test. Under the influence of the load, the sliding parts are gradually moving apart from each other, through sliding over the 45° inclined surface of the base, and the initial crack is grown due to the friction force developed at the interface between the device and the specimen. The main feature of the device is to have control on the width of crack during the test so that it allows measurement of the permeability of the specimens over a wide range of crack width in the third stage.

During this stage, the loading rate was selected 0.1 mm/sec. Since at high temperatures, the required energy for fracture test is high (Zhu, 2017), therefore, the room temperature (25 ± 1 °C) was adopted to distinguish better the reference and reinforced asphalt mixes. The displacement and applied force from the MTS press were recorded for each reinforced and reference specimen.

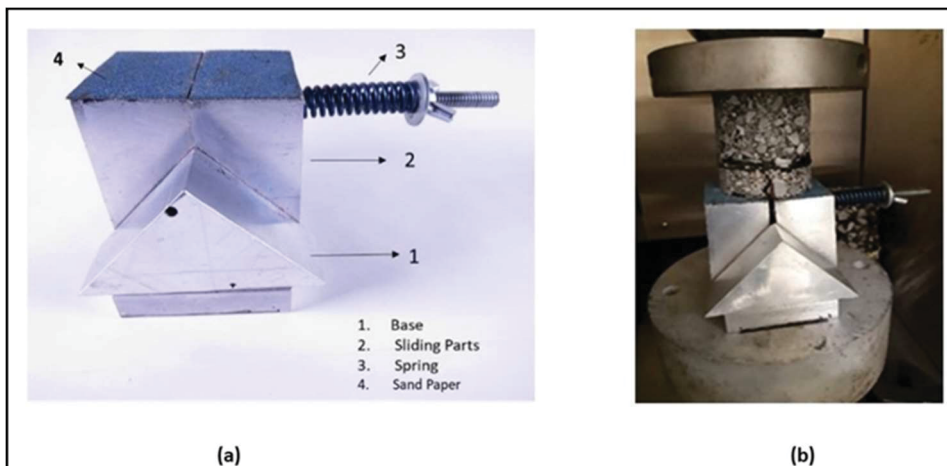


Figure 4.3 Crack Widening Device (CWD) (a) schematic design (b) test setup

4.4.2.3 Water-Vacuum Permeability Device (WVPD)

During this stage, the permeability of specimens in a cracked condition was measured. The permeability shows how fast water moves in a porous medium. Because the existing laboratory test methods, such as falling or constant head test methods, are basically suitable for high porosity materials, the water-vacuum permeability device (WVPD) was designed and assembled (Figure 4.4). The WVPD is a modified version of the falling head test method, which is basically suitable for an asphalt mix with low air-void content.

The device comprises a latex membrane to encompass the specimen, two porous stones placed on two ends, and a head that carries water to the top surface of the specimen. In addition, a mechanical pump was used to apply suction force (-100 kPa) to the bottom of the specimen in order to accelerate the movement of water through the specimen, and a cell was employed to apply a positive confinement pressure (+140 kPa) to restrain the percolation of water between the membrane and the specimen. By taking advantage of a stopwatch, the required time for a certain volume of distilled water (50 ml) to fall in a graduated cylinder was recorded and used as an input to calculate the permeability of the system in m^3/sec per meter length of crack.

It should be noted that under the effect of negative pressure applied during the permeability test, the water flow cross section may change and this in turn, affects the coefficient of permeability of the system. However, this method can be regarded as a suitable tool to evaluate the permeability of reinforced asphalt specimens against that of reference specimens through making comparison with the same crack width.

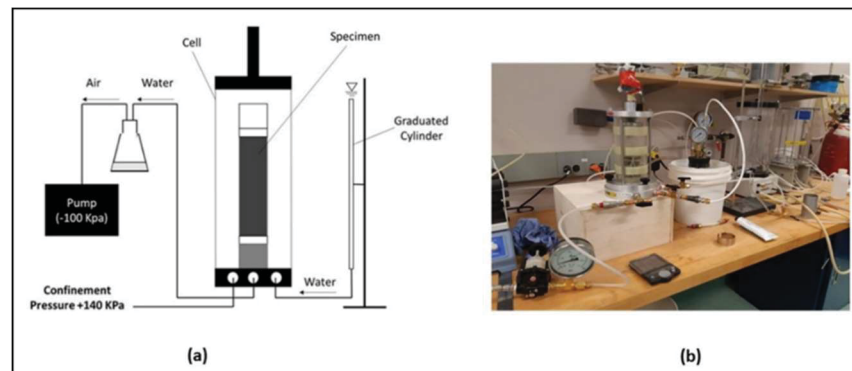


Figure 4.4 Water-Vacuum Permeability Device (WVPD) (a) schematic design (b) test setup

In order to make sure that during the permeability test, water moves only through the specimen, it is necessary to seal the entire system. This was accomplished by applying some grease, right below and above the specimen under the latex membrane, taking advantage of two pairs of elastic rings, along with the confinement pressure applied to the sides of the specimen in the cell.

Once the specimens were cracked to the desired width by taking advantage of the CWD, it was essential that they were fixed in their cracked positions by applying epoxy on the cracked wall because under applied confinement pressure, the crack would close. In order to prevent the puncture of the latex membrane under the influence of applied pressure due to the sharp edges, the sides of the specimens were taped.

4.5 Results and discussion

The results of the testing program are presented in this section. Specifically, the following subsections present the path and required force for crack formation in specimens with and without paving fabric. In addition, a comparison is provided between load - displacement relationships of reference and reinforced cases. Finally, the permeability test results and their changes with crack width are revealed.

4.5.1 Crack resistance and formation

Figure 4.5 illustrates the results of the crack generation test performed by 3-PBT at room temperature (25 ± 1 °C) on reinforced and reference specimens. The specimens on the right hand side of Figure 4.5 show the crack formation path from the tip of the notch to the top surface of the specimen under the influence of compressive load.

In addition, the values shown on the vertical axes of the diagram are the differences from the average force required for crack generation among 16 specimens of each type, recorded when the crack appeared at the top surface of the specimen. Based on the results obtained from the 3-PBT, the required force for crack generation under the influence of tensile stress for the reinforced specimens is 13.47 kN which is slightly higher than 11.58 kN for reference ones. In addition, the standard deviation (STD) of the results from mean force for reinforced specimens is equal to $STD= 0.264$ compared to $STD=0.747$ for reference specimens, which

shows the low variability of the results for reinforced specimens. Furthermore, since there is no overlap between standard deviation bars, the difference of mean values may be meaningful that needs to be confirmed by performing a statistical analysis such as Independent T Test to draw a valid conclusion.

The results obtained from the independent T test has shown in Table 4.4. The p-value is the most important statistic in this table. Since the p-value in one-tail and two-tail T tests is less than significance level, i.e. 0.05, the null hypothesis based on the equality of mean values are rejected.

Table 4.4 T-Test: Two-Sample Assuming Unequal Variances

| | | |
|------------------------------|----------|-------------|
| Mean | 13,459 | 11,520375 |
| Variance | 0,264532 | 0,747225125 |
| Observations | 8 | 8 |
| Hypothesized Mean Difference | 0 | |
| df | 11 | |
| t Stat | 5,451307 | |
| P(T<=t) one-tail | 0,0001 | |
| t Critical one-tail | 1,795885 | |
| P(T<=t) two-tail | 0,0002 | |
| t Critical two-tail | 2,200985 | |

In addition, based on the observation, when the crack reached to the paving fabric level, its path was redirected to the sides and followed two paths instead with a narrower width for all the reinforced specimens tested. While for reference specimens, the crack developed along a rather straight line from the tip of the notch to the top surface, as shown in the right hand side of Figure 4.5.

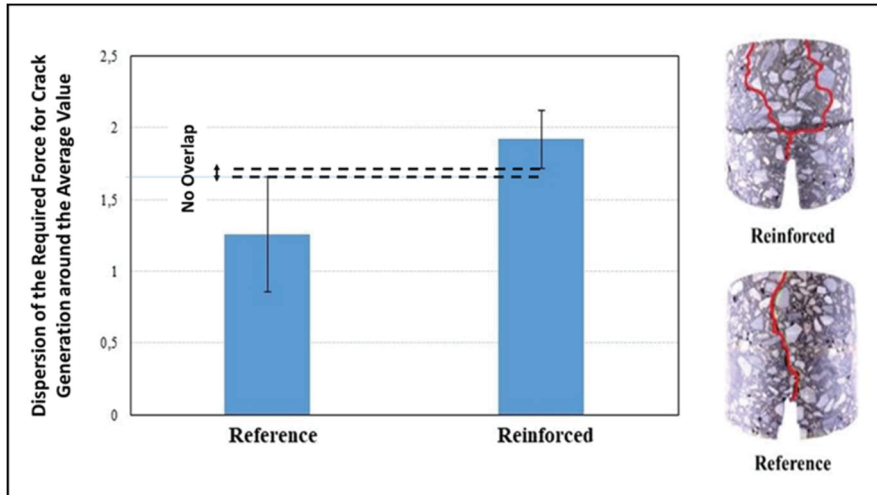


Figure 4.5 Comparative results in required force for crack generation and crack formation in reference and reinforced cases

4.5.2 Load-displacement relationship

Figures 4.6 provide the results of crack widening performed by the CWD on reinforced and reference specimens. Eight specimens in each case were tested under the effect of shear forces imposed at the bottom side of the specimens. The result of one reference specimen was removed from Figure 4.6-b because of failure at an earlier stage of the test.

As can be seen from Figure 4.6-a, most of the reinforced specimens followed a similar linear trend. Moreover, there is no discontinuity in the force, which means that the paving fabric could effectively transfer the shear stresses from the bottom to the top asphalt layer so that the entire system resisted the crack propagation. This reinforcement benefit can also be indicated through one-half higher maximum force undergone by reinforced specimens compared with reference ones. Another positive point of using paving fabric, inferred from Figure 4.6-a, is that there is a high degree of conformity among the load-displacement curves which in turn provides a reliable mechanical behavior of the reinforced asphalt overlay during its service life. However, for the reference materials, a wide discrepancy was found even though they follow a similar pattern from the initial point to the end. It starts with a linear part on which force and displacement have a linear relationship. Then, the behavior follows a non-linear proportionality with a decreasing rate until it reaches a maximum value at the interface between two asphalt layers based on the observations made during the test. Here after, a sudden fall in

force accompanied by a considerable deflection occurred which could be explained by the sliding of the upper asphalt layer over the bottom layer. After that, a hardening effect was manifested by an increasing rate in the force-displacement curve from the resistance of the top asphalt layer until the specimen breaks under pressure.

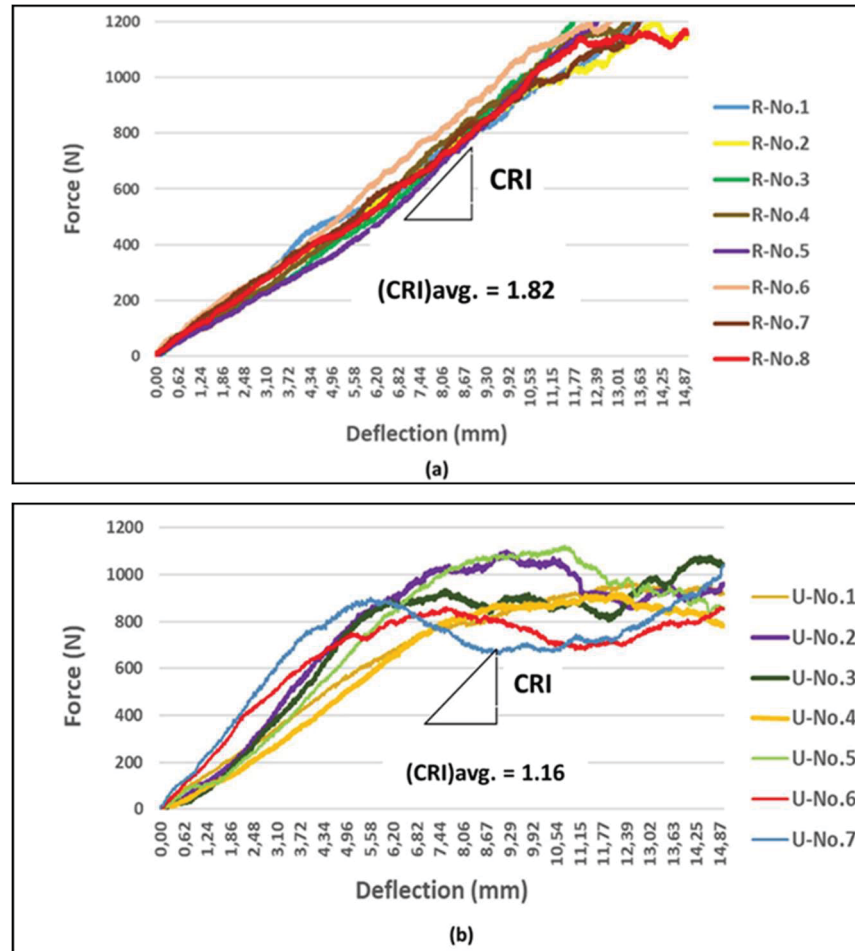


Figure 4.6 Load-displacement behavior of specimens under the influence of shear stresses (a) reinforced case (b) reference case

Another valuable finding from Figure 4.6 is that, for all the specimens, there are linear parts, whose slope can be treated as an index for the resistance of the system against crack growing. As can be seen, In reinforced case, there is just one slope from the initial point to the end, while for the reference case, there are two different slopes indicating the resistance of two asphalt layers against crack propagation that needs to be averaged to better reflect the resistance of the whole system. Based on the comparison, on average, the reinforced specimens have notable

crack resistance index compared with the reference materials, which in turn could result in higher structural capacity of the system.

4.5.3 Water permeability result

Prior to performing the permeability test, the crack-widening test was performed on 8 specimens of each case (reinforced and reference) in order to obtain a variety of crack widths. Then the widths of cracks were measured at the top of the specimen with a digital microscope, as shown in Figure 4.7, and at the bottom via caliper. This measurement was conducted from two aspects: 1) to obtain the same width of crack at the bottom surface of reference and reinforced specimens in each step of the permeability test and 2) To compare the width of crack reflected at the top surface due to the propagation process.

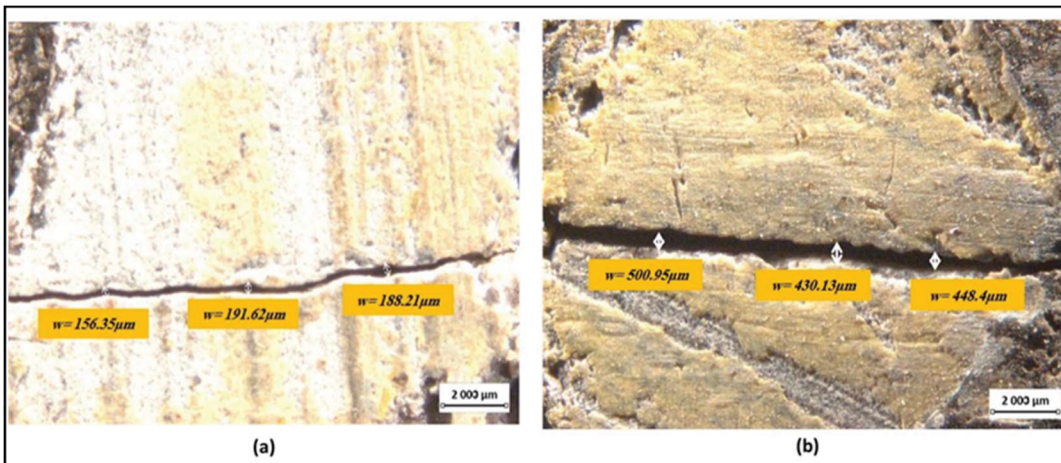


Figure 4.7 Typical view of crack at the top surface of the specimen measured by microscope for (a) reinforced and (b) reference specimens

Figure 4.8 shows the result of the permeability test for a variety of widths of cracks for specimens without paving fabric. However, no permeability was recorded for specimens with paving fabric used in this study with almost the same width of crack at the bottom surface within 24 hours of running the tests.

From Figure 4.8-a, the variation in crack width reflected at the top surface for the same crack width at the bottom for reference and reinforced specimens has been depicted. It can be seen, for reinforced materials, the crack width is considerably lower. This seems to be due in part to the fact that the paving fabric dissipates some of the stress coming from the bottom. Also, the

changes in crack width at the top for reference material, to a great degree, are dictated by the width of crack at the bottom, while this is not the case for reinforced materials.

Finally, Figure 4.8-b demonstrates the variations in permeability as a function of the crack width at the top surface of the specimen. It can be seen, when the crack becomes wider, the permeability increases. This relationship can be described by a polynomial equation of second order, as indicated on Figure 4.8-b. Moreover, despite the permeability test for reference and reinforced materials being performed with the same width of crack at the bottom, no flow rate was recorded during 24 hours of the test. This proves the waterproofing benefit that using paving fabric could bring for the entire compound system.

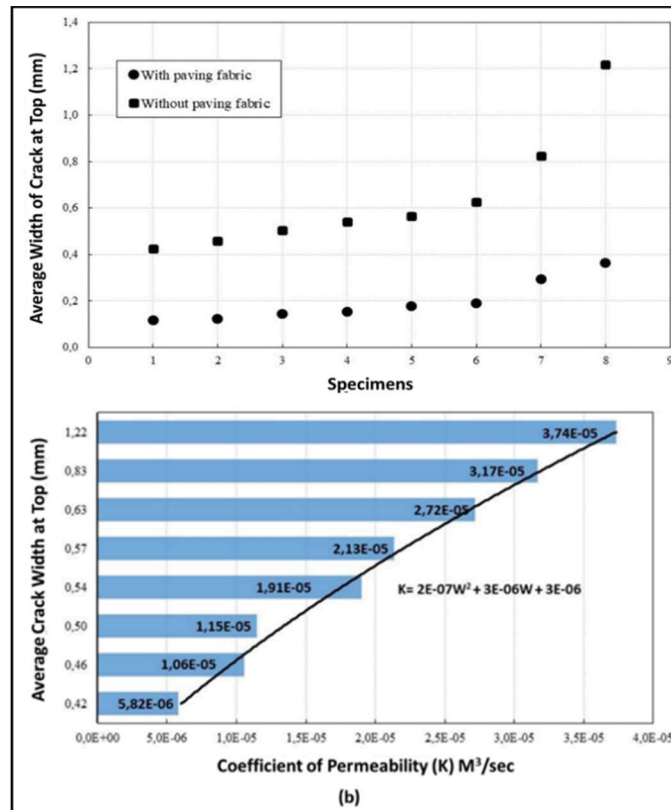


Figure 4.8 The result of permeability tests: (a) the width of crack at the top surface measured with a digital microscope for reference and reinforced specimens; (b) the results of permeability tests on reference specimens

4.6 Conclusion

In this study, new experimental methodologies were employed to investigate the effect of inclusion of paving fabrics on the mechanical behavior of the asphalt layer. To this end, two types of specimen, one with paving fabric and the other without, as the reference material, were used. 3-PBT and CWD were developed to simulate the crack initiation and propagation at laboratory scale. At first, the mechanical performance of specimens was quantified in terms of the crack width and crack resistance index (CRI) of the system and then, the permeability of the reference and reinforced materials were evaluated at a variety of crack widths through the proposed WVPT method. Based on the results obtained from this experimental study, the following conclusions could be drawn:

- Because the reflected cracks at the surface have 3 times lower width, the possibility of water infiltration and the following erosive effects would considerably reduce in the case of using paving fabrics in asphalt overlays.
- The required force in 3-PBT for the crack to reach the surface of a new asphalt overlay is almost 13 percent higher for reinforced specimens.
- Based on the laboratory results, the water-vacuum permeability test method is an effective tool to evaluate the waterproofing effect of pavement systems with paving fabrics in a cracked condition based on the comparison between the coefficient of permeability in reinforced and reference specimens at the same width of the crack.
- The result of cracking tests (crack generation and propagation tests) showed that the inclusion of paving fabric could enhance the crack resistance of the entire system as much as 60 percent. In addition, it makes the mechanical behavior of asphalt overlay more predictable, an issue associated with typical asphalt overlays implemented on cracked existing asphalt layers.
- The methodology developed in this study can be employed to evaluate the performance of any interlayer systems in an overlay and even to investigate the quality of typical asphalt overlays implemented on the existing surface in terms of its adhesion to the old asphalt surface and its adequacy to seal the pavement structure.

CHAPTER 5

EXPERIMENTAL MEASUREMENTS OF INTERFACIAL MECHANICAL PROPERTIES BETWEEN REHABILITATED BITUMINOUS LAYERS USING INNOVATIVE APPROACHES

Ehsan Solatiyan^a, Nicolas Bueche^b, Alan Carter^c

^{a, c} Department of Construction Engineering, École de Technologie Supérieure (ÉTS),
1100 Rue Notre-Dame O, Montréal, QC H3C1K3, Canada

^b Department of Architecture-Wood-Civil Engineering, Bern University of Applied Sciences
(BFH), Pestalozzistrasse 20, CH-3401 Burgdorf, Switzerland

Paper accepted for publication in *Materials in Civil Engineering*, September 2020

5.1 Abstract

Bituminous pavements frequently fail at an early age well below the predicted design life, which in turn necessitate taking rehabilitation actions to recover the serviceability to an acceptable level for the users. Two rehabilitation techniques have been the focus of the engineering community: a traditional method known as the mill and fill and the other, which attracts increasing interest, is to take advantage of an interlayer before resurfacing. This rehabilitation technique is more challenging from the theoretical point of view since the traditional test methods need to be adapted to capture the mechanical properties that, in the presence of the interlayer, may emerge.

On this ground, the focus of this paper is to gain an in-depth understanding of mechanical properties developed at the interface between two asphalt layers as in an unreinforced case and between a layer of paving fabric (a system composed of binder and synthetic fabric) and asphalt layers as in a reinforced case. To achieve this goal, three main properties were addressed: the anti-reflective property of the interface against crack propagation was examined via a modified 3-Point Bending Test (3-PBT) by calculating the J-integral and measuring the crack width below and above the interface. Besides, the stiffness properties in two perpendicular directions

at the interface were separately studied through novel approaches to finding out the possible mechanical effects induced by the interlayer on structural responses of a composite structure. The experimental results derived from this study revealed that the reinforced interface, including the paving fabric, had about 5 times the higher capacity in delaying the propagation of bottom-up cracking than unreinforced one. However, this promising result was accompanied by 2.5 and 1.5 reductions in bonding quality and dynamic modulus, respectively, at the reinforced interface, which in turn necessitates introducing the real mechanical behavior of the reinforced system into design methods.

5.2 Introduction

Bituminous pavements are subjected to premature failures arising from the application of improper design methods, high traffic loads, and severe environmental changes. Overlaying a deteriorated surface with a thin HMA overlay (usually between 25 to 50 mm) has been adopted over the years as a common technique to restore the structural integrity of the pavement system to an acceptable condition. However, this traditional method has been plagued with the reappearance of existing cracks and discontinuities to the new surface, known as reflective cracking. This phenomenon has been identified as the most serious issue associated with asphalt overlays (Cleveland et al. 2002; Dempsey 2002; Engle 2001; Bhosale et al. 2008; Khodaii et al. 2008; Solatiyan et al. 2020a). Although a variety of factors are responsible for the occurrence of reflective cracking in bituminous pavements, the principal sources are attributed to the horizontal and vertical movements induced by the combined effects of traffic loads and temperature oscillation (Palacios et al. 2008; Von Quintus et al. 2007; Moses 2011; Vervaeche et al. 2008).

The engineering community has battled reflective cracking for years by adopting various measures (Kretor and Gorelysheva 2000; Mukhtar and Dempsey 1996; Vespa 2005; Brown et al. 2001). Among them, taking advantage of stress-relieving interlayers such as paving fabrics (a system composed of bitumen and non-woven fabric) to delay reflective cracking, have drawn a lot of attention over other alternatives from practical and economic points of view. Paving fabrics are able to absorb the energy induced at the tip of the crack by their horizontal elongation without transferring large tensile stresses to the fresh asphalt overlay (Solatiyan et

al. 2020b). Notwithstanding, the presence of paving fabrics may lead to debonding between asphalt layers and adversely affect the structural integrity of the pavement system in terms of horizontal and vertical stiffness (Hakim 2002; West et al. 2005). Consequently, the occurrence of distresses such as top-down cracking, slippage cracking, and surface delamination in zones with high horizontal shear loads would be inevitable (Canestrari et al. 2015; Charmot et al. 2005; Zamora et al. 2011). On this basis, a legitimate measurement to quantify the mechanical properties of a reinforced system is of paramount importance for the betterment of interpretation of factors involved in reinforced pavement design methods.

5.3 Research background

Paving fabrics are typically employed at the bottom of the asphalt overlay to prevent infiltration of water to the underlying untreated layers, thus maintaining the structural capacity of the pavement system for a more extended period of time. This advantage was highlighted by measuring the coefficient of water permeability with Water Vacuum Permeability Device (WVPD) in a variety of crack width and then comparing the results with control specimens (Li et al. 2013; Solatiyan et al. 2020b). Another benefit of the application of paving fabric brings into a new asphalt overlay is to retard the propagation of reflective cracking (Amini 2005; Elseifi 2003). This benefit can be described as follows (Elseifi 2003): the existing discontinuity in the asphalt surface starts to grow upward due to movements driven by temperature and/or traffic loads as long as it crosses the interface. Afterward, the paving fabric elongates along its axial direction and absorbs a large part of the energy of the crack, which in turn, delays the vertical crack growth. By mobilizing enough energy from further movements, the crack restarts to propagate from a new deviated location to the surface. A field study conducted at the Illinois Department of Transportation (IDOT) illustrated that the delayed action of paving fabric on reflective cracking could extend the mean service life of asphalt overlay for up to 2 years (Buttlar et al. 2000).

Nevertheless, the shear strength of the rehabilitated system, which is substantially controlled by the bonding condition at the interface of attached layers is another crucial design consideration, which plays a pivotal role in the redistribution of stresses and delaying reflective cracking (Sudarsanan et al. 2018; Raab et al. 2017; Noory et al. 2018; Panda et al. 2013; Jaskula

and Rys 2017). To comparatively evaluate the quality of bonding provided at the interface, a great variety of laboratory devices, which basically measure the shear strength under the effect of static or dynamic loadings, have been developed. Marshall stability loading press (Molenaar et al. 1993), Ancon Shear Testing Research and Analysis (ASTRA) (Canestrari et al. 2005), Swiss LPDS Tester (Roffe and Chaignon 2002), Sapienza Inclined Shear Test Machine (SISTM) (D'Andrea and Tozzo 2012), FDOT Bond Strength Device (Sholar et al. 2004), ATACKER™ Device (ATACKER 2005), Tschegg Device (Tschegg et al. 1995), Krakow Technological University test device (Grzybowska 1993), Amirkabir University of Technology Shear Lab Tester (AUT-SLT) (Noory et al. 2018), Louisiana Interlayer Shear Strength Tester (LISST) (Bae et al. 2010) and Advanced Shear Tester (Zofka et al. 2015) are just a few to name. However, because of the complexity of these pieces of equipment, the details pertaining to the test conditions and their procedures are, to a great extent, ambiguous and the results suffer from heterogeneity. In addition, the test methods designed to take advantage of the Marshall testing device employ a constant rate of displacement of 50 mm/min, which often exaggerates the shear strength (Sudarsanan 2018, Solatiyan. et al. 2020a). As for the geometry of the specimens, a cylindrical shape of 100 mm or 150 mm in diameter is usually employed, and the preparation of cylindrical specimens are time-consuming in terms of coring and grinding. Also, the specimens are either glued into plates or gripped into molds. Because of the uncertainty in the quality of gluing and easy handling, clamping mechanism outperforms other handling methods (Raab 2010). Another common factor between different shear test devices is the gap width provided at the interface, which ranges from 0 to 10 mm. A small gap may not be enough to take the thickness of the interlayer into account, while a big gap width results in variability of the results due to the effect of bending accompanied by shearing (Raab 2010). Limited thickness of the asphalt layer is another barrier in shear test devices designed based on the Leutner method. To overcome this deficiency, attaching the steel plates at two surfaces was recommended to enlarge layer thickness (Sutanto 2009). It is, therefore, essential to develop a shear test method that covers the above-mentioned points.

Additionally, it is evident that introducing a layer of paving fabric between asphalt layers leads to a change in axial stiffness of the combined system, which in turn could affect the structural response in terms of stress and strain distribution. According to the literature, this matter was

not the subject of any previous studies, and there is a lack of a rheological model to realistically describe the mechanical behavior of the reinforced system as a whole and the reinforced interface with paving fabric. However, in case of the implementation of geogrid between asphalt layers, a laboratory study showed that the 2 Springs, 2 Parabolic Elements, and 1 Dashpot (2S2P1D) model could be utilized to predict the mechanical behavior of the reinforced interface (Freire et al. 2018).

On top of that, plenty of studies have been conducted to evaluate the influencing factors on interlayer shear strength such as the type of mix, type of geosynthetic materials, temperature, the dosage of tack coat, surface roughness and loading rate (Brown et al. 2001; Pasquini et al. 2014; Saride and Kumar 2017; Kumar et al. 2017; Walubita et al. 2018, Solatiyan et al. 2020a). However, only limited studies have concentrated explicitly on paving fabric as an anti-reflective interlayer placed between different mixes, while over 24000 lane-Km of paving fabrics are implemented annually in North America (Carmichael and Marienfeld 1999). Furthermore, the computation of the interlayer bonding condition has also not been the focus of these studies. In this context, there is a lack of methodology, which adequately provides a connection between interlayer test results and the ability of paving fabrics to mitigate the energy and width of reflected cracks.

The objectives of this study are to evaluate the impact of the addition of a paving fabric on the stiffness at the interface of a reinforced pavement system and to evaluate the reflective cracking resistance of this system. More precisely, a comparative study of the influence of paving fabrics on stiffness properties at the interface in two orthogonal directions through innovative approaches was performed first. Then, by adopting new instrumentation for the 3-point bending test, the potency of paving fabrics to mitigate reflective cracking in terms of the width of the reflected crack and the dissipated energy required for crack initiation and propagation was quantified.

5.4 Experimental program

This research aimed at assessing the contribution of paving fabrics on the mechanical performance of the reinforced asphalt overlay. To this purpose, double-layered specimens, composed of three different types of mixes with and without paving fabric at the interface,

were prepared in the laboratory to simulate the field characteristics. Given that the reinforcement effect of paving fabric largely relies on its friction with adjacent materials, it was assumed that different types of mixes might result in changes in the mechanical behavior of the reinforced interface. For this purpose, the interface shear test and complex modulus test with specific configurations were designed to measure and highlight the differences in terms of horizontal and vertical stiffnesses at the interface of unreinforced and reinforced specimens. Besides, a new methodology to perform a 3-point bending test with three crack gauges installed at different locations was proposed to gain an insight into crack generation and propagation behavior from an existing discontinuity to the surface.

5.4.1 Materials and Specimen Preparation

In this study, three different types of asphalt mixtures, commonly used in Quebec (Canada), were designed according to Transport Quebec's standard (LC 4202) for experimental investigation: (I) a surface course mix with a nominal maximum aggregate size (NMAS) of 10 mm (ESG-10); (II) a binder course mix with an NMAS of 14mm (ESG-14); and (III) a base course mix with an NMAS of 20 mm (GB-20). The designed aggregate gradations of mixes are shown in Figure 5.1 and pertinent technical specifications are summarized in Table 5.1.

The paving fabric is composed of two essential elements: a needle-punched nonwoven fabric along with an asphalt binder PG 64-34 as an adhesive material. The main physical properties of the fabric, supplied by the company, are presented in Table 5.2. In order to seek for the effect of the type of mix on mechanical properties at the interface, the paving fabric was inserted between the layers of two types of structures: one ESG-10 as a surface course and ESG-14 as a binder course and the other ESG-14 as a binder course and GB-20 as an asphaltic base course. The same structures without paving fabric were also fabricated as a benchmark, which simulates the traditional method of overlaying with a tack coat, to make a comparison between the results.

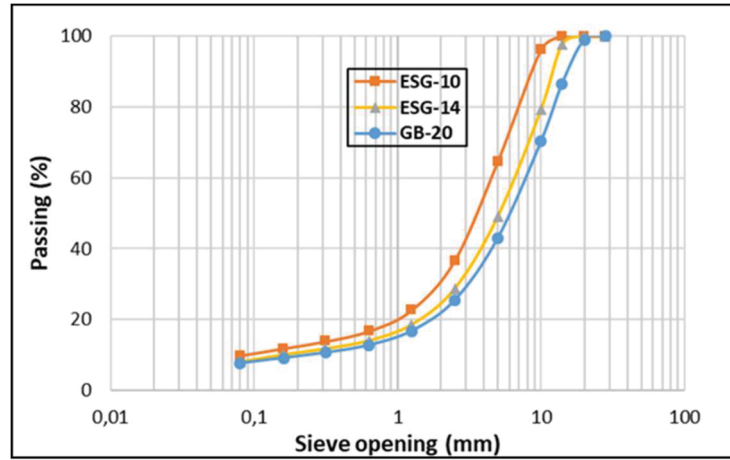


Figure 5.1 Gradation curves of mixes

Table 5.1 Experimental design

| Technical specifications of mixes | | | | | |
|---------------------------------------|----------|--|---------------------------|---------------------------|--|
| Mixture | | ESG-10 | ESG-14 | GB-20 | |
| Binder Type | | PG 58-28 | PG 58-28 | PG 58-28 | |
| Binder Content (% mass) | | 5.45 | 5.22 | 5.14 | |
| Air Void Content (%) (ASTM D2726M) | | 2.2 | 3.6 | 4.8 | |
| Water Sensitivity (LC 26-001) (%) | Measured | 97.3 | 85.5 | 86.5 | |
| | Required | ≥ 70 | ≥ 70 | ≥ 70 | |
| Rutting Resistance (LC 26-410) (%) | Measured | After 1000 = 6.6 After 3000 = 8.2 | 7.2 | 9.1 | |
| | Required | (After 1000 cycles) ≤ 10 (After 3000 cycles) ≤ 15 | (After 30000 cycles) ≤ 10 | (After 30000 cycles) ≤ 10 | |

Table 5.2 Main Technical Specification of Fabric (Supplied by the Company)

| Specification | Test Method | Unit | Value |
|-------------------------|-------------------|------------------|---------|
| Grab tensile elongation | CAN 148.1 No. 7.3 | % | 45–105% |
| Grab tensile strength | CAN 148.1 No. 7.3 | N | 550 |
| Mullen burst | CAN 4.2 No. 11.1 | kPa | 1585 |
| Bitumen retention | ASTM D6140 | L/m ² | 1.15 |

The mechanical properties at the interface were examined using double-layered specimens taken from small-sized laboratory asphaltic slabs. The preparation of each slab was conducted by bonding two different small plates (i.e., ESG-10 over ESG-14 and ESG-14 over GB-20) of 500 mm in length and 180 mm in width. For the sake of shear and crack resistance tests, the thickness of each plate was chosen at 50 mm, while for the complex modulus test, a 75 mm thickness for each plate was required.

The composite structure was made first by the preparation and compaction of the bottom layer, followed by the application of tack coat (with/without fabric) and then the implementation and compaction of the upper layer over the bottom layer. The compaction procedure was carried out according to the French Roller Compactor, complying with European Standard EN 12697-33, at 135 ± 2 °C in accordance with the type of bitumen (i.e., PG 58-28) employed in this research.

To ensure the monolithic action of the composite structure, asphalt emulsion type SS-1h with the dosage of 180 gr/m² of residual bitumen (i.e., 59.6%) was used as tack coat in control slabs between two asphalt plates, while 110 gr/m² of a PG 64-34, according to the specification provided by the company, was applied as an adhesive agent between fabric and the bottom asphalt plate for the reinforced systems. It needs to be underlined that for the complete breakage of the asphalt emulsion, five hours curing time was assigned before the implementation of the upper asphalt layer, while for the reinforced structure, the dispersion of adhesive and overlayment process were performed one after another with no delay.

A total of 12 slabs were assembled for both reinforced and unreinforced structures: eight out of 12 had a total thickness of 100 mm assigned for crack resistance and shear tests and four slabs, with a total thickness of 150 mm, for complex modulus test. The shape and dimension

of specimens employed for crack resistance and shear tests were cubes by size $80 \times 80 \times 80$ mm (sawed in slabs), and for complex modulus test was cylinders by size 75×135 mm (cored in slabs). The arrangement and physical dimension of the specimens are schematically demonstrated in Figure 5.2. The specimen preparation pertaining to each test will be described later.

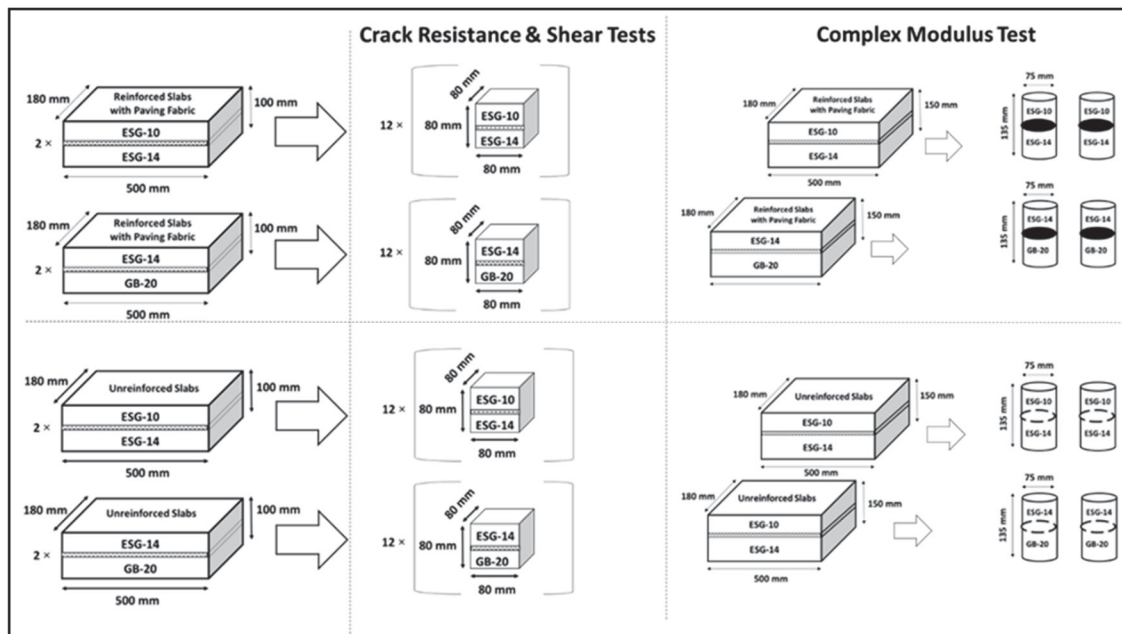


Figure 5.2 Schematic presentation of the shape and number of specimens for each type of test

5.4.2 Test Methods

In this research, an effort was devoted toward gaining an in-depth understanding of mechanical characteristics of a reinforced interface with a layer of paving fabric and then extracting the differences with a reference interface, which more commonly exists in practice. To this end, the 3-Point Bending Test (3-PBT) with a new set-up was employed to see how the insertion of the paving fabric between different types of asphalt layers affects the initiation and propagation of the crack from an existing notch in the structure, in terms of crack width below and top of the interface, and the dissipation of energy required for crack opening in mode I.

Furthermore, from the stiffness perspective, novel approaches were adopted to investigate the structural response of the composite structure to the horizontal and vertical displacement

induced at the interface. In this context, a new version of the slant shear device was developed to measure the main interface properties in the tangential direction of the in contact layers, including shear strength, shear stiffness, and sliding coefficient. Besides, a new arrangement of complex modulus test in the tension-compression mode of loading was tested to inspect the differences in structural responses in various levels of specimen normal to the interface at a variety of frequencies and temperatures.

It was postulated that the presented methodologies would result in better insight into mechanical properties at the interface. The following subsections describe in detail the test methods taken into account for this project.

5.4.2.1 3-point bending test (3-PBT)

This test was initially designed to simulate the mode I of crack generation and propagation on cylindrical specimens reinforced with paving fabric (Solatiyan et al. 2020b). However, for the sake of this project, the cubic shape specimens were substituted to provide a flat surface for crack gauge installation. Three sets of crack gauges were employed, as shown in Figure 5.3-a: one at the bottom to control the starting point of the crack propagation, and the two others to measure the crack width under and over the interface during the crack propagation stage to have a better insight into the anti-reflective cracking properties provided at the interface. Moreover, by taking advantage of a vertical linear variable deflection transformer (LVDT) to measure the vertical displacement, fixed on a thin narrow aluminum plate attached to the bottom of the specimen, the pre-cracking and post-cracking behaviors of double-layered specimens were evaluated by developing force-displacement curves (Fig. 5.3-c). Also, in order to provide enough space for the specimen movement during bending while assuring the stability of the system, the equipped specimen accompanied by the rolling supports were placed on a U-shape basis, as shown in Figures 5.3-a & 5.3-b.

The test was performed in a displacement control mode at a rate of 2 mm/min, and at the ambient temperature of 20 ± 1 °C according to ASTM D8044-16, since at low or high temperatures, it is difficult to differentiate between the asphaltic specimens in terms of non-linear energy release rate (Zhu et al. 2017) and also it is remarked that bottom-up cracking more frequently appears in intermediate temperature (Gauthier 2012). Moreover, for the study

of the fracture energy, three different depths of notches, which acted as stress concentrators with a notch to depth ratio (a/W) ranging from 0.250 to 0.375 were made at the midpoint of the bottom side of each double-layered specimens by a water-cooled masonry saw with a 3.5 mm wide blade according to ASTM E399 (ASTM E399; Ahmed et al. 2012). It is worth mentioning that using higher a/W ratios may result in biased test results due to the specimen's weight. The test results and the pertaining discussion will be introduced later.

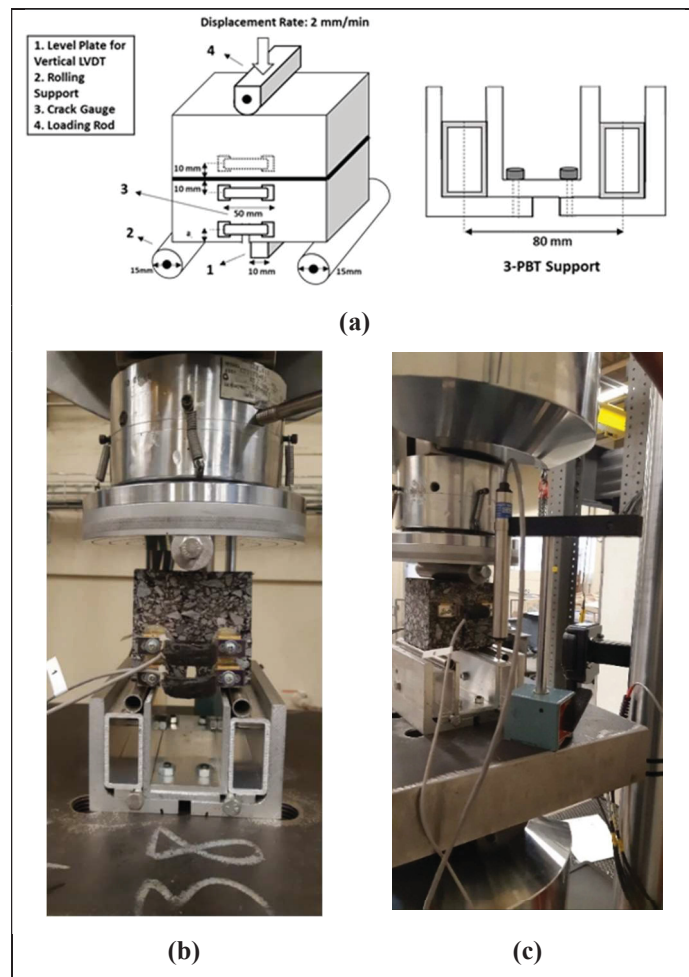


Figure 5.3 Scheme of 3-PBT: (a) schematic design; (b) test setup; (c) vertical displacement measurement by an LVDT

5.4.2.2 Interface shear test

Concerning the shear test, an effort was devoted toward developing a new test method, which was not complicated in terms of configuration and specimen installation and able to measure the shear properties at the interface, including an interlayer compressed between two different types of asphalt layers with the same thickness. For this purpose, the slant shear device, previously employed in the cement concrete realm (Diab et al. 2017; Liu et al. 2018), was adopted with some modifications in its structure. Figure 5.4-a illustrates a schematic of the device designed for this project. The device, which runs in a monotonic loading condition of 2mm/min (same as in 3-PBT), is composed of two aluminum pieces, one movable over a rail track and the other fixed with a screw to the loading arm of an MTS press (MTS-810). Putting the pieces with the same dimensional size, one over the other, provides enough space to accommodate a double-layered cubic specimen of 80 mm in thickness, leaned on a 45° inclined surface. This configuration allows us to mimic the actual loading condition in which the interface experiences both the vertical and shear loads at the same time. It is believed that the effect of the type of mixture in terms of surface texture on shear strength becomes significant when the normal load is applied at the interface (Noory et al. 2019). Another noteworthy feature of the developed method is the horizontal movement of the bottom part on a frictionless track, which can prevent crushing the specimen during loading (Figure 5.4-b). Furthermore, the horizontal movement was recorded by taking advantage of an LVDT, magnetically attached to the bottom-loading arm of the press (Figure 5.4-c).

As far as the gap width is concerned, it was proven that its influence is of paramount importance in the case of shear strength of an interface composed of two comparable layers in gradation and mechanical characteristics (Raab 2010). Under such conditions, taking a large gap width leads to less concentrated shear stress at the interface, which in turn could result in underestimation of the shear strength. In this project, from a practical point of view, the gap width between the device and the interface, according to Figure 5.4-c was considered 5 ± 1 mm, which was earlier employed in the Sapienza Horizontal Shear Test Machine (D'Andrea and Tozzo 2012).

As for the test temperature, the moderate temperature, equals to the one selected for the crack resistance test (i.e., 20 ± 1 °C), was considered from different perspectives: (I) a significant

dependency of the shear test to the temperature (Raab 2010); (II) to lessen the danger of damaging to the specimen and the device during the test at high or low temperatures. However, it is interesting to note that the flexibility of the device allows us to perform the shear test in a wide range of temperatures and frequencies under haversine kind of loading, which will be the subject of further research.

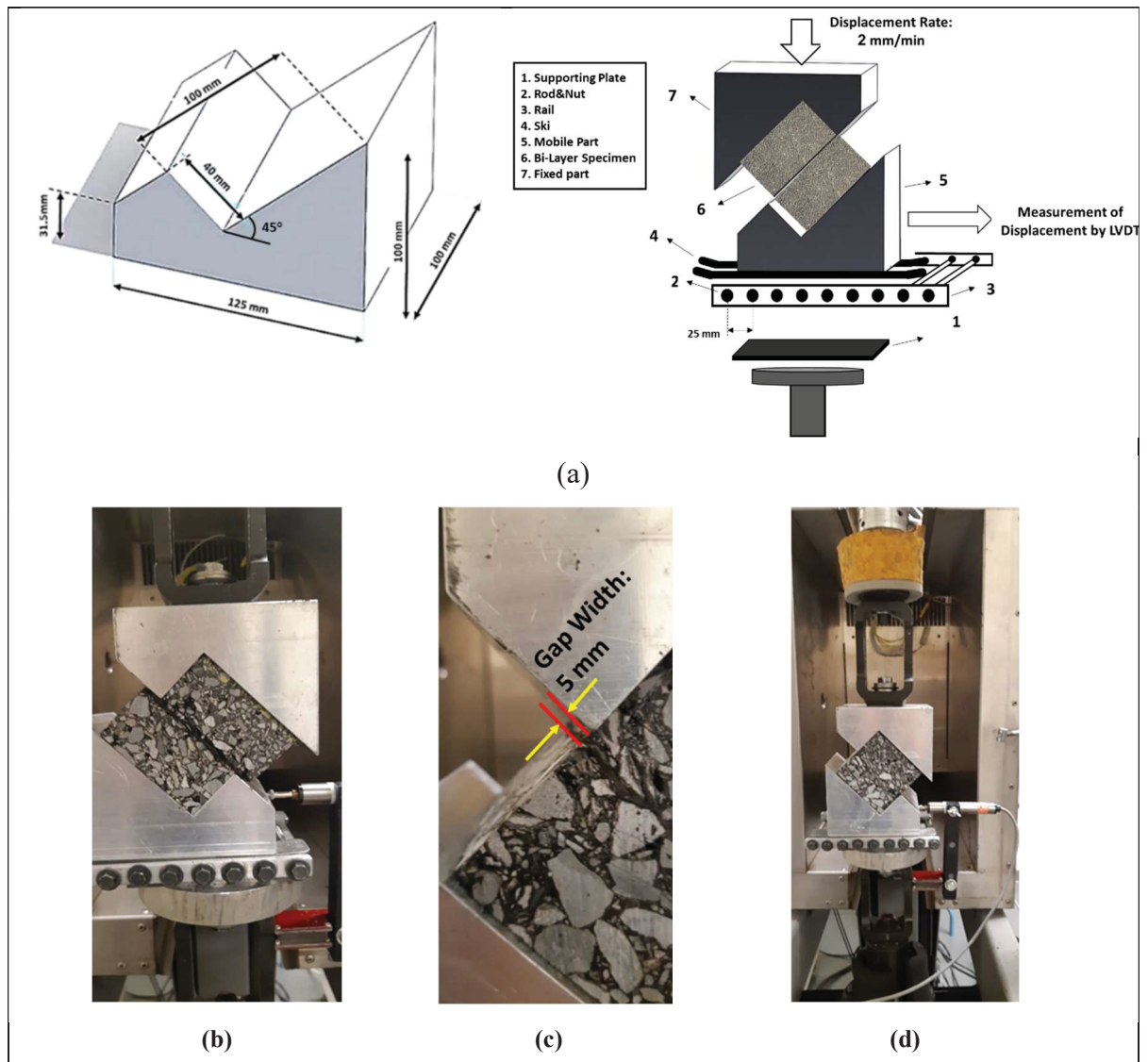


Figure 5.4 Scheme of modified slant shear device: (a) schematic design; (b) freely movement of the bottom part on rail track; (c) gap width provided at the interface; (d) test setup

5.4.2.3 Complex Modulus Test

The viscoelastic behavior of asphalt mixtures could be reflected by performing the complex modulus test at a low strain level. Among different types of loadings employed to perform this test, a tension-compression sinusoidal loading mode, applied in the longitudinal direction of the glued specimens, was selected for the purpose of this project because of its popularity in simulating the real field situation that mixture could undergo. The test was carried out in a servo-hydraulic Material Testing System (MTS 810) with a loading capacity of 100 kN and a ± 50 mm axial stroke in a controlled strain amplitude (Basueny et al. 2016). The temperature of the specimen was monitored during the test in a thermal chamber by taking advantage of three sets of surface temperature probes (PT100), fixed to the side of the specimen with a rubber band.

The specimen preparation was carried out with respect to Transport Quebec's standard (LC 26-690). On this basis, the prepared slabs were initially cut using a sawing machine in two pieces to obtain two asphalt blocks of 250 mm \times 180 mm \times 100 mm. The ends of the blocks were then further cut to obtain two blocks of 150 mm \times 180 mm \times 100 mm. From the center, two cylindrical test pieces of 75 mm (± 1 mm) in diameter by 150 mm in height were cored perpendicular to the compaction direction. Finally, the ends of the specimens were leveled with a precision saw and grinding machine to make test pieces 75 mm in diameter and 135 mm (± 2 mm) in height and glued to the caps. According to the standard, the coring was performed 24 hours after the completion of compaction. Also, the cored specimens were cured one week before the test at ambient temperature and humidity by laying them on their longitudinal axis on a soft sand bed covered to the center.

The mean values of strain measurements derived from three couples of extensometers with different initial length (i.e., 25 mm, 50 mm and 100 mm) located at 180 °C from one another, were employed to determine the axial strains induced at different height of the specimen (Figure 5.5-a). Special attention was also paid during mounting the extensometers so that a half-length of each extensometer was placed on each side of the interface, and that the extensometers were aligned with the loading axis. The average of measurements made by two 25 mm extensometers was assigned to monitor the strain amplitude to assure the linear viscoelasticity behavior of the material during the test. Moreover, the data acquisition was

conducted in 100 points per cycle (100 Hz), and the quality of signals in two successive cycles was controlled through a quality index (QI) defined by the dispersion of the measured data compared to a sinusoidal function. The data with high QI (i.e., $\geq 15\%$) were removed. Figure 5.5-b shows the configuration of the test and Figure 5.5-c illustrates the instrumented specimen from the top and side views.

Furthermore, the test was repeated on two replicates of each type of reinforced and unreinforced structures. Also, eight different temperatures varied from -35 to $+35$ °C, and 7 different frequencies ranged from 10 to 0.01 Hz were selected to cover all the impact of temperature and frequency variations and their possible combinations, compatible with Canada's roads.

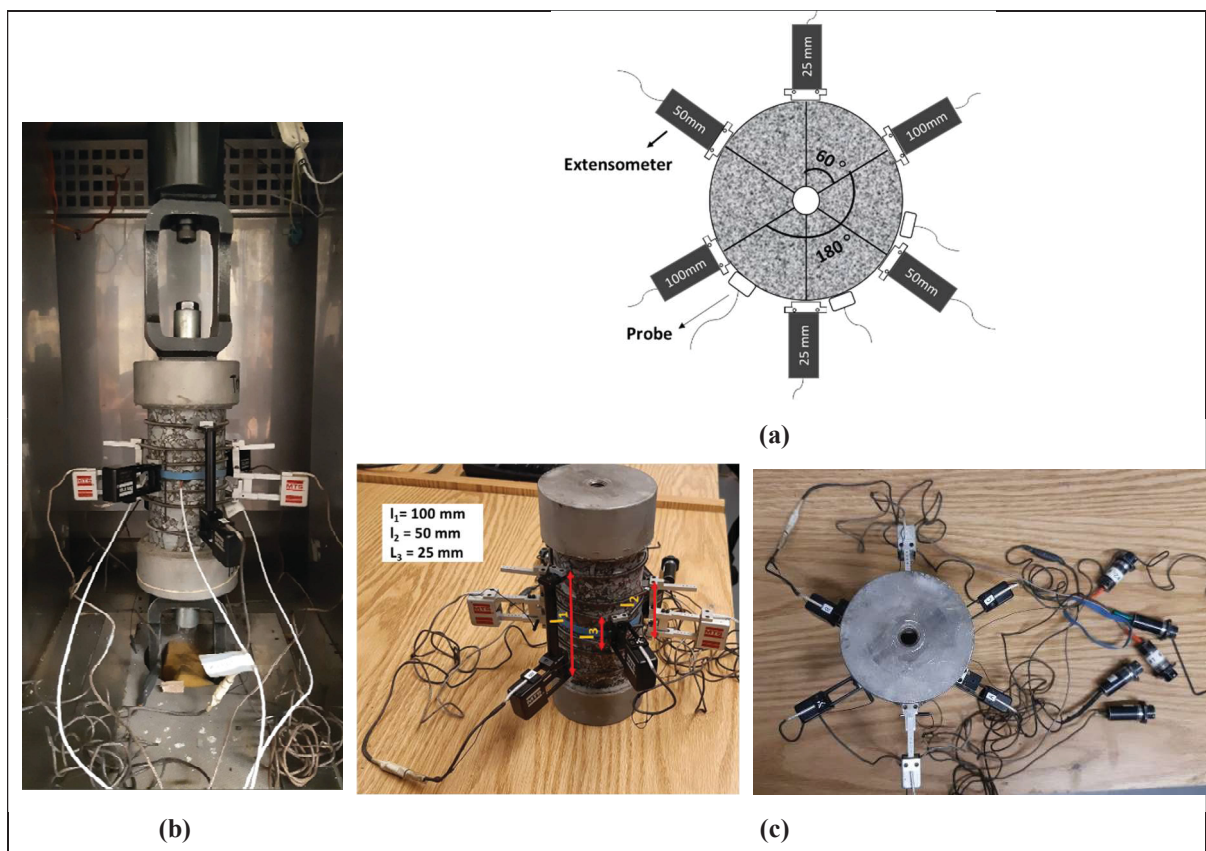


Figure 5.5 Scheme of adjusted complex modulus test: (a) the arrangement of extensometers with different initial length around the specimen; (b) instrumented specimen in the thermal chamber; (c) side and top views of the instrumented specimen.

5.5 Results and discussions

In this section, the mean results obtained from each type of test are introduced and discussed in detail. Specifically, the following subsections disclose the anti-reflective properties of reinforced and unreinforced specimens. In addition, the stiffness characteristics in two perpendicular directions at the interface are discussed in detail.

5.5.1 Results and Discussions on Anti-Reflective Properties at the Interface

Figure 5.6 demonstrates the load-displacement curves obtained from the average of three replicates of 3-PBT in three distinct depths of notches for four different types of structures studied in this research. It is worth mentioning that the coefficient of variance (COV) of the maximum loads in each depth of notch were controlled to be lower than 25%, which could be regarded acceptable according to the specifications of an ideal cracking test given by the NCHRP 9-57 (Zhou et al., 2017). Also, Table 5.3 provides an average of dimensional details of handmade notches and relevant calculations of the area surrounded by the load-displacement curves and the J-integral.

It can be observed that the curves for each type of structure followed a rather similar trend from the beginning of the loading up to the failure point with different depth of notches and within each type of structure, and the values of maximum deflection at failure were somewhat close to each other. Besides, it was found that all the specimens in different types of structures have an initial linear part, which can be explained as the pre-cracking phase. During this phase, the presence of the interlayer has no significant effect on the mechanical behavior of the double-layered specimen. However, in the crack propagation phase, the reinforced and unreinforced structures have entirely different patterns. As for the unreinforced specimens, a sudden decrease in load-carrying capacity could be observed. However, for reinforced specimens, a short-delayed phase was followed by an extended strain-hardening behavior, which generally led to a 40-50 % higher maximum force compared with the corresponding unreinforced structure.

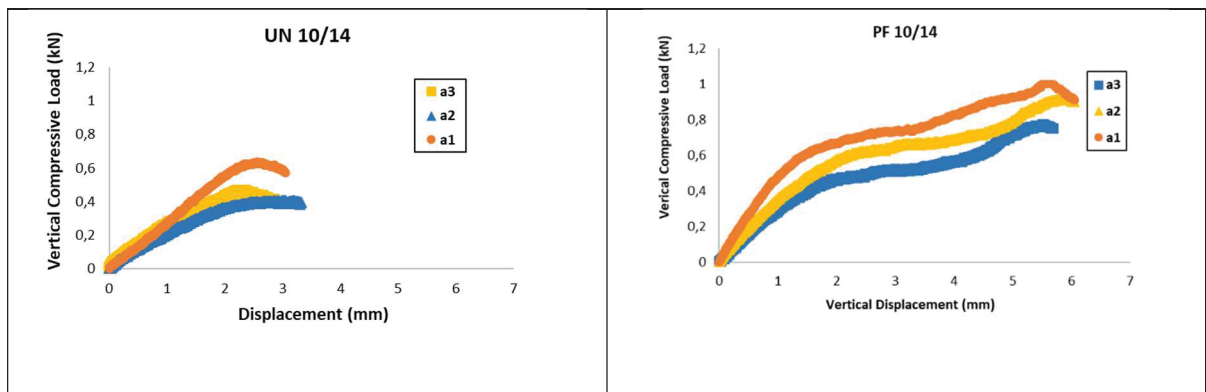
The significant difference between reinforced and unreinforced structures was related to the energy dissipated in mode I of the crack opening phase, known as J-Integral, which its value could be computed according to Equation (5.1) (Anderson 1991).

$$J = -\frac{1}{B} \left(\frac{dU_T}{da} \right) \quad (5.1)$$

where J is the non-linear energy release rate in J/m^2 ; B is the specimen thickness in m; U_T is the total strain energy in J (calculated by the area under the load-displacement curve up to failure); a is the notch depth in m; and $\frac{dU_T}{da}$ is the decreasing rate in fracture energy with notch depth.

According to the results indicated in the last column of Table 5.3, the reinforced structures had four to five times higher amount of energy dissipation in comparison with unreinforced structures.

Another finding of interest was obtained from the crack gauges installed under and over the interface to monitor the crack propagation from the top of a notch of depth a_2 (specified in Table 5.3) to the top surface. As seen in Figure 5.7, the steeper initial slopes, higher maximum force at the failure point, and larger differences between the crack widths at the bottom and the top of the reinforced interfaces (i.e. PF 10/14 and PF 14/20) all lead to a higher capability of the reinforced interface to retard crack propagation from its bottom side to the top, which was quantified by ΔA , as shown in Figure 5.7. This parameter is calculated by subtracting the areas surrounded by the load-crack width curve at the bottom and the top of the interface. This feature was more highlighted in coarse-graded reinforced structure (i.e. PF 14/20).



(a)

Figure 5.6 The load-displacement curve for different notch depths (a_1 , a_2 and a_3 : see Table 3) for composite structures including: (a) ESG10 over ESG 14; (b) ESG 14 over GB20 (UN: unreinforced structure; PF: reinforced structure with paving fabric)

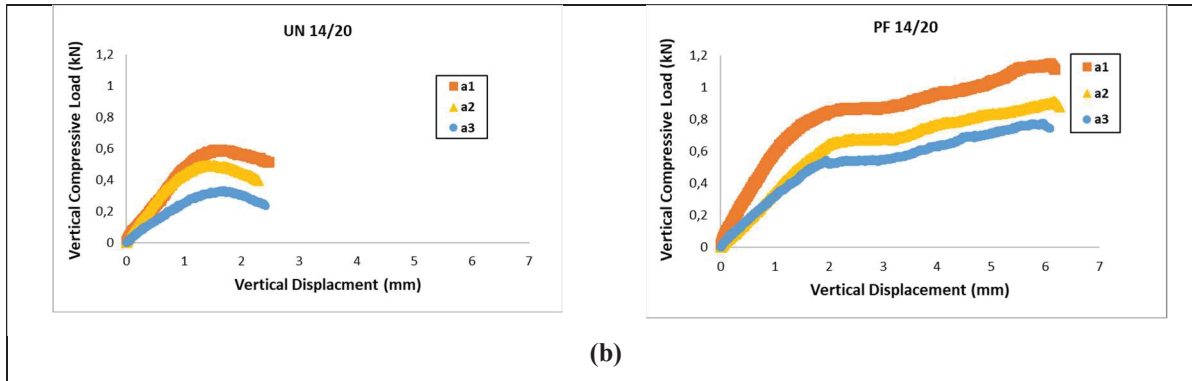
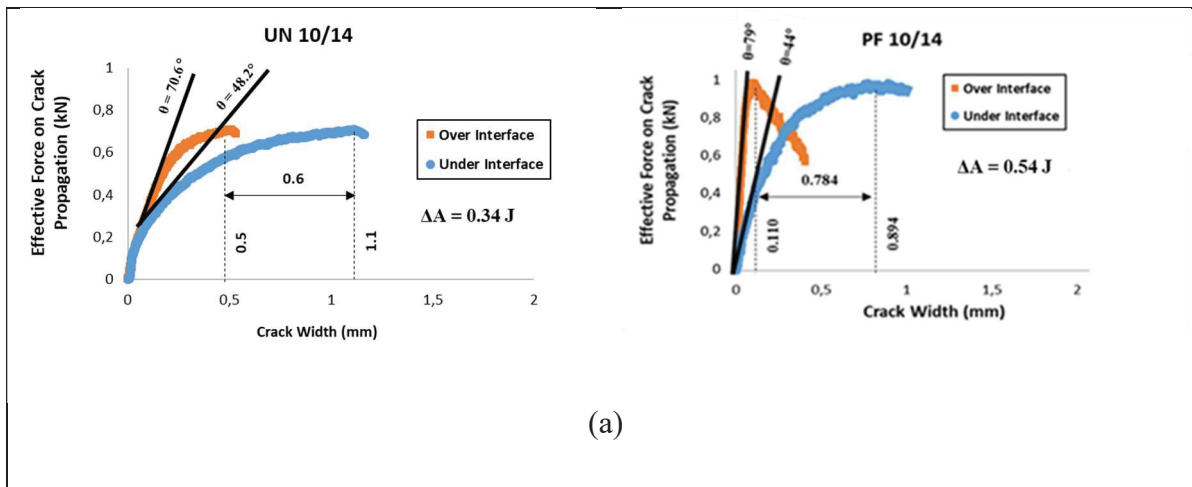


Figure 5.6 (Continued)

Table 5.3 Dimensional details of mechanical notch and energy dissipation in mode I of crack development

| Type of Structure | Notch Depth a (mm) | | | Notch Width w (mm) | | | Specimen Height B (mm) | | | Strain Energy at Failure U (J) | | | dU/da | J-Integral (J/m ²) |
|-------------------|--------------------|----------------|----------------|--------------------|----------------|----------------|------------------------|----------------|----------------|--------------------------------|----------------|----------------|--------|--------------------------------|
| | a ₁ | a ₂ | a ₃ | w ₁ | w ₂ | w ₃ | B ₁ | B ₂ | B ₃ | U ₁ | U ₂ | U ₃ | | |
| UN 10/14 | 18.8 | 23.8 | 31.0 | 3.8 | 3.7 | 3.6 | 80.3 | 78.9 | 82.9 | 0.9 | 0.8 | 0.6 | -22.8 | 286.8 |
| UN 14/20 | 18.9 | 27.0 | 31.0 | 3.7 | 3.9 | 3.7 | 84.5 | 85.6 | 82.9 | 0.6 | 0.5 | 0.3 | -29.0 | 344.4 |
| PF 10/14 | 19.0 | 25.2 | 32.1 | 3.8 | 3.6 | 3.6 | 80.8 | 83.2 | 85.3 | 4.2 | 3.4 | 2.5 | -122.0 | 1469.1 |
| PF 14/20 | 20.5 | 27.0 | 36.1 | 3.5 | 3.7 | 3.5 | 86.6 | 85.6 | 85.5 | 5.0 | 3.8 | 3.1 | -140.0 | 1628.1 |



(a)

Figure 5.7 Crack width development below and above the interface during crack propagation stage in a₂ depth of notch for composite structures including: (a) ESG10 over ESG 14; (b) ESG 14 over GB20 (UN: unreinforced structure; PF: reinforced structure with paving fabric)

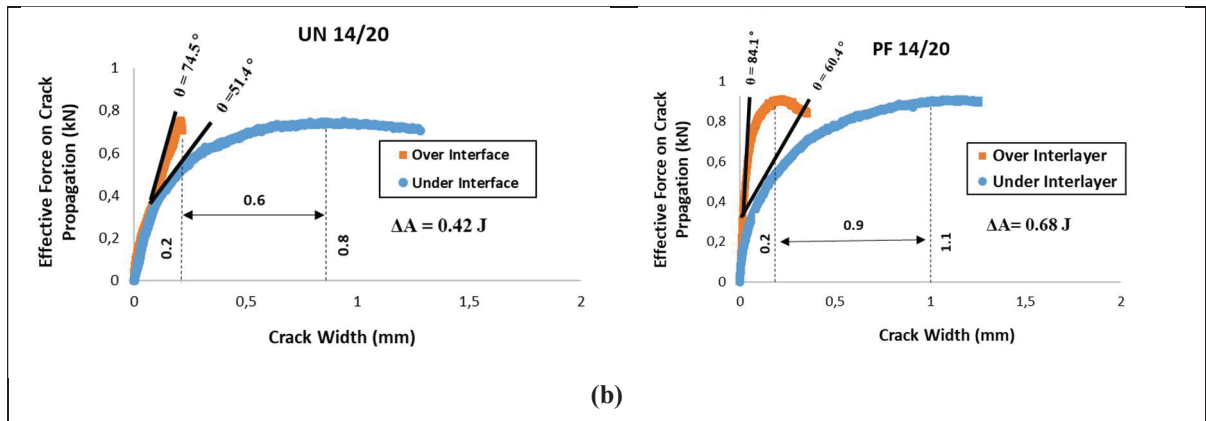


Figure 5.7 (Continued)

5.5.2 Results and discussions on the shear test

The mean results of three replicates derived from the modified slant shear device are illustrated in Figure 5.8. In order to gain a better vision on interlayer shear stiffness, some parameters were highlighted on each developed curve as Maximum Interlayer Shear Strength (ISS_{Max}); Interlayer Shear Displacement (ISD) at maximum shear strength point; Coefficient of Interface Bonding (CIB) and shear stiffness (E_T) defined as the slope of the initial linear part of the curve.

As far as the shear strength is concerned, the presence of the paving fabric as an interlayer between two asphalt layers resulted in 30% and 48% reduced shear strength in reinforced structures of ESG10/ESG14 and ESG14/GB20, respectively. Furthermore, the reduction in shear stiffness (E_T) was more significant for the ESG14/GB20 structure.

The sliding between the layers can be evaluated by the introduction of CIB, which is the quotient of ISS_{max} and ISD ($CIB = \frac{ISS_{max}}{ISD}$). On this ground, the higher CIB indicates the higher bonding quality between the layers, while lower CIB means reverse. As can be seen, in both of the structures, the bonding quality was reduced as much as 50-60 percent.

Despite the reduced shear properties and bonding quality at the interface, it is crucial to bear in mind that the reinforced structure maintained its structural integrity even in a large shear displacement induced at the interface. In contrast, in the unreinforced structure, the shear strength was sharply decreased after its maximum value and the structure failed in a considerably lower horizontal displacement. It is worth mentioning that, because of large

displacement before failure in reinforced structures, which could result in the slippage of the bottom part over the rail, and also to set a fair sustainable threshold between reinforced and unreinforced structures, it was decided to define the failure point as the force underwent by the structure at 80 percent of its maximum shear strength.

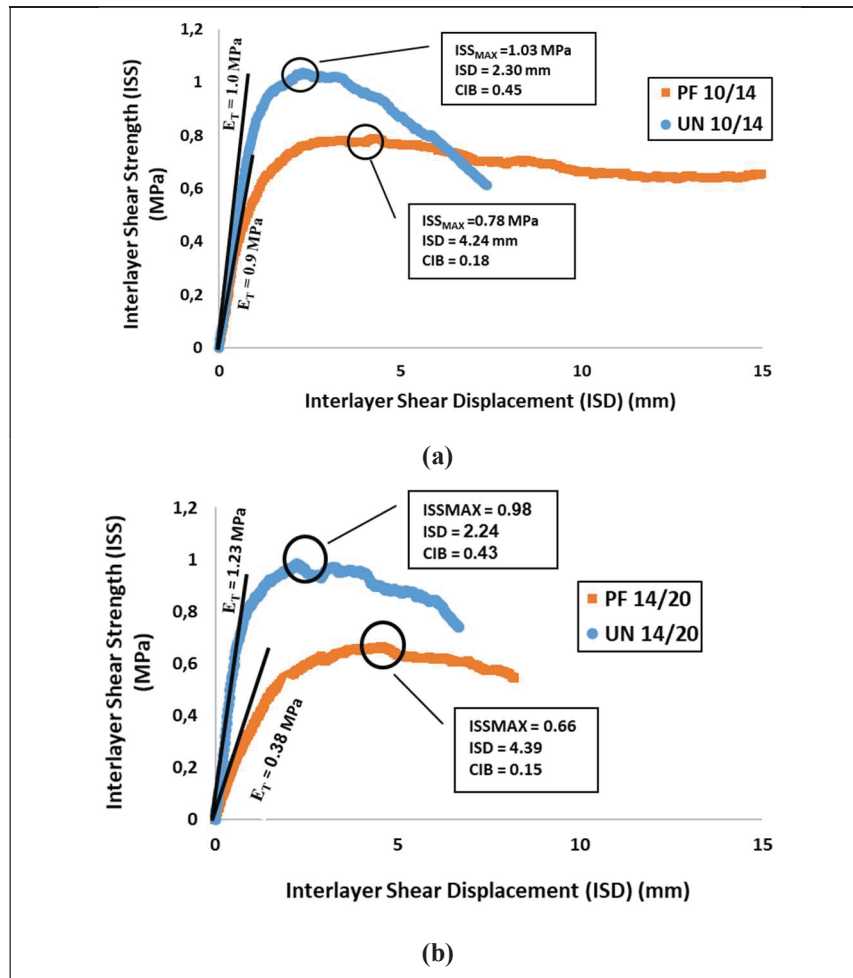


Figure 5.8 Interlayer shear strength versus interlayer shear displacement at 25 °C and 2 mm/min loading rate: (a) ESG10 over ESG 14; (b) ESG 14 over GB20 (UN: unreinforced structure; PF: reinforced structure with paving fabric)

5.5.3 Results and Discussions on Complex Modulus Test

Experimental results for complex modulus tests on reinforced and unreinforced structures are plotted in Figures 5.9 & 5.10 in terms of the Cole-Cole diagram ($E_{Imaginary}$, E_{Real}) and the black diagram ($|E^*|$, ϕ). Each test was conducted twice to ensure the repeatability of the results. As

can be seen, the measured values followed a unique pattern, which implied the applicability of Time-Temperature Superposition Principle (TTSP) and the possibility of fitting a rheological model to justify the changes. However, a valuable finding, which could be deduced from the data was that for all the structures, the complex modulus data measured by 50 and 100 mm extensometers were largely superimposed on the Cole-Cole diagram. On the other hand, the 25 mm extensometer had distinguishably lower values in comparison. This could be explained by the mechanical effect of the interface, which was preponderant in the 25 mm extensometer domain but very small on other sizes of extensometers. Nevertheless, it is vividly seen in Figure 5.10 that the mechanical effect of the interface was not outstanding in the black diagram. Therefore, the measurements derived from the 25 mm extensometer could be treated as a useful tool to compare the complex modulus of reinforced and unreinforced structures in a variety of temperatures and frequencies.

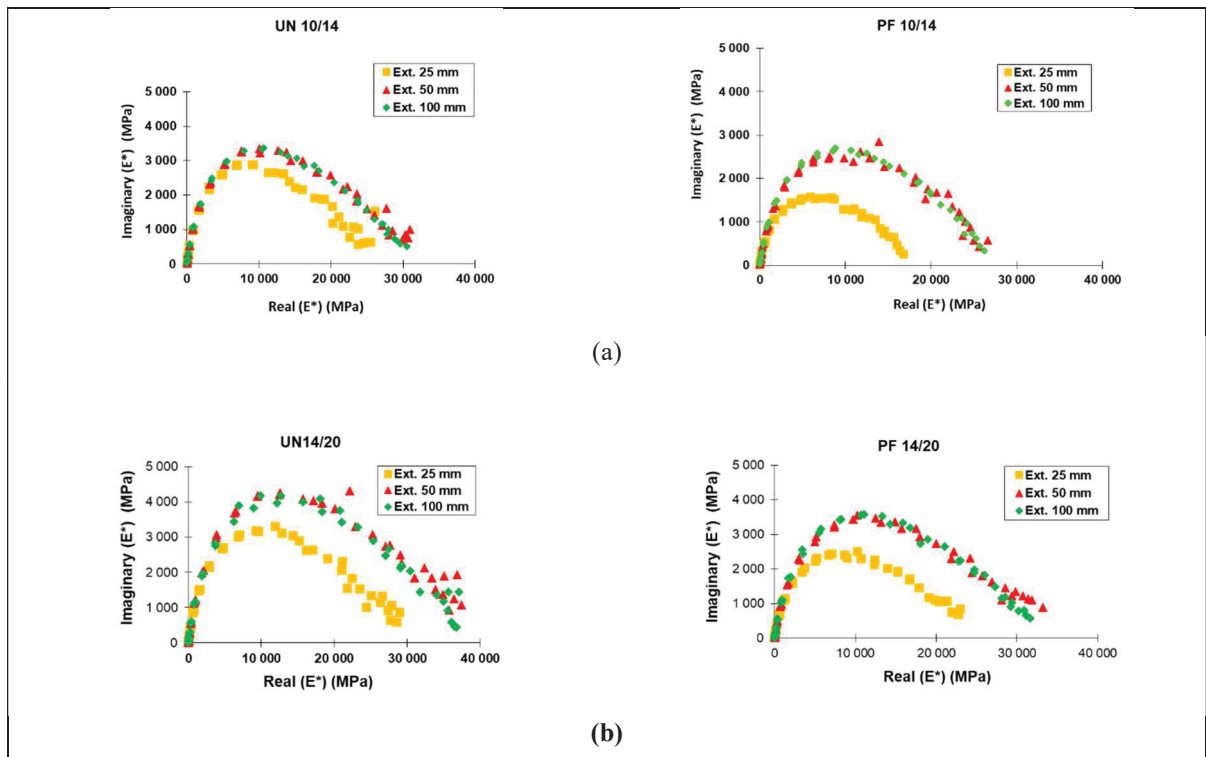


Figure 5.9 The Cole-Cole diagram developed based on the measured data from complex modulus test (a) ESG10 over ESG 14; (b) ESG 14 over GB20 (UN: unreinforced structure; PF: reinforced structure with paving fabric)

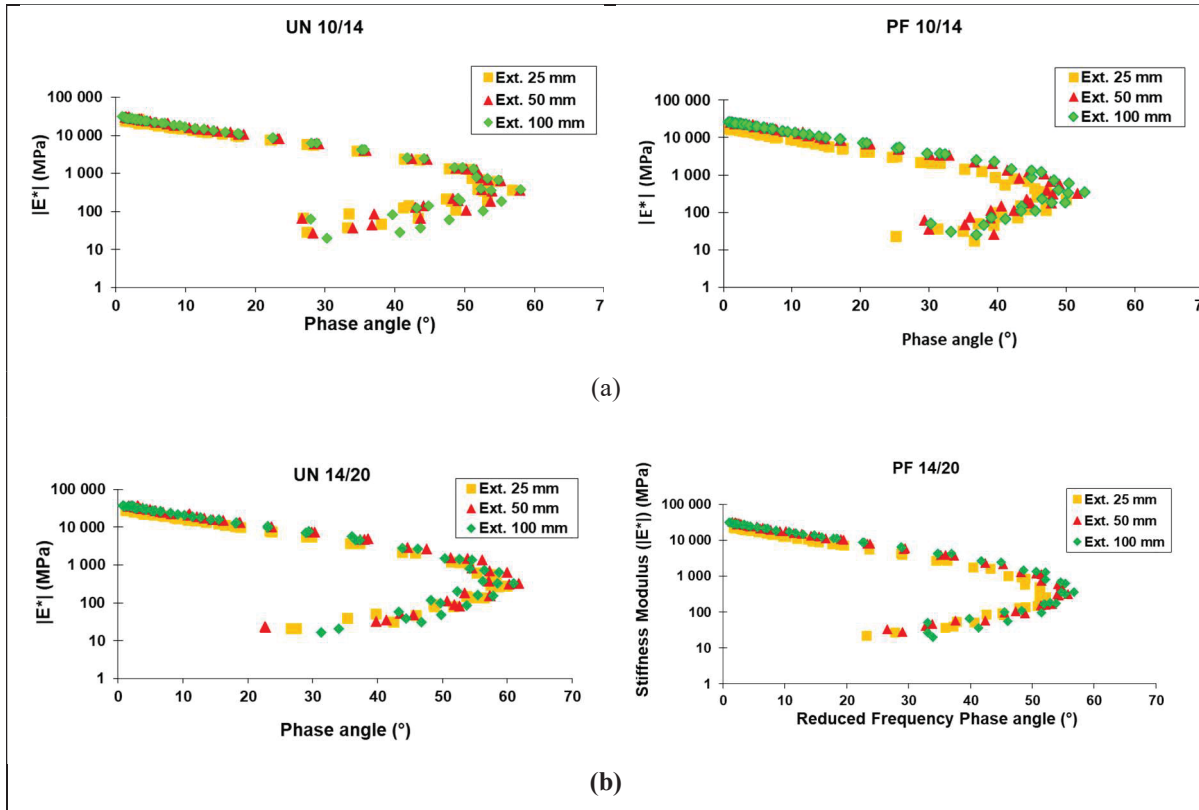


Figure 5.10 The Black diagram developed based on the measured data from complex modulus test (a) ESG10 over ESG 14; (b) ESG 14 over GB20 (UN: unreinforced structure; PF: reinforced structure with paving fabric)

A variety of rheological models have been presented in the literature to justify the viscoelastic behavior of bituminous mixture under different temperatures and load frequencies. Based on the nature of representation, these models could be classified into mathematical expressions and advanced analogical models. However, because of having a physical illustration of the elements involved in the model, the advanced rheological models have received much attention over the mathematical expressions. In this connection, 2S2P1D model (two Springs, two Parabolic creep elements, and one Dashpot) amidst others, could reliably be utilized to predict the behavior of bituminous mixture from very low frequencies to very high ones (Olard and Di Benedetto 2003). The analytical expression to compute the complex modulus based on the 2S2P1D model is given by the Equation (5.2).

$$E_{2S2P1D}^* = E_{00} + \frac{E_0 - E_{00}}{1 + \delta(i\omega\tau)^{-k} + (i\omega\tau)^{-h} + (i\omega\beta\tau)^{-1}} \quad (5.2)$$

where i the imaginary unit; ω angular frequency; E_0 glassy modulus ($\omega \rightarrow \infty$); E_{00} static modulus ($\omega \rightarrow 0$); k , h , and δ calibration constants; β parameter related to Newtonian viscosity of the dashpot; and τ_E characteristic time value varied with temperature. The calibration of the model parameters based on the experimental data obtained from Ext. 25 mm, for all designated structures are listed in Table 5.4.

Table 5.4 2S2P1D model parameters

| Model Parameters | Types of Structures | | | |
|-------------------------------------|---------------------|----------|----------|----------|
| | UN 10/14 | UN 14/20 | PF 10/14 | PF 14/20 |
| E_{∞} | 35 | 20 | 15 | 18 |
| E_0 | 26200 | 30000 | 17500 | 24200 |
| K | 0,2 | 0,2 | 0,2 | 0,2 |
| h | 0,6 | 0,6 | 0,6 | 0,6 |
| δ | 1,8 | 1,8 | 2,7 | 2,12 |
| τ_E (s) ($T_{ref} = -5.4$ °C) | 2 | 2 | 2 | 2 |
| β | 100 | 100 | 1000 | 250 |

According to Table 5.4, the k and h values, which are linked to the binder rheology, were not changed among the structures. However, the result showed that the presence of a different type of binder as an adhesive between the asphalt layer and the paving fabric, (i.e., PG 64-34) than the one employed in the asphalt mixture (i.e., PG 58-28) resulted in a variation of δ and β values (shape factors) which was highlighted in PF 10/14 structure. Another interesting finding was that both the glassy modulus (E_0) and the static modulus (E_{00}) were higher in unreinforced structures than the corresponding type of the reinforced structure. This negative effect could be explained by the high air-void content surrounding the reinforced interface due to incomplete compaction (Solatiyan et al. 2020b).

Figure 5.11 demonstrates the relative differences between the measured and simulated values for stiffness modulus ($|E^*|$) at a reference temperature ($T_{ref} = -5.4$ °C). On this ground, low differences in Y-axis imply the ability of the 2S2P1D model to predict the mechanical behavior at that reduced frequency ($a_T \cdot f_r$). Accordingly, the results showed that the 2S2P1D model was a reliable tool to predict the mechanical behavior of the reinforced and unreinforced interface, especially for high frequencies or low temperatures. At high temperatures, because of the creep deformations pertaining to the asphalt mixture and subsequent stress relaxation over time, the

more heterogeneity in the mechanical behavior of involved surfaces would be expected, which negatively affects the accuracy of the model.

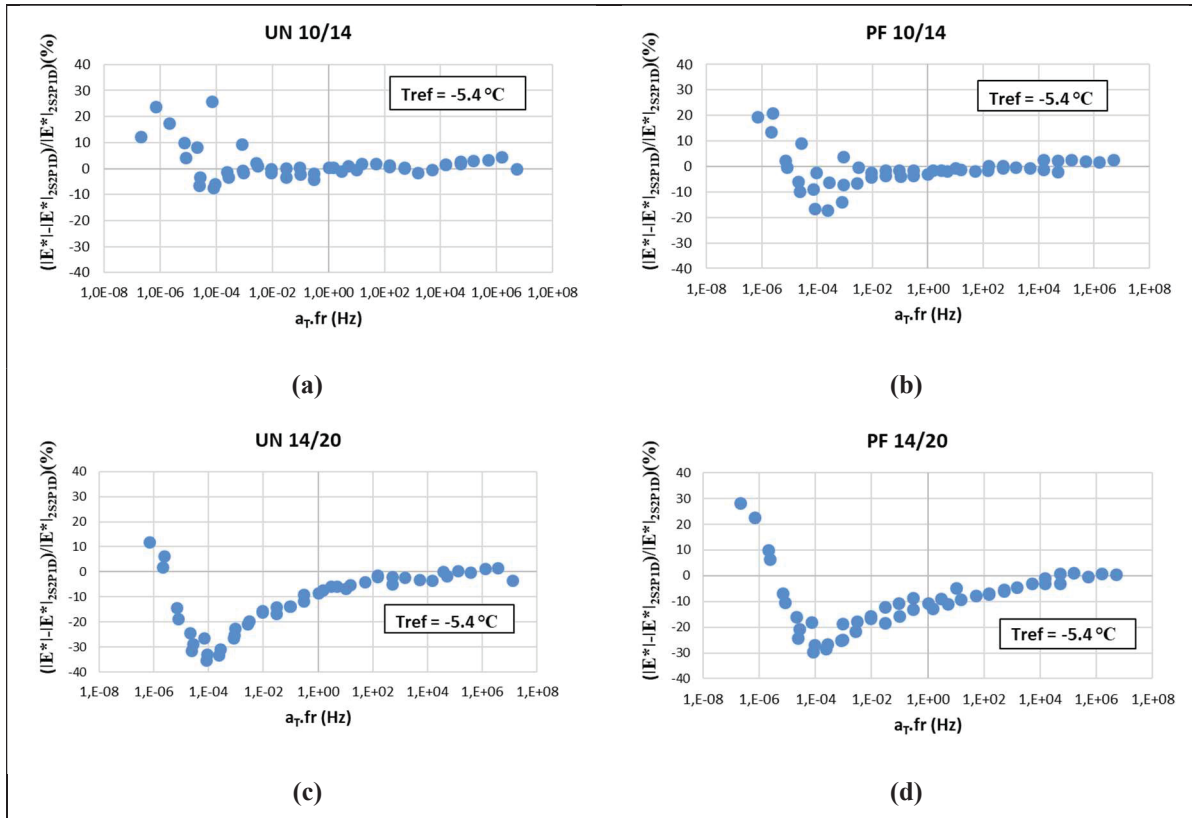


Figure 5.11 Difference in the norm of complex modulus between experimental and 2S2P1D model values: (a) Unreinforced structure with ESG10 over ESG14; (b) reinforced structure with ESG10 over ESG14; (c) Unreinforced structure with ESG14 over GB 20; (d) reinforced structure with ESG14 over GB20

To define viscoelastic behavior of bituminous materials in terms of the stress-strain relationship into finite element design methods (e.g. Abaqus software), Prony series in the form of shear modulus defined by Equation (5.3) could be utilized (Dogan 2007):

$$g(t) = 1 - \sum_{i=1}^N g_i \left(1 - e^{\left(\frac{-t}{\tau_i}\right)} \right), \quad g(t) = \frac{G(t)}{G(t=0)} \quad (5.3)$$

In which $g(t)$ is the shear modulus ratio, which is defined as the ratio of shear modulus at any time like $t, G(t)$, to the shear modulus at the first stage ($t = 0, G(t = 0)$). τ_i and g_i are Prony constants, which are determined based on the material properties and entered into the Abaqus

software, and N is considered as the number of terms used in Prony series which is suggested to take as $N = 5$ to obtain accurate results (Liao and Sargand 2010).

On the other hand, Shear modulus, $G(t)$, is determined from the relaxation modulus, $E(t)$, according to the Equation (5.4).

$$G(t) = \frac{E(t)}{2(1 + \nu)} \quad (5.4)$$

where $E(t)$ is the relaxation modulus, determined by converting the dynamic modulus master curve; and ν is the Poisson's ratio, which can be logically assumed to be 0.35. Once $G(t)$ is calculated the ratio of $g(t)$ could be easily determined as indicated in Equation (5.3).

Figure 5.12 demonstrates the changes in dynamic modulus master curves by the length of extensometers for different types of structures studied in this research. As evident, in unreinforced structures (i.e. UN 10/14 and UN 14/20) all the master curves, developed based on each length of extensometer, are well superimposed on each other. However, in reinforced structures (i.e. PF 10/14 and PF 14/20), the master curve derived from 25 mm extensometer is positioned below the two others especially at high frequency domain.

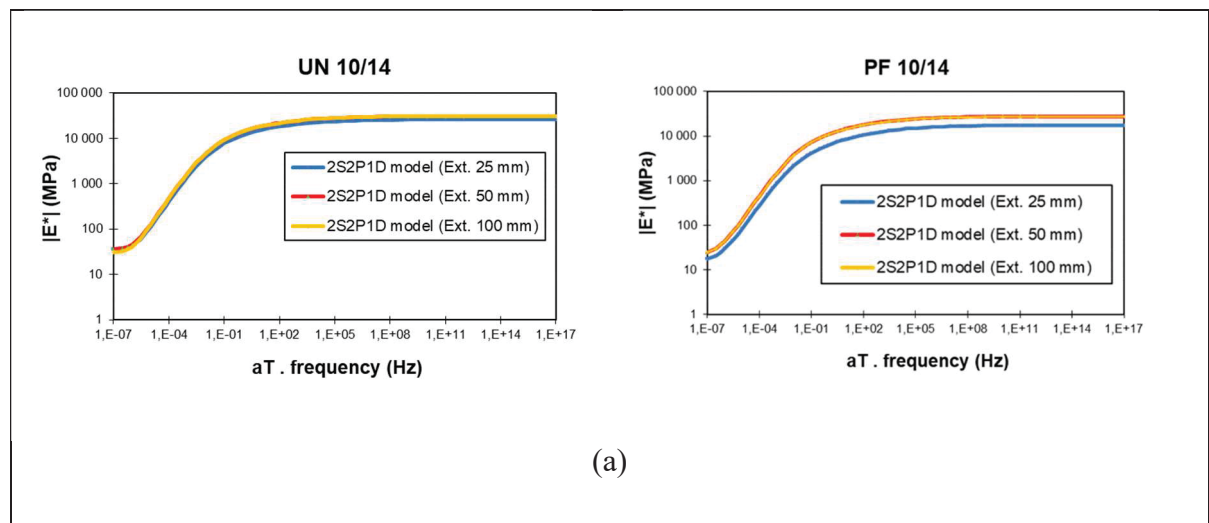


Figure 5.12 Changes in dynamic modulus master curves by the length of extensometers for each type of structure (a) ESG-10 over ESG-14, (b) ESG-14 over GB-20

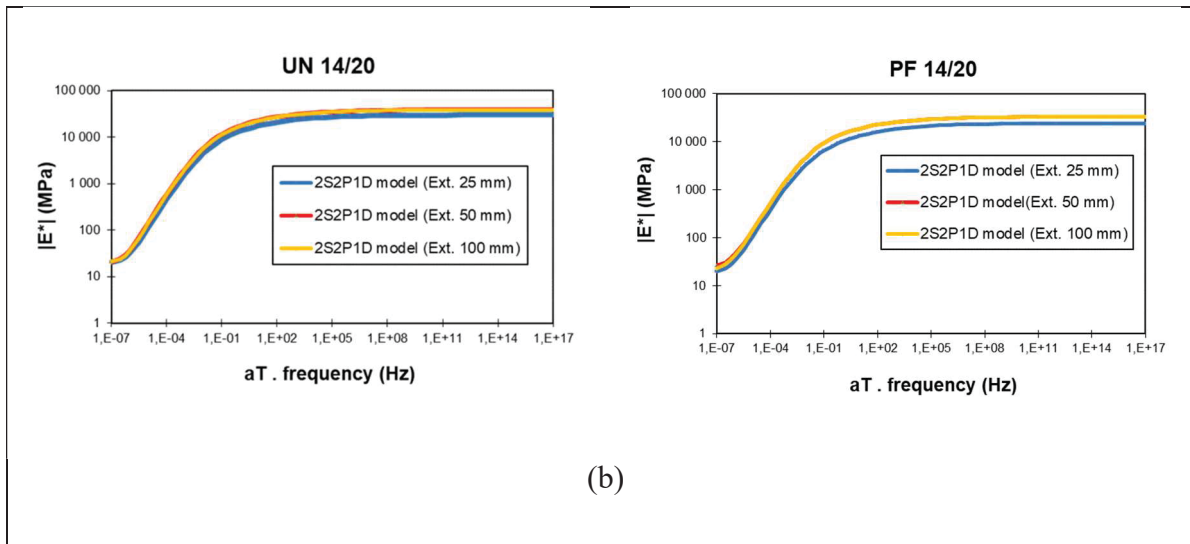


Figure 5.12 (Continued)

Figure 5.13 illustrates a comparison in master curves developed for reinforced and unreinforced interfaces by a 25 mm extensometer. As can be seen, the master curves of reinforced interfaces in both of the structures were well situated below the unreinforced cases. This discrepancy was highlighted for an arbitrary point $f = 10$ Hz and $T_{ref} = -5.4$ °C as an example on the graph. The results showed that the reinforced interfaces, especially the one surrounded by ESG-10 and ESG-14, underwent a meaningful reduction in terms of dynamic modulus and a slight increase in the phase angle compared to unreinforced ones, especially at higher frequencies or lower temperatures. This could suggest developing the 2S2P1D model of reinforced interface with paving fabric by taking its actual model parameters into account while seeking for the real structural responses from mechanistic-based design methods.

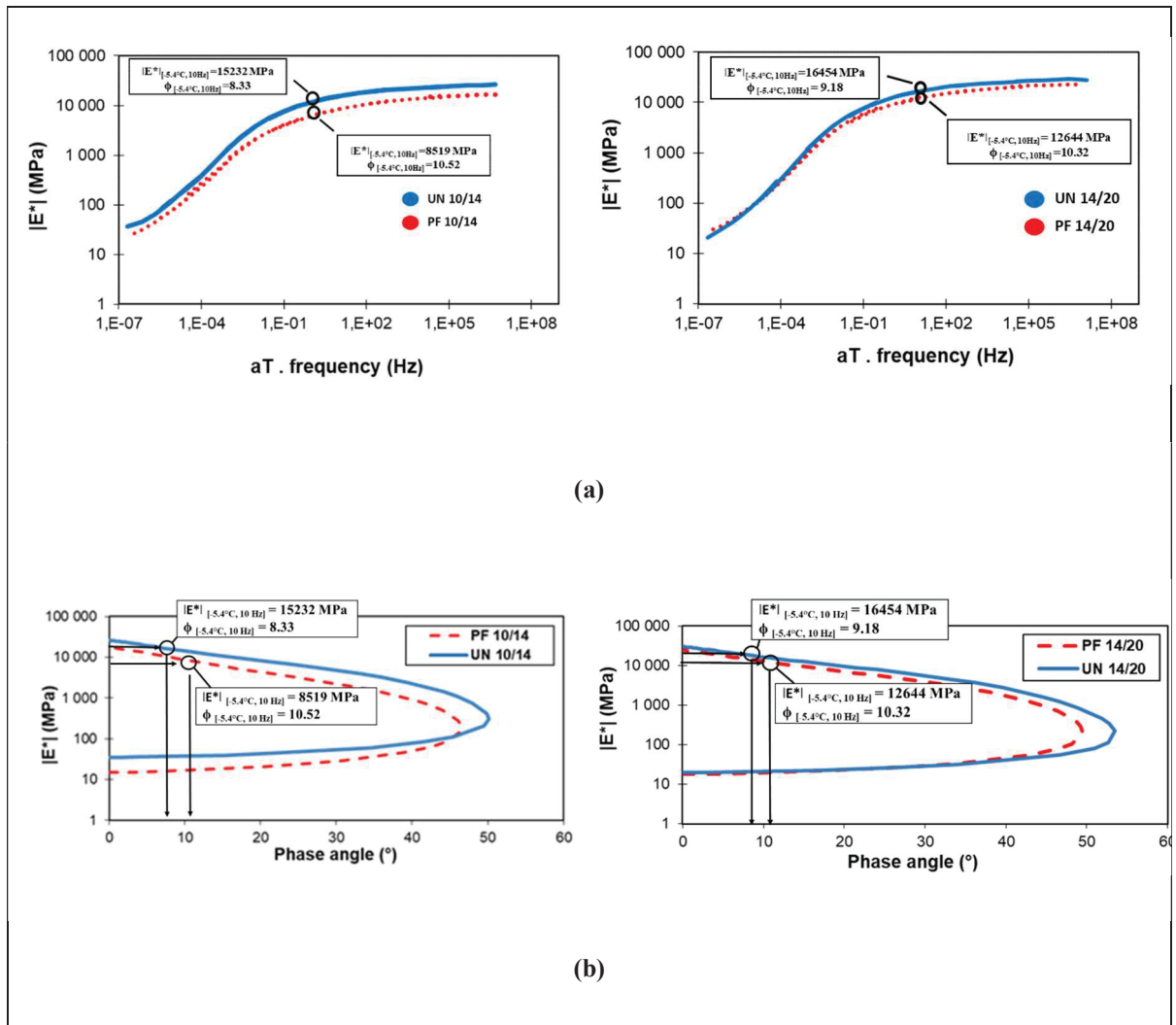


Figure 5.13 A comparison of dynamic modulus and phase angle at $T = -5.4 \text{ }^\circ\text{C}$ and $f = 10 \text{ Hz}$ from (a) dynamic modulus master curve and (b) black diagram; developed for reinforced and unreinforced interfaces based on 25 mm extensometer

5.6 Conclusions

The focus of this study was to experimentally evaluate the mechanical properties at the interface of bituminous layers reinforced with paving fabric compared to the unreinforced one through novel approaches. The following conclusions could be extracted from this study:

- In the 3-PBT, it was revealed that the reinforced interface with paving fabric outperforms the unreinforced interface in terms of J-integral and crack retardation capability. This advantage was more dominant when paving fabric introduced between bituminous layers with higher NMAS.

- In the shear test, the unreinforced interface provided an appreciable level of shear strength and shear stiffness, which resulted in higher bonding quality in terms of CIB. However, the ability of the reinforced interface to maintain the structural integrity of the composite structure even at large horizontal displacements needs to be respected in design methods.
- The complex modulus of rehabilitated bituminous structures, composed of different layers with or without paving fabric, could be reliably predicted by the 2S2P1D model in high frequency domain (1 to 1E7 Hz).
- The mechanical effect of the interface on the complex modulus of the composite structure was highlighted in the Cole-Cole diagram, black diagram and dynamic modulus master curve by distinct rheological behavior measured through the 25 mm length extensometer.
- The actual dynamic modulus master curve of the reinforced interface with paving fabric is required to be considered in mechanistic-based pavement design methods, which would yield valid structural responses especially at higher frequencies or low temperatures.
- Generally, the application of paving fabric between bituminous layers with a higher NMAS could lead to enhanced anti-reflective property against the bottom-up cracking with a less negative effect on stiffness properties at the interface.

CHAPTER 6

MECHANICAL PERFORMANCE OF REHABILITATED BITUMINOUS LAYERS WITH PAVING FABRIC UNDER CYCLIC LOADING

Ehsan Solatiyan^a, Nicolas Bueche^b, Alan Carter^c

^{a, c} Department of Construction Engineering, École de Technologie Supérieure (ÉTS),
1100 Rue Notre-Dame O, Montréal, QC H3C1K3, Canada

^b Department of Architecture-Wood-Civil Engineering, Bern University of Applied Sciences
(BFH), Pestalozzistrasse 20, CH-3401 Burgdorf, Switzerland

Paper submitted for publication in *Road Materials and Pavement Design*, August 2020

6.1 Abstract

The application of paving fabric (a system composed of a layer of geotextile along with asphalt cement) between an existing deteriorated bituminous layer and a fresh asphalt overlay, as a newly developed rehabilitation strategy, has proved its effectiveness in terms of delaying the propagation of reflective cracks. Nevertheless, this application requires an in-depth knowledge of the mechanical behavior of the composite system including paving fabric under cyclic loading in order to predict its performance during the design life. In this context, rutting resistance and fatigue failure are commonly employed as major failure criteria in mechanistic-based design methods. The objective of this study was to understand the possible mechanical changes in composite structures made of different hot mixtures reinforced with paving fabric compared with unreinforced ones. To this end, two types of double-layered structures, normally recognized in a bituminous pavement cross-section, were addressed: a fine-graded structure found in the upper bituminous layers and a coarse-graded structure positioned in the lower bituminous layers. Rutting resistance of the composite structure was evaluated using the French Laboratory Rut Tester (FLRT) device and fatigue behavior was studied via a method developed in Département de Génie Civil et Bâtiment (DGCB). The results showed that the composite structure including paving fabric had lower rutting resistance and accelerated rut

depth evolution, especially at higher number of cycles, but about 30 percent enhanced fatigue life compared with unreinforced structures. This study also suggested that the placement of paving fabric between coarse-graded mixtures could strike a balance between rutting resistance and fatigue performance.

6.2 Introduction

Application of paving fabric, a system composed of geotextile and asphalt cement as a tack coat, between bituminous layers is an alternative way to the usual mill and fill to restore the serviceability of the road surface for the users. This type of geosynthetic, a geotextile, has received much attention from the engineering community for economic reasons and because of its ease of implementation (Golestani et al., 2016). It not only waterproofs the system against the percolation of water through fractures and discontinuities on the surface but also prolongs the life cycle of the pavement system by retarding the manifestation of the reflective cracking from bottom layers (Solatiyan et al., 2020a). Nevertheless, their mechanical interactions with adjacent asphalt layers need to be further examined to provide a better vision into the design of new rehabilitation projects based on the mechanistic methods.

Permanent deformation or rutting is a common type of distress in bituminous pavements, which appears at the road surface by accumulated permanent deformation along the wheel path due to excessive shear strain (Said et al., 2016). In mechanistic-based design methods, rutting is considered a critical criterion because of its high impact on driving quality and safety (Liao et al., 2018; Xu & Huang, 2012). It is believed that a hot mix asphalt layer placed near the surface contributes more than granular base layers in the occurrence of the rutting (White et al., 2002). In this respect, among many factors that are influential on rutting resistance of bituminous layers, the mechanical properties and gradation of aggregates employed in the asphalt mixture play pivotal roles in reducing the shear strain induced in the bituminous layer (Khan, 2010; Khedr & Breakah, 2011; Yang et al., 2006). In addition, in reinforced rehabilitated bituminous layers, the specifications of the interlayer system and its installation procedure are other important considerations that govern the regime of shear strains induced at the interface (Ling & Liu, 2001; Mounes et al., 2014; Tang et al., 2016). Several semi-empirical test methods have been utilized to measure the rutting resistance of asphalt mixture.

Among which the Asphalt Pavement Analyzer (APA) (AASHTO TP 63-07, 2007), the Humburg Wheel Tracking Device (HWTD) (Mahoney and Zinke, 2008), the French Laboratory Rut Tester (FLRT) (MTQ- LC26-410, 2018), repeated-load creep test (RLC) (Behbahani et al., 2009) and the Asphalt Mixture Performance Tester (AMPT) (Bonaquist, 2010) are the most common.

Fatigue failure, caused by the accumulated damage under the repetitive action of traffic loads, is another important criterion in the pavement design process, which could lead to a decline in the stiffness modulus of the bituminous layers, as the number of load cycles increases, and finally degradation of the whole pavement structure (Carter et al., 2018). In this connection, the mechanical behavior of bituminous layer to repetitive loads is dominated by a series of factors including (Abojaradeh, 2003; Khateeb et al. 2011):

- The specifications of the mix design such as aggregate gradation, air void content, bitumen content, and type of bitumen;
- The environmental effect such as temperature;
- Load type, configuration, and its frequency;
- Specimen preparation and compaction procedures.

A common method to evaluate the fatigue resistance of a bituminous layer is to determine the evolution of its stiffness modulus by the number of load cycles, which is normally composed of three distinct stages from the instant of loading to the failure point (Baaj et al., 2005). At the early stages, the stiffness modulus sharply decreases, which can be attributed to the temperature increment due to the internal friction in the bituminous layer and in turn a reversion in the thixotropy effect of the bitumen. Right after the first stage, the reduction in the stiffness modulus follows a linear trend (constant rate), as a result of the formation of microcracks in the structure. The failure of the material (third stage) occurs when the coalition of microcracks turns into macrocracks and consequently losing the structural capacity of the system (Tapsoba et al. 2013; Carter et al., 2018). In this context, a variety of criteria has been suggested to determine the transition point from stage 2 to 3 as the failure point in fatigue resistance of the material or system (Perraton et al. 2015; Tapsoba et al. 2013). Among them, $N_{f50\%}$ is a conventional fatigue criterion, which is defined based on a 50% reduction in the initial stiffness modulus of the bituminous layer (Perraton et al. 2015, Orešković et al. 2019).

Four-point bending test (4-PBT) (ASTM D7460, or AASHTO T321) and the uniaxial tension-compression test procedure developed in Département de Génie Civil et Bâtiment (DGCB) (Di Benedetto et al. 2011) are commonly employed to measure the fatigue resistance of a bituminous mixture. To perform conventional fatigue tests on the reinforced structure, it is essential to assume that the geosynthetic is installed at the middle of a double-layer structure and perfectly attached to the bottom layer with no slippage at the interface (Sudarsanan et al. 2020). These tests are usually performed at one temperature and one frequency and different strain levels (at least three levels) and the pertinent results are presented on a log-log graph of the number of cycles at failure against the amplitude of the strain level. The fitted curve on the failure points ($N_{f50\%}$ derived from each strain level) is called the Wöhler curve and follows a straight line given by the Equation (6.1) (Baaj et al., 2005; Perraton et al., 2015):

$$N_f = K_1 \cdot \varepsilon^{-K_2} \quad (6.1)$$

where N_f is the number of cycles; K_1 and K_2 are coefficient depending on material and ε is the axial strain amplitude. If the failure point is assumed at one million cycles, the pertinent strain level, ε_6 , could be derived from Equation (6.2):

$$\frac{N_f}{10^6} = \frac{\varepsilon^{-K_2}}{\varepsilon_6} \quad (6.2)$$

With respect to the context introduced above, the objective of this study is to evaluate the rutting resistance and fatigue performance of double-layered rehabilitated bituminous structures with and without paving fabric to cyclic loading applied at the top surface, under field-like conditions in the laboratory. This is necessary for establishing an in-depth knowledge of the mechanical behavior of a reinforced bituminous layer in mechanistic-based design methods and to select the proper type and location of paving fabric in pavement rehabilitation strategies. From this perspective, three specific objectives are addressed throughout this research:

- (1) Development of the rut depth in a composite structure manufactured of different bituminous layers in terms of Nominal Maximum Aggregate Size (NMAS);

- (2) Evolution of the rut depth in reinforced and unreinforced double-layered bituminous structures;
- (3) Quantifying the changes in initial stiffness modulus and the failure criterion among reinforced and unreinforced bituminous composite structures.

This paper is arranged in five sections. First, a review of relevant studies on fatigue behavior and the rutting resistance of reinforced-rehabilitated bituminous layers are introduced. Then, a description of the materials used to manufacture the specimens are presented. This is continued in the third section with a description of test methods employed to meet the objectives of this research. The fourth section will demonstrate the experimental results, followed by a detailed analysis. In the end, a summary of the outcomes is given.

6.3 Research Background

Permanent deformation or rutting is a crucial factor in mechanistic-based design methods because of its impact on the performance of a road. A variety of methods and additives has been recommended to enhance the anti-rutting property of a bituminous layer. These alternatives can be classified into three distinct categories. In some studies, the high-temperature rheological properties of the bitumen have been addressed by adding polymer-based modifiers such as styrene-butadiene-styrene (SBS), rubber and fibers to restrain the lateral flowing out of the material under traffic loads (Bostancioglu & Oruc, 2016; Fontes et al. 2010; Guo et al., 2015; Shafabakhsh et al., 2014 Alatas & Kizirgil, 2013; Babagoli et al., 2015; Bernier et al. 2012; Tayfur et al., 2007). In addition, introducing additives such as diatomite and glass fiber (Guo et al. 2015), RAP (Cooper et al., 2016), and rubber (Moreno-Navarro et al. 2014) into the hot mixture could effectively enhance the resistance of the bituminous layer against rutting. On the other hand, physical and mechanical specifications of the aggregate have been the focus of other studies to increase the shear strength of the asphalt mixture (Muraya et al., 2009; Singh et al., 2016).

Taking advantage of a layer of geosynthetic material over a rehabilitated bituminous layer, as an interlayer, is another approach to increase the shear stiffness of the system against rutting, which has received a lot of interest from the engineering community (Ling & Liu 2001; Mounes et al., 2014; Tang et al., 2016). According to (Correia & Zornberg (2016), the presence

of a geosynthetic in a bituminous pavement could result in a rutting resistance up to four times better than that of an unreinforced structure). It was also found that the rut depth and the modulus of elasticity of a reinforced bituminous layer with geosynthetic are correlated with each other and in this connection, the type of geosynthetic material plays an important role (Laurinavičius and Oginskas, 2006). In addition, a review of studies shows that the performance of reinforced bituminous layer to lateral plastic flow is governed by the position of geosynthetic in asphalt overlay and the adhesion quality provided at the interface and it is independent of the geosynthetic stiffness at the ambient temperature (Solatiyan et al. 2020b). However, at high temperature, the elastic modulus of the geosynthetic material and its bonding quality to the adjacent asphalt layer are of great importance on the effectivity of the interlayer system on rutting (Shamami & Khiavi, 2017; Lee et al., 2015). Nevertheless, most of these studies were concentrated on the application of geogrids placed between two layers of the same bituminous mixture. Only a few researches have been assigned to reinforced bituminous layers with paving fabrics, implemented between two different types of mixtures. Besides, the possible changes in the evolution of rutting in the presence of a layer of paving fabric could provide a better insight into the development of a suitable failure criterion in mechanistically based design methods.

Fatigue failure is another important design consideration, which directly influences the design life of a pavement structure. A series of factors are influential on fatigue performance of a geosynthetic-reinforced bituminous structure including the type of pavement, the quality of the adhesion between the geosynthetic and the adjacent bituminous layers, the type of raw material employed in geosynthetic fabrication, the type and dosage of tack coat, the position of the geosynthetic in the structure, the temperature and the loading type and magnitude (Nithin et al., 2015).

A review of pertinent literature on the fatigue behavior of geosynthetic-reinforced bituminous structure revealed that the placement of geosynthetic between bituminous layers results in a higher fatigue life varying between 2 and 10 times than unreinforced structure (Solatiyan et al. 2020b). This improvement in the fatigue life relies on the stiffness of the geosynthetic to the bituminous layer and on the bonding strength supplied at the interface. In this respect, the reduced bonding strength compared to the unreinforced case leads to a higher improvement in

the fatigue life due to increased ductility of the system (Sudarsanan et al. 2020). Same as for a single material. The fatigue behavior of a double layer structure relies on the failure criterion (Orešković et al. 2019). In this regard, different approaches have been adopted to capture the fatigue life of a bituminous structure. In a controlled-strain mode of fatigue test (ASTM D7460), in which the strain remains constant and the stress is decreasing, four different indices are of interest. $N_{f50\%}$ is a classical index related to the number of cycles when the initial stiffness modulus reaches its half value (Basueny et al., 2014). $N_{f\Delta\epsilon_{ax}}$ is defined based on the 25% difference in strain amplitude recorded by three separate extensometers. $N_{f\Delta\phi}$ corresponds to a difference of more than 5° of the phase angle recorded by each extensometer from the mean value. Finally, $N_{f\phi_{max}}$ considers the evolution of phase angle during the test. The number of cycles related to the maximum value of the phase angle is defined as the failure point of the structure. It is believed that all these criteria usually give similar results (Tapsoba et al. 2013). On this basis, Because of its ease of application, the classical index of fatigue failure was selected for the sake of this project.

The main purpose of this study is to understand the possible changes in rutting and fatigue behavior of bituminous double-layered structures, with embedded paving fabric. This study helps for the betterment in the design of reinforced structure with paving fabric.

6.4 Material and methods

The evaluation of the changes in rutting resistance and fatigue performance of double-layered structures, made of different mixtures, due to the placement of paving fabric at the interface of two bituminous layers compared to corresponding unreinforced structures are the objectives of this study. To this end, double-layer bituminous specimens, based on three kinds of mixes with and without paving fabric, were manufactured in the laboratory to simulate field conditions. Since the surface texture at the interface of two different bituminous layers plays a pivotal role in the reinforcement mechanism of paving fabric, it was assumed that the mechanical performance of the composite structure varies by the changes in the type of mixture used below and above the interface. Two significant failure criteria in pavement design methods were addressed during this study: the rutting resistance of the composite structure was investigated by the French Laboratory Rut Tester (FLRT), and the DGCB procedure was

employed to examine the fatigue behavior of reinforced and unreinforced specimens.

6.4.1 Materials

This research utilized two types of double-layered bituminous structures made of three different mixtures normally applied in Quebec (Canada), with and without paving fabric as the reinforcement interlayer installed at the interface of bituminous layers. The hot mixtures were designed in accordance with Transport Quebec's standard (LC 4202) as follows: (I) a surface course mixture with a nominal maximum aggregate size (NMAS) of 10 mm (ESG-10); (II) a binder course mixture with an NMAS of 14mm (ESG-14); and (III) a base course mixture with an NMAS of 20 mm (GB-20). Mix design gradation curves are illustrated in Figure 6.1, and relevant technical properties are given in Table 6.1.

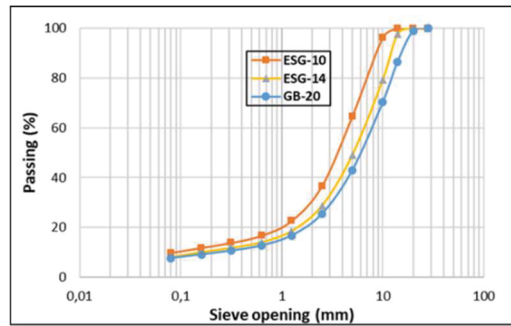



Figure 6.1 Mix design sieve curves

Table 6.1 Technical specifications of hot mixes

| Mixture | | ESG-10 | ESG-14 | GB-20 |
|--|----------------------------------|--|--------------------------------|--------------------------------|
| Binder Type | | PG 58-28 | PG 58-28 | PG 58-28 |
| Binder Content (% mass) | | 4.0 | 3.7 | 3.5 |
| Air Void Content (%) | | 3.8 | 4.1 | 4.8 |
| Mean Texture Depth (MTD) (mm) (ASTM E965) | | | 3.6 | 4.4 |
| Water Sensitivity (LC 26-001) (%) | Measured | 95.4 | 88.3 | 82.3 |
| | Required | ≥ 70 | ≥ 70 | ≥ 70 |
| Rutting Resistance (LC 26-410) (%) | Measured (After 30000 cycles) | 7.8 | 8.5 | 9.1 |
| | Required | (After 1000 cycles) ≤ 10 (After 3000 cycles) ≤ 15 | (After 30000 cycles) ≤ 10 | (After 30000 cycles) ≤ 10 |

The paving fabric is composed of two parts: a needle-punched nonwoven fabric together with asphalt cement type PG 64-34 as tack coat material applied on the top surface of the bottom asphalt layer. The principal mechanical specifications of the fabric, provided by the company, are presented in Table 6.2.

Table 6.2 Principal mechanical specification of fabric (provided by the company)

| Specification | Test Method | Unit | Value |
|---|-------------------|------------------|---------|
| Grab tensile elongation | CAN 148.1 No. 7.3 | % | 45–105% |
| Grab tensile strength | CAN 148.1 No. 7.3 | N | 550 |
| Mullen burst | CAN 4.2 No. 11.1 | kPa | 1585 |
| Bitumen retention | ASTM D6140 | L/m ² | 1.15 |
|  | | | |

Two types of double-layered structures by taking advantage of three different types of hot mixes were fabricated in the laboratory (Figure 6.2). In one of them, the ESG-10 was placed at the top as a surface course and the ESG-14 at the bottom as a binder course (i.e. ESG10/ESG-14). In the other one, the ESG-14 was employed at the top as a binder course and GB-20 at the bottom as a bituminous base course (i.e. ESG14/GB20). For each type of structure, two types of rehabilitation strategies were examined. First, a conventional method is considered as an unreinforced case, in which the top layer is applied on the bottom layer utilizing asphalt emulsion as tack coat. Second, a reinforced case by introducing paving fabric at the interface of bituminous layers.

The double-layered structure was prepared first by the implementation and compaction of the lower layer, succeeded by the spreading of tack coat (with/without fabric) and then the placement and compaction of the upper layer over the bottom layer. The compaction procedure, done at 135 ± 2 °C selected based on the type of bitumen (i.e., PG 58-28), was conducted in compliance with the French Roller Compactor, according to the European Standard EN 12697-33, .

Asphalt emulsion type SS-1h with a dosage of 180 gr/m^2 of residual bitumen was employed at the interface of unreinforced specimens, while 110 gr/m^2 of a PG 64-34, based on the specification supplied by the company was utilized between the fabric and the bottom bituminous layer in reinforced specimens. In order to complete breakage of the asphalt emulsion, five hours curing time was respected before the placement of the top hot mix layer. For the reinforced specimens, the application of asphalt cement and implementation of the top hot mix layer was carried out successively (no cure).

A total of eight reinforced and unreinforced slabs of size $500 \times 180 \times 100 \text{ mm}$ were prepared for rutting test and four slabs of size $500 \times 180 \times 150 \text{ mm}$ were manufactured for the fatigue test to extract three cylindrical shape specimens of size $135 \times 75 \text{ mm}$. A schematic view of specimens and their geometrical dimensions are presented in Figure 6.2.

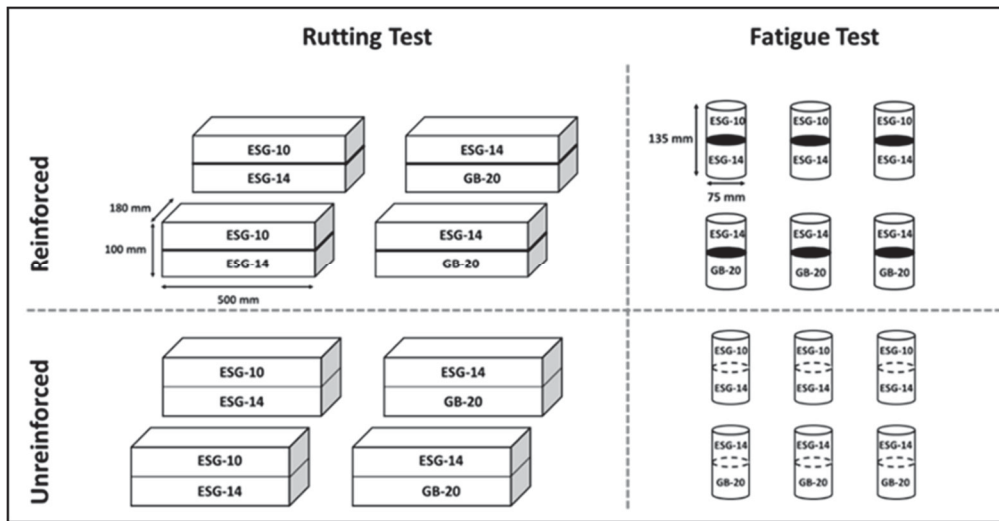


Figure 6.2 A schematic view of specimens prepared for each type of test

6.4.2 Test methods

The mechanical behavior of double-layered structures made of different types of hot mixes under cyclic loading was studied in order to highlight the reinforcement effect of a layer of paving fabric installed at the interface of bituminous layers compared to unreinforced double-layered structures. To this end, two fundamental failure criteria in mechanistic-based design methods were addressed. The rutting resistance of the composite system was examined through the French Laboratory Rut Tester (FLRT) and the fatigue performance of the system under repeated action of cyclic loads was evaluated by performing the fatigue test based on the

method developed at DGCB (Département de Génie Civil et Bâtiment) at the ENTPE (École Nationale de Travaux Publics de l'État, (Lyon, France). The details pertaining to each type of test will be discussed in detail in the following subsections. It was hypothesized that the adopted test methods would shed light on the mechanical properties of reinforced and unreinforced structures, necessary to be taken into account in design methods.

6.4.2.1 French laboratory rut tester (FLRT)

The resistance of hot mixes to flow rutting is evaluated in Quebec (Canada) by taking advantage of the FLRT, developed by France's Laboratoire central des ponts et chaussées (LCPC). For the sake of this project, the $500 \times 180 \times 100$ mm bituminous slabs, designed according to Transport Quebec's standard (LC 4202) (MTQ, 2018), were compacted in the laboratory by the means of a LCPC-type plate compactor, as shown in Figure 6.3. The reinforcement and the upper layer were added directly in the mold and compacted. The test was conducted at 58°C according to the type of bitumen employed in the hot mixture. Rut depths are measured as an average of 15 points on the surface after 1000, 3000, 10000 and 30000 cycles. Normally, with the FLRT, the rut depths are given as a percentage of the thickness of the slabs. Here, since ruts are measured on a system and not a single material, the rut depths are given directly in mm.

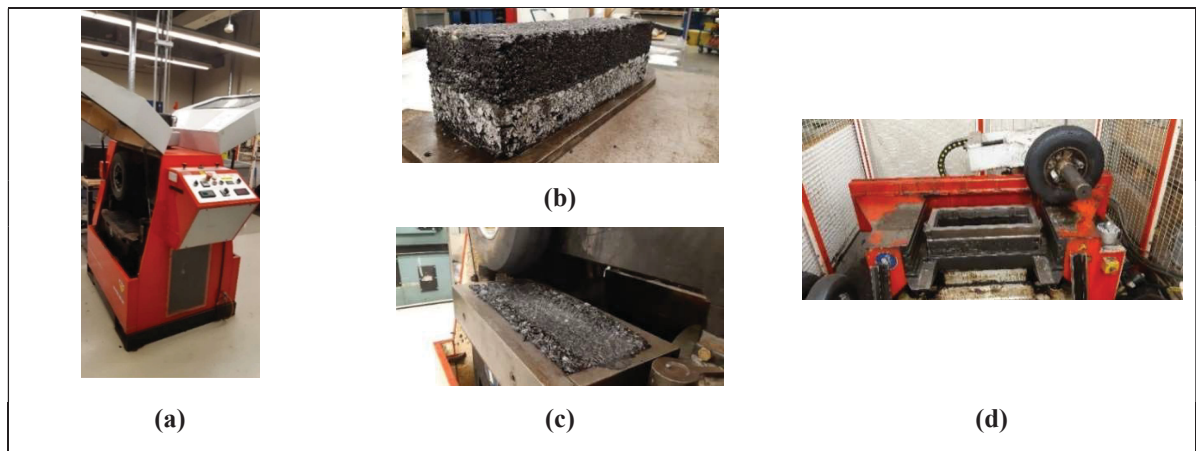


Figure 6.3 A view of rutting test: (a) French Laboratory Rut Tester (FLRT); (b) a double-layered reinforced structure; (c) wheel path imprint (rut depth) on the slab surface; (d) LCPC compactor

6.4.2.2 DGCB fatigue test method

The fatigue behavior of double-layer structures was investigated by the tension-compression method developed in the “ENTPE” (Di Benedetto et al., 2011). The homogeneity state of responses, in terms of stress and strain, induced in the specimen is the main feature of this test. The test was carried out at 10 ° C and a frequency of 10 Hz on cylindrical specimens with the same size as those used in the complex modulus test (i.e. 135 mm in height and 75 mm in diameter) by the cyclic solicitation of axial strain amplitude. The evolution in stiffness modulus of the specimens by the number of cycles was observed at three different strain levels to develop Wöhler’s curve for each type of structure. Figure 6.4 demonstrates a general view of the fatigue test.

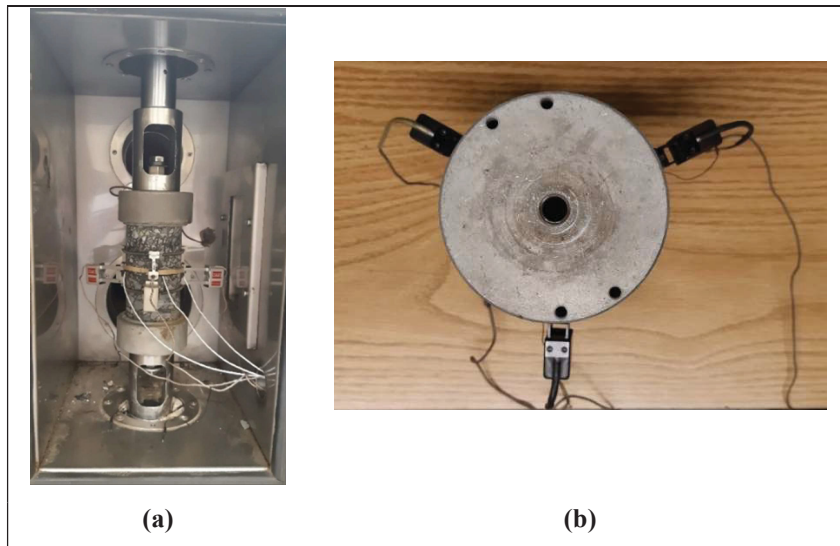


Figure 6.4 A view of fatigue test: (a) test setup; (b) arrangement of extensometers

6.5 Results and discussions

Presented in this research is a laboratory effort to comprehend the mechanical differences of two rehabilitation strategies on bituminous pavements under cyclic loading. The following subsections present details on the rutting and fatigue tests conducted on unreinforced and reinforced bituminous specimens.

6.5.1 Rutting test

Figure 6.5 illustrates the changes in the mean rut depth obtained from two slabs, and measured at four specified number of cycles (i.e. 1000, 3000, 10000 and 30000) for different types of reinforced and unreinforced structures. As can be seen, at the early stages of load passing (i.e. at 1000 and 3000 number of cycles) the rut depth increased sharply because of the densification effect and reduction in air voids, while after 10000 cycles, it followed a rather steady state increment trend. This can be attributed to the effects of post compaction and tertiary flow. This feature was found to be common in different types of structures. On this basis, if the rut depth between 10000 and 30000 cycles are considered in the calculation of rut development, a better indication of the actual rutting evolution in the field is expected (Yang et al., 2006). The slope of the evolution curve indicated on Figure 6.5 by S in mm per cycle, suggest that by placing the paving fabric between fine-graded hot mixtures (i.e. ESG-10 over ESG-14), the growth rate in the rut depth is almost doubled, whilst between coarse-graded hot mixtures, the evolution pattern was not influenced. Another point of interest was that the rut depth in unreinforced structures was clearly distinguished between ESG-10 over ESG-14 and ESG14 over GB-20 whereas this distinction was not obvious between different mixtures of reinforced types of structures. In addition, unreinforced composite structures (UN 10-14 and UN 14-20) have considerably lower rut depth compared with corresponding reinforced ones at any number of cycles. Moreover, the fine-graded composite structures (ESG-10 over ESG-14) outperformed the coarse-graded composite structures (ESG-14 over GB-20) in terms of rut depth. However, at a higher number of cycles (more than 20000 cycles) the rut depth in fine-graded reinforced composite structures surpassed over the coarse-grade ones. Figure 6.6 also demonstrates a comparison in rut depth between different types of composite structures. It is worth mentioning that this result was obtained while each mixture applied at the bottom and top of the interface respected the Quebec's standard (LC 26-001), as indicated in Table 6.1.

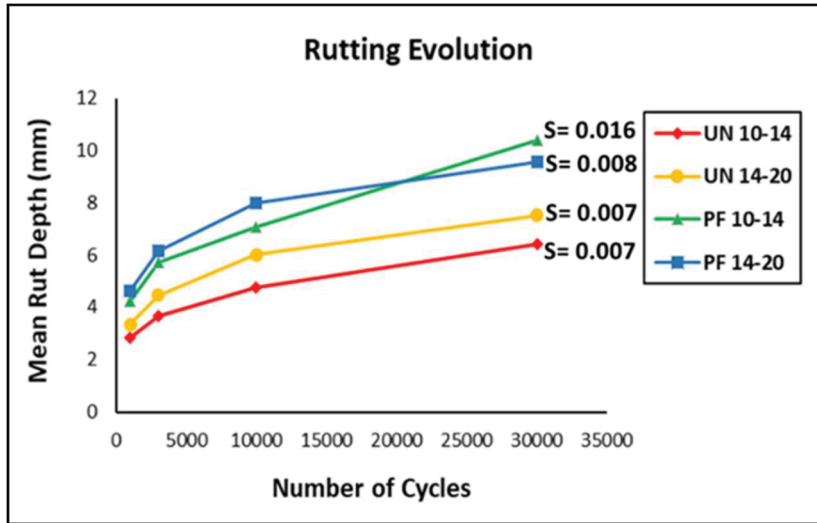


Figure 6.5 Rutting depth evolution by the number of cycles for different types of reinforced and unreinforced structures (UN: unreinforced structure; PF: reinforced structure with paving fabric)

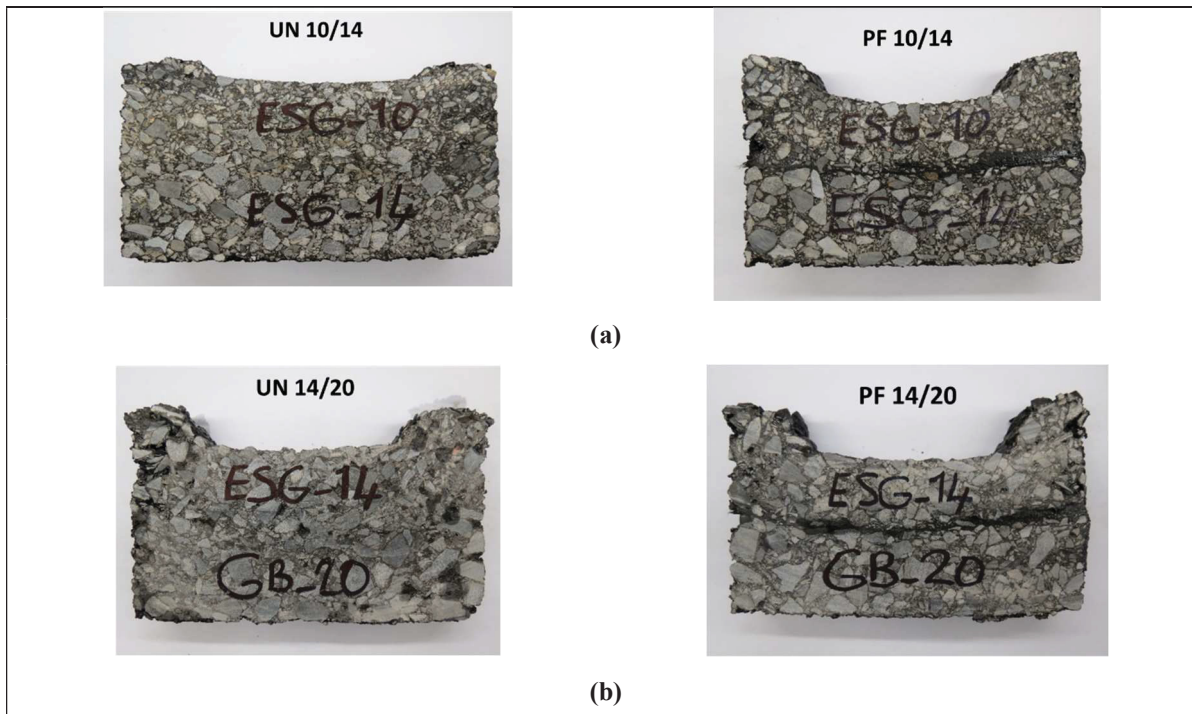


Figure 6.6 The rut depth after 30000 cycles taken from different types of composite structures (UN: unreinforced structure; PF: reinforced structure with paving fabric): (a) ESG 10 over ESG 14; (b) ESG 14 over GB-20

Figure 6.7 also shows the rut depth in a cross-sectional view in the middle of the specimen positioned in French Rutting Tester (FRT) (i.e. at the intersection of vertical line 3 with horizontal A-F axes) after 30000 cycles. It could be recognized that the placement of a layer of paving fabric between different types of hot mixtures, regardless of the size of material surrounding the paving fabric, acted reversely on the capability of the structure against flowing out the material under cycling loads. This negative effect could be partially explained by the lack of interlocking between the aggregates in adjacent hot mixture layers in the presence of the paving fabric.

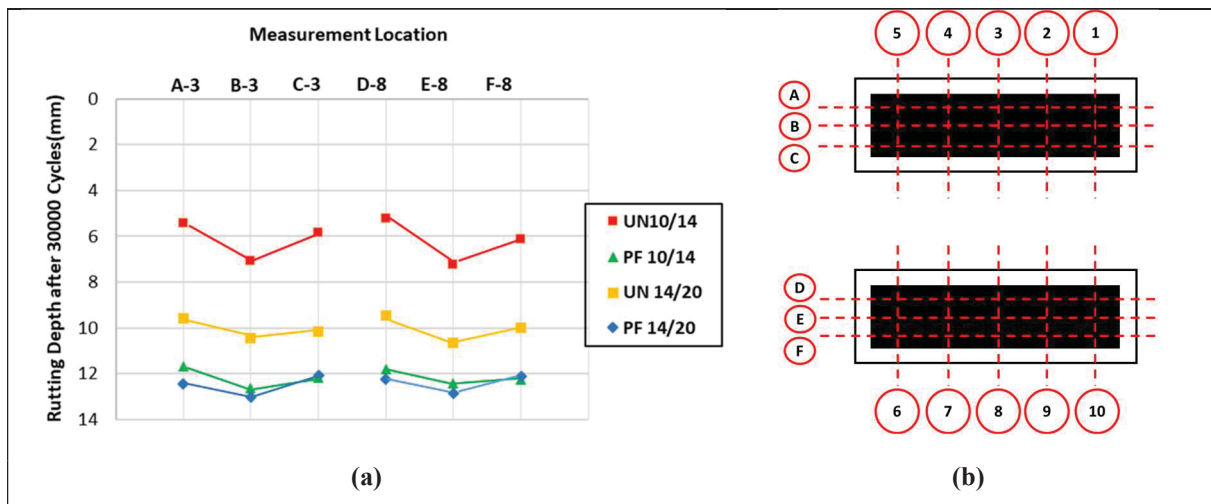


Figure 6.7 The rut depth measured at different locations of mid-span after 30000 cycles: (a) changes in rut depth for different types of structures; (b) axing plan of slabs under inner and outer wheels of French Rutting Tester

In general, the introduction of a layer of paving fabric between hot mixtures led to a higher rut depth with a remarkable rate of growth when surrounded by finer-graded mixtures.

6.5.2 Fatigue Test

The fatigue tests were performed on different types of reinforced and unreinforced structures at three different strain levels, complying with the DGCB method. The actual axial strain amplitudes, captured at $T=10\text{ }^{\circ}\text{C}$ and $f=10\text{ Hz}$, the value of the initial stiffness modulus denoted by $|E_0^*|$ derived from each strain level and its mean value for each type of structure are specified in Table 6.3. As evidenced, the initial modulus of the composite systems with and without paving fabrics was almost the same between the structures composed of similar mixes.

It could be inferred that the placement of paving fabric between different hot mixtures has no meaningful influence on the initial modulus of the system.

Table 6.3 Fatigue test specifications at $T= 10\text{ }^{\circ}\text{C}$ and $f= 10\text{ Hz}$

| Structure | Axial Strain Amplitude ($\mu\text{m/m}$) | Initial Modulus $ E_0^* $ (MPa) | |
|-----------|---|---------------------------------|---------|
| | | Value | Average |
| UN 10/14 | 66.5 | 6924 | 6981 |
| | 74.6 | 6874 | |
| | 99.1 | 7146 | |
| UN 14/20 | 64.8 | 4759 | 4479 |
| | 73.3 | 4425 | |
| | 95.3 | 4255 | |
| PF 10/14 | 65.7 | 6849 | 6903 |
| | 87.1 | 6906 | |
| | 97.2 | 6955 | |
| PF 14/20 | 67.1 | 4528 | 4539 |
| | 85.6 | 4477 | |
| | 96.4 | 4612 | |

Figure 6.8 illustrates the $N_{f50\%}$'s Wöhler curve for the reinforced and unreinforced structures composed of different mixtures. The vertical axis is the number of cycles at failure and the horizontal axis shows the actual applied strain level during the test, both axes in logarithmic scales. Table 6.4 also presents fatigue parameters indicated in Equations (6.1) and (6.2) based on $N_{f50\%}$ fatigue failure for each type of structure.

As shown in Figure 6.8, the Wöhler curve for reinforced structures (i.e. PF 10/14 and PF 14/20) are distinctly placed over the corresponding unreinforced structure (i.e. UN 10/14 and UN 14/20). Another point of interest was that the slope of the Wöhler curve in unreinforced structures is steeper than the pertinent reinforced structure, which indicates that the stiffness modulus in unreinforced structures was decreased more rapidly than that in reinforced ones to the respective failure values. Additionally, R^2 values shown on each curve indicates that the regression line fitted on the data could suitably justify changes, which in turn proves the

adequacy of the $N_{f50\%}$ failure criterion to study the fatigue behavior of structures under cyclic loadings.

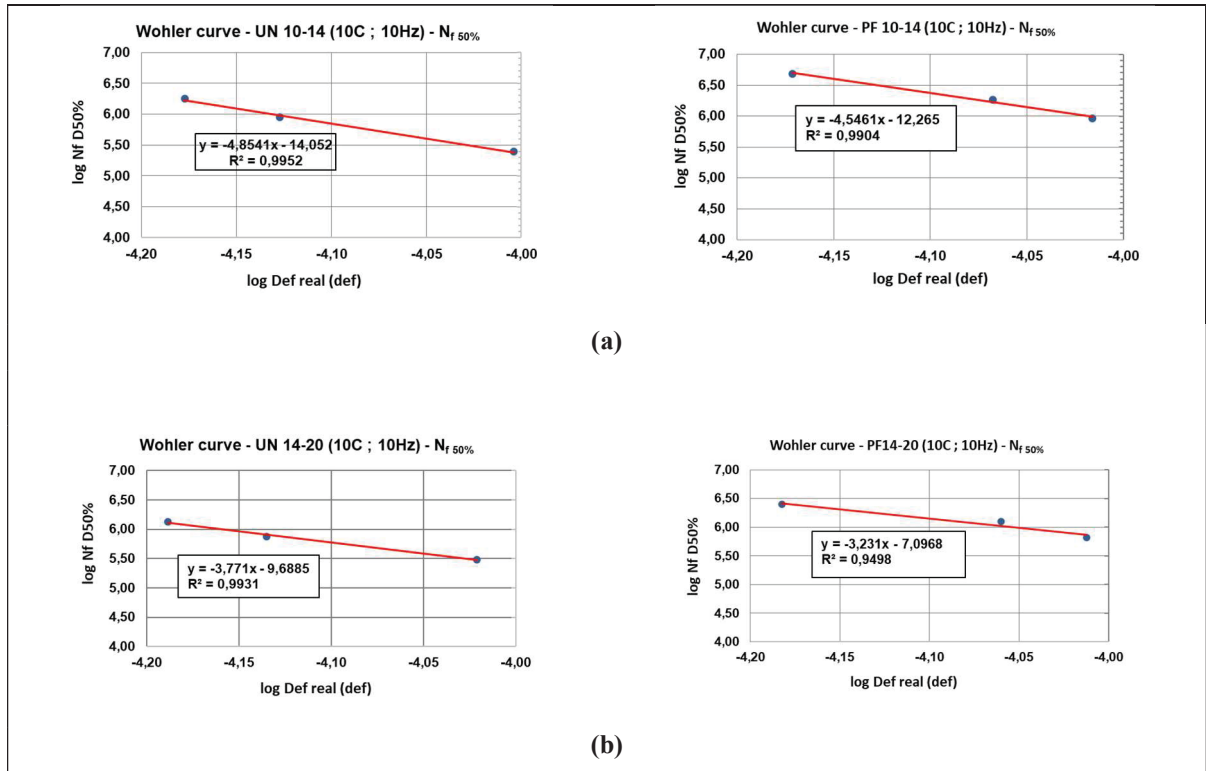
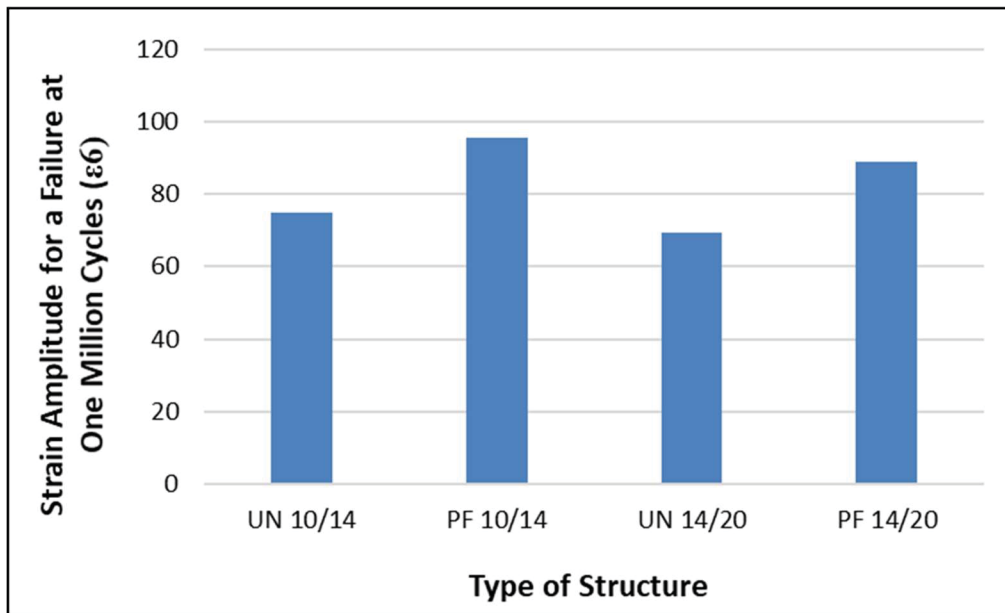


Figure 6.8 Wöhler curve developed for each type of composite structure at $T = 10\text{ }^\circ\text{C}$ and $f = 10\text{ Hz}$ (UN: unreinforced structure; PF: reinforced structure with paving fabric): (a) ESG 10 over ESG-14; (b) ESG-14 over GB-20

Table 6.4 presents a comparison in material-dependent coefficients (i.e. K_1 and K_2), R-squared (R^2) and axial strain at one million cycles (ϵ_6) between different types of structures. As can be seen, the ϵ_6 values, calculated according to Equations (6.1) and (6.2), are about 30 percent higher in reinforced structures than those in corresponding unreinforced structures. It could be deduced that the reinforced structure with paving fabric has considerably higher fatigue life than the unreinforced structure. As shown in Figure 6.9, this advantage was more highlighted in the reinforced structure composed of fine-graded mixtures (i.e. PF 10/14).

Table 6.4 Comparison of fatigue parameters based on NF50% failure criterion

| Structure | Fatigue Parameters for $N_{f50\%}$ Criterion | | | |
|-----------|--|-------|--------|--------------|
| | K_1 | K_2 | R^2 | ϵ_6 |
| UN 10/14 | 8.88 E -15 | 4.85 | 0.9952 | 74.8 |
| UN 14/20 | 2.05 E-10 | 3.77 | 0.9931 | 69.5 |
| PF 10/14 | 5.43 E-13 | 4.55 | 0.9904 | 95.5 |
| PF 14/20 | 8.0 E -8 | 3.23 | 0.9498 | 88.9 |

Figure 6.9 Comparison of parameter ϵ_6 for the reference and reinforced structures composed of different mixtures

This attribute could be explained by the presence of the asphalt cement at the interface of a reinforced structure as tack coat material compared to the asphalt emulsion employed in the same location of an unreinforced structure. This could bring more structural integrity to the composite system at low and medium temperatures, which is usually encountered in Canada's roads.

6.6 Conclusion

In this study, the mechanical behavior of two rehabilitation strategies applied on a bituminous

layer under cyclic loading was examined. First, a conventional method in which a new bituminous layer is directly spread over the existing one along with a thin film of the asphalt emulsion to provide adhesion at the interface (tack coat). In the second one, an interlayer composed of a layer of fabric (nonwoven geotextile) accompanied with the asphalt cement, called paving fabric, is implemented over the existing bituminous layer before the application of the upper bituminous layer. The possible mechanical changes in introducing a layer of paving fabric between two bituminous layers in two different types of structures were studied by comparing the results with those derived from the corresponding unreinforced structure. Two principal failure criteria, commonly used in mechanistic-based design methods, were addressed; permanent deformation or rutting and fatigue failure. The following conclusions were found:

- The placement of a layer of paving fabric between bituminous layers of different sizes led to higher rut depth compared with corresponding unreinforced cases. Meanwhile, the rutting growth rate in a reinforced structure composed of fine-graded hot mixtures was considerably higher than that embedded in coarse-graded mixtures.
- The rut depth in reinforced structures at higher number of cycles (i.e. 30000 cycles) was not influenced by the type of mixture surrounding the paving fabric. In addition, the initial stiffness modulus of the composite structure was independent of the type of material employed at the interface of bituminous layers.
- The fatigue failure criterion defined in terms of $NF_{50\%}$ was a suitable tool to predict the fatigue life of reinforced or unreinforced composite structures made of different hot mixtures. On average, the ϵ_6 (strain amplitude at one million cycles) in reinforced structures was 30 percent higher than that in unreinforced ones.
- The application of paving fabric between bituminous layers resulted in lower rutting resistance but increased fatigue life compared with unreinforced structures. In this connection, the introduction of paving fabric between coarse-graded mixtures (i.e. ESG-14 over GB-20) presented a fair balance between rutting resistance and fatigue performance of the composite structure under cyclic loading.

CHAPTER 7

LABORATORY EVALUATION OF INTERFACIAL MECHANICAL PROPERTIES IN GRID-REINFORCED BITUMINOUS LAYERS

Ehsan Solatiyan^a, Nicolas Bueche^b, Alan Carter^c

^{a, c} Department of Construction Engineering, École de Technologie Supérieure (ÉTS),
1100 Rue Notre-Dame O, Montréal, QC H3C1K3, Canada

^b Department of Architecture-Wood-Civil Engineering, Bern University of Applied Sciences
(BFH), Pestalozzistrasse 20, CH-3401 Burgdorf, Switzerland

Paper accepted for publication in *Geotextiles and Geomembranes*, Dec 2020

7.1 Abstract

In this study, the mechanical properties of composite bituminous structures with grid products, used as an interlayer between different types of bituminous mixtures, at a constant temperature were examined. A twofold experimental program based on new approaches was selected. A new configuration of the 3-Point Bending Test (3-PBT) was adopted to capture the J-integral and crack resistance property defined by crack resistance index (CRI) at the interface against bottom-up crack propagation. The bonding quality at the interface was also defined through a new index named coefficient of interface bonding (CIB), which was measured via a modified version of the slant shear device. The results derived from this research revealed that reinforcement of the interface, with varying degree of surface texture, by grid products significantly enhances the fracture toughness of the whole system in terms of the J-integral, which could be properly connected to the combined functions of bonding quality and crack resistance indices defined at the interface.

7.2 Introduction

Resurfacing an existing deteriorated bituminous surface layer with a layer of hot mix asphalt (HMA) is viewed as a prevalent rehabilitation technique to upgrade the ride quality for users.

However, the occurrence of premature failures in the form of reflective cracking endangers the service life of this strategy, which is in conflict with the growing demand for more sustainable roads. This phenomenon is almost exclusively attributed to the movements induced at any form of discontinuities in the pavement structure, triggered by temperature oscillations and wheel loads (de Bondt, 2000; Mandal et al. 2018; Moghadas Nejad et al. 2016). In this context, thermally driven reflective cracks, which occur in pure mode I of crack opening mechanism (Solatiyan et al. 2020a; Kim and Buttlar, 2002), contributes more than traffic loads to minimize the efficiency of the overlayment (Gonzalez-Torre et al., 2015; Noori et al., 2014). Accordingly, many remedial techniques have been recommended to retard the appearance of reflective cracking (Brown et al., 2001; Nguyen et al. 2013; Prieto et al., 2007). Among them, taking advantage of polymeric-based grid as an interlayer between a rehabilitated surface layer and a fresh overlay has drawn a lot of attention from the engineering community owing to its adaptability to asphaltic materials (Ahmed et al. 2018, Solatiyan et al. 2020b).

The anti-reflective property measurement of grid products embedded in bituminous layers has been the subject of interest in recent years (Prieto et al., 2007; Khodaii et al., 2009; Gonzalez-Torre et al., 2015; Ingrassia et al. 2020). Based on digital imaging techniques, on the rate of crack growth measurements, and on the development of load-displacement curves, it is understood that grid-reinforced bituminous layers are capable of extending the pavement service life by deviating the crack path from bottom to the top surface and by dissipating the energy of crack during propagation stage (Moghadas Nejad et al., 2014; Sobhan et al., 2005; Ling et al., 2019; Saride and Kumar, 2017; Romeo et al., 2014; Moaydi et al. 2009). However, in parallel studies, it was realized that this asset is linked to appropriate bonding quality provided at the interface of the grid and adjacent asphalt layers (Brown et al., 2001; Barraza et al., 2010; Pasquini et al., 2015; Canestrari et al., 2013, Solatiyan et al., 2020b). Nevertheless, the specific connection between crack resistance property at the interface, the pertaining energy dissipation capability and the bonding quality between the layers are unclear.

Introducing interlayer systems between bituminous layers could change the mechanical properties of the system in terms of stiffness modulus, crack initiation in the lower layer, crack propagation in the upper layer, fracture toughness and shear strength of the system. However, the objective of the present study would be on changes in anti-reflective and shear properties

emerged in the presence of the reinforced and unreinforced interfaces and their interconnections. Their possible mechanical variations in stiffness modulus of the system is the subject of another undergoing project.

This study is necessary to gain an in-depth knowledge that allows selecting a viable interlayer for the pavement rehabilitation purposes. It is mandatory to study bituminous systems, asphalt mix-geogrid-asphalt mix or asphalt mix-tack coat-asphalt mix, and not simply asphalt mixes by themselves or just the grids in order to well understand the reinforcement at the pavement structure scale.

This paper is organized into five sections. A review of studies on fracture and shear tests are first presented, and this is continued with a description of the materials employed to fabricate the specimens. The subsequent section will introduce the experimental results, followed by a detailed analysis. Finally, a summary of the findings is listed.

7.3 Research background

In order to shed light on the efficiency of any anti-crack treatments employed as an interlayer between bituminous layers, the fracture toughness parameters derived from fracture tests including stress intensity factor (K), Crack Mouth Opening Displacement (CMOD) and energy release rate per unit area of the crack surface (J-integral) have broadly been utilized. In this regard, the stress intensity factor was the interest of a study to understand how the number of freeze-thaw cycles and water saturation could influence the thermal cracking development in asphaltic mixtures under different modes of loadings (Fakhri et al., 2020). In another study, the fracture parameters, including the J-integral and the CMOD were employed to study the fracture behavior of bituminous mixtures containing reclaimed asphalt pavement (RAP) (Tang, 2014). Accordingly, the mechanical behavior of interesting materials and the dimension of the fracture process zone (FPZ) are key factors in selecting the appropriate parameter to evaluate and compare the fracture resistance of the material (Wu et al., 2005). Concerning the asphalt mixture subjected to ambient temperature, J-integral and CMOD are good indications to account for the plastic deformations around the crack tip (Zhu et al., 2012). In this context, the J-integral can be quantified experimentally by developing a load-displacement curve, and CMOD is determined by measuring the displacement close to the crack tip induced by elastic

and plastic deformations. However, energy-based indices could effectively take the effect of both stress and strain into account and lessen the dimensional effect from the size of specimen and depth of notch in the characterization of crack extension (Zhu et al., 2017).

In reference to fracture tests, various types of test methods and devices such as Disc-Shaped Compact Tension (DCT), Single Edge Notched Beam (SENB) and Semi-Circular Bend (SCB) have been employed by researchers (Artamendi and Khalid, 2006; Molenaar et al., 2000; Li et al., 2004; Wagoner et al., 2005; Pirmohammad and Kiani, 2016). However, because of the complex specimen preparation, geometry-dependency of the test results along with the self-weight effect on crack initiation, the SCB test has been recognized as an attractive test method over others (Nsengiyumva et al. 2015). SCB Tests, consisting of a three-point bending configuration along with semi-circular shaped specimen with a mechanical notch on straight edge, have been conventionally applied to asphalt mixtures at intermediate temperatures (ASTM D8044-16). Nevertheless, in the case of reinforced layers with grids, the specimen preparation procedure is not convenient and not a good representative of field conditions. Moreover, the fracture energy obtained from this test is not a suitable indicator for the evaluation of materials, which exhibit large elastic-plastic behavior under loading.

Additionally, the connectivity of anti-crack properties provided at the reinforced interface with the shear test result is another missing point, which needs to be taken into account to properly address the mechanical effect of introducing a layer of the grid on the structural integrity of the whole system. The quality of bonding between the connected layers is of paramount importance in shear stiffness at the interface (Sudarsanan et al., 2018; Noory et al., 2019; Jaskula and Rys, 2017). A variety of devices have been developed to measure the shear strength of grid-reinforced interface under monotonic or dynamic loadings (Molenaar, 1993; Canestrari et al., 2005; Roffe and Chaignon, 2002; D'Andrea and Tozzo, 2012; Sholar et al., 2004; Tschegg et al., 1995; Noory et al., 2018). However, even if interesting results were obtained, the complexity of these devices, which introduce appreciable levels of bias into test results and the deficiency in simulating the field condition on laboratory scale specimens led to incoherent interpretations of the real mechanical behavior. As regards to the geometry of the specimens, cylindrical shape specimens require great manipulation in terms of coring and grinding, but the main issue resides in controlling the number of meshes in the specimens under

investigation, while in the case of cubic shape specimens, these restrictions are mostly trivial. Besides, any attempts to confine the specimen into molds or gluing the ends of the specimen into plates can result in a stress redistribution or a concentration effect, which may affect the structural response of the system.

It has been recognized that the halting effect against crack growth in grid-reinforced bituminous layers was attributed to the bond strength at the interface (Sudarsanan et al., 2018). In this sense, most of the pertinent research relied on shear force-shear displacement diagram to establish this mindset (Wanga et al., 2020; Walubita et al., 2018; Sagnol et al., 2019). However, regarding the ability of reinforced structures to undergo large shear deformation before failure, limited studies have specifically focused on developing an index, based on the bonding quality, which concurrently takes the effect of shear strength and shear displacement into account.

To attain a general understanding of the effect of grid-reinforced interface on fracture toughness and shear stiffness of the composite structure, a novel experimental survey and an analytical investigation were adopted. The following objectives were studied: (I) how the fracture toughness emerged at the reinforced interface influences the crack evolution (II) how the shear stiffness and fracture toughness affects each other in different interface settings in terms of the type of mixture and grid. This study is indeed vitally important to appropriately define the interaction of newborn interface properties in the presence of the grid into mechanistic-based design methods and also as a practical tool to distinguish between poor and good reinforced interfaces.

7.4 Material and Methods

The variation in mechanical properties of the pavement system by the placement of grid products at the interface of different asphalt layers is the subject of this study. To this end, bi-layer bituminous specimens, based on three kinds of mixes with and without grid-based interlayers, were fabricated in the laboratory to resemble in-site characteristics. Since the surface texture provided at the interface plays an important role in the reinforcement effect derived from grids, it was postulated that the mechanical behavior of the system in reinforced and unreinforced specimens changes by the variation in type of mixes applied below and over

the interface. Two main mechanical properties were addressed during this research: the shear responses of the composite structure were examined through a new version of slant shear device, and a novel configuration of the 3-point bending test was designed to perceive the mechanical reaction of the system against crack initiation and development from the bottom layer to the top surface.

7.4.1 Materials

In this research, three different types of asphalt concrete mixture, composed of the same kind of PG 58-28 asphalt binder but with varying gradations, were designed according to Transport Quebec's standard (LC 4202) (MTQ, 2018). The first mixture is referred to as ESG-10 specified by a nominal maximum aggregate size (NMAS) of 10 mm, typically applied as a surface course, while the second and third mixtures, called ESG-14 and GB-20 with the NMAS 14 mm and 20 mm respectively, are standard binder and base course mixes. The gradations of the designed mixes are shown in Figure 7.1 and all three mixes properties are given in Table 7.1.

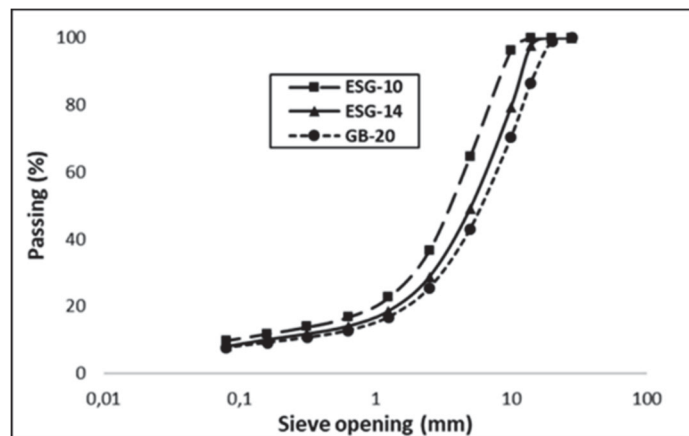


Figure 7.1 Gradation curves of the mixes

Table 7.1 Mechanical specifications of asphalt concrete mixtures

| Technical specifications of mixes | | | | | |
|--|----------|--|---------------------------|---------------------------|--|
| Mixture | | ESG-10 | ESG-14 | GB-20 | |
| Binder Type | | PG 58-28 | PG 58-28 | PG 58-28 | |
| Binder Content (% mass) | | 5.45 | 5.22 | 5.14 | |
| Mean Texture Depth (MTD) (mm) | | | 3.6 | 4.4 | |
| Water Sensitivity (LC 26-001 ¹) (%) | Measured | 97.3 | 85.5 | 86.5 | |
| | Required | ≥ 70 | ≥ 70 | ≥ 70 | |
| Rutting Resistance (LC 26-410 [*]) (%) | Measured | After 1000 = 6.6 After 3000 = 8.2 | 7.2 | 9.1 | |
| | Required | (After 1000 cycles) ≤ 10 (After 3000 cycles) ≤ 15 | (After 30000 cycles) ≤ 10 | (After 30000 cycles) ≤ 10 | |

* LC standards are Quebec Ministry of Transportation's standards

Four types of grids with different raw material and mechanical properties were employed as the interlayer between the above mentioned mixes. The main technical properties of the grids are listed in Table 7.2. GW, GB, and GR grids are coated with bitumen, while GV is a geocomposite composed of a non-woven fabric attached to the bottom side of the grid.

Table 7.2 Technical properties of grids (provided by the geogrid supplier)

| Name | Abbreviated Name | Raw Material / Transversal Strength (kN) | Raw Material / Longitudinal Strength (kN) | Protective Layer on the Grid | Elongation | | Mesh size (square shape) (mm) |
|----------------------|------------------|--|---|------------------------------|-----------------------|------------------------|-------------------------------|
| | | | | | Transversal Direction | Longitudinal Direction | |
| Glasphalt G 120/120 | GW | Glass fibers / 120 | Glass fibers / 120 | Plastic foil | <3% | <3% | 20 |
| Carbophalt G 120/200 | GB | Glass fibers / 120 | Carbon fibers / 200 | Plastic foil | <3% | <1.5% | 20 |
| Carbophalt G 200/200 | GR | Carbon fibers / 200 | Carbon fibers / 200 | Plastic foil | <1.5% | <1.5% | 20 |
| Glasphalt GV 120/120 | GV | Glass fibers / 120 | Glass fibers / 120 | non-woven | <3% | <3% | 20 |

- A total of 20 slabs of $500 \times 180 \times 100$ mm, 16 slabs for reinforced structure and four slabs for unreinforced one, were prepared. For each slab, first, the bottom layer (ESG 14 or GB-20) was fabricated by mixing the aggregates and the asphalt binder at $150\text{ }^{\circ}\text{C}$ and then compacted at $135\text{ }^{\circ}\text{C}$ with French Roller compactor, complying with European Standard EN 12697-33. After one day of curing, in order to assure proper bonding between the grid and the bottom slab, a thin layer of slow-setting asphalt emulsion was uniformly applied on the surface. The dosage of the tack coat type SS-1h (slow setting) was selected 180 g/m^2 of residual bitumen for geogrids and unreinforced surface and 270 g/m^2 of residual bitumen for geocomposite, according to the specifications given by the company. Two different approaches were followed for the placement of the grids on the emulsified surface: for the surface reinforced with geogrids and unreinforced surface, three hours of curing time was respected for complete breakage of the emulsion. Then, for the reinforced case, the grid was installed by the steady-state movement of a gas blow torch on the bottom side of the grid to adequately mild the bitumen coated the side surface of geogrids.
- For the surface reinforced with geocomposite, it was directly installed on the wet surface with no curing time.

The experimental program was continued by laying a surface layer of asphalt mix (ESG-10 or ESG-14) over the bottom layer and the compaction of the whole composite structure with the same procedure and temperature as mentioned above. This construction plan is illustrated in Figure 7.2.

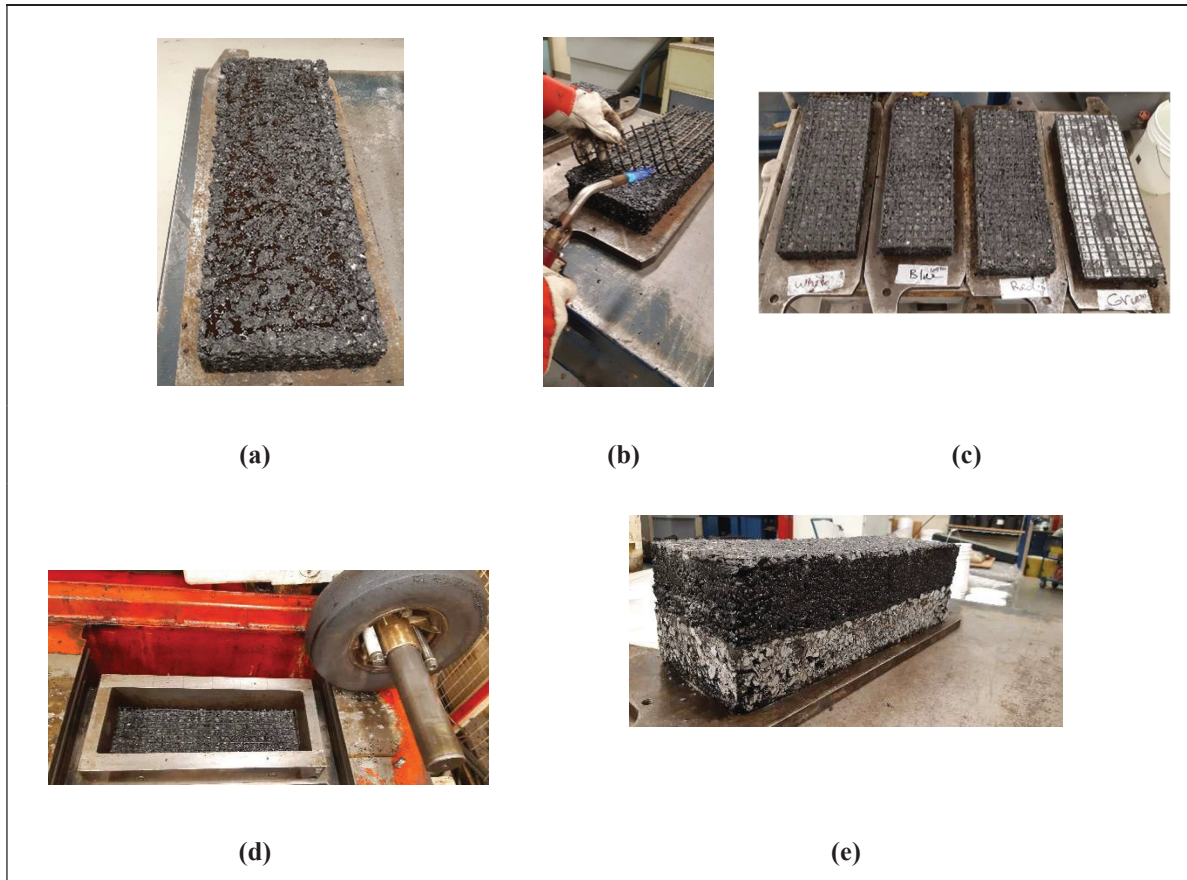


Figure 7.2 Experimental procedure followed for each slab: (a) emulsified surface of the bottom slab; (b) application of gas blowtorch below the G-products after completion of breakage; (c) prepared reinforced surfaces with G & GV products; (d) preparation for the implementation of the top slab over bottom-reinforced slab; (e) Reinforced composite structure

After the preparation of double layer slabs, four cubic specimens were extracted with dimensions of $80 \times 80 \times 80$ mm from the slabs. This process was performed based on the recommendation reported by Romeo et al. (2014). Two types of tests were established for the sake of this project: a modified configuration of the 3-point bending test (3-PBT) for crack resistance evaluation of the composite structures and shear test based on a novel apparatus to examine the bonding quality at the interface. Both of the tests were carried out on three replicates of each type of structure at 20 ± 1 °C according to ASTM D8044-16 to make sure of the viscoelastic behavior of the material. Figure 7.3 schematically presents the arrangement and dimensional details of specimens for each type of test.

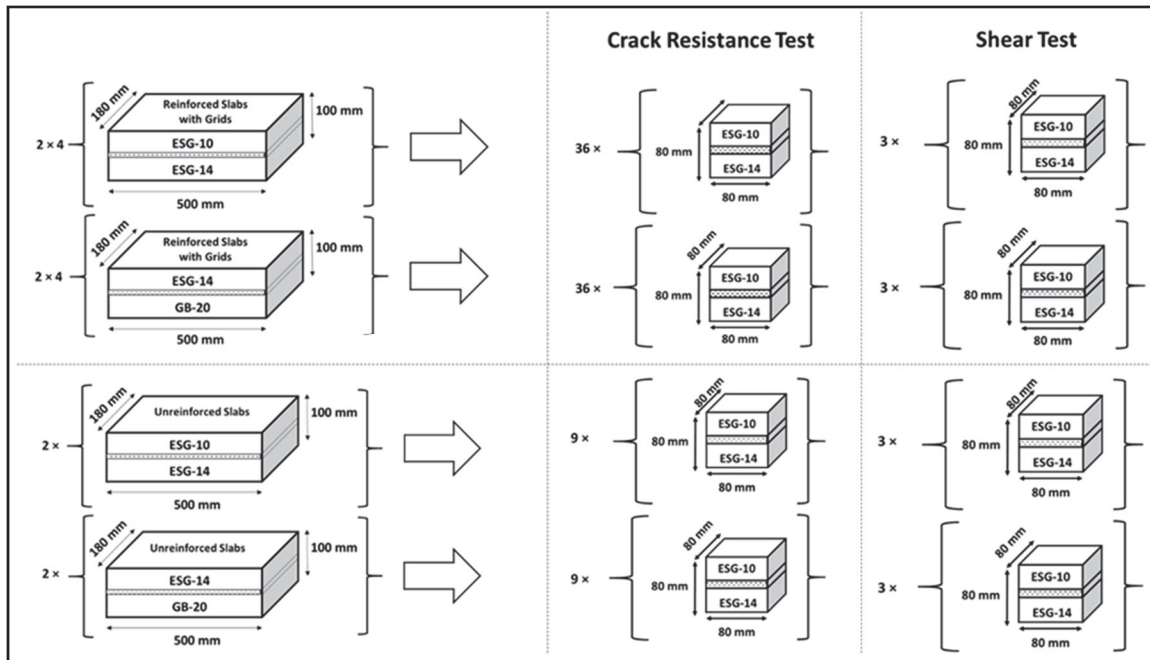


Figure 7.3 A schematic of size and number of specimens for each type of test

7.4.2 Test methods

The presence of an interlayer between bituminous layers improves the anti-crack property of the system (Elseifi, 2003). However, this benefit is dependent on the bonding quality provided at the interface (Sudarsanan et al., 2018). In the present study, an attempt was made to characterize the connection between interfacial mechanical properties and fracture parameters. This objective was realized through the development of two pieces of equipment. The modified version of the 3-point bending test (3-PBT) was used to capture the fracture parameters in terms of the J-integral and crack resistance index at the interface of both reinforced and unreinforced specimens. Additionally, a new shear test setup was designed to quantify the bonding quality at the interface between different types of grids and mixes. These test methods are direct representations of the field behavior where cracking advances from a discontinuity in the existing surface under the effect of a sudden drop in the temperature and then at the interface level, depending on the bonding quality between the layers, the system reacts with different degrees to the crack propagation. It was assumed that this methodology would result in gathering better insight into the fracture behavior of reinforced and unreinforced composite

structures. The following subsections will give a detailed description of the introduced test methods.

7.4.2.1 3-point bending test (3-PBT)

This test was an updated version of the method initially employed to study the crack initiation and propagation in notched bituminous specimens, including paving fabric (Solatiyan et al., 2020a). The differences include the specimen geometry, modified loading plate and raised supporting base. This configuration allows simulating mode I of loading perpendicular to the notch plane, and providing enough space to equip the specimen with measuring instruments. In this context, three sets of crack gauges were utilized. One at the mid-height of a notch to control the propagation of crack and the two others below and above the interface to monitor the crack growth under applied tensile stresses to develop a new crack resistance index (CRI) based on the energy dissipated across the interface, which encompasses the effect of both stress and strain in their maximum value. In addition, a vertical linear variable differential transformer (LVDT) was attached at the bottom of the specimen through a thin plate to develop the force-displacement curve required to study the energy dissipation over the test. The test setup is shown in Figure 7.4.

The test was run in an MTS press in a controlled-displacement mode of 2 mm/min because the fracture energy reduces by increasing the loading rates and increases as the loading rate decreases at all range of temperatures (Stempihar et al., 2013). It is worth mentioning that under tensile mode of loading (mode I) the effect of loading rate on fracture behavior of bituminous mixture, with low air void content, at intermediate temperature is insignificant (Aliha et al., 2018). The test was performed at an intermediate temperature of 20 ± 1 °C. At low or high temperature it is difficult to rank the specimen based on the energy dissipation ability during crack development (Zhu et al., 2017) and also because the bottom-up cracking is more frequently observed in intermediate temperature (Gauthier, 2012). Furthermore, to gain knowledge on fracture energy, three different mechanical notches with notch depth to specimen height ratio between 0.25 to 0.375, according to ASTM E399 (ASTME399-90, 2008), were tested. Details on the dimensions will be further presented.

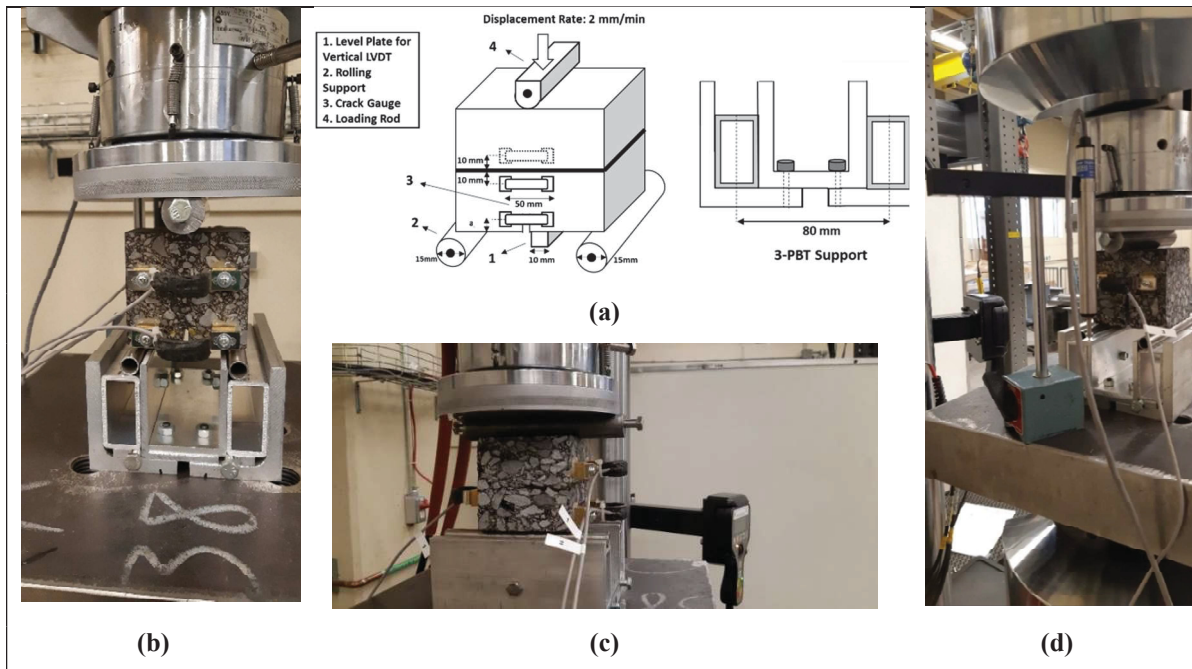


Figure 7.4 A scheme of 3-PBT setup: (a) schematic design; (b) front view of the device mounted on MTS press; (c) location of crack gauges; (d) back view representing the placement of crack gauge above the interface and LVDT

7.4.2.2 Interface shear test

The necessity of a test method with the least complexity in terms of device configuration and specimen preparation and greatest proximity to the field condition inspired the development of a modified slant shear device, as shown in Figure 7.5, which was initially employed in the cement concrete domain (Diab et al., 2017) and modified to satisfy the need of this study. The device is composed of two aluminum parts with the same dimensions, one fixed at the top and the other movable with a rocker ski over a steel-made rail at the bottom, both mounted in an MTS servo-hydraulic loading system. This setup allows to run the test in different temperatures and modes of loading (static or cyclic) with less effort in specimen preparation, free of gluing and molding, and high flexibility in vertical adjustment to accommodate the specimen with various heights into the device. Moreover, the test device is able to simultaneously apply the vertical and horizontal stresses to the interface, which is normally the case in field conditions. Furthermore, the degree of freedom provided in the horizontal direction by means of the ski and the rail prevents crushing the specimen under the compressive load applied at the top. It is worth mentioning that the flat part in the middle with a raised tail at the end of the designed

ski provides a very good floating condition of the device over the rail with a negligible effect from the friction. The horizontal displacement during the test was recorded through an LVDT, attached to the bottom-loading arm, and the vertical load was directly recorded by the machine, which was further broken down into normal and tangential components knowing the inclined surface of 45° .

For the sake of this research, the test was performed in a constant displacement mode of loading 2 mm/min, similar to the 3-PBT at the same temperature as $20 \pm 1^\circ\text{C}$. Besides, the gap width between the interface and the edge of the top part, as shown in Figure 7.5, is 5 mm, as earlier considered in the Sapienza Horizontal Shear Test Machine (D'Andrea and Tozzo 2012).

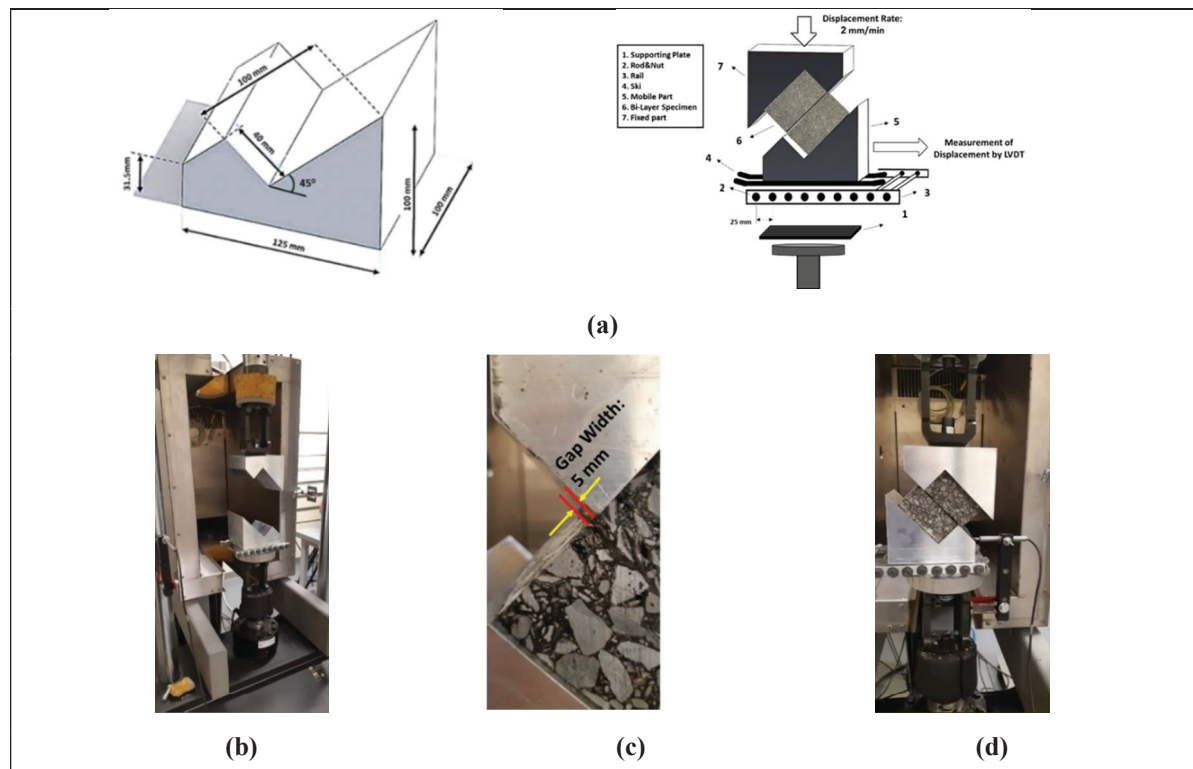


Figure 7.5 Scheme of slant shear device: (a) schematic design; (b) shear test setup; (c) gap width between the interface and the edge of top part; (d) a frame of the test run

7.5 Results and analysis

In this section, the new findings on 3-PBT and shear tests and their interrelations are presented and discussed. As far as the 3-PBT is concerned, the fracture behavior of reinforced and unreinforced structures during crack propagation in mode I of opening are evaluated and

compared in terms of J-integral and crack resistance index measured by means of crack gauges installed below and above the interface. Afterward, the results of the interface shear test are given and discussed to search for a meaningful connection with fracture parameters obtained from the 3-PBT.

7.5.1 3-PBT results and discussions

Figures 7.6 and 7.7 present the load-displacement curves developed for two different types of structures (i.e. ESG-10 over ESG-14 and ESG-14 over GB-20), based on the materials surrounding the interface, and five interfacial conditions in terms of being unreinforced or reinforced with different kinds of grids, in three different depth of notches. These results were obtained as the mean value of three replicates in each depths of the notch. Figure 7.8 illustrates the changes in the load-displacement curve for GR 10/14 in depth of notch a_2 as a representative case. It is worth pointing out that the coefficient of variance (COV) of the maximum loads in each depth of notch were below 25%, which could be considered acceptable based on the specifications of an ideal cracking test given by the NCHRP 9-57 (Zhou et al., 2017). The geometrical details on the artificial notch and the critical value of J-integral calculated based on Equation (7.1) (Anderson et al., 1991) are summarized in Table 7.3.

$$J = -\frac{1}{B} \left(\frac{dU_T}{da} \right) \quad (7.1)$$

where J non-linear energy release rate in J/m^2 ; B specimen thickness in m; U_T total strain energy in J (calculated by the area under the load-displacement curve up to failure); a notch depth in m; and $\frac{dU_T}{da}$ the decreasing rate in fracture energy with notch depth.

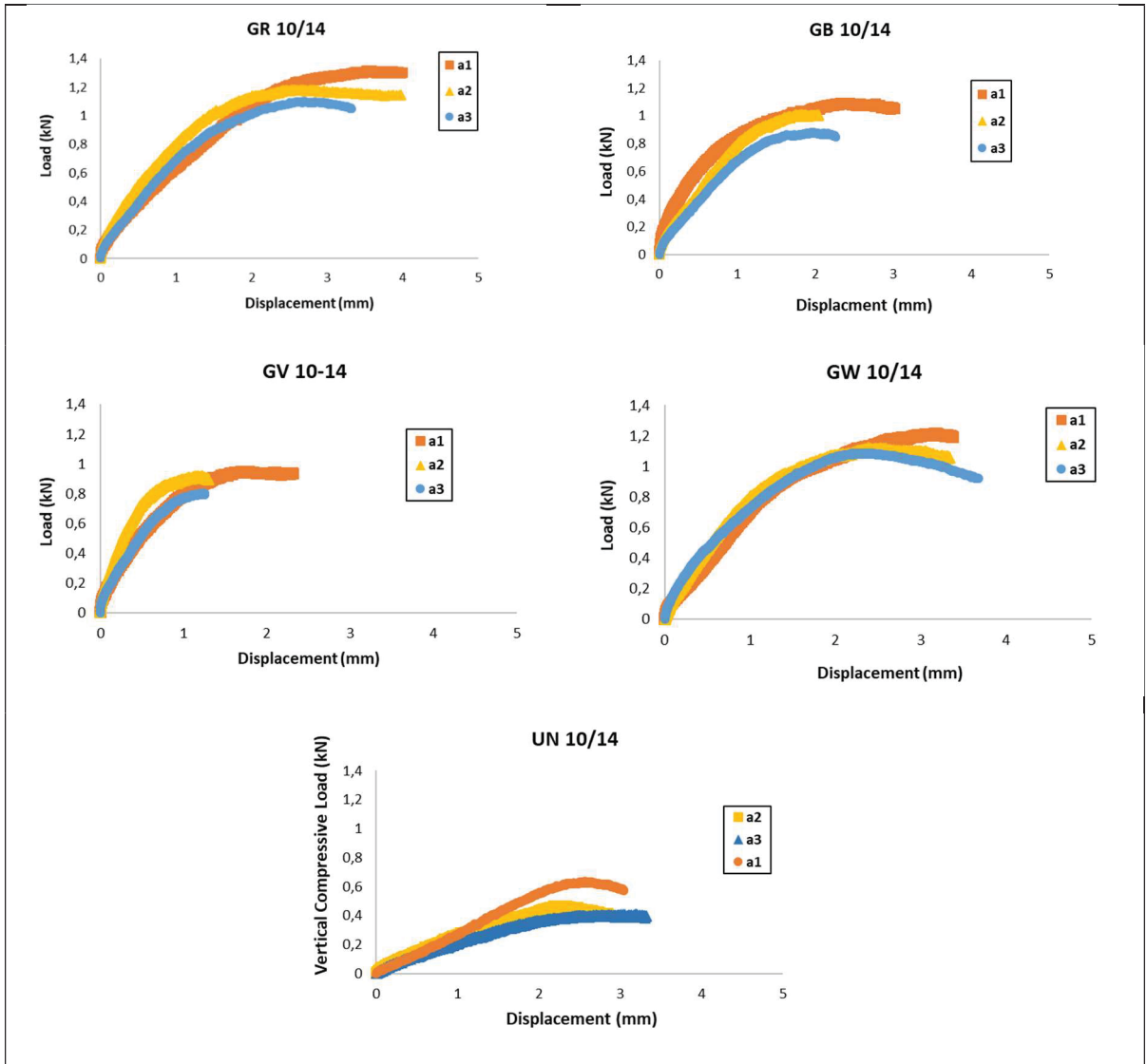


Figure 7.6 Average (n=3) load-displacement curve in different depth of notch for composite structures including ESG10 as the top layer and ESG 14 as the bottom layer in different interfacial conditions

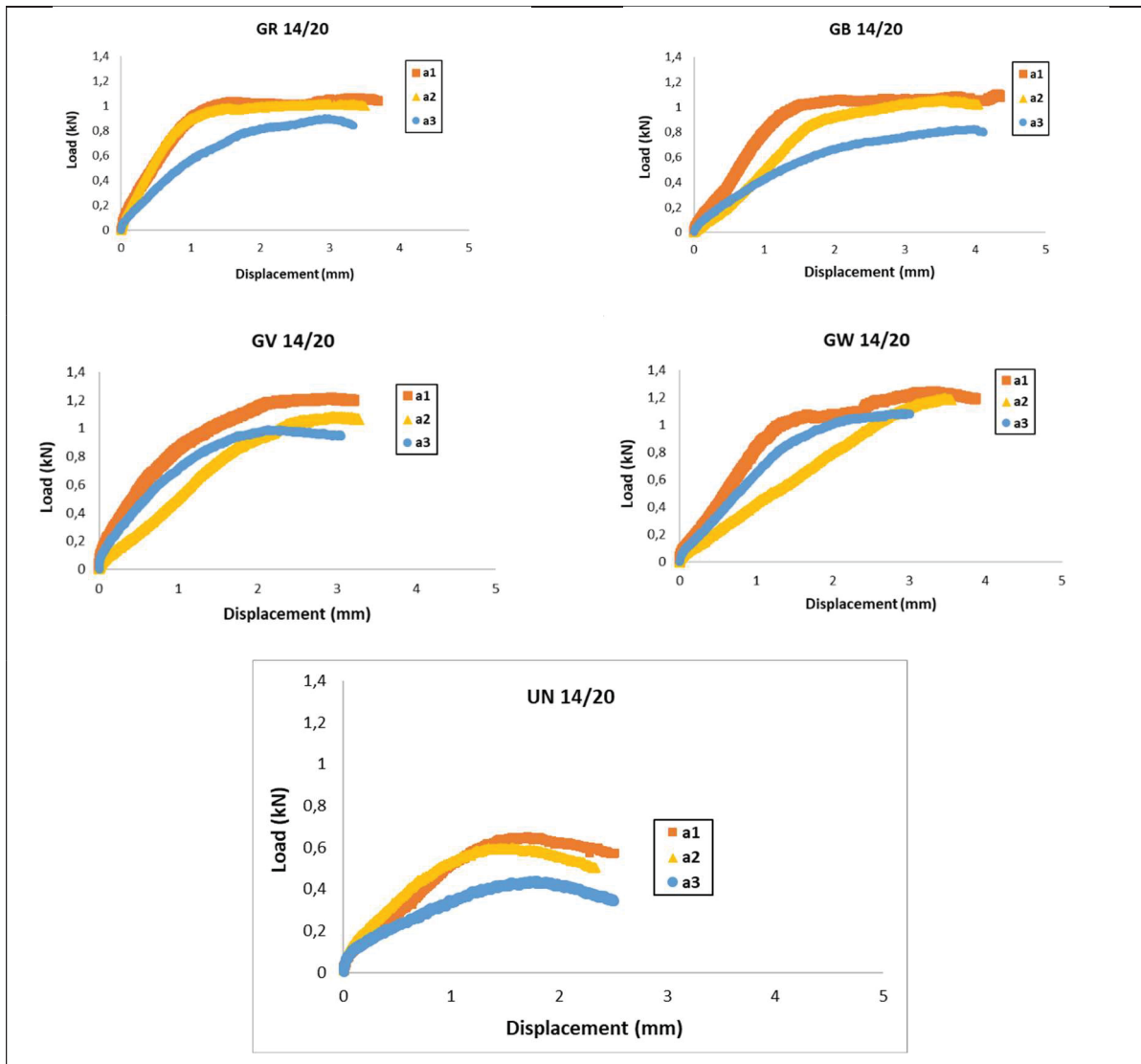


Figure 7.7 Average (n=3) load-displacement curve in different depth of notch for composite structures including ESG14 as the top layer and GB 20 as the bottom layer in different interfacial conditions

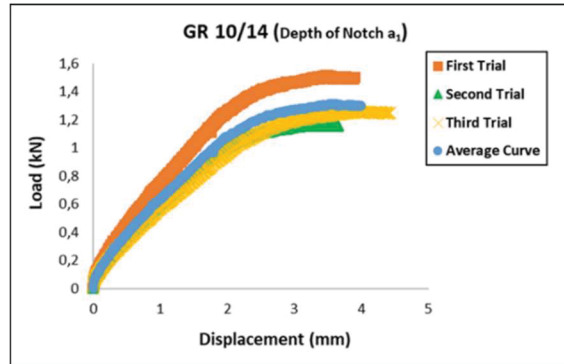


Figure 7.8 The changes in load-displacement curve for GR 10/14 specimen in depth of notch a_1

Table 7.3 J-Integral values for the different systems tested

| Structure | Notch Depth a (mm) | | | Notch Width w (mm) | | | Specimen Height B (mm) | | | Strain Energy at Failure U (J) | | | dU/da | J-Integral (J/m ²) |
|-----------|--------------------|----------------|----------------|--------------------|----------------|----------------|------------------------|----------------|----------------|--------------------------------|----------------|----------------|--------|--------------------------------|
| | a ₁ | a ₂ | a ₃ | w ₁ | w ₂ | w ₃ | B ₁ | B ₂ | B ₃ | U ₁ | U ₂ | U ₃ | | |
| GR 10/14 | 18.6 | 24 | 32.5 | 3.9 | 3.9 | 3.6 | 83.6 | 80.1 | 80.8 | 3.1 | 2.3 | 1.9 | -107.1 | 1314,2 |
| GB 10/14 | 20.1 | 24.5 | 33.3 | 3.4 | 3.8 | 3.5 | 81.2 | 80.2 | 81.2 | 1.8 | 1.2 | 1.1 | -97.0 | 1199,5 |
| GV 10/14 | 18.9 | 23.4 | 33.6 | 3.9 | 3.7 | 3.4 | 79.8 | 80.0 | 80.2 | 2.6 | 2.0 | 1.6 | -99.8 | 1246,8 |
| GW 10/14 | 18.8 | 24.3 | 31.6 | 3.8 | 3.6 | 3.6 | 90.8 | 82.6 | 83.4 | 2.6 | 1.9 | 1.7 | -85.8 | 1051 |
| UN 10/14 | 18.8 | 23.8 | 31 | 3.8 | 3.7 | 3.5 | 80.3 | 78.9 | 82.9 | 0.9 | 0.8 | 0.6 | -22.8 | 286,8 |
| GR 14/20 | 21.0 | 24.9 | 30.0 | 3.9 | 3.8 | 3.8 | 88.1 | 90.3 | 83.2 | 2.8 | 2.2 | 1.8 | -128.4 | 1473,6 |
| GB 14/20 | 17.5 | 25.1 | 33.6 | 3.9 | 3.6 | 3.9 | 81.1 | 80.6 | 81.8 | 3.8 | 2.5 | 2.2 | -101.5 | 1250 |
| GV 14/20 | 20.9 | 24.1 | 29.4 | 3.9 | 3.7 | 3.8 | 89.9 | 88.1 | 82.9 | 2.6 | 2.1 | 1.5 | -124.9 | 1437,9 |
| GW 14/20 | 20.6 | 24.7 | 33.0 | 3.7 | 3.8 | 3.8 | 81.0 | 83.8 | 80.1 | 2.9 | 2.3 | 2.1 | -89.8 | 1046,8 |
| UN 14/20 | 18.9 | 27.0 | 31.0 | 3.7 | 3.9 | 3.7 | 84.5 | 85.6 | 83.0 | 0.6 | 0.5 | 0.3 | -29.0 | 344,4 |

From Table 7.3, it is eminent that both of the reinforced structures benefit from 3 to 4.5 times higher capability in energy dissipation during crack extension compared to corresponding unreinforced structures. In this regard, the structure including ESG 14 and GB 20, outperformed the one constructed from ESG 10 and ESG 14. Another quantitative result of interest from this test was the higher level of energy dissipation in carbon-grid products

compared with glass-grid products in both of the fine- and coarse-graded double-layered structures, which could be related to the high tensile strength and low deformability of carbon-made strands, as indicated in Table 7.2. Another valuable finding was that, on average, the value of the J-integral in coarse-graded composite structures were higher than that in fine-graded ones, which could be explained by the longer path that a crack in the coarse-graded body required passing alongside the perimeter of aggregates. This in turn necessitates more energy dissipation during the crack extension phase. In addition, the differences in the J-integral between reinforced interfaces embedded in the coarse-graded structures were more obvious. It is worth mentioning that the test method appears to be sensitive to the type of the interface since it provides comparable results in different mixtures and grid types.

To investigate the ability of the interface against crack reflection from the bottom side to the top, the crack resistance index (CRI) was defined based on the energy dissipated across the interface. This objective was realized by the installation of crack gauges below and above the interface and developing the force–displacement curves and then calculation the areas up to the maximum point. The net value obtained from subtracting the surrounded areas to the load-displacement curves developed for the crack gauges installed below and above the interface gives an indication of the interface's ability against the crack propagation while taking the effect of both stress and strain into account. Figures 7.9 and 7.10 show the resulting curves for each type of structure and interface conditions. Table 7.4 provides the relevant CRI values derived from three replicates. It is seen from Table 7.4 that all the reinforced structures have higher CRI compared to the corresponding unreinforced ones, and this value is highlighted at the interface reinforced with carbon-grid (GR) followed by the geocomposite reinforcement (GV).

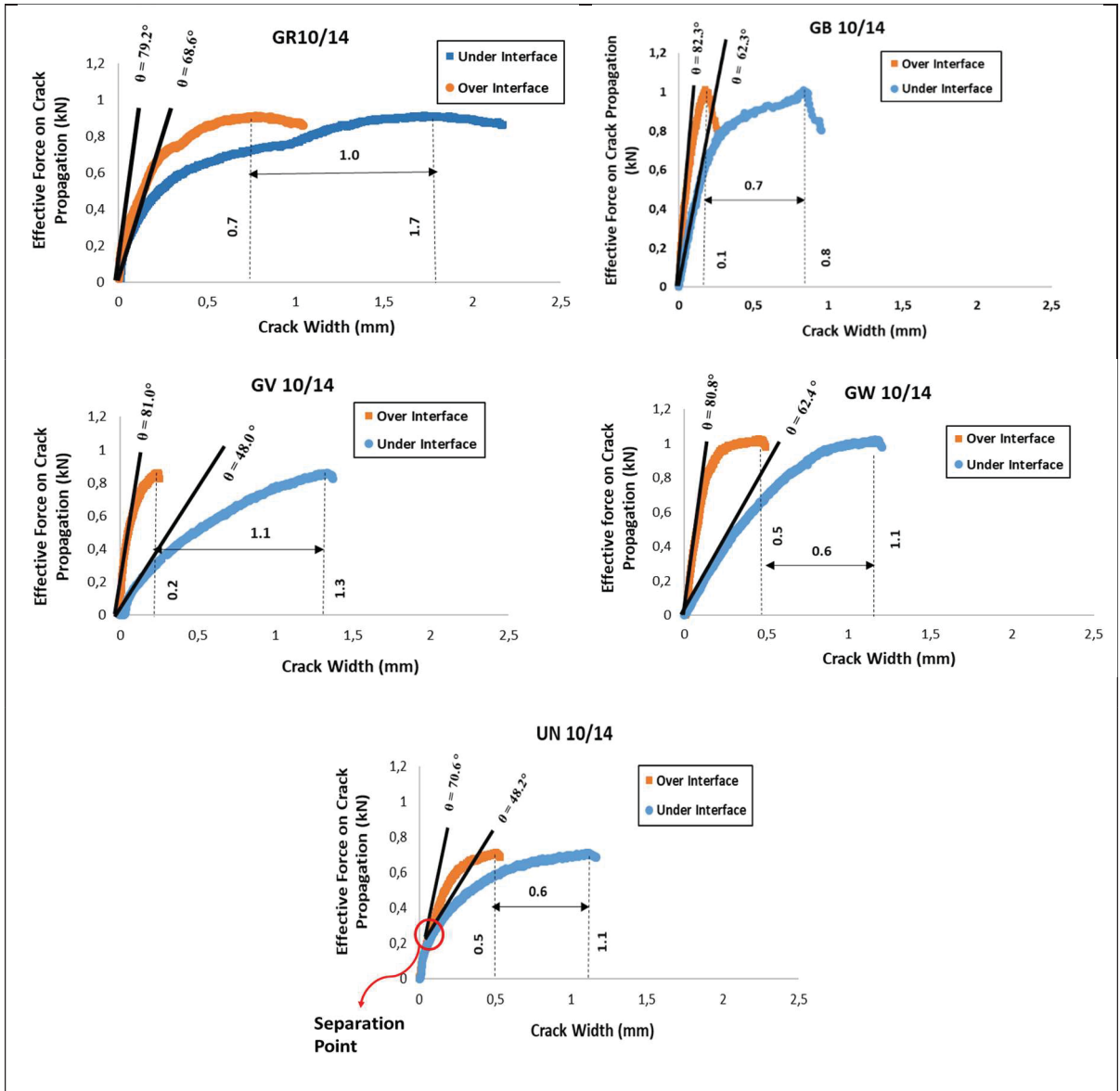


Figure 7.9 Crack propagation under and over the interface in different interface conditions in ESG10/ESG14 structure

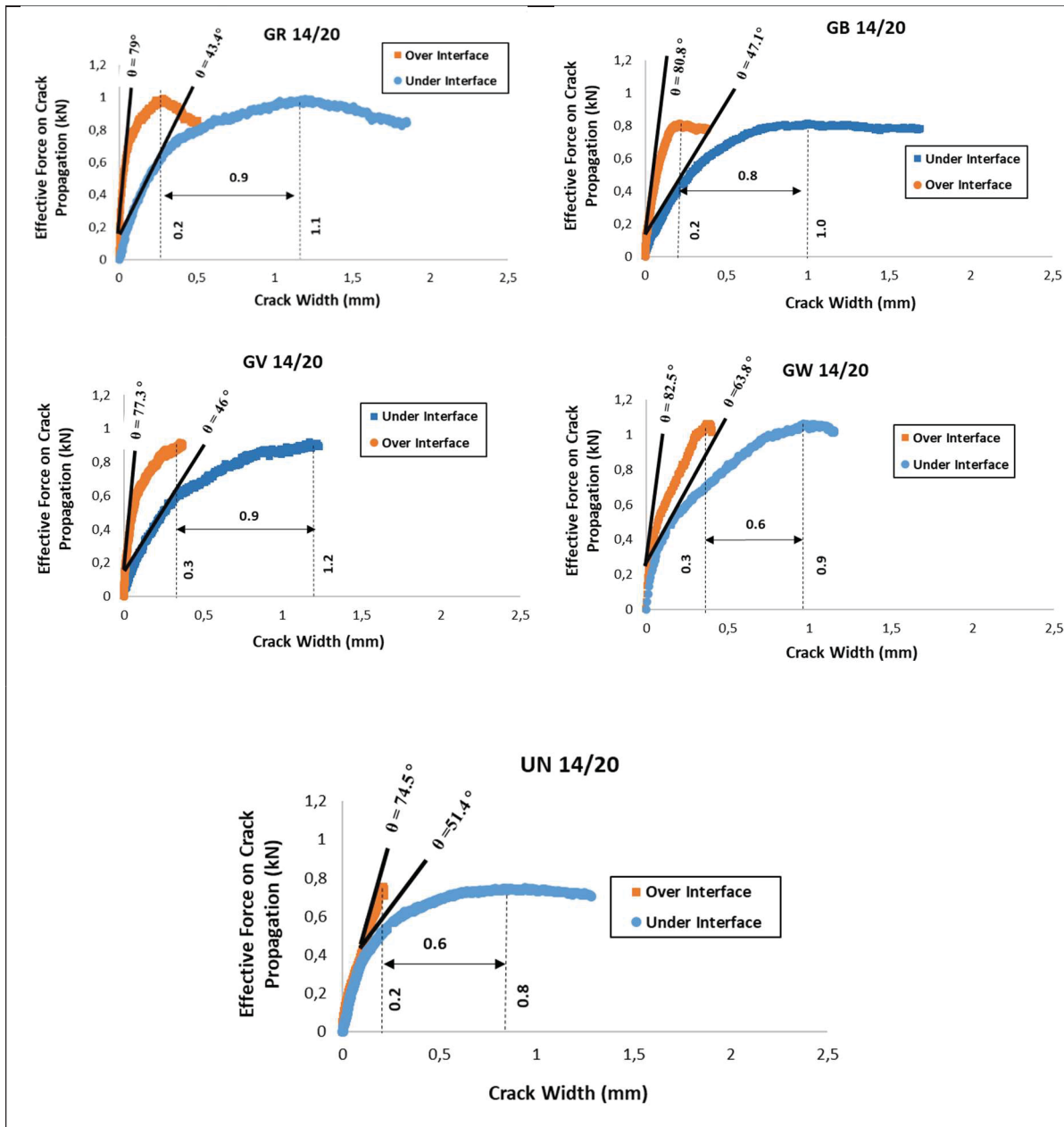


Figure 7.10 Crack propagation under and over the interface in different interface conditions in ESG14/GB 20 structure

Table 7.4 Crack Resistance Index (CRI) for each type of structure and interface condition

| Type of Interface | Energy at Bottom Level of Interface (J) | Energy at Top Level of Interface (J) | Crack Resistance Index (CRI) |
|-----------------------|---|--------------------------------------|------------------------------|
| ESG 10 / ESG14 | | | |
| GR 10/14 | 1.29 | 0.67 | 0.62 |
| GB 10/14 | 0.63 | 0.11 | 0.52 |
| GV 10/14 | 0.74 | 0.15 | 0.58 |
| GW 10/14 | 0.81 | 0.39 | 0.42 |
| UN 10/14 | 0.60 | 0.26 | 0.33 |
| ESG 14 / GB 20 | | | |
| GR 14/20 | 0.87 | 0.21 | 0.65 |
| GB 14/20 | 0.59 | 0.12 | 0.47 |
| GV 14/20 | 0.80 | 0.25 | 0.54 |
| GW 14/20 | 0.71 | 0.26 | 0.45 |
| UN 14/20 | 0.51 | 0.18 | 0.32 |

The slope of tangents, drawn from the separation point on each load-crack width curve, with the horizon, indicated by θ on Figure 7.9 and 7.10, was treated as the stiffness of material right below and above the interface against crack propagation. The position of the separation point on the load-crack width curve was typically shown on Figure 7.9 for unreinforced structure. As shown in Figure 7.11, the changes in the θ value between below and above the interface ($\Delta\theta$) in reinforced structures including GR and GB grids were more significant in the case of surrounding by coarse-graded mixtures (i.e. ESG-14 over GB-20). This outstanding feature could be related to the low deformation and high tensile strength of the strands in GR and GB grids in the longitudinal direction, as specified in Table 7.2, perpendicular to the crack development path. In this case, the interlocking effect between coarse aggregates trapped in grid apertures involves more contribution from the grid to mitigate the crack propagation phenomena while in fine-graded mixtures (ESG-10 over GB-20) this contribution from the grids is tangibly lower. In this respect, the interfaces reinforced with the GV and GW grids had almost the same crack retardation abilities in both of the structures, which could be justified by the lack of interlocking effect and higher deformation (or lower tensile strength) in GV and GW grids, respectively.

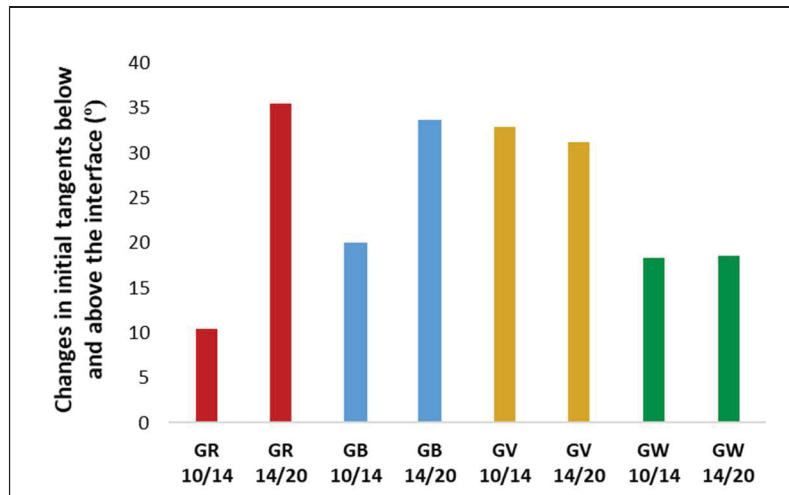


Figure 7.11 Changes in crack development angles below and above the interface among different types of reinforced structures

7.5.2 Interface Shear Test Result and Discussion

In order to take into account the effect of high shear displacement capability before failure in reinforced structures, as shown in Figure 7.12, it is of vital importance to define a proper coefficient to realistically reflect the bonding quality at the interface. This parameter, called the Coefficient of Interface Bonding (CIB), is obtained from the quotient of maximum interlayer shear strength (ISS_{max}) and the pertinent interlayer shear displacement (ISD) ($CIB = \frac{ISS_{max}}{ISD}$). On this basis, the higher CIB values indicate higher bonding quality, while lower CIB means reverse. The results of CIB values are summarized in Table 7.5. Experimental results obtained from the interface shear test for two types of structures are illustrated in Figures 7.13 and 7.14. As it can be observed in Table 7.5, in general, the interface surrounded in ESG14/GB 20 structure had a higher level of CIB values, which is caused by the lower level of horizontal displacement before failure. Furthermore, in both of the structures, the unreinforced specimens had better bonding quality compared with reinforced specimens, which confirms the fact that the presence of the interlayer could have a debonding effect (Vanelstraete & Francken, 1997; Brown et al., 2001; Canestrari et al., 2013; Zamora-Barraza et al., 2011; Sudarsanan et al., 2018).

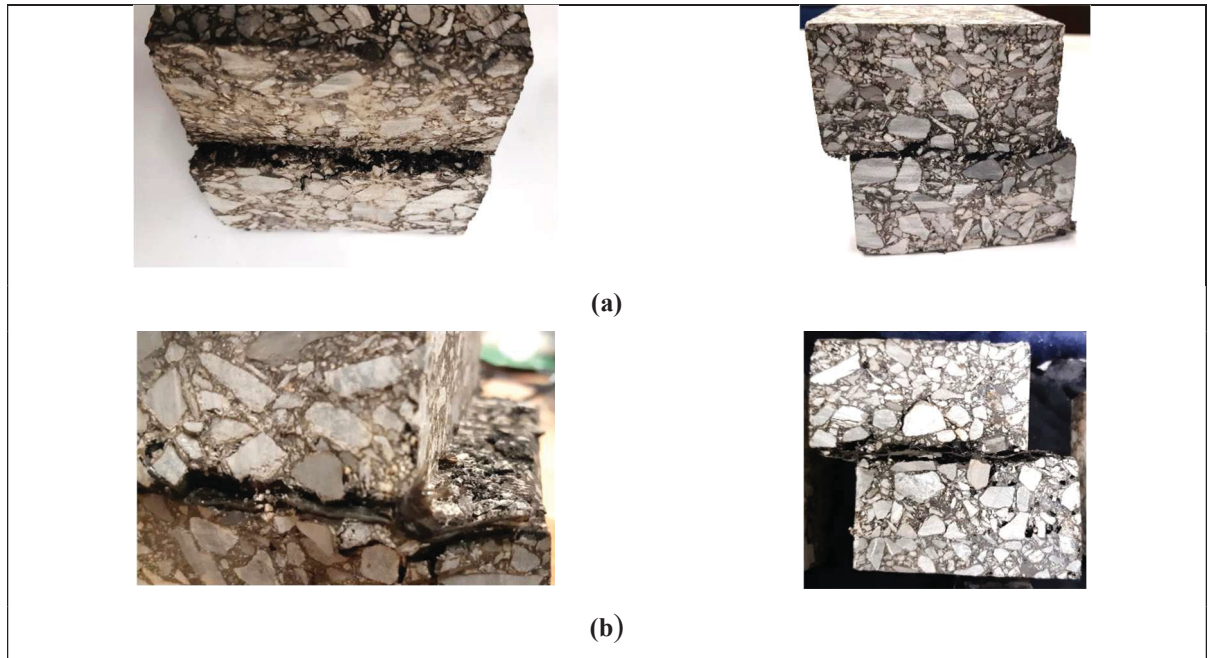


Figure 7.12 Shear displacement at the interface: (a) Unreinforced specimen; (b) reinforced specimen

Table 7.5 Average values (n=3) of Coefficient of Interface Bonding (CIB) obtained from the interface shear test

| Type of Interface | Interlayer Shear Strength (ISS) (MPa) | Interlayer Shear Displacement (ISD) (mm) | Coefficient of Interface Bonding (CIB) |
|----------------------|---------------------------------------|--|--|
| ESG 10/ ESG14 | | | |
| GR 10/14 | 1.01 | 2.55 | 0.40 |
| GB 10/14 | 1.12 | 3.84 | 0.29 |
| GV 10/14 | 0.98 | 2.74 | 0.35 |
| GW 10/14 | 1.02 | 3.68 | 0.27 |
| UN 10/14 | 1.03 | 2.30 | 0.45 |
| ESG 14/ GB 20 | | | |
| GR 14/20 | 0.99 | 2.42 | 0.41 |
| GB 14/20 | 0.94 | 2.90 | 0.32 |
| GV 14/20 | 1.03 | 2.66 | 0.38 |
| GW 14/20 | 0.94 | 2.72 | 0.34 |
| UN 14/20 | 1.19 | 2.75 | 0.43 |

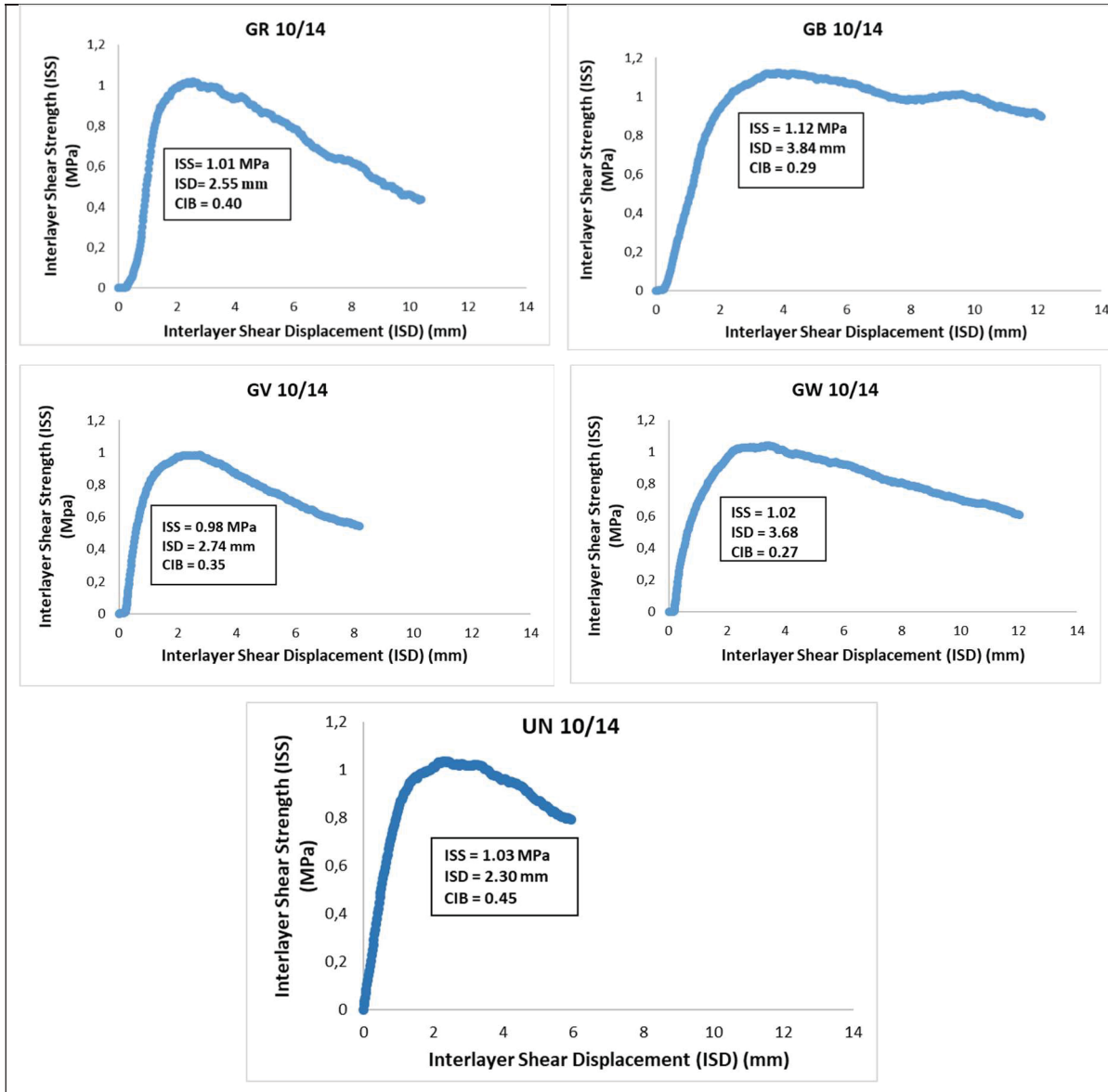


Figure 7.13 Average (n=3) load-shear displacement curves developed for different types of interface in ESG-10 over ESG 14 structure

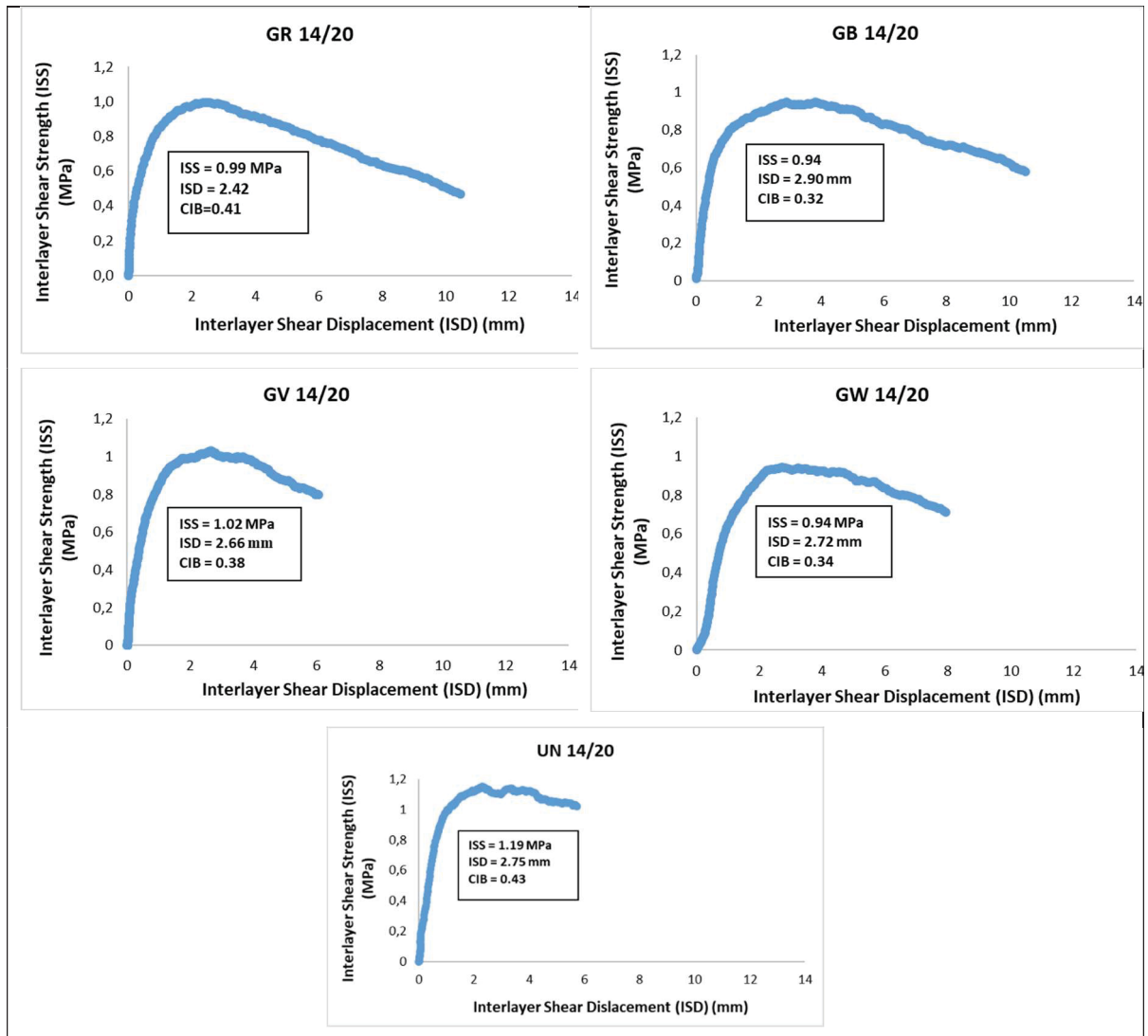


Figure 7.14 Average (n=3) load-shear displacement curves developed for different types of interface in ESG-14 over GB-20 structure

7.5.3 Combined Analysis of 3-PBT and Interface Shear Test Results

In this section, the interrelation between the J-integral as a fracture parameter on one hand and CRI and CIB, as representatives of interface properties, on the other hand are investigated. Figure 7.15 provides a better vision of the discrepancy of the values of CRI and CIB for different types of structures and interfaces. Apart from unreinforced structures, the CRI values were significantly higher than CIB values for all the reinforced structures. This could infer an existing connection between these values in the presence of a reinforcement layer between the bituminous layers.

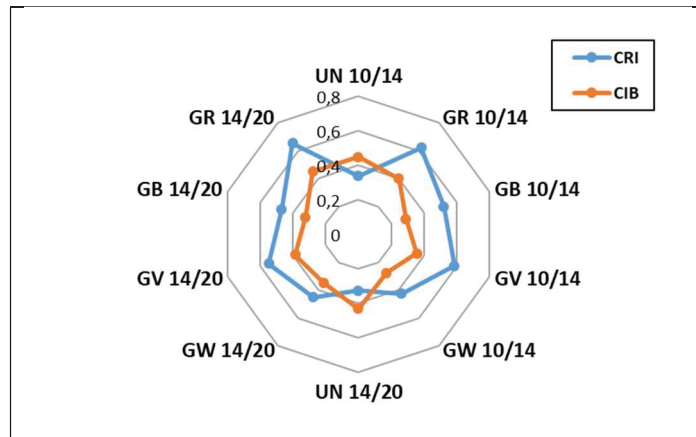


Figure 7.15 Radar plot indicating the changes in CRI values to CIB values around different structures and interfaces

On this basis, for the reinforced interface enclosed by fine mixtures, a strong linear relationship between the J-integral and the CRI was identified while in coarse graded mixtures the changes in the J-integral with the CRI was justified by a second-order polynomial equation, as shown in Figure 7.16 a. This difference could stem from the fact that, in the coarse-graded mixture, the crack path is highly affected by the aggregate shape, size and its strength. Nonetheless, as illustrated in Fig. 7.16 b, the changes in the J-integral with the CIB was not straight enough. In this regard, a third-order polynomial equation would best describe the interconnection between these two parameters. However, more research with different types of grids and structures is required to better justify this interrelationship.

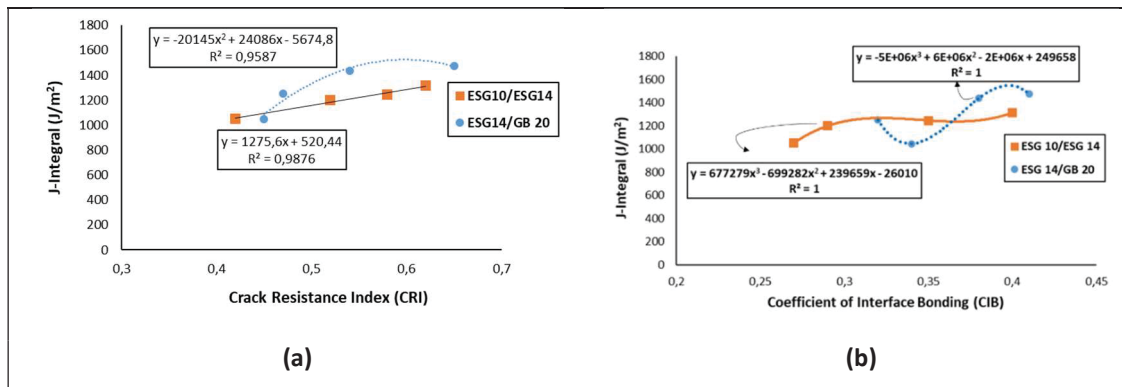


Figure 7.16 Sensitivity of the J-integral in fine and coarse-graded mixtures to mechanical indices defined at the interface level: (a) changes in J-integral by CRI; (b) changes in the J-integral by CIB

On the other hand, between CRI and CIB in each type of the reinforced structure in terms of type of mixture employed in, a straight linear relationship was found, as shown in Figure 7.17. On this basis, as the bonding quality increases (i.e. CIB) at the interface, the ability of the interface to mitigate the crack reflection from its bottom side to the top proportionally enhances (i.e. CRI). In other terms, higher bonding quality involves more contribution of the grid in reducing the crack width at the interface level.

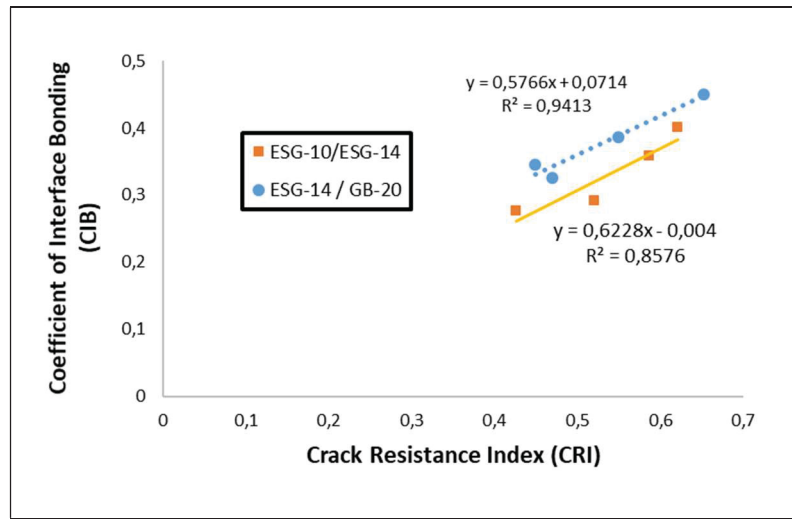


Figure 7.17 Interrelationship between CIB and CRI for each type of structure

In addition, the total results from the 3-PBT and the interface shear test were comparatively analyzed through the ANOVA test to investigate the dependency of the results for both of the reinforced and unreinforced structures. Table 7.6 provides a list of test summaries based on a 95% confidence interval. The $F \geq F_{crit}$ and P-value suggested that the values of CRI and CIB were independent of each other.

Table 7.6 ANOVA summary results

| | SS | DF | MS | F-Value | P-Value | Fcrit |
|-----------------------|-------|----|--------|---------|---------|-------|
| Between Groups | 0.08 | 1 | 0.08 | 10.062 | 0.0052 | 4.413 |
| Within Groups | 0.143 | 18 | 0.0079 | - | - | - |
| Total | 0.223 | 19 | | | | |

Finally, an analysis by means of MINITAB software release 15 was carried out to understand how the changes in CRI and CIB values justify the changes in J-integral for both reinforced and unreinforced systems. In this regard, the suitability of the following second-order regression model, as shown in Equation (7.2), was verified by the analysis of the ANOVA test ($P \leq 0.05$), according to Table 7.7.

Table 7.7 ANOVA result for the regression model

| | DF | SS | MS | F | P-Value |
|-------------------|----|----------|----------|-------|---------|
| Regression | 5 | 1539146 | 307829.1 | 30.94 | 0.0027 |
| Residual | 4 | 39792.98 | 9948.244 | | |
| Total | 9 | 1578939 | | | |

$$J = -65.71 + 7946.3 (CRI) - 13956.14 (CRI)^2 + 21773.18 (CRI \cdot CIB) - 7143.35 (CIB) - 3948.71 (CIB)^2 \quad (R^2 = 0.97) \quad (7.2)$$

Where J is the J-integral in J/m^2 , and CRI and CIB are the crack resistance index and coefficient of interlayer bonding, respectively. It is noteworthy that the resultant coefficient of determination ($R^2 = 0.97$) suggested a good proficiency of the proposed model.

According to Equation (7.2), a curvilinear relationship exists between the dependent variable in terms of the J-integral and combined effect of interfacial mechanical properties in terms of CRI and CIB. As expected, in the linear component of the equation (i.e. $-65.71 + 7946.3 (CRI) - 7143.35 (CIB)$), the J-integral is directly related to the CRI, which means that more resistance from the interface against the crack propagation could result in higher J-integral value. In contrast, the CIB factor acts in a reverse direction on the J-integral value. In other words, by increasing the bonding quality at the interface, as is the case in unreinforced structure, the J-integral value is negatively affected. In addition, the interaction component of Equation (7.2) (i.e. $21773.18 (CRI \cdot CIB)$) illustrates that the effect of the CRI on the J-integral value is different at various levels of the CIB. Another way of saying this is that the slope of regression lines between the J-integral and the CRI are different for different levels of CIB in which the coefficient 21773.18 indicates how different those slopes are. In general, this interaction has a positive impact on the J-integral. Furthermore, from the quadratic component of Equation (7.2) (i.e. $-13956.14 (CRI)^2 - 3948.71 (CIB)^2$) it could be perceived that the

changes in the J-integral with respect to CRI and CIB values justifies by a curvilinear shape with a curvature downwards. As previously mentioned in Figure 7.16, the accuracy of the model could enhance in further research if the effect of the aggregate size in a body, in which the crack propagation occurs, could be introduced into the model. This is in connection with what previously observed in Figure 7.11 that the crack mitigation property of high strength grids such as the GR and the GB were highly dependent on the type of the structure in terms of the nominal maximum aggregate size.

7.6 Conclusion

Rehabilitation of an existing deteriorated bituminous surface with a new asphalt overlay with or without the application of an interlayer system such as geogrid or geocomposite could change the structural response of the system against the initiation and extension of reflective cracking. From this perspective, the interconnection of fracture toughness parameters in terms of J-integral and CRI obtained from 3-PBT, and the bonding quality in terms of CIB, derived from modified slant shear device was studied in this research. Three different types of grids and one type of geocomposite were placed between two types of structures, while the effect of influential parameters such as temperature and loading rate were assumed constant. Following conclusions were reached:

- Introducing grid products regardless of its raw material and tensile strength resulted in 4-5 times higher resistance of the bi-layer structure against the crack extension.
- The fracture toughness of the interface against crack reflection can be described by the crack resistance index (CRI). The result of this study revealed that, on average, reinforced structures profit from 1.5 to 1.6 higher CRI compared to unreinforced ones.
- The binding quality provided at the different types of interfaces could properly be reflected through defining the coefficient of interface bonding, which is able to take the effect of both shear strength and shear displacement into account. The interface shear test results showed that introducing an interlayer between coarse-graded bituminous mixtures maintained the structural integrity against shear forces owing to limited shear displacement before failure.

- The crack mitigation property of high strength grids is highly dependent on the size of the aggregates employed in their surrounding mixtures.
- The quadratic polynomial regression model, developed based on the experimental data, could reliably predict the J-integral of the composite structure based on the CIB and CRI values.

It is noteworthy that the result derived from this study is only valid for the studied materials and testing condition. Along with the present experimental program, more laboratory work is required to confirm the validity of the proposed model in different temperatures, loading rates, in the presence of the moisture at the interface, and on aged materials to check the changes in fracture toughness parameters in relation to the bonding quality between the connected reinforced-rehabilitated layers. In addition, the cost-effectiveness of using the interlayer products employed in this research could be the subject of further research to better evaluate the short-term and long-term return of initial investment.

CHAPTER 8

MECHANICAL CHARACTERIZATION OF GRID-REINFORCED INTERFACES WITHIN BITUMINOUS LAYERS

Ehsan Solatiyan¹, Nicolas Bueche², Alan Carter³

^{a, c} Department of Construction Engineering, École de Technologie Supérieure (ÉTS),
1100 Rue Notre-Dame O, Montréal, QC H3C1K3, Canada

^b Department of Architecture-Wood-Civil Engineering, Bern University of Applied Sciences
(BFH), Pestalozzistrasse 20, CH-3401 Burgdorf, Switzerland

Paper submitted for publication in *Construction and Building Materials*, October 2020

8.1 Abstract

The installation of a layer of the grid, as an interlayer between bituminous layers, enhances the mechanical performance of the entire system under repetitive action of traffic loads, typically by increasing the tensile and shear strength at the interface level. At the same time, this mechanical improvement is accompanied by changes in mechanical responses of the system in terms of axial stiffness and structural integrity, which needs to be well defined in performance-based design methods. This research was dedicated to know how to characterize the mechanical alterations at the reinforced interface of bituminous layers from different mixtures, concerning axial stiffness and adhesion quality through a comparative analysis with corresponding unreinforced cases. In doing so, a new configuration of extensometers in the tension-compression complex modulus test was suggested to elucidate the changes in structural responses at different heights relative to the interface. Furthermore, a uniaxial tension-compression test was utilized to evaluate the structural integrity of the system at the interface level. The results demonstrated that the proposed methodology of doing complex modulus test could be employed as a practical tool to compare the rheological behavior of the interfaces with dissimilar conditions. In addition, the 2S2P1D model could be reliably employed to predict the mechanical behavior of any type of interface at high frequencies or low

temperatures. Also, the fatigue life of the bituminous mixture, determined at one million loading cycles, ϵ_6 , provided a proper indication of the structural integrity of the reinforced and unreinforced systems under cyclic loading.

8.2 Introduction

The installation of grid products at the interface of a deteriorated existing bituminous layer and a new hot mixture overlay has proved its effectiveness as a novel rehabilitation strategy to enhance the mechanical performance and to extend the service life of the pavement system (Zielnski, 2008; Lee, 2008; Zamora-Barraza et al., 2011; Montestruque et al., 2004; Kim et al., 2009; Ferrotti et al., 2012; Virgili et al., 2009). Nevertheless, the key requirement to ensure the reinforcement effect induced by the interlayer product is the reliable adhesion provided at the interface of adjacent layers in the pavement system (Zamora-Barraza et al., 2010; Canestrari et al., 2012), which in the case of debonding effect, the structural enhancement of the system could be jeopardized by the fatigue failure under repetitive loadings (Graziani et al., 2014).

A rehabilitated bituminous structure usually engages different layers with individual thicknesses and mechanical properties. A conventional method to characterize the rehabilitated structure into mechanistic-based design methods is to perform a series of laboratory tests independently in order to provide a full mechanical description of each layer and then to assume a full bonding between considered layers. However, it has been well understood that any changes in the interface condition could influence the structural behavior of the entire system (Wu et al., 2017; Galaviz-González et al., 2019; Romanoschi & Metcalf, 2001), which in turn might undermine the design alternative proposed for the rehabilitated structure. On this basis, an improvement in the current design methods would be acquired by taking the real interfacial mechanical behavior into account.

This study is essential to capture a profound knowledge that helps to analyze the structural responses of a rehabilitated bituminous structure, composed of different hot mixtures and grid types, exposed to in-field load condition. It also provides new insight into selecting a proper type of reinforcement material for the sake of the pavement rehabilitation project.

This paper is partitioned into five separate sections. First, a research background on studies carried out on the mechanical response of a double-layer bituminous structure at the interface

is introduced and followed by the characterization of the materials used to prepare specimens. Then, experimental results will be delivered with a detailed subsequent discussion. In the end, the paper is concluded with a list of outcomes along with future recommendations.

8.3 Research background

A review of pertinent studies indicates that, in general, two approaches have been adopted by the researchers to introduce the reinforcement effect of geosynthetics into pavement design methods. Initially, an empirical approach in which based on establishing specific failure criteria including fatigue cracking and rutting, empirical coefficients, such as Traffic Benefit Ratio (TBR) and Base Course Reduction (BCR), are defined by making a comparison between the reinforced and unreinforced structures to reach a specific level of failure (Zornberg, 2011). This approach is rather proprietary and depends on the reinforcement material and test environment under which these coefficients are developed (Zornberg & Gupta, 2010). On the other hand, a performance-based design approach such as the mechanistic-empirical (M-E) pavement design method, released by NCHRP project 1-37A, is still unable to predict the mechanical behavior of reinforced bituminous structure because of the complexity of the system induced by the involvement of a myriad of factors (Solatiyan et al., 2020). Type of geosynthetic (Brusa et al., 2016); Type of overlay and its thickness (Button & Lytton, 2007); the design life of the interlayer system and long-term field calibration (Jenner & Uijting, 2004); mechanical specifications of the geosynthetic (De Bondt, 2000); type of loading (De Bondt, 2009); and economic considerations (Zofka & Maliszewski, 2019) are just a few factors required to be specified in any design method designated for the reinforced-rehabilitated bituminous structure. Among all these factors, considering the real mechanical behavior of the interface between geosynthetic and surrounding bituminous layers is of paramount importance (Solatiyan et al., 2020).

A variety of mechanical models to predict the behavior of the reinforced bituminous overlay have been developed based on controlling a specific type of damage. A simple layered elastic theory (LET) model was developed based on the falling weight deflectometer (FWD) test by comparing the structural responses of a reinforced overlay in comparison with an unreinforced one. On this basis, the modulus of the upper bituminous layer relative to the lower bituminous

layer was increased so that the horizontal and transversal strains measured in the field correspond well to those predicted by the model (Canestrari et al., 2018). In another effort, a reflective cracking (RC) model was proposed which was able to predict the percentage area stricken by reflective cracking, during the service life of the reinforced overlay (Zofka & Maliszewski, 2019). The Bodin damage model, which was a damage model in an elastic continuum space, was employed to anticipate the fatigue performance of a composite bituminous structure including a grid based on a reduction in dynamic modulus of the system under cyclic loading (Arsenie et al., 2017). Also, a continuum composite model, which was an energy model derived from differentiating the stored strain energy of a composite structure including hot mixture and grid, was utilized to analyze the reinforced bituminous structure with the grid, simply by considering the orthotropic effect of the grid instead of modeling the meshed structure of the grid (Gajewski & Jemioło, 2014). To predict the rut depth growth of a reinforced hot mixture overlay with the number of load cycles, a shift model, which was able to take the effect of temperature, load frequency and deviator stress on rut growth, was calibrated on the results obtained from triaxial stress sweep (TSS). This model was then incorporated into a finite element based program, called LVECD, for the analysis of the reinforced structure. The conformity of the derived results from this program with field measurements was further proved its capability on the prediction of permanent deformation of bituminous pavement (Choi & Kim, 2014). Furthermore, a finite element based program, named OLCRACK, was released to tackle the prediction of both bottom-up and top-down reflective cracking in a bituminous mixture reinforced with the grid. To this end, the new bituminous overlay was assumed as a sole linear elastic material placed over a cracked existing layer. The effect of the grid at the interface was considered by a decreased shear stiffness of the new overlay (Thom, 2000). CAPA is the name of another finite element program, mainly designed to address the propagation of reflective cracks in the grid-reinforced overlay. By allocating the interface elements at the region of connection between the grid and adjacent asphalt layer and bar- type element to simulate the reinforcement effect induced by the grid, this model was able to evaluate the contribution of reinforcement in crack growth deceleration (Scarpas & De Bondt, 1996). In general, two different models were employed in the FEM method to model the reinforced structure with geosynthetic (Ghadimi, 2015): "linear elastic,

cross-anisotropic model" and "non-linear viscoelastic model". The reason to choose a simplified model like the linear elastic model instead of non-linear one could be explained by the fact that bituminous pavements are only able to undergo a small range of permanent deformation. Accordingly, the structures with geogrid could be assumed to act in a linear domain (Solatiyan et al., 2020). However, in the case of demanding a higher level of precision, non-linear behavior could be utilized (Ghadimi, & Nikraz, 2017). On this ground, a variety of programs, working based on the finite element method, have been employed to simulate the reinforced bituminous structure such as Abaqus (able to consider both the linear and non-linear behavior), CAPA-2D (based on non-linear behavior) and Supersap (assuming linear behavior) (Bohagr, 2013). A review of pertinent literature shows that the linear elastic model was predominantly applied in FEM models as a constitutive model of the geosynthetic with a full bonding provided at its interface with an adjacent bituminous layer (Montestruque et al., 2004; Correia et al., 2018; Coni & Bianco, 2000; Buonsanti & Leonardi, 2012; Abdesssemed et al., 2015; Taherkhani & Jalali, 2016; Calvarano et al., 2017; Hojat Shamami & Khiavi, 2017). As can be noticed, all these above-mentioned models treated the reinforced asphalt overlay as a system. However, it was demonstrated that the interface by itself in reinforced bituminous specimens behaves as a linear viscoelastic material, which its mechanical behavior could be modeled by the 2S2P1D model (2 Springs, 2 Parabolic elements and 1 Dashpot) (Freire, 2018). As far as the mechanical performance of the reinforced structure under cyclic loading is concerned, a review of pertinent studies on a reinforced bituminous layer with geosynthetic unfolded that the fatigue life could enhance significantly compared with the unreinforced structure (Solatiyan et al., 2020). In this regard, the relative stiffness of the geosynthetic to the bituminous layer and the quality of adhesion provided at the interface of successive layers play pivotal roles. Another important consideration is to select an appropriate failure criterion (Orešković et al., 2019). On this basis, different failure criteria have been suggested to specify the fatigue life of a bituminous structure. In a controlled-strain mode of fatigue test (ASTM D7460), four types of indices were the subject of studies. $N_{f50\%}$ is a classical index related to the number of cycles when the initial stiffness modulus reaches its half value (Basueny et al., 2014). $N_{f\Delta\epsilon_{ax}}$ is defined as the 25% difference in strain amplitude registered by three different extensometers. $N_{f\Delta\phi}$ relates to more than 5° difference in the phase angle recorded by each

extensometer from the average value. Finally, $N_{f\phi max}$ takes the evolution of the phase angle over the test into account. On this ground, the number of cycles connected to the maximum value of the phase angle is considered as the failure point. It is worth mentioning that all these criteria could provide comparable outcomes (Tapsoba et al., 2013). Two laboratory methods are applicable to evaluate the fatigue life of double-layered reinforced structure: Four-point bending test (4-PBT) (ASTM D7460, or AASHTO T321) and the uniaxial tension-compression test procedure established in Département de Génie Civil et Bâtiment (DGCB) (Di Benedetto et al. 2011). Both of these tests are usually carried out at one frequency and one temperature (e.g. 10 °C & 10Hz) and at different strain levels in order to develop the Wöhler curve, which is a suitable way to predict the design life of a structure in terms of ϵ_6 (i.e. the number of cycles at one million cycles) (Baaj et al., 2005; Perraton et al., 2015). However, the suitability of the DGCB method over the 4-PBT method is because of the fact that the same specimen derived from the complex modulus test, which is actually a non-destructive test, could be utilized for the DGCB fatigue test. Therefore, less material and time, needed for specimen preparation, are expected. In addition, the test procedure is very suitable to evaluate the quality of adhesion at the interface, an important factor affecting the fatigue performance, under specific temperature and load frequency.

The abovementioned review reveals that the need for a more accurate and practical method to include the rheological behavior of the reinforced interface into mechanistic-based design methods is still not properly responded to. The purpose of this research is to provide a better understanding of the necessary changes in terms of the mechanical behavior that emerges at a reinforced interface with geogrid, which are required to be taken into account in design methods.

8.4 Experimental program

The present study aims to develop a laboratory methodology for describing and modeling the interfacial behavior of grid reinforced specimens composed of different types of hot mixtures subjected to in-site loading conditions. In this context, an investigation of possible changes in the fatigue life, defined by ϵ_6 , owing to the variation in the quality of adhesion at the interface, and also the axial stiffness in terms of the complex modulus of the composite system and the

interface by itself, was carried out for two types of grids embedded in two different mixtures. Then the results were compared with an unreinforced case of the same type of the structure as a benchmark. To fulfill these objectives, double layer specimens with different types of hot mixtures were prepared by assuming that the complex modulus and fatigue behavior might change in different structures with regard to the nominal maximum aggregate size (NMAS).

8.4.1 Materials and specimen preparation

In the current study two kinds of hot mixtures with respect to the nominal maximum aggregate size (NMAS), conventionally employed in Quebec (Canada), with the same type of bitumen type PG 58-28, were assigned complying with Transport Quebec's standard (LC 4202) (MTQ, 2018): (I) a wearing course mixture with an NMAS of 10 mm (indicated by ESG-10); and (II) a binder course mixture with an NMAS of 14 mm (indicated by ESG-14. The gradation curve and mechanical properties of each type of mixture are illustrated in Figure 8.1 and Table 8.1, respectively.

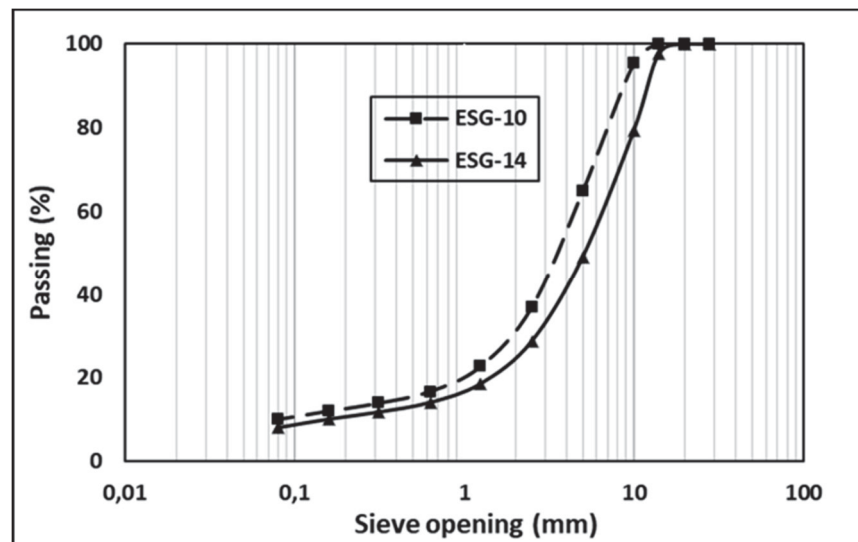


Figure 8.1 Gradation curves of each type of hot mixture

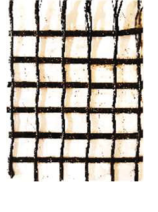

Table 8.1 Mechanical specifications of asphalt concrete mixtures

| Technical specifications of mixes | | | |
|--|----------|--|---------------------------|
| Mixture | | ESG-10 | ESG-14 |
| Binder Type | | PG 58-28 | PG 58-28 |
| Binder Content (% mass) | | 5.45 | 5.22 |
| Mean Texture Depth (MTD) (mm) (ASTM E965) | | 3.1 | 3.6 |
| Water Sensitivity (LC 26-001 ¹) (%) | Measured | 97.3 | 85.5 |
| | Required | ≥ 70 | ≥ 70 |
| Rutting Resistance (LC 26-410*) (%) | Measured | After 1000 = 6.6 After 3000 = 8.2 | 7.2 |
| | Required | (After 1000 cycles) ≤ 10 (After 3000 cycles) ≤ 15 | (After 30000 cycles) ≤ 10 |

* LC standards are Quebec Ministry of Transportation's standards

Double-layered structures were prepared by putting the ESG-10 over the ESG-14. In the case of reinforced structures, two types of grids, according to the specifications given in Table 8.2, were introduced at the interface of bituminous courses along with a thin film of asphalt emulsion type SS-1h (slow-setting) as the tack coat to ensure the monolithic action of the grid with the lower bituminous layer. As shown in Table 8.2, GB stands for a type of the grid coated with bitumen at its bottom side and GV indicates a grid accompanied by a layer of fabric attached underneath the grid and covered the apertures. The main reason behind the selection of these two types of grids was to examine the effect of the adhesion quality at the interface, presented by the different dosage of the tack coat, the implementation process demanded by each type of the grid, and the structure of the grid itself on possible changes on fatigue behavior and axial stiffness of the system.

Table 8.2 Technical properties of grids (supplied by the company)

| Name | Symbol | Raw Material / Transversal Strength (kN) | Raw Material / Longitudinal Strength (kN) | Protective Layer on the Grid | Mesh size (square shape) (mm) | Plan View |
|----------------------------|--------|--|---|------------------------------------|-------------------------------------|---|
| Carbophalt G 120/200 | GB | Glass fibers / 120 | Carbon fibers / 200 | Plastic foil | 20 |  |
| Glasphalt GV 120/120 | GV | Glass fibers / 120 | Glass fibers / 120 | non-woven | 20 |  |

The formation of each composite structure was started by the preparation of a bottom bituminous slab at a mixing temperature of 150 °C, in a mold of size 500 × 180 × 75 mm and then its compaction, employing the French Roller Compactor (FRC), according to European Standard EN 12697-33, at 135±2 °C in compliance with the type of bitumen (i.e., PG 58-28), utilized in this research. After 24 hours of curing time, two different procedures, specified by the company, were followed for the installation of each type of the grid on the dried and clean surface of the bottom slab as shown in Figure 8.2.

- For a reinforced structure with the GB grid as well as unreinforced one, a slow setting type of emulsion (SS-1h) with the amount of 180 gr/m² of residual bitumen was uniformly spread out on the surface with the aid of a syringe. After five hours of curing time for the complete breakage of the emulsion, the grid was laid out on the surface by means of a blow torch, slowly and steadily moved on the bottom side of the grid in order to sufficiently soften the bitumen coated the bottom surface of the grid.
- For a reinforced structure with the GV grid, the placement of the grid was immediately performed after the application of the tack coat with the same type as mentioned for the GB grid but with different dosage (i.e. 270 g/m² of residual bitumen).

The preparation of the composite structure was then moved forward by the application of the top bituminous slab, with the same dimensional size as the bottom slab, directly on the grid

and then the compaction of the whole structure through the FRC, at the same temperature as mentioned for the bottom slab.

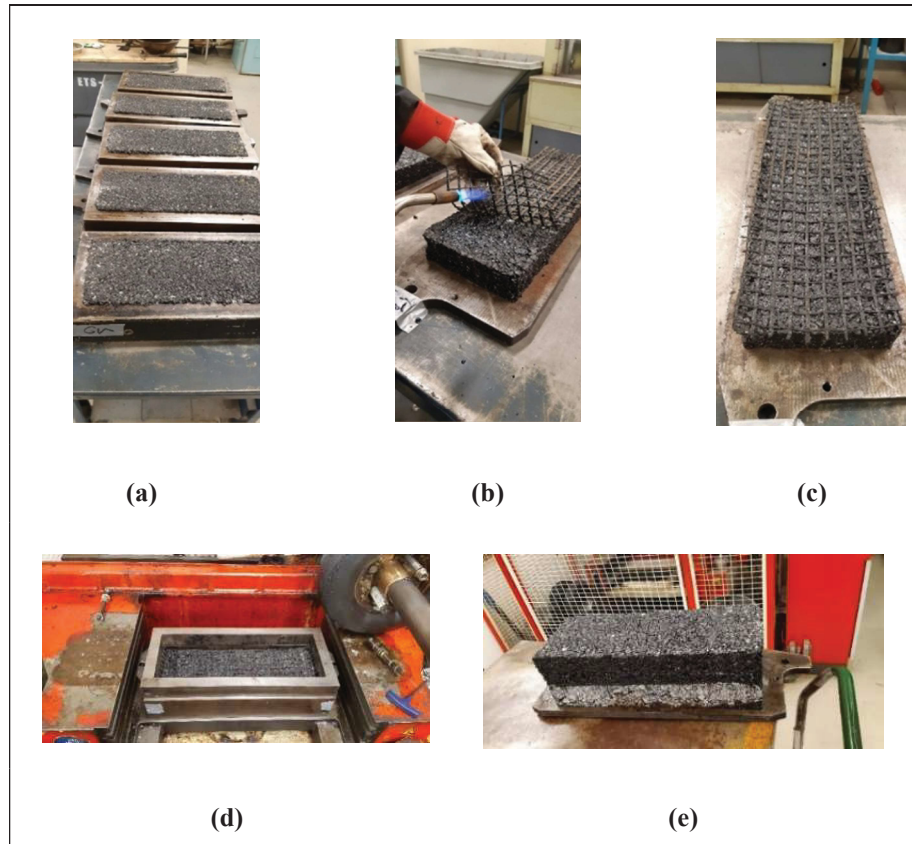


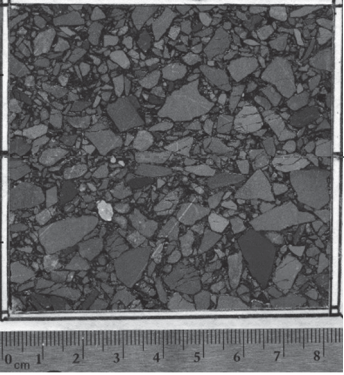
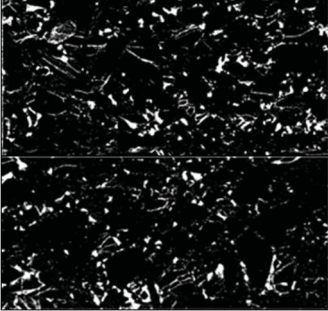
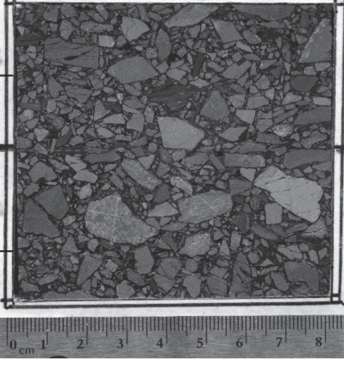
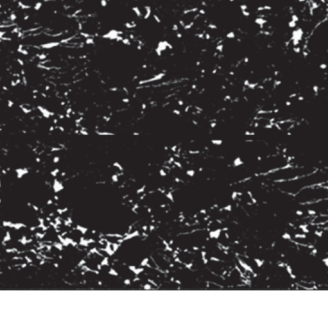
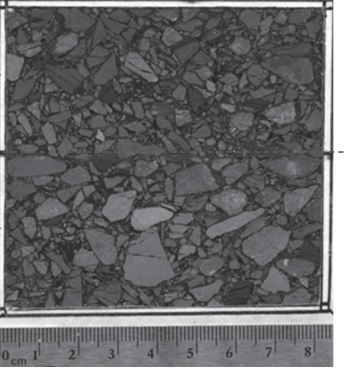
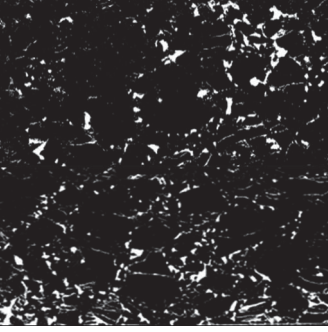
Figure 8.2 Experimental procedure followed for each slab: (a) preparation of the bottom slab; (b) application of gas blow torch below the GB grid after the breakage of emulsion; (c) prepared reinforced surfaces with GB product; (d) the bottom slab along with the grid before spreading the top hot mixture accompanied by the compaction with FRC method; (e) prepared composite structure

In addition of the composite structure with different types of mixtures at the bottom and top of the interface, a composite structure with the same type of one mixture (i.e. ESG-10) surrounded the interface was constructed to look for the effect of changing in the type of the mixture employed at the bottom side on the complex modulus of the system and the interface. Furthermore, two plain structures, made of only one type of mixture (i.e. ESG-10 and ESG-14) were fabricated to see how the complex modulus changes if it is separately defined than the case that it is viewed as a property of the system in design methods.

In total, six composite slabs both unreinforced and reinforced with grids with different types of mixtures around the interface, one unreinforced slab with the same type of the mixture below and above the interface (i.e. ESG-10/ESG-10) and two plain structures of one type of the mixture (i.e. ESG-10 and ESG-14) were constructed for the sake of this project.

One of the main aspects affecting the performance of bituminous structures under cyclic loading is the amount of air voids in the structure (Prowell, 2010; Abojaradeh, 2003). In order to reduce the variability of the results and in turn decrease the number of specimens to be tested, it is necessary that this parameter be taken into account. In this connection, since the application of the volumetric method to measure the air void content in a composite structure made of two different types of mixtures is impractical, and also in order to have a better vision of connected water paths distributed below and above the interface, an image analysis procedure was employed which had formerly been used to measure the percentage of air void in mortar and concrete materials by taking advantage of a Matlab script written for this purpose (Fonseca & Scherer, 2015). The code receives an image from the specimen's cross-section in Matlab as a scanned file and then calculates the ratio of white parts, as air void, to total solids comprising aggregate, binder, and white spots. Likewise, this technique was utilized to measure the air void content in a bituminous composite structure studied in this research. The mean air void contents obtained from three specimens via the image analysis method and a typical scanned image of the specimen's cross-section for each type of structure are demonstrated in Table 8.3. A general view of the shape and size of slabs and specimens is schematically illustrated in Figure 8.3.

Table 8.3 Mean value of air void content measured by image analysis method for the bottom and top mixture of each type of structure

| Type of Structure | Mean Air Void (%) | Typical Raw Image | Typical Processed Image |
|-------------------|-------------------|--|---|
| UN 10/14 | 3.403 |  <p>Top Side (ESG-10)</p> |  |
| | 4.353 | | |
| GB 10/14 | 3.796 |  <p>Top Side (ESG-10)</p> |  |
| | 4.67 | | |
| GV 10/14 | 3.243 |  <p>Top Side (ESG-10)</p> |  |
| | 4.173 | | |

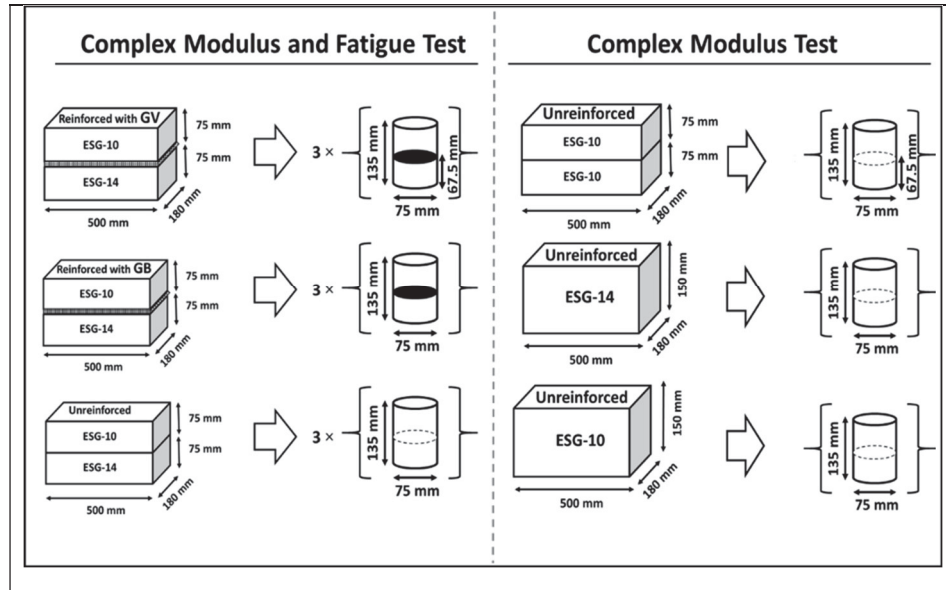


Figure 8.3 A schematic view of the arrangement and dimensional size of bituminous slabs and cylindrical specimens employed for the complex modulus test

8.4.2 Test methods

In order to understand the mechanical behavior of a grid-reinforced interface embedded in bituminous layers of different mixtures, a new arrangement of extensometers in the conventional complex modulus test with MTS press was proposed and the result was compared with a same type of the structure without the grid, which is conventionally encountered in traditional rehabilitation strategy. On the other hand, the quality of adhesion supplied at the interface, which rules out the fatigue behavior of the composite system with and without the grid, was assessed by performing the DGCB test method to see how the presence of a reinforcement interlayer could influence the structural response of the system in terms of ϵ_6 (i.e. number of cycles in one million cycles). The following subsections present details associated with each type of test. It was conjectured that the proposed test methods would help to a better understanding of possible changes that introducing a layer of the grid could bring in the structural response of the system, which is required to be included in mechanistically based design methods.

8.4.2.1 Complex modulus test

The complex modulus test was carried out on cylindrical specimens of 135 mm in height and 75 mm in diameter in a tension-compression sinusoidal mode of loading, complying with Transport Quebec's standard (LC 26-700) (MTQ, 2018). By taking advantage of a servo-hydraulic Material Testing System (MTS 810) with a loading capacity of 100 kN and a ± 50 mm axial stroke in a controlled strain amplitude, the mechanical behavior of the structure was controlled to be in the viscoelastic domain (Basueny et al., 2016). The test was conducted in a thermal chamber. Three sets of surface temperature probes (PT 100), attached to the middle height of the specimen with an elastic band, were responsible for monitoring and recording any changes in the temperature in the course of the test.

Preparing of specimens was performed in accordance with Transport Quebec's standard (LC 26-690) (MTQ, 2018). First, the prepared slabs were split in half by means of a sawing machine. The end parts of each block were subsequently trimmed off to receive two blocks of size 150 mm \times 180 mm \times 150 mm. From the center of each block, derived from each slab, two cylindrical specimens 75 mm (± 1 mm) in diameter by 150 mm in height were cored in a vertical direction to the interface. Eventually, the ends of the specimens were further processed with sawing and grinding machines to obtain test specimens with a flat surface of 75 mm in diameter and 135 mm (± 2 mm) in height. After drying, the loading caps were glued to the ends of each specimen. As indicated in the standard, it is necessary that the specimen be laid down on a soft sand bed for at least one week at ambient temperature before the day of the test. As shown in Figure 8.4, three couples of extensometers of different lengths (i.e. 25 mm, 50 mm, and 100 mm) separated at 60° from each other, were employed to capture the induced strain at different levels of the specimen. It was controlled that each half of the extensometer length be placed on each side of the interface. The mean of two measurements derived from 25 mm size of extensometers was set to control the strain amplitude during the test. Besides, the data acquisition was performed in 100 points per cycle (100 Hz), and the quality of signals in two consecutive cycles was checked by using a quality index (QI) which is calculated from scattering the measured data from a sinusoidal function that needs to be lower than 15%. Moreover, the test was executed in eight different temperatures changed from -35 to +35 °C, and seven distinct frequencies varied from 10 to 0.01 Hz, in order to cover a wide range of

temperature-frequency combinations, usually encountered in Canada's roads. The results originated from the complex modulus test are ordinarily displayed in the form of isothermal curves, the master curve at a reference temperature, Cole-Cole diagram, and Black diagram, which will be presented and discussed in the following section.

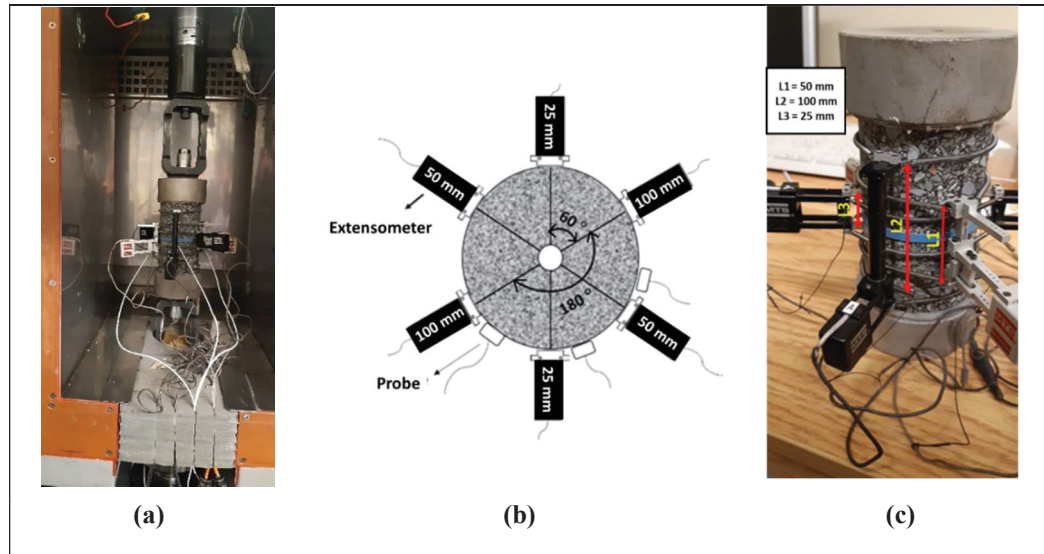


Figure 8.4 A view of complex modulus test: (a) test setup; (b) the arrangement of extensometers around the specimen; (c) a side view of the instrumented specimen

8.4.2.2 Fatigue test (DGCB Method)

The DGCB method was employed to study the adhesion quality at the interface of reinforced composite structures in terms of ϵ_6 since, as mentioned earlier, it determines the fatigue behavior of a composite structure. The reason to choose this test method instead of the 4-PBT was because of its similarity with complex modulus test in size and shape of the specimen, which considerably saves the time required for the specimen preparation. The DGCB test was carried out at an MTS press, with an environmental chamber, at a temperature of 10°C and a loading frequency of 10 Hz, applied at three different levels of axial strain amplitude. To this end, three sets of 50 mm length of extensometers, located at 120° from one another at the perimeter of specimen, were assigned to record the changes in length of the specimen from the initial values. In addition, to control the temperature oscillation during the test, three sets of surface temperature probes (PT 100) was installed at the mid-height of the specimen by using

a rubber band. Figure 8.5 gives further details of the DGCB test method.

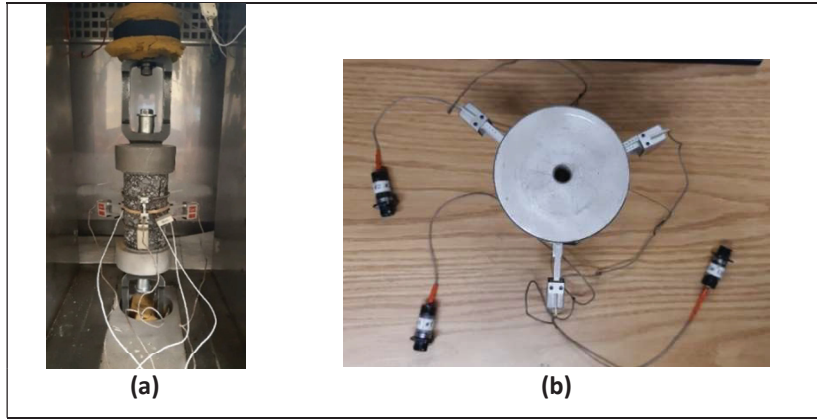


Figure 8.5. A view of DGCB test method: (a) test setup; (b) arrangement of extensometers; (c) failure at the interface

As indicated in Figure 8.3, the DGCB test was performed on three different types of structures including GB 10/14, GV 10/14, and UN 10/14 in which the suffixes 10 and 14 refer to the type of mixture applied at top and bottom of the interface.

8.5 Results and discussions

This research is an experimental work to understand the differences in the mechanical behavior of two rehabilitation techniques on bituminous pavements. To this end, the complex modulus test was performed on different types of composite structures with and without the grid to see how the complex modulus varies in different heights relative to the interface, captured by different lengths of extensometers. Also, the effect of using dissimilar mixtures around the interface on axial stiffness was examined. On the other hand, the adhesion quality at the interface of composite structures was tested through the DGCB procedure in order to find out how could the placement of a layer of the grid from two separate types between bituminous mixtures influences the structural response of the system to cyclic loading in terms of ϵ_6 . The results of this research could provide better insights into the considerations required to be considered in the application of mechanistically based design methods for reinforced bituminous structures with grids.

8.5.1 Results and discussion on complex modulus test

The results obtained from the complex modulus test on reinforced and unreinforced structures are plotted in Figures 8.6 & Figure 8.7 in terms of the Cole-Cole diagram ($E_{\text{Imaginary}}$, E_{Real}) and the Black diagram ($|E^*|$, ϕ), respectively. As evidenced, the measured values on each type of diagram were traced out a unique pattern, which could be inferred from the applicability of the Time-Temperature Superposition Principle (TTSP). In addition, in all the Cole-Cole diagrams for different types of composite structures (i.e. UN 10/14, GV 10/14, GB 10/14 and ESG-10/ESG-10), a distinguished pattern in measured values by the 25 mm-extensometer on one hand, and the 50 and 100 mm length of extensometers from the other hand could be recognized, which varied with different extents among the structures. This appreciable difference could be considered as a practical tool to evaluate the effect of the interface state on the complex modulus of the system. Another valuable finding was understood by comparing the unreinforced structure of the same type of the mixture below and above the interface (i.e. ESG 10/ESG 10) with a similar unreinforced structure but with dissimilar types of mixture surrounding the interface (i.e. UN 10/14). This could convey that by the application of a mixture with greater air void content than the one used at the top of the interface, the complex modulus of the system at the interface level was more negatively affected by the lower modulus at higher frequencies. Notwithstanding, comparing the Black diagrams among different types of structures with various interface conditions showed that the variation in measured values by different sizes of extensometers was not highlighted.

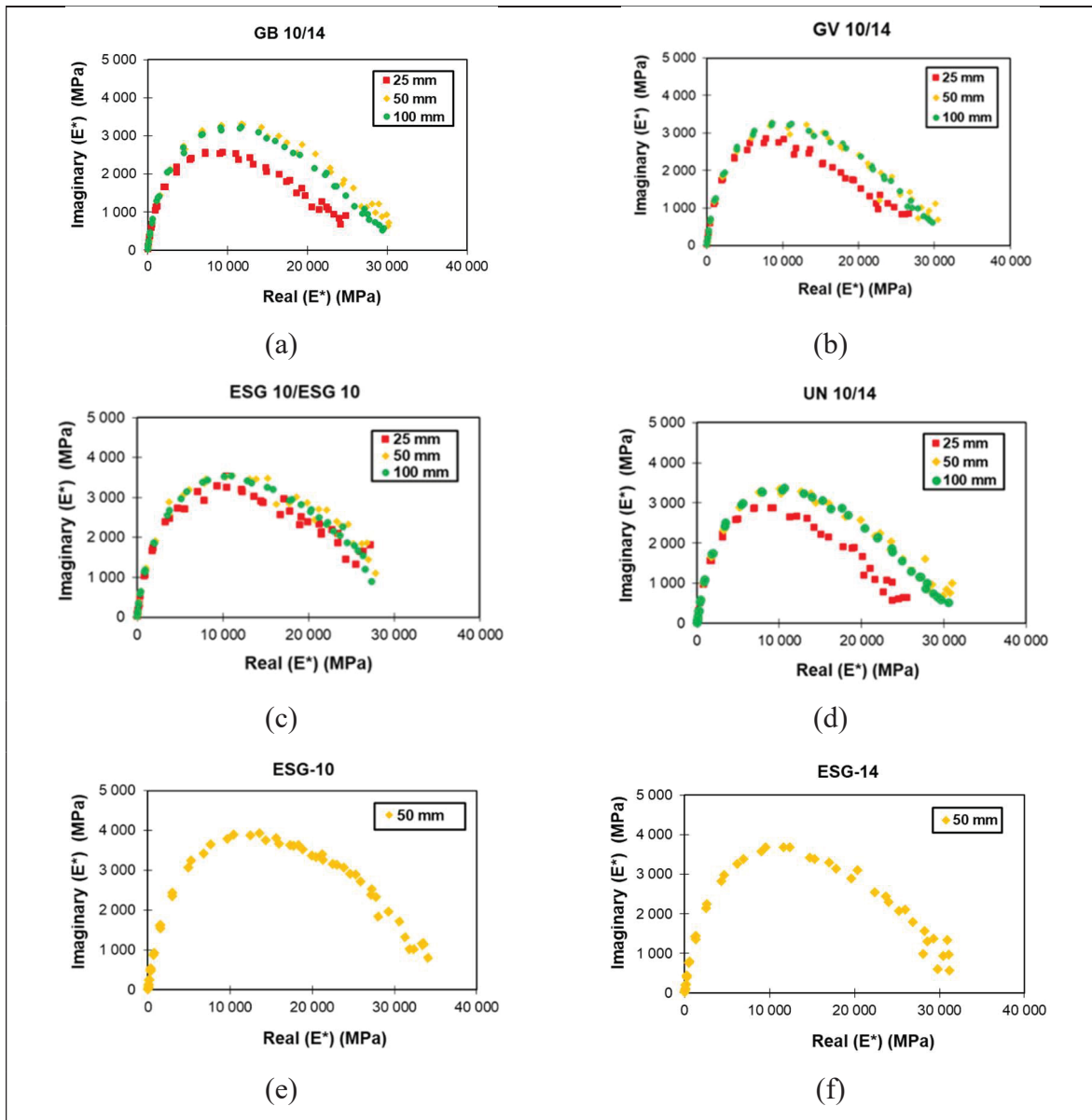


Figure 8.6 The Cole-Cole diagram measured with different sizes of extensometers for: (a) reinforced structure with GB grid surrounded by ESG-10 and ESG14; (b) reinforced structure with GV grid surrounded by ESG-10 and ESG14; (c) unreinforced structure with the same type of mixture ESG-10 at the bottom and top of the interface; (d) unreinforced structure with different types of mixtures around the interface; (e) plain structure of ESG-10; (f) plain structure of ESG-14

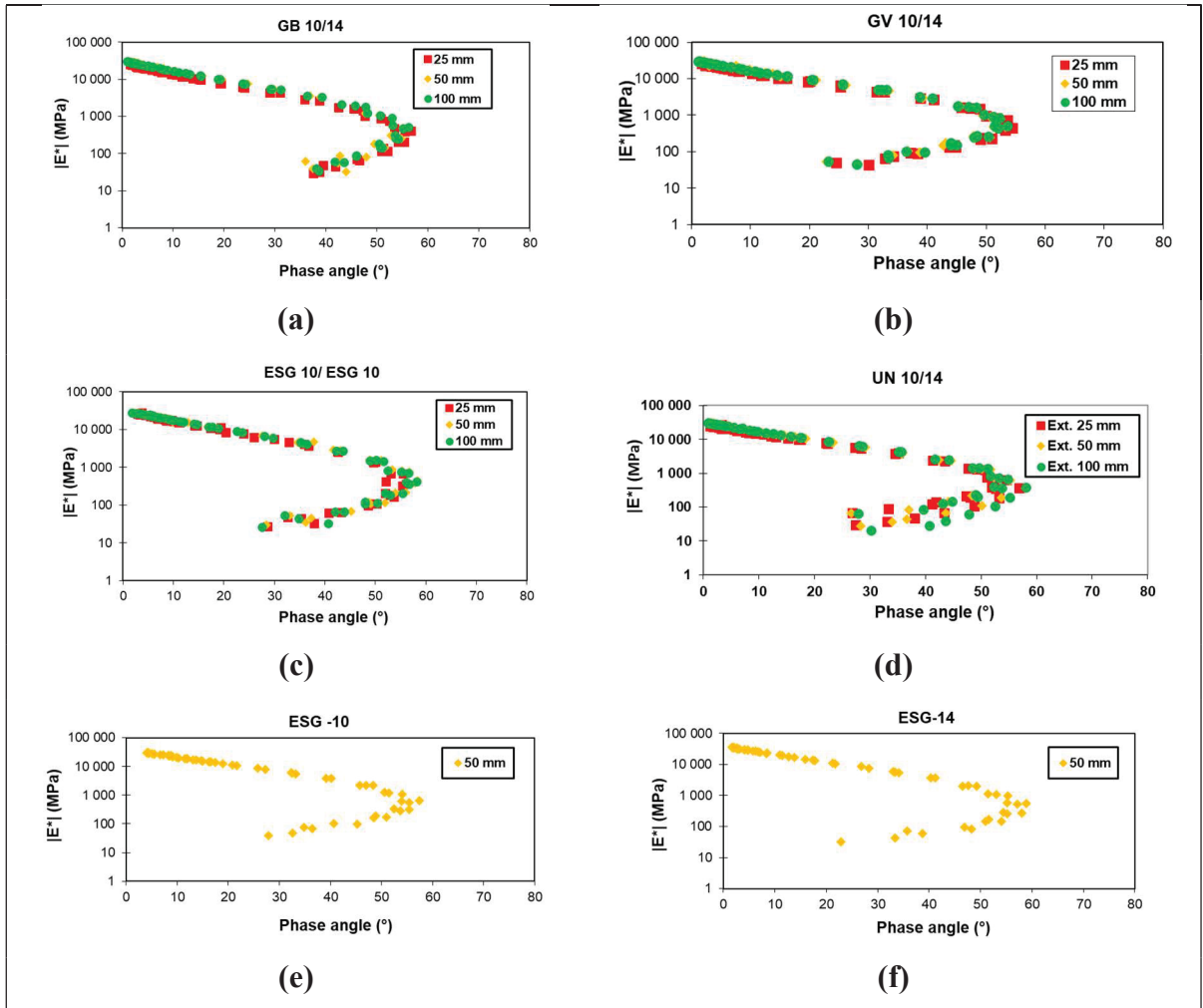


Figure 8.7 The Black diagram measured with different sizes of extensometers for: (a) reinforced structure with GB grid surrounded by ESG-10 and ESG14; (b) reinforced structure with GV grid surrounded by ESG-10 and ESG14; (c) unreinforced structure with the same type of mixture at the bottom and top of the interface; (d) unreinforced structure with different mixture around the interface; (e) simple mixture of ESG-10; (f) simple mixture of ESG-14

A broad range of mechanical models, either with mathematical or analogical nature, have been proposed to justify the changes in the modulus of bituminous layers by the temperature and load frequency (Olard & Di Benedetto, 2003). Among them, the 2S2P1D model (two Springs, two Parabolic creep elements, and one Dashpot) has received much attention over others because of its capability to predict the mechanical behavior of bituminous mixtures from very low to very high frequencies. Equation (8.1) presents the mathematical form of this model:

$$E_{2S2P1D}^* = E_{00} + \frac{E_0 - E_{00}}{1 + \delta(i\omega\tau)^{-k} + (i\omega\tau)^{-h} + (i\omega\beta\tau)^{-1}} \quad (8.1)$$

where i the imaginary unit; ω angular frequency; E_0 glassy modulus ($\omega \rightarrow \infty$); E_{00} static modulus ($\omega \rightarrow 0$); k , h , and δ calibration constants; β parameter related to Newtonian viscosity of the dashpot; and τ_E characteristic time value varied with temperature. On this basis, Table 8.4 provides a fair comparison between 2S2P1D model parameters, obtained from its fitting with the experimental data measured by the Ext. 25 mm, for different types of structures. As can be seen, the values of glassy modulus (i.e. E_0) and static modulus (i.e. E_{00}) were highly affected in different types of structures while other parameters remained almost unchanged. This suggested that the interface behavior in design methods could be defined only by the adjustment of two threshold values of modulus (i.e. E_0 and E_{00}). Also, the glassy modulus for the structures composed of dissimilar mixtures were tangibly lower than that of the structure made of only one type of mixture (i.e. ESG 10/10). This could be explained by the higher air void content in the bottom layer mixture in the case of unlike layers. Furthermore, in double-layered structures composed of different mixtures, the interface reinforced with the GV grid showed almost the same static and glassy modulus compared with the unreinforced structure. This could be attributed to the higher dosage of tack coat used for the installation of the GV grid compared to the GB one, which positively keeps the stiffness of the structure at high frequencies or low temperatures the same as that in the unreinforced structure.

Table 8.4. 2S2P1D model parameters fitted with the experimental data from Ext. 25 mm

| Model Parameters | Types of Structures | | | |
|--|---------------------|----------|----------|-----------|
| | UN 10/14 | GB 10/14 | GV 10/14 | ESG 10/10 |
| E_{∞} | 35 | 20 | 35 | 25 |
| E_0 | 26200 | 25300 | 26700 | 31000 |
| K | 0,2 | 0,2 | 0,2 | 0,2 |
| h | 0,6 | 0,6 | 0,6 | 0,6 |
| δ | 1,8 | 2 | 2 | 2 |
| τ_E (s) ($T_{ref} = -5.4 \text{ }^\circ\text{C}$) | 2 | 2 | 2 | 2 |
| β | 100 | 100 | 100 | 100 |

Furthermore, a comparison between the model parameters derived from each type of mixture (i.e. ESG-10 and ESG-14) measured independently with a 50 mm length of extensometer, with

those acquired from a composite system through the same size of extensometer is shown in Table 8.5. It could be perceived that treating the complex modulus as a system property resulted in an almost unique pattern, more closely to the complex modulus of the bottom layer (i.e. ESG-14) than that for the top layer (i.e. ESG-10). In addition, the glassy modulus (E_0) of each individual layer was markedly affected when it was studied in a compound system of layers.

Table 8.5 2S2P1D model parameters fitted with the experimental data from Ext. 50 mm

| Model Parameters | Types of Structures | | | | | |
|---|---------------------|----------|----------|-----------|--------|--------|
| | UN 10/14 | GB 10/14 | GV 10/14 | ESG 10/10 | ESG 10 | ESG 14 |
| E_{∞} | 35 | 23 | 35 | 25 | 30 | 24 |
| E_0 | 31200 | 31800 | 30800 | 32500 | 38000 | 33000 |
| K | 0.2 | 0.2 | 0.2 | 0.2 | 0.2 | 0.2 |
| h | 0.6 | 0.6 | 0.6 | 0.6 | 0.6 | 0.6 |
| δ | 1.8 | 2 | 1.9 | 1.9 | 1.9 | 1.8 |
| $\tau_E(s)$ ($T_{ref} = -5.4\text{ }^{\circ}C$) | 2 | 2 | 2 | 2 | 2 | 2 |
| β | 100 | 100 | 100 | 100 | 100 | 100 |

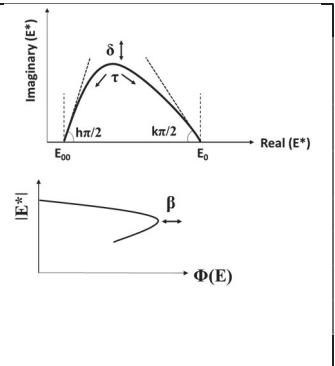


Figure 8.8 shows relative differences in the percentage between the stiffness modulus obtained from the Ext. 25 mm and pertinent predicted values by the 2S2P1D model at a reference temperature ($T_{ref} = -5.4\text{ }^{\circ}C$). On this basis, for all three structures a low discrepancy in Y-axis (lower than 10 percent) at higher frequencies or low temperatures referred to the accuracy of the 2S2P1D model to predict the mechanical behavior of reinforced and unreinforced interfaces. However, at low frequencies or high temperatures up to $a_T \cdot f_r$ equals to $1E-05$ the 2S2P1D model is still reliable for the unreinforced structure but for the reinforced structure with the GB grid the model started to lose its accuracy way earlier as $a_T \cdot f_r$ getting smaller than $1 E+00$. In the case of the structure with the GV grid, the 2S2P1D model kept its accuracy before $a_T \cdot f_r$ equals to $1E-05$ with some exceptions at middle points from $1 E-02$ to $1E-03$.

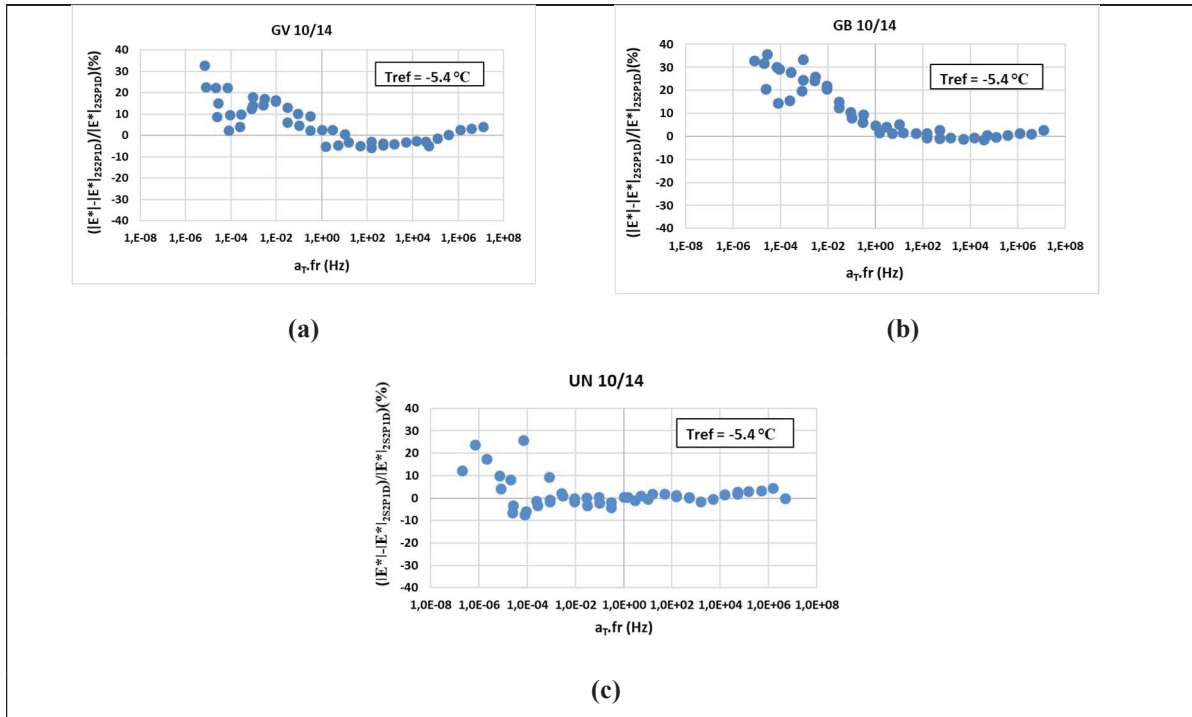


Figure 8.8 Changes in the stiffness modulus between measured and predicted values by the 2S2P1D model: (a) reinforced structure with GV grid; (b) reinforced structure with GB grid; (c) Unreinforced structure

The viscoelastic behavior of bituminous layers could be introduced into design software, working based on the finite element method, through the Prony series as defined by Equation (8.2) (Dogan, C. 2007):

$$g(t) = 1 - \sum_{i=1}^N g_i \left(1 - e^{\left(\frac{-t}{\tau_i}\right)} \right), \quad g(t) = \frac{G(t)}{G(t=0)} \quad (8.2)$$

In which $g(t)$ is the shear modulus ratio, defined by the ratio of shear modulus at any time like t , (*i.e.* $G(t)$), to the shear modulus at the first stage ($t = 0$, $G(t = 0)$). τ_i and g_i are the Prony constants, which are specified based on the material properties, and N is the number of terms used in the Prony series (normally takes $N = 5$) (Liao & Sargand, 2010).

Shear modulus, $G(t)$, is obtained from the relaxation modulus, $E(t)$, according to the Equation (8.3):

$$G(t) = \frac{E(t)}{2(1 + \nu)} \quad (8.3)$$

where $E(t)$ is the relaxation modulus, defined by transforming the dynamic modulus master curve; and ν is the Poisson's ratio, normally assumed 0.35. Once $G(t)$ gets clear the ratio of $g(t)$ could be easily computed by Equation (8.2).

On this basis, it is necessary to study the changes in the dynamic modulus master curve in the presence of a grid-reinforced interface. Figure 8.9 provides a comparison in master curves measured by different lengths of extensometers for different types of structures. To have a better vision, the dynamic modulus at the reference temperature (i.e. $-5.4\text{ }^{\circ}\text{C}$) and an arbitrary point of frequency (i.e. 10 Hz) are also displayed. It could be observed that there was a meaningful distinction between the dynamic modulus captured by Ext. 25 mm from the others, in each type of the structure, especially for the GB 10/14. However, the master curves developed for Ext. 50 mm and Ext. 100 mm are almost superimposed on each other.

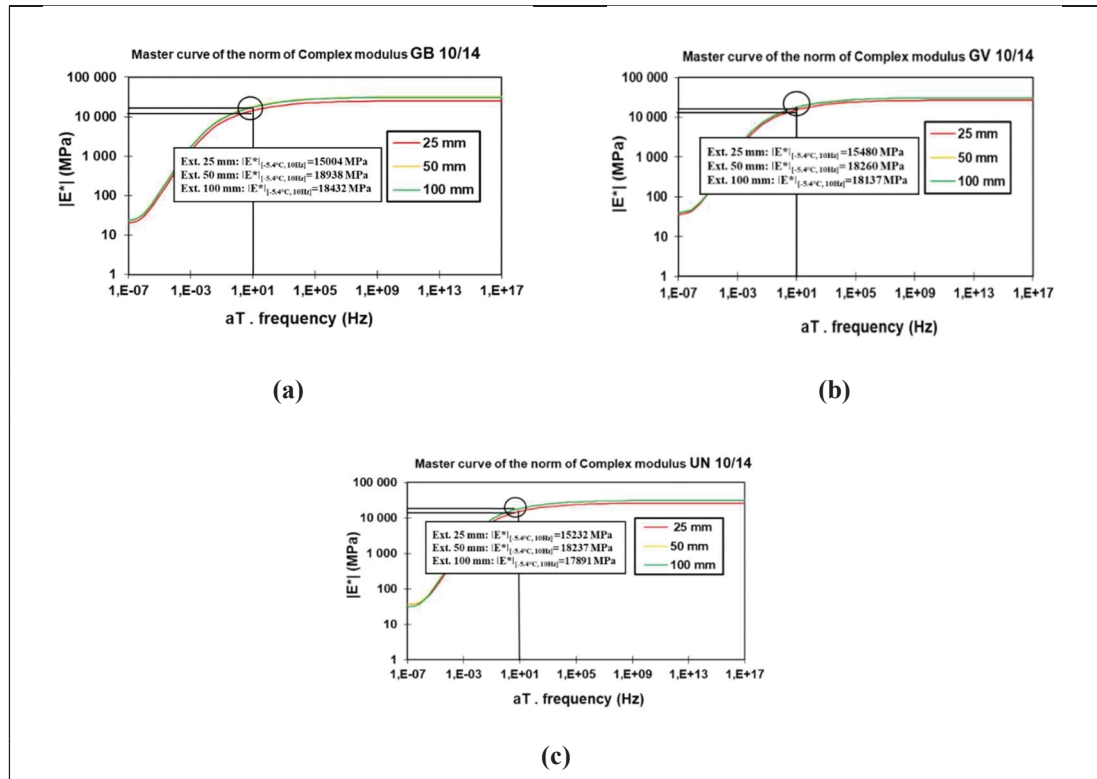


Figure 8.9 Changes in dynamic modulus master curves developed by the 2S2P1D model for different lengths of extensometers for: (a) reinforced structure type GB 10/14; (b) reinforced structure type GV 10/14; (c) unreinforced structure UN10/14

Figure 8.10 also makes a comparison in dynamic modulus and phase angle derived by Ext. 25 mm for various interfaces at the reference temperature (i.e. -5.4 °C) and a frequency 10Hz. As can be seen, the highest dynamic modulus and the lowest phase angles are related to the reinforced structure made of the GV grid, which it could be inferred that the structure reinforced with the GV grid received more solid behavior from the interface compared with the structure reinforced with the GB grid, which under cyclic loading it could be regarded as positive mechanical effect.

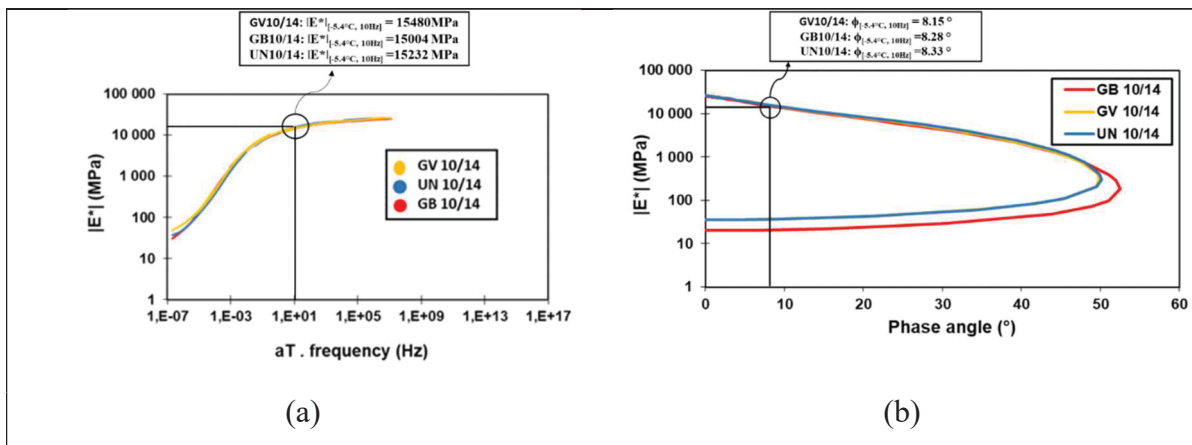


Figure 8.10 A comparison of dynamic modulus and phase angle at $T = -5.4 \text{ }^\circ\text{C}$ and $f = 10 \text{ Hz}$ from (a) dynamic modulus master curve and (b) black diagram; predicted by the 2S2P1D model for reinforced and unreinforced interfaces based on 25 mm extensometer

The results showed that the proposed methodology provided a practical tool to evaluate the axial stiffness of reinforced and unreinforced interfaces through the measurements using the Ext. 25 mm. It also revealed that treating the axial stiffness in a composite structure as a system property than that when the specification of each layer, without the presence of other layers, are defined into the design methods could result in a more realistically solution.

8.5.2 Results and discussion on fatigue test

Table 8.6 presents a comparison among various structures in terms of the average of initial modulus $|E_0^*|$ obtained from different levels of axial strains. This value was derived from the first cycle, which was extrapolated by presuming a linear trend between 2 and 50 cycles. It could be deduced that in both of the reinforced structures, the composite system received more

axial stiffness from the interface than the unreinforced case. This characteristic was also more meaningful for the structure reinforced with the GB type of the grid.

Table 8.6 Fatigue test specifications at $T= 10\text{ }^{\circ}\text{C}$ and $f= 10\text{ Hz}$

| Structure | Axial Strain Amplitude ($\mu\text{m/m}$) | Initial Modulus $ E_0^* $ (MPa) | |
|-----------|---|---------------------------------|---------|
| | | Value | Average |
| UN 10/14 | 66.5 | 6924 | 6981 |
| | 74.6 | 6874 | |
| | 99.1 | 7146 | |
| GV 10/14 | 76.6 | 7243 | 7445 |
| | 88.4 | 6920 | |
| | 96.7 | 8172 | |
| GB 10/14 | 77.8 | 8175 | 7762 |
| | 87.5 | 7059 | |
| | 98.5 | 8054 | |

The Wöhler curve for three structures, both reinforced and unreinforced ones, are demonstrated in Figure 8.11. The classical failure criterion was considered, $N_{f50\%}$ was considered to study the integrity of the structure under cyclic loading at temperature $10\text{ }^{\circ}\text{C}$ and frequency 10 Hz . The vertical axis is the number of cycles up to the half value of the initial modulus and the horizontal axis is the real axial strain level registered in the course of the test. Both of the axes are defined in logarithmic scales. It could be seen that in both of the reinforced structures, the slope of the curve was lower than the unreinforced case. This could be translated by the higher number of cycles required for the reinforced structure before failure at high strain amplitude (heavy loads). Moreover, the R^2 value, given on each curve, indicates that the $N_{f50\%}$ failure criterion is a suitable index to study the adhesion quality at the interface of a composite structure.

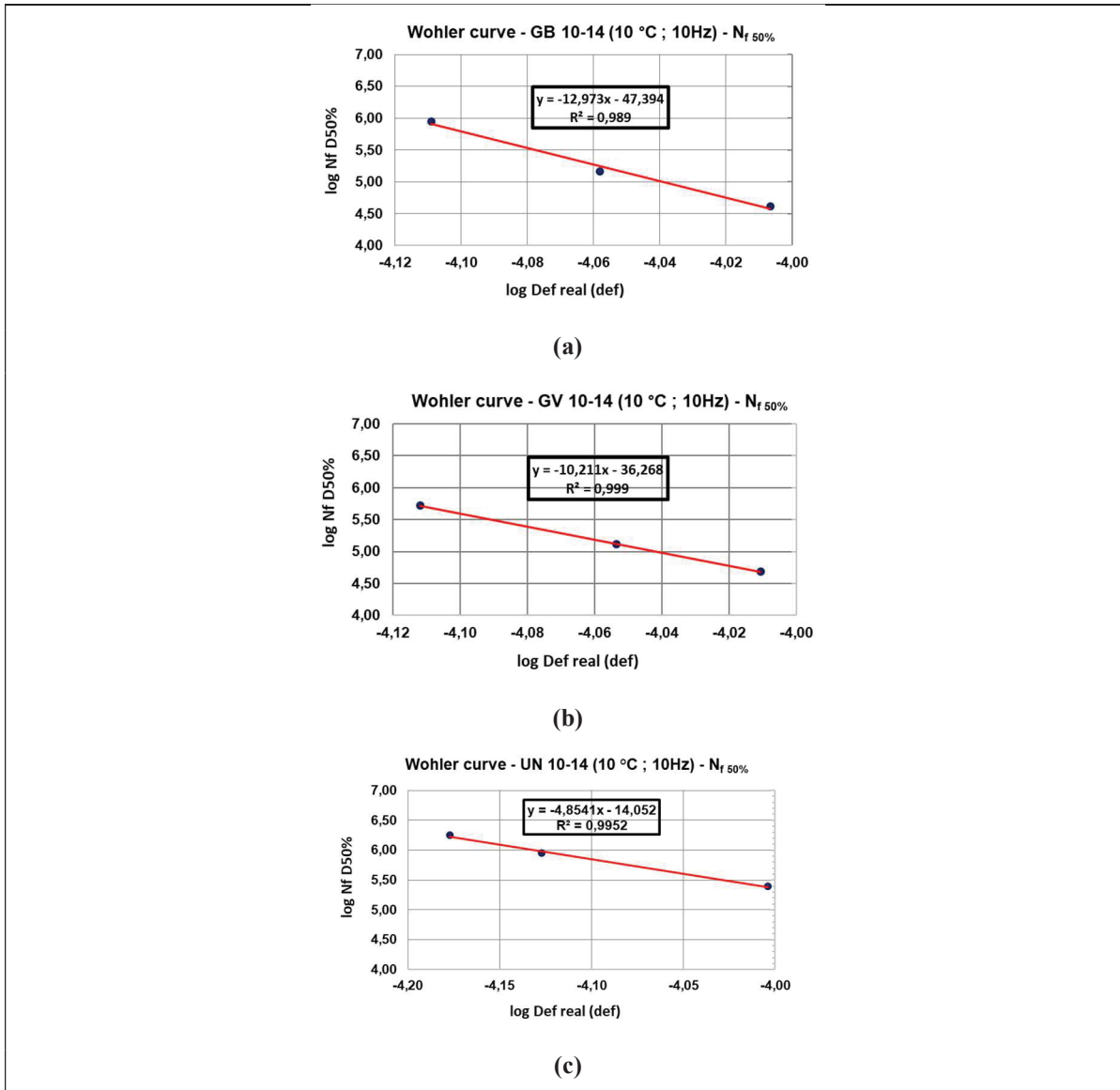


Figure 8.11 Wöhler curve for each type of structure developed at $T = 10\text{ °C}$ and $f = 10\text{ Hz}$:
 (a) reinforced structure with the GB grid; (b) reinforced structure with the GV grid; (c) unreinforced structure

A mathematical form of the Wöhler curve can be shown by Equation (8.4).

$$N_f = K_1 \cdot \varepsilon^{-K_2} \tag{8.4}$$

where K_1 and K_2 are empirical constants dependent on the type of material, N_f is the number of cycles and ε is the axial strain, which its value at failure is considered ε_6 . A fair comparison of these parameters for various types of structures is given in Table 8.7. A higher ε_6 value

obtained for the reinforced structure with the GB grid, as shown in Figure 8.12, suggested that the reinforced interface could tangibly integrate a system composed of different layers compared with the unreinforced structure. Nonetheless, a system reinforced with the GV grid may act in the opposite direction.

Table 8.7 A Comparison of parameters employed in development of Wöhler curve

| Structure | Fatigue Parameters for $N_{f50\%}$ Criterion | | | |
|-----------|--|-------|-------|--------------|
| | K_1 | K_2 | R^2 | ϵ_6 |
| UN 10/14 | 8.88 E -15 | 4.85 | 0.99 | 74.8 |
| GV 10/14 | 5.39 E -37 | 10.21 | 0.99 | 71.6 |
| GB 10/14 | 4.04 E -48 | 12.97 | 0.94 | 76.4 |

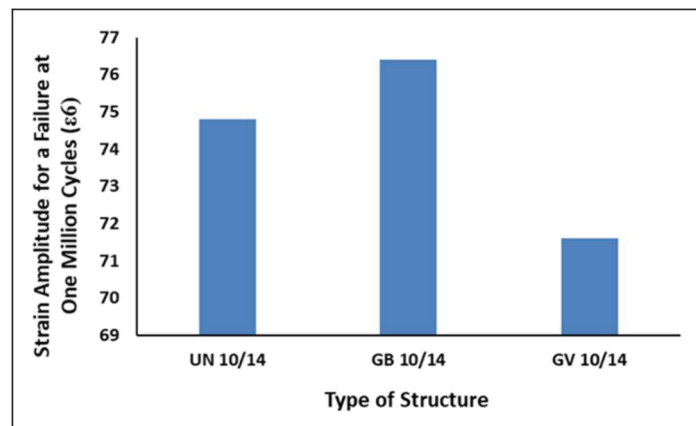


Figure 8.12 Comparing the ϵ_6 value among different structures (UN: unreinforced structure; GB: reinforced structure with the GB grid; GV: reinforced structure with the GV grid)

Overall, by comparing the results obtained from the DGCB method for both reinforced and unreinforced structures, it could be notified that using the grid at the interface of dissimilar mixtures could enhance the mechanical performance of the system in terms of the initial modulus and number of cycles before failure at high strain levels. However, only the grid without fabric covering its aperture (i.e. GB grid) could provide monolithic action of the system at failure point compared with the unreinforced structure. This could be explained by

the lack of interlocking effect between the aggregate in different mixtures around the interface in the case of using the GV grid.

8.6 Conclusion and recommendations

The proposed methodologies described in this paper were allocated to learn how the placement of a layer of the grid with different specifications and installation process could influence the axial stiffness and integrity of a bituminous structure composed of different mixtures under cyclic loading compared with unreinforced structures. To fulfill these objectives, the conventional tension-compression complex modulus test with a new configuration in extensometers was proposed to account for the changes in axial stiffness caused by a reinforced interface. In addition, the uniaxial tension-compression DGCB test method was employed to evaluate the structural integrity of reinforced structures in terms of the axial strain, tolerated by the structure at one million cycles, expressed by ϵ_6 . The following result can be drawn from this study:

- The mechanical effect of a reinforced and unreinforced interface can be extracted from Ext. 25 mm. On this basis, the rheological behavior of the reinforced and unreinforced interfaces could be reliably predicted by the 2S2P1D model at high frequencies or low temperatures.
- Among the 2S2P1D model parameters, using the glassy modulus (E_0) could provide a practical tool to compare the changes in axial stiffness between different interface conditions and various structures.
- Using the complex modulus as a system property in a structure made of dissimilar mixtures could result in a more realistic mechanical behavior than when introducing the specification of each layer separately into design methods.
- The reinforced structure with the GV grid behaved more like the unreinforced structure under cyclic loadings. However, the GB grid contributed more to enhance the initial stiffness and the fatigue life of the system.
- The initial modulus and number of cycles at failure at high axial strain levels are affected by the presence of a reinforced interface with the grid. In this connection, the application of the classical $N_{f50\%}$ failure criterion is a suitable tool to study the quality

of adhesion at the interface with different conditions in terms of axial strain at one million cycles or ϵ_6 .

CONCLUSION AND RECOMMENDATIONS

Rehabilitation or reinforcement of bituminous layers within the flexible pavement by introducing geosynthetic materials has been the focus of the engineering community as an alternative way to the traditional approach called mill and fill from economical and mechanical performance points of view. However, the mechanistic-empirical (M-E) design approach, which has been accepted for the design of the conventional structure of the flexible pavement, can not be used for reinforced or rehabilitated structures with geosynthetics mainly due to the lack of laboratory equipment to allow a better characterization of the mechanical behavior of the composite system, while establishing an appropriate design method for reinforced or rehabilitated structures is imminent in the widespread usage of interlayer products in the market. To this end, 44 double-layer slabs of size $500 \times 180 \times 100$ mm and 16 slabs of size $500 \times 180 \times 150$ mm, composed of three different hot mixtures in terms of NMAS, were fabricated during almost 2 years. As a result of this effort, two new devices were built: the CWD to control the width of the crack reflected to the surface during the water permeability test, and the interface shear tester to evaluate the shear strength and shear displacement applied at the interface at the same time. Also, the new configuration of falling head permeability test was made to accommodate bituminous specimens of size 50 mm in diameter and allow water to percolate through different width of cracks from the top to the bottom surface of the specimen in an accelerated way. Moreover, a new arrangement of extensometers in the complex modulus test was proposed to predict the rheological behavior of the interface under different temperatures and loading frequencies. Furthermore, the crack resistance ability of the interlayers surrounded by different hot mixtures was studied through a new configuration of the 3-PBT. Besides, the adhesion quality at the interface was evaluated at 10 °C and 10 Hz by means of the DGCB test method and the axial strain at one million cycles was opted as a basis to compare the reinforced and rehabilitated structures with corresponding unreinforced ones.

The following conclusions can be derived from this study:

- The proposed laboratory methodologies provide reliable inputs for mechanistic- based design methods according to the low range of variability of $\pm 15\%$ obtained from three replicates around the mean value.
- The permeability of double-layer structures was predicted by the width of the crack opening, reflected from the bottom layers to the surface, by a second-order polynomial equation. In addition, taking advantage of the water-vacuum permeability device (WVPD) showed that the rehabilitated system with paving fabric was impervious to water. This effect in the design method is translated by using low drainage coefficient for granular layers and high retained modulus for granular and bituminous layers, which are placed underneath.
- The ability of double-layer reinforced or rehabilitated bituminous structures against crack initiation from an existing notch at the bottom bituminous layer was examined through a new configuration of the 3-PBT by calculating the J-integral parameter.
- The structural performance of a double-layer system to crack propagation was assessed by the Crack Resistance Index (CRI). This parameter in rehabilitated structures is defined based on the slope of the force-displacement curve measured through Crack Widening Device (CWD) to simulate thermally-driven cracks, while in reinforced structures it is calculated from subtracting the areas surrounded by the force-crack width opening, below and above the interface measured by two crack gauges employed in the 3-PBT to resemble traffic driven cracks.
- Although the shear strength in double-layer structures is negatively affected by the placement of the geosynthetic at the interface, the Coefficient of Interface Bonding (CIB) measured by the interface shear tester showed that the ability of reinforced or rehabilitated structures in maintaining their structural integrity, even in large shear displacement, could not be ignored. In this regard, the French Rutting Tester (FRT) demonstrated that the installation of the paving fabric between coarse-graded bituminous mixtures resulted in a rather similar evolution pattern as that in unreinforced structures.

- In reinforced structures with geogrid, the J-integral was connected to the bonding quality and the crack resistance property of the interface, defined by CIB and CRI parameters respectively, through a second-order linear regression equation. In this regard, the J-integral of the rehabilitated system was found higher than the reinforced case. However, it is possible that in reinforced specimens with a size larger than the ones studied in the research, the more contribution from the grid on crack halting is observed.
- Complex modulus of rehabilitated and reinforced double layer structures, which forms the backbone of the response model in the M-E design method, was reliably predicted by the 2S2P1D model especially at high frequencies or low temperatures. In addition, the mechanical response of interlayers to cyclic loadings in the linear viscoelastic range of material's behavior was learned by the 25-mm extensometer. Also, employing the same type of material as the tack coat in reinforced and unreinforced structures only resulted in variation of static modulus and glassy modulus, while using a different type of the tack coat material, as the one applied in the rehabilitated structure, would also change the shape parameters (β and δ) in the 2S2P1D model.
- The adhesion quality provided at the interface of double-layer bituminous structures was evaluated by performing the uniaxial tension-compression fatigue test (the DGCB method). The results showed that using the classic fatigue criterion, $N_{f50\%}$ justified the evolution of axial stiffness of reinforced and rehabilitated structures under cyclic loadings. In addition, the DGCB test method revealed that the initial stiffness modulus of reinforced structures was tangibly higher than that of rehabilitated structures.
- The negative effect of using paving fabric on rutting resistance of double-layer hot mixtures, do not compromise its great advantage in crack retardation ability and maintain the structural integrity of the system under shear stress and cyclic loadings. However, a full ME pavement analysis is required to be done to confirm that.

In addition, following considerations are required to be taken into account in M-E design approaches for reinforced and rehabilitated structures:

- In terms of the response model, from chapters 5 and 8, it was found that the reinforced and rehabilitated bituminous interfaces had different rheological behaviors from their surrounding mixtures with respect to E_0 , E_{00} , δ , β . Therefore, it is recommended that rheological behavior of the interface is defined independently into the mechanistic design methods. Furthermore, it was recognized that a more precise rheological model to justify the mechanical responses of the interface at low frequencies or high temperatures is still in demand.
- From the distress prediction model's perspective, it was recognized in chapter 6 that the rut depth prediction model needs to be adjusted. In this connection, both the initial rut depth and the slope of rutting evolution were both affected by the placement of paving fabric at the interface. Therefore, it is suggested that the initial rut depth in rehabilitated structures including ESG-10 over ESG-14 and ESG-14 over GB-20 increases up to 1.5 and 1.3 respectively, compared to corresponding unrehabilitated cases. Also, a factor of 2 is necessary to apply to the slope of rut evolution in rehabilitated structures including ESG-10 over ESG-14. Regarding fatigue failure studied in chapters 6 and 8 two modifications are necessary to be made in the prediction model: first the allowable value of ϵ_t needs to be corrected according to the modified ϵ_6 . In this respect, it was found that the modified ϵ_6 in rehabilitated structure was 30 percent higher than that in the structure without interlayer. However, no significant change was observed in the reinforced case. Also, it is suggested that the dynamic modulus of the combined system is used in the prediction model. In this sense, the dynamic modulus of the combined system in reinforced structures was 10 percent higher than that in the unreinforced case. Concerning reflective cracking, it is suggested, based on the results obtained from chapter 5 and 7, that in the reflective cracking prediction model, the delay retardation ability of the system (factor d in prediction model) is selected according to the J-Integral calculations. This parameter, in case of grid-reinforced interfaces, is in close relationship with crack resistance index (CRI) and Coefficient of Interface Bonding (CIB) as demonstrated in chapter 7. On this

basis, it was found from chapters 5 and 7 that the rehabilitated and reinforced structures had, on average, 5 and 3 times higher fracture toughness, respectively, compared to the untreated systems.

Along with this study, more research is required to predict the behavior of reinforced and rehabilitated structures at low frequencies or high temperatures. Also, the effect of any structural discontinuity in the bottom hot mix layer, as is the case in reality, on rheological behavior of the composite system could be studied further. Also, the validity of the results obtained from this study could be verified further by using different hot mixtures and interlayer products. Besides, the suitability of failure criteria and performance indices discussed in this research could be evaluated and compared under different temperatures and load frequencies in field conditions. Last but not the least, the required changes in the geometrical design of a road, rehabilitated with a layer of paving fabric, in terms of side slope and longitudinal slope need to be further studied to lessen the trapping effect of water in the surface layer on its mechanical characteristics.

APPENDIX

Table-A I-1 Studies on the effect of geosynthetics on fatigue life

| Researchers | Research Topic | Type of Test | Major Findings |
|---------------------------|---|--|--|
| Safavizadeh et al. (2019) | Studied the effect of reinforced asphalt concrete beam with fiberglass grid on reflective cracking | Four-point bending notched beam tests | The fatigue life is extended by the application of a high-quality tack coat at the interface |
| Cho et al. (2004) | Examined the crack resistance of bituminous pavements including reinforced asphalt overlay with glass-fiber sheet | Three-point bending beam test | 1- Higher fatigue load results in low reinforcement effect 2- The fatigue life of reinforced asphalt layer is increased between 6-10 times higher than unreinforced layer |
| Arsenie et al. (2017) | Laboratory investigation of fatigue behavior of grid-reinforced asphalt layer with glass fiber | Four-point bending beam test | In reinforced specimens: 1- Enhancement of fatigue life (N_f) by 50% 2- Increase of ϵ_6 (strain at fatigue failure for 10^6 cycles) by 10.52% 3- Increase in b (the slope of fatigue curve) up to 11.55% |
| Polidora et al. (2019) | Studied the effects of inclusion geosynthetics between different asphalt layers and locations | Four-point bending test on notched beams | 1- In static mode of testing, the specimens reinforced with geosynthetics in two layers have higher resistance against fatigue failure compared to single-layer reinforced specimens and unreinforced ones 2- According to the Paris law, in cyclic mode of test, the double-layer reinforced specimens have the least rate of crack growth |

Table A-I-1 (Continued)

| Researchers | Research Topic | Type of Test | Major Findings |
|---------------------------------|---|---|---|
| Kumar and Saride (2017) | Studied the flexural behavior of reinforced asphalt beams with three different types of geogrids by digital image correlation (DIC) technique | Four-point bending test | 1- The DIC method is a helpful method to study the formation and evolution of fatigue cracks. 2- The reinforced structures with geogrids made of polyester material has 22 times higher fatigue life compared to the application of fibers fabricated with geojute materials |
| Hosseini et al. (2009) | Applied a mechanistic approach to explain crack propagation in reinforced specimens with geosynthetics | Four-point bending test | 1- Based on fatigue versus damage evolution curves, the reinforced overlays have a lower rate of crack propagation. 2- The reinforced specimens with low strain level of geotextiles and high strain level of geogrids have the least crack propagation rate. |
| Požaryckia and Garbowski (2013) | Investigate the type of geosynthetic on fatigue life of reinforced asphalt overlay | Schenck strength device | The fatigue life of asphalt overlay is extended by 16% in the case of geogrid and up to 35% for geocomposite. |
| Nguyen et al. (2013) | Field examination of pavement structures with and without glass grid through the accelerated pavement testing facility of the IFSTTAR to compare the structural responses under traffic loading | Field investigation of structural response by taking advantage of strain gauges installed on the grid | The placement of a grid near the bottom of the asphalt overlay remarkably enhance the fatigue life of the system |

Table-A I-2 Studies on the effect of geosynthetic on permanent deformation (rutting)

| Researchers | Research Topic | Type of Test | Major Findings |
|-----------------------------|--|-----------------------------------|---|
| Correia and Zornberg (2016) | Laboratory study of the effect of geosynthetics in asphalt overlay on plastic deformation | Wheel tracking device | <p>1- Reinforced asphalt overlays have 4 times higher service life than unreinforced ones in terms of rutting</p> <p>2- Dynamic vertical stress at the bottom of the reinforced asphalt overlay and at the top of the subgrade are reduced 32% and 36% respectively</p> |
| Ingrassia et al. (2020) | To evaluate the effect of geocomposite embedded in thin asphalt overlay on pavement response | Fast Falling Weight Deflectometer | Reinforced specimens have 5-10% reduced compressive strain at the top of the subgrade |
| Mounes et al. (2014) | A review on improved rutting resistance of reinforced asphalt overlay | | <p>1- Placement of geogrid in the mid-depth of asphalt overlay has more influence on improving rutting compared to that at the bottom</p> <p>2- The resistance of asphalt overlay on rutting depend on its elastic modulus which improves by adding the geosynthetic</p> <p>3- The mesh size and adhesion quality provided at the interface govern the resistance of reinforced asphalt overlay to plastic flow</p> |

Table A-I-2 (Continued)

| Researchers | Research Topic | Type of Test | Major Findings |
|-----------------------------|---|--|---|
| Guler and Atalay (2016) | To investigate the rutting resistance of different geosynthetic products in different asphalt mixes | Hamburg Wheel Tracking Device | The improved rutting resistance of reinforced asphalt overlays is independent of the stiffness of the geosynthetics |
| Bertuliene et al. (2011) | To develop a theoretical model to explain the function of geosynthetics in asphalt overlay | | Rut depth in reinforced sections are 1.4 times lower than the reference ones |
| Laurinavičius et al. (2006) | To examine the connection between geosynthetic type and loading with rut depth | Static plate load tests on field section | 1- During cold seasons asphalt concrete elasticity determines the rut depth development while in hot seasons, the asphalt concrete viscosity controls the rutting. 2- In reinforced sections with geogrids, the rheological characteristics of asphalt mix are higher than the ones constructed with geotextile. |
| Lee et al. (2015) | Studied rutting performance of different types of geosynthetics | Third-scale model mobile loading simulator (MMLS3) | 1- The rutting depth is highly dependent on the type of geosynthetic applied for reinforcement 2- Geogrid-reinforced specimens exhibit higher resistance against shear flow. 3- The rutting resistance of sheet-reinforced specimens are similar to the unreinforced ones. 4- The geogrid reinforced specimens have higher air void content at the interface which may adversely affect the pavement performance |

Table A-I-2 (Continued)

| Researchers | Research Topic | Type of Test | Major Findings |
|----------------------|--|---------------------|---|
| Wasage et al. (2004) | Laboratory evaluation of rut depth in reinforced specimens with different types of geosynthetics | Wheel tracking test | Geogrids provide a uniform distribution of applied loads which in turn lead to reduced rut depth of the whole structure |

Table-A I-3 Studies on the effect of geosynthetic on reflective cracking

| Researchers | Research Topic | Type of Test | Major Findings |
|------------------------------|--|---|---|
| Safavizadeh et al. (2019) | Studied the effect of reinforced asphalt concrete beam with fiberglass grid on reflective cracking | Four-Point Bending Notched Beam Tests | 1- different interlayer conditions do not reflect a unique failure mechanism 2- Reinforced asphalt beams perform better than unreinforced ones |
| Moghadas Nejad et al. (2016) | Examined the effect of geosynthetics on propagation of reflective cracking in reinforced asphalt overlay by taking the effect of crack width, geosynthetic type, temperature and their interactions into account | Cyclic loading applied by UTM-25 servo-hydraulic dynamic testing machine | 1- Geogrid outperform geotextile in delaying the reflective cracking 2- Temperature is the most influential factor on the number of cycles to failure (N_f) due to reflective cracking followed by the type of geosynthetic |
| Moghadas Nejad et al. (2015) | Laboratory simulation of reflective cracking initiation and propagation | Notched two-layer beam loaded by a small plate under cyclic haversine loading | 1-High-modulus geosynthetics are more efficient in thick asphalt overlay. 2- In reinforced overlays, the number of cycles prior to failure, the speed of crack propagation, rate of displacement at the bottom of the overlay are all dependent on the modulus of geosynthetic |

Table A-I-3 (Continued)

| Researchers | Research Topic | Type of Test | Major Findings |
|-----------------------|--|---|---|
| Khodaii et al. (2009) | Studied the effect of influential factors like temperature, geogrid position, type of existing layer on the propagation of reflective cracks | Repeated loading applied by hydraulic dynamic loading frame | Placing of geogrid at one-third depth from the bottom of the asphalt overlay leads to higher mitigation of reflective cracking |
| Sobhan et al. (2005) | To study the effect of the placement of geosynthetic in asphalt overlays on reflective cracking propagation and permanent deformation | Asphalt overlay beam placed over a joint and loaded by an MTS servo-hydraulic machine in two different conditions: i)static test to simulate the initiation and propagation of reflective cracks and ii) cyclic test to evaluate the fatigue behavior | <ol style="list-style-type: none"> 1- Reinforced specimens outperform the unreinforced ones in terms of reflective cracking and rutting 2- The enhanced mechanical behavior of reinforced asphalt overlay is strongly dependent on solid adhesion at the interface 3- Deeper placement of geosynthetic in asphalt overlay leads to extended fatigue life and increased rutting resistance |
| Ling et al. (2019) | Laboratory study of both traffic and thermally induced reflective cracking in asphalt overlays reinforced with geotextile, SAMI, and atactic polypropylene by taking the effect of temperature, load combination, type of mixture and compaction effort into account | A newly developed device named Joint Motion Simulation System (JMSS) | <ol style="list-style-type: none"> 1- Separately considering the effect of horizontal and vertical loads on crack initiation and propagation results in higher number of cycles to failure which may exaggerate real service life 2- The growth of reflective cracks are nonlinear in nature which means it rapidly grows in earlier stages followed by reduced rates at later stages 3- In comparison, geotextile can effectively retard reflective cracking. |

Table A-I-3 (Continued)

| Researchers | Research Topic | Type of Test | Major Findings |
|----------------------------|---|--|--|
| Solatiyan et al. (2020) | Laboratory evaluation of paving fabrics to mitigate reflective cracking | 3-point bending test on notched specimens and new crack widening device (CWD) | Reinforced specimens have: 1- Three times lower crack width reflected at the surface 2- 60 percent higher crack resistance index |
| Saride and Kumar (2017) | Examined the mechanical behavior of pre-cracked asphalt overlays reinforced with geosynthetics | Four-point bending beam test on notched beams | Reinforced overlays with high shear and pull-off tensile strength interlayers have significantly higher potential to control the cracking |
| Torre et al. (2015) | Studied the influence of different types of geosynthetics to control reflective cracking in reinforced specimens under traffic loads and temperature fluctuations | Modified three-point bending test with a combination of sinusoidal and triangular loadings | 1- The type of interlayer controls its positive effect on retarding the reflective cracking. The grids accompanied by a textile in their structures have low influential impacts because of low adhesion made at the interface. 2- High secant modulus and proper adhesion provided at the interface determine the anti-reflective cracking properties of geosynthetics in asphalt overlays |
| Al-Qadi and Elseifi (2004) | Investigated the effect of various design factors on the effectiveness of interlayer systems in retarding the reflective cracking | Field Investigation | 1- Application of steel reinforcement is more efficient in asphalt overlays with lower than 25 mm thickness 2- The more contribution of interlayer system in delaying reflective cracking is provided when it is placed near to the crack generation point. |

BIBLIOGRAPHY

- Abdessemed, M., Kenai, S., & Bali, A. (2015). Experimental and numerical analysis of the behavior of an airport pavement reinforced by geogrids. *Construction and Building Materials*, 94, 547-554.
- Abdi, M. R., & Zandieh, A. R. (2014). Experimental and numerical analysis of large scale pull out tests conducted on clays reinforced with geogrids encapsulated with coarse material. *Geotextiles and Geomembranes*, 42(5), 494-504.
- Abojaradeh, M. (2003). Predictive fatigue models for Arizona asphalt concrete mixtures. (Doctoral dissertation, Arizona State University).
- Ahlich, R. C. (1986). Evaluation of Asphalt Rubber and Engineering Fabrics as Pavement Interlayers (No. WES/MP/GL-86-34). Army Engineer Waterways Experiment Station Vicksburg MS Geotechnical Lab.
- Ahmed, S., Dave, E. V., Buttlar, W. G., & Behnia, B. (2012). Compact tension test for fracture characterization of thin bonded asphalt overlay systems at low temperature. *Materials and structures*, 45(8), 1207-1220.
- Ahn, J., Jalmasco, M., Suk Shin, H., Jung, J. (2017). Test equipment and procedure to evaluate permeability characteristics of permeable pavements. *Journal of the Korean Society of Hazard Mitigation*. 17(6):359-365.
- Alataş, T., & Kızırgıl, M. E. (2013). The effects of using Styrene-Butadiene-Styrene and fly ash together on the resistance to moisture-induced damage, permanent deformation and fatigue of hot mixture asphalt. *KSCE Journal of Civil Engineering*, 17(5), 1030-1039.
- Aliha, M. R. M., Fakhri, M., Kharrazi, E. H., & Berto, F. (2018). The effect of loading rate on fracture energy of asphalt mixture at intermediate temperatures and under different loading modes. *Frattura ed Integrità Strutturale*, 12(43), 113-132.
- Al-Khateeb, L. A., Saoud, A., & Al-Msouti, M. F. (2011). Rutting prediction of flexible pavements using finite element modeling. *Jordan Journal of Civil Engineering*, 159(2980), 1-18.
- Al-Qadi, I. L., & Elseifi, M. A. (2004). Field installation and design considerations of steel reinforcing netting to reduce reflection of cracks. In *Proceedings of the International RILEM Conference* (No. 37, pp. 97-104).

- Al-Qadi, I. L. (2006). Pavement interlayer system mechanisms: separation reinforcement and reflective cracking control. Lecture, Chinese Soc. of Pavement Engineering, Taipei, Taiwan.
- Al-Qadi, I. L., Dessouky, S. H., Kwon, J., & Tutumluer, E. (2008). Geogrid in flexible pavements: validated mechanism. *Transportation Research Record*, 2045(1), 102-109.
- Al-Qadi, I. L., Morian, D. A., Stoffels, S. M., Elseifi, M., Chehab, G., & Stark, T. (2008). Synthesis on use of geosynthetics in pavements and development of a roadmap to geosynthetically-modified pavements. Federal Highway Administration, McLean, VA, Report No. FHWAHRT, 1-195.
- Al-Qadi, I. L., Carpenter, S. H., Leng, Z., Ozer, H., & Trepanier, J. (2009). Tack coat optimization for HMA overlays: Accelerated pavement test report. Illinois Center for Transportation (ICT).
- Al-Qadi, I. L., Buttlar, W., Baek, J., & Kim, M. (2009). Cost-effectiveness and performance of overlay systems in Illinois volume 1: effectiveness assessment of HMA overlay interlayer systems used to retard reflective cracking. Illinois Center for Transportation (ICT).
- Al-Qadi, I. L., Ozer, H., Lambros, J., El Khatib, A., Singhvi, P., Khan, T., ... & Doll, B. (2015). Testing protocols to ensure performance of high asphalt binder replacement mixes using RAP and RAS. Illinois Center for Transportation/Illinois Department of Transportation.
- Alvarez, A. D. C. (2008). Repaving Principal Highways in Caracas-Venezuela using nonwoven needle punched, and impregnated with Asphalt Emulsion Geotextiles. In *Proceedings of the first Pan American Geosynthetics Conference & Exhibition*, Cancun, Mexico (pp. 1078-1087).
- American Association of State Highway and Transportation Officials (AASHTO). (2008). *Mechanistic-empirical pavement design guide—a manual of practice*.
- American Association of State Highway and Transportation Officials (AASHTO TP 63-07). (2007). Determining rutting susceptibility of hot mix asphalt (HMA) using the asphalt pavement analyzer (APA). AASHTO Provincial Standards, Washington, D.C.
- Amini, F. (2005). Potential applications of paving fabrics to reduce reflective cracking (No. FHWA/MS-DOT-RD-05-174). United States. Federal Highway Administration.
- Amini, F., & Wen, K. (2016). Long-term field monitoring of paving fabric interlayer systems to reduce reflective cracking (No. FHWA/MS-DOT-RD-16-184). Mississippi. Dept. of Transportation.

- Anderson, D. A., Dongre, R., Christensen, D. W., & Dukatz, E. L. (1992). Effects of minus no. 200-sized aggregate on fracture behavior of dense-graded hot-mix asphalt. In *Effects of aggregates and mineral fillers on asphalt mixture performance*. ASTM International.
- Apeageyi, A. K., Dave, E. V., & Buttlar, W. G. (2008). Effect of cooling rate on thermal cracking of asphalt concrete pavements. *Asphalt Paving Technology-Proceedings*, 77, 709.
- Arsenie, I. M., Chazallon, C., Duchez, J. L., & Mouhoubi, S. (2017). Modelling of the fatigue damage of a geogrid-reinforced asphalt concrete. *Road Materials and Pavement Design*, 18(1), 250-262.
- Arsenie, I. M., Chazallon, C., Duchez, J. L., & Hornych, P. (2017). Laboratory characterisation of the fatigue behaviour of a glass fibre grid-reinforced asphalt concrete using 4PB tests. *Road Materials and Pavement Design*, 18(1), 168-180.
- Artamendi, I., & Khalid, H. A. (2006). A comparison between beam and semi-circular bending fracture tests for asphalt. *Road Materials and Pavement Design*, 7(sup1), 163-180.
- Asphalt Interlayer Association (AIA). (1999). *Fabric Interlayer Guide*. Retrieved from <http://www.aia-us.org/interlayer-guideline-options/interlayer-guide/>.
- ASTM E399-90 (2008). Standard test method for plane-strain fracture toughness of metallic materials. *Annual Book of ASTM Standards*, (03.01), 443–473.
- ASTM D8044 – 16. (2016). Standard Test Method for Evaluation of Asphalt Mixture Cracking Resistance using the Semi-Circular Bend Test (SCB) at Intermediate Temperatures. Retrieved from <https://standards.globalspec.com/std/10041469/ASTM%20D8044>.
- ASTM E399-90. (2008). Standard test method for plane-strain fracture toughness of metallic materials. *Annual Book of ASTM Standards*, (03.01), 443–473.
- ATACKER™ A Tack Coat Testing Device, Operator's Guide, InstroTek, Inc. 2005.
- Austin, R. A., & Gilchrist, A. J. T. (1996). Enhanced performance of asphalt pavements using geocomposites. *Geotextiles and Geomembranes*, 14(3-4), 175-186.
- Avesani Neto, J. O., Bueno, B. S., & Futai, M. M. (2013). A bearing capacity calculation method for soil reinforced with a geocell. *Geosynthetics International*, 20(3), 129-142.
- Baaj, H., Di Benedetto, H., & Chaverot, P. (2005). Effect of binder characteristics on fatigue of asphalt pavement using an intrinsic damage approach. *Road Materials and Pavement Design*, 6(2), 147-174.

- Bae, A., Mohammad, L. N., Elseifi, M. A., Button, J., & Patel, N. (2010). Effects of temperature on interface shear strength of emulsified tack coats and its relationship to rheological properties. *Transportation research record*, 2180(1), 102-109.
- Babagoli, R., Hasaninia, M., & Mohammad Namazi, N. (2015). Laboratory evaluation of the effect of Gilsonite on the performance of stone matrix asphalt mixtures. *Road Materials and Pavement Design*, 16(4), 889-906.
- Baek, J., Al-Qadi, I. L., Xie, W., & Buttlar, W. G. (2008). In situ assessment of interlayer systems to abate reflective cracking in hot-mix asphalt overlays. *Transportation research record*, 2084(1), 104-113.
- Baek, J. (2010). Modeling reflective cracking development in hot-mix asphalt overlays and quantification of control techniques (Doctoral dissertation, University of Illinois at Urbana-Champaign).
- Barksdale, R. D., Brown, S. F., & Chan, F. (1989). Potential benefits of geosynthetics in flexible pavement systems (No. 315).
- Basueny, A., Perraton, D., & Carter, A. (2014). Laboratory study of the effect of RAP conditioning on the mechanical properties of hot mix asphalt containing RAP. *Materials and structures*, 47(9), 1425-1450.
- Basueny, A., Carter, A., Perraton, D., & Vaillancourt, M. (2016). Laboratory evaluation of complex modulus and fatigue resistance of asphalt mixtures with RAP. In 8th RILEM International Symposium on Testing and Characterization of Sustainable and Innovative Bituminous Materials (pp. 521-532). Springer, Dordrecht.
- Behiry, A. E. A. E. M. (2013). Laboratory evaluation of resistance to moisture damage in asphalt mixtures. *Ain Shams Engineering Journal*, 4(3), 351-363.
- Benjamim, C., Bueno, B., & Zornberg, J. G. (2007). Field monitoring evaluation of geotextile-reinforced soil-retaining walls. *Geosynthetics International*, 14(2), 100-118.
- Berg, R. R., Christopher, B. R., & Perkins, S. W. (2000). Geosynthetic reinforcement of the aggregate base course of flexible pavement structures. GMA White Paper II, Geosynthetic Materials Association, Roseville, MN, USA, 130.
- Bernier, A., Zofka, A., & Yut, I. (2012). Laboratory evaluation of rutting susceptibility of polymer-modified asphalt mixtures containing recycled pavements. *Construction and Building Materials*, 31, 58-66.
- Bertuliene, L., Oginskas, R., & Bulevicius, M. (2011). Research of rut depth in asphalt pavements reinforced with geosynthetic materials. In *Environmental Engineering. Proceedings of the International Conference on Environmental Engineering*.

- ICEE (Vol. 8, p. 1039). Vilnius Gediminas Technical University, Department of Construction Economics & Property.
- Bhattacharjee, S., Mallick, R. B., & Daniel, J. S. (2009). Small scale accelerated pavement testing in the laboratory for the fatigue characterization of hot mix asphalt. In *Pavements and Materials: Modeling, Testing, and Performance* (pp. 56-63).
- Bhosale S. S. and Mandal J. N. (2008). Open graded asphalt concrete for mitigation of reflection cracking on asphalt concrete overlays. 12th International Conference of International Association for Computer Methods and Advances in Geomechanics (IACMAG), India. 4409-4416.
- Biglari, M., Asgharzadeh, S. M., & Sharif Tehrani, S. (2019). Evaluation of factors affecting tack coat bond strength. *Canadian Journal of Civil Engineering*, 46(6), 270-277.
- Bohagr, A. A. (2013). *Finite Element Modeling of Geosynthetic Reinforced* (Doctoral dissertation, Washington State University).
- Bolt, A. F., & Duszynska, A. (2000, October). Pull-out testing of geogrid reinforcements. In *Proceedings of Second European Geosynthetics Conference Eurogeo*.
- Bonaquist, R. F. (2010). Wisconsin mixture characterization using the asphalt mixture performance tester (AMPT) on historical aggregate structures. Wisconsin Highway Research Program.
- Bondt, A. D., Schrader, J., Bijsterveld, W. V., & Long, D. (2005). *Scientific Background of ARCDESO-version April 2005*. Internal Report-Ooms Nederland Holding.
- Bostancioğlu, M., & Oruç, Ş. (2016). Effect of activated carbon and furan resin on asphalt mixture performance. *Road Materials and Pavement Design*, 17(2), 512-525.
- Bozkurt, D., & Buttlar, W. G. (2002, May). Three-dimensional finite element modeling to evaluate benefits of interlayer stress absorbing composite for reflective crack mitigation. In *Proc., Federal Aviation Administration Airport Technology Transfer Conference*.
- Brown, S. F., Hughes, D. A. B., & Brodrick, B. V. (1983). *Grid Reinforcement for Asphalt Pavements*. University of Nottingham, Report submitted to Netlon Ltd and SERC.
- Brown, S. F., Brunton, J. M., Hughes, D. A. B., & Brodrick, B. V. (1985, February). Polymer grid reinforcement of asphalt. In *Annual Meeting of the Association of Asphalt Paving Technologists*, Texas.
- Brown, S. F., Thom, N. H., & Sanders, P. J. (2001). A study of grid reinforced asphalt to combat reflection cracking (with discussion). *Journal of the Association of Asphalt Paving Technologists*, 70.

- Brown, S. F. (2009). An assessment of geogrid use in railways and asphalt applications. In Proceedings of Jubilee Symposium on Polymer Geogrid Reinforcement.
- Brusa, N., Crowther, D., & Pezzano, P. (2016). Asphalt reinforcement through geosynthetics: design method and UK experience. In Proc. of the LJMU 15th Annual International Conference on Asphalt Pavement Engineering and Infrastructure (pp. 24-25).
- Bueno, B. S., Benjamim, C. V. S., & Zornberg, J. G. (2005). Field performance of a full-scale retaining wall reinforced with Nonwoven geotextiles. In Slopes and retaining structures under seismic and static conditions (pp. 1-9).
- Buonsanti, M., & Leonardi, G. (2012). FEM analysis of airport flexible pavements reinforced with geogrids. *Advanced Science Letters*, 13(1), 392-395.
- Buttlar, W. G., Bozkurt, D., & Dempsey, B. J. (2000). Cost-effectiveness of paving fabrics used to control reflective cracking. *Transportation Research Record*, 1730(1), 139-149.
- Buttlar, W. G., Chabot, A., Dave, E. V., Petit, C., & Tebaldi, G. (Eds.). (2018). *Mechanisms of cracking and debonding in asphalt and composite pavements*. Springer International Publishing.
- Button, J. W., & Lytton, R. L. (2007). Guidelines for using geosynthetics with hot-mix asphalt overlays to reduce reflective cracking. *Transportation research record*, 2004(1), 111-119.
- Calvarano, L. S., Palamara, R., Leonardi, G., & Moraci, N. (2017). 3D-FEM analysis on geogrid reinforced flexible pavement roads. In *IOP Conference Series: Earth and Environmental Science* (Vol. 95, No. 2, p. 022024). IOP Publishing.
- Canestrari, F., Ferrotti, G., Partl, M. N., & Santagata, E. (2005). Advanced testing and characterization of interlayer shear resistance. *Transportation Research Record*, 1929(1), 69-78.
- Canestrari, F., Pasquini, E., & Belogi, L. (2012). Optimization of geocomposites for double-layered bituminous systems. In *7th RILEM International Conference on Cracking in Pavements* (pp. 1229-1239). Springer, Dordrecht.
- Canestrari, F., Ferrotti, G., Lu, X., Millien, A., Partl, M. N., Petit, C., Phelipot-Mardelé, A., Piber, H., & Raab, C. (2013). Mechanical testing of interlayer bonding in asphalt pavements. In *Advances in interlaboratory testing and evaluation of bituminous materials* (pp. 303-360). Springer, Dordrecht.
- Canestrari, F., Belogi, L., Ferrotti, G., & Graziani, A. (2015). Shear and flexural characterization of grid-reinforced asphalt pavements and relation with field distress evolution. *Materials and Structures*, 48(4), 959-975.

- Canestrari, F., D'Andrea, A., Ferrotti, G., Graziani, A., Partl, M. N., Petit, C., Raab, C., & Sangiorgi, C. (2018). Advanced interface testing of grids in asphalt pavements. In *Testing and Characterization of Sustainable Innovative Bituminous Materials and Systems* (pp. 127-202). Springer, Cham.
- Carmichael III, R. F., & Marienfeld, M. L. (1999). Synthesis and literature review of nonwoven paving fabrics performance in overlays. *Transportation Research Record*, 1687(1), 112-124.
- Carter, A., Donovan, H., MacInnis, K., & Strynadka T. (2018). Hot mix asphalt. Canadian Technical Asphalt Association, first edition. ISBN: 978-0-9869141-8-8.
- Chang, D. T., Lai, R. Q., Chang, J. Y., & Wang, Y. H. (1998). Effects of geogrid in enhancing the resistance of asphalt concrete to reflection cracks. In *Flexible Pavement Rehabilitation and Maintenance*. ASTM International.
- Charmot, S., Romero, P., & Dunning, M. (2005). Forensic analysis of slippage cracking. In *Proceeding of the 84th TRB annual meeting*. Washington.
- Chehovits, J., & Galehouse, L. (2010). Energy usage and greenhouse gas emissions of pavement preservation processes for asphalt concrete pavements. In *Proceedings on the 1st International Conference of Pavement Preservation*, 27-42.
- Chen, Q., Abu-Farsakh, M., & Tao, M. (2009). Laboratory evaluation of geogrid base reinforcement and corresponding instrumentation program. *Geotechnical testing journal*, 32(6), 516-525.
- Chen, J. S., & Huang, C. C. (2010). Effect of surface characteristics on bonding properties of bituminous tack coat. *Transportation research record*, 2180(1), 142-149.
- Cho, Y. H., McCullough, B. F., & Weissmann, J. (1996). Considerations on finite-element method application in pavement structural analysis. *Transportation Research Record*, 1539(1), 96-101.
- Cho, S. D., Kim, N. H., Lee, D. Y., & Kim, J. H. (2004). A study on the performance of crack resistance for glass fiber-sheet reinforced asphalt pavement. *Proceedings of the 3rd Asian Regional Conference on Geosynthetics—Now and Future of Geosynthetics in Civil Engineering*, 453-462.
- Chowdhury, A., Button, J. W., & Lytton, R. L. (2009). Tests of HMA overlays using geosynthetics to reduce reflection cracking (No. FHWA/TX-10/0-1777-3). Texas Transportation Institute.

- Choi, Y. T., & Kim, Y. R. (2014). Implementation and verification of a mechanistic permanent deformation model (shift model) to predict rut depths of asphalt pavement. *Road materials and pavement design*, 15(sup1), 195-218.
- Cleveland, G. S., Button, J. W., & Lytton, R. L. (2002). Geosynthetics in flexible and rigid pavement overlay systems to reduce reflection cracking. Texas Transportation Institute, Texas A & M University System.
- Collop, A. C., Thom, N. H., & Sangiorgi, C. (2003, November). Assessment of bond condition using the Leutner shear test. In *Proceedings of the Institution of Civil Engineers-Transport* (Vol. 156, No. 4, pp. 211-217). Thomas Telford Ltd.
- Coni, M., & Bianco, P. M. (2000). Steel reinforcement influence on the dynamic behaviour of bituminous pavement. In *Proceedings of the 4th International RILEM Conference-Reflective Cracking in Pavements*, Ottawa, Canada (pp. 3-12).
- Cooper Jr, S. B., Mohammad, L. N., & Elseifi, M. A. (2017). Laboratory performance of asphalt mixtures containing recycled asphalt shingles, reclaimed asphalt pavement, and recycling agents. *Journal of Materials in Civil Engineering*, 29(3), D4016001.
- Copeland, A. R. (2007). Influence of moisture on bond strength of asphalt-aggregate systems (Doctoral dissertation).
- Correia, N. D. S. (2014). Performance of flexible pavements enhanced using geogrid-reinforced asphalt overlays (Doctoral dissertation, Ph. D. dissertation, Univ. of Sao Paulo).
- Correia, N. S., & Zornberg, J. G. (2016). Mechanical response of flexible pavements enhanced with geogrid-reinforced asphalt overlays. *Geosynthetics International*, 23(3), 183-193.
- Correia, N. S., Esquivel, E. R., & Zornberg, J. G. (2018). Finite-Element Evaluations of Geogrid-Reinforced Asphalt Overlays over Flexible Pavements. *Journal of Transportation Engineering, Part B: Pavements*, 144(2), 04018020.
- Darling, J. R., & Woolstencroft, J. H. (2004). Fibreglass pavement reinforcements used in dissimilar climatic zones for retarding reflective cracking in asphalt overlays. *Cracking in Pavements, Mitigation, Risk Assessment and Prevention*, 435-442.
- Dave, E. V., Song, S. H., Buttlar, W. G., & Paulino, G. H. (2007). Reflective and thermal cracking modeling of asphalt concrete overlays. *Advanced Testing and Characterization of Bituminous Materials*, 2, 1241-1252.
- Dave, E. V., Braham, A. F., Buttlar, W. G., Paulino, G. H., & Zofka, A. (2008). Integration of laboratory testing, field performance data, and numerical simulations for the study of low-temperature cracking. In *Proceedings of the 6th RILEM International Conference on Cracking in Pavements* (Vol. 1, pp. 369-378). Taylor and Francis.

- Dave, E.V., Hanson, C. E., Helmer, B., Dailey, J., Hoplin, C. (2015). Laboratory performance test for asphalt concrete (report MN/RC 2015-24). St. Paul, MN: Minnesota Department of Transportation.
- D'Andrea, A., & Tozzo, C. (2012). Interlayer shear failure evolution with different test equipments. *Procedia-Social and Behavioral Sciences*, 53, 556-567.
- De Bondt, A. H. (2000). Anti-reflective cracking design of (reinforced) asphaltic overlays.
- De Bondt, A. (2000). Effect of Reinforcement Properties. In *Proceedings of the 4th International RILEM Conference on Reflective Cracking in Pavements-Research in Practice*, RILEM Publications SARL, Paris, France, pp. 13–22.
- De Bondt, A. H. (2009). Research on geogrids in asphalt pavements. In *Jubilee Symposium on Polymer Geogrid Reinforcement*, London, United Kingdom.
- De Bondt, A. H. (2012). 20 Years of Research on Asphalt Reinforcement—Achievements and Future Needs. In *7th RILEM International Conference on Cracking in Pavements* (pp. 327-335). Springer, Dordrecht.
- De Souza Correia, N., & de Souza Bueno, B. (2011). Effect of bituminous impregnation on nonwoven geotextiles tensile and permeability properties. *Geotextiles and Geomembranes*, 29(2), 92-101.
- Dempsey, B. J. (2002). Development and performance of interlayer stress-absorbing composite in asphalt concrete overlays. *Transportation Research Record*, 1809(1), 175-183.
- Dhakal, N., Elseifi, M. A., & Zhang, Z. (2016). Mitigation strategies for reflection cracking in rehabilitated pavements—A synthesis. *International Journal of Pavement Research and Technology*, 9(3), 228-239.
- Diab, A. M., Abd Elmoaty, M., & Eldin, M. R. T. (2017). Slant shear bond strength between self compacting concrete and old concrete. *Construction and Building Materials*, 130, 73-82.
- Diakhaté, M. (2007). *Fatigue et comportement des couches d'accrochage dans les structures de chaussée* (Doctoral dissertation).
- Di Benedetto, H., Delaporte, B. and Sauzéat, C. (2007). Three-dimensional linear behavior of bituminous materials: experiments and modeling. *International Journal of Geomechanics*, 7(2), 149-157.

- Di Benedetto, H., Nguyen, Q. T., & Sauzéat, C. (2011). Nonlinearity, heating, fatigue and thixotropy during cyclic loading of asphalt mixtures. *Road Materials and Pavement Design*, 12(1), 129-158.
- Donovan, E. P. (1999). Determination of optimum tack coat application rate for geocomposite membrane use in roads and overlaid bridge decks (Doctoral dissertation, Virginia Tech).
- Dougan, C. (2007). Mechanistic-Empirical Pavement Design Guide: project level pavement management. Lecture Session 1a: PMS to support New MEPDG Norfolk, VA.
- Du, Y., Chen, J., Han, Z., & Liu, W. (2018). A review on solutions for improving rutting resistance of asphalt pavement and test methods. *Construction and Building Materials*, 168, 893-905.
- Dykes, J. W. (1980). The Use of fabric interlayers to retard reflective cracking. In *Association of Asphalt Paving Technologists Proceedings* (Vol. 49).
- Ebnesajjad, S. (2010). *Handbook of adhesives and surface preparation: technology, applications and manufacturing*. William Andrew.
- Elias, J. M. (2004). Building Roads on Sabkha Soils with Geosynthetic Systems. In *Proceedings of 2nd Golf Conference, Abu Dhabi, UAE* (pp. 1-12).
- Elseifi, M. (2003). Performance quantification of interlayer systems in flexible pavements using finite element analysis, instrument response, and non destructive testing (Doctoral dissertation, Virginia Tech).
- Elseifi, M. A., & Al-Qadi, I. L. (2005). Effectiveness of steel reinforcing nettings in combating fatigue cracking in new flexible pavement systems. *Journal of Transportation Engineering*, 131(1), 37-45.
- Engineers, U. A. C. O. (2003). Use of geogrids in pavement construction TECHNICAL LETTER ETL 1110-1-189. WASHINGTON DC.
- Engle, E. (2001). Field evaluation of engineering fabrics for asphalt concrete resurfacing-Audubon County (No. HR-360). Ames, Iowa, United States: Iowa Department of Transportation.
- Faheem, H., & Hassan, A. M. (2014). 2D PLAXIS finite element modeling of asphalt-concrete pavement reinforced with geogrid. *Journal of Engineering Sciences Assiut University Faculty of Engineering*, 42(6), 1336-1348.
- Fakhri, K., Darban, A. K., and pasquini. H.R.A. (2009). The effect of geosynthetic reinforcement on the damage propagation rate of asphalt pavements. *Scientia Iranica* Vol. 16.1, pp: 26-32.

- Fakhri, M., Siyadati, S. A., & Aliha, M. R. M. (2020). Impact of freeze–thaw cycles on low temperature mixed mode I/II cracking properties of water saturated hot mix asphalt: An experimental study. *Construction and Building Materials*, 261, 119939.
- Fallah, S., & Khodaii, A. (2015). Reinforcing overlay to reduce reflection cracking; an experimental investigation. *Geotextiles and Geomembranes*, 43(3), 216-227.
- Fannin, J. (2007). The use of geosynthetics as filters in civil engineering. In *Geosynthetics in Civil Engineering* (pp. 127-147). Woodhead Publishing.
- Ferrotti, G., Canestrari, F., Pasquini, E., & Virgili, A. (2012). Experimental evaluation of the influence of surface coating on fiberglass geogrid performance in asphalt pavements. *Geotextiles and Geomembranes*, 34, 11-18.
- Flutcher, S., & Wu, J. T. (2013). A state-of-the-art review on geosynthetics in low-volume asphalt roadway pavements. *International Journal of Geotechnical Engineering*, 7(4), 411-419.
- Fonseca, P. C., & Scherer, G. W. (2015). An image analysis procedure to quantify the air void system of mortar and concrete. *Materials and Structures*, 48(10), 3087-3098.
- Ferreira, J. A., & Zornberg, J. G. (2015). A transparent pullout testing device for 3D evaluation of soil–geogrid interaction. *Geotechnical Testing Journal*, 38(5), 686-707.
- Fontes, L. P., & Triches, G. (2010). Jorge. C. Pais and Paulo AA Pereira. (2010). Evaluating Permanent Deformation in Asphalt Rubber Mixtures. *Construction and Building Materials*, 24, 1193-1200.
- Freire, R., Di Benedetto, H., Sauzéat, C., Pouget, S., & Lesueur, D. (2018). Linear Viscoelastic Behaviour of Geogrids Interface within Bituminous Mixtures. *KSCE Journal of Civil Engineering*, 22(6), 2082-2088.
- Fuller, A. L. (1997). On the comparative behaviour of geogrids in tension and pullout (Doctoral dissertation, University of British Columbia).
- Fwa, T. F., Tan, S. A., & Guwe, Y. K. (1999). Laboratory evaluation of clogging potential of porous asphalt mixtures. *Transportation Research Record*, 1681(1), 43-49.
- Fyfe, R., Australasia, G., & Australia, S. (2011). Geotextile reinforced seals under asphalt. Paper Publication. *Geofabrics Australasia*, 1.
- Gajewski, M., & Jemioło, S. (2014). Orthotropic composite constitutive model of mineral–asphalt mix reinforced with grid and its approximation with an isotropic model. *Road Materials and Pavement Design*, 15(3), 521-538.

- Galaviz-González, J. R., Avalos Cueva, D., Limón Covarrubias, P., & Zamora Palacios, M. (2019). Bonding evaluation of asphalt emulsions used as tack coats through shear testing. *Applied Sciences*, 9(9), 1727.
- Gallego, J., & Prieto, J. N. (2006). New laboratory equipment for study of reflective cracking in asphalt overlays. *Transportation research record*, 1970(1), 215-222.
- Gauthier, G. G. (2012). Evaluation of low-temperature fracture properties of asphalt binder. (Master Thesis. The Pennsylvania State University).
- Geminger, T., & Jarka, S. (2016). Injection molding of multimaterial systems. In *Specialized injection molding techniques* (pp. 165-210). William Andrew Publishing.
- Ghadimi, B. (2015). Numerical modelling for flexible pavement materials applying advanced finite element approach to develop Mechanistic-Empirical design procedure (Doctoral dissertation, Curtin University).
- Ghadimi, B., & Nikraz, H. (2017). A comparison of implementation of linear and nonlinear constitutive models in numerical analysis of layered flexible pavement. *Road Materials and Pavement Design*, 18(3), 550-572.
- Giroud, J. P., & Noiray, L. (1981). Geotextile-reinforced unpaved road design. *Journal of geotechnical and geoenvironmental engineering*, 107(ASCE 16489).
- Golestani, B., Nam, B., Noori, M., An, J., & Tatari, O. (2018). An optimum selection strategy of reflective cracking mitigation methods for an asphalt concrete overlay over flexible pavements. *International Journal of Pavement Engineering*, 19(1), 48-61.
- Gonzalez-Torre, I., Calzada-Perez, M. A., Vega-Zamanillo, A., & Castro-Fresno, D. (2015). Experimental study of the behaviour of different geosynthetics as anti-reflective cracking systems using a combined-load fatigue test. *Geotextiles and Geomembranes*, 43(4), 345-350.
- Gonzalez-Torre, I., Calzada-Perez, M. A., Vega-Zamanillo, A., & Castro-Fresno, D. (2015). Evaluation of reflective cracking in pavements using a new procedure that combine loads with different frequencies. *Construction and Building Materials*, 75, 368-374.
- Goud, G. N., Ramu, B., Umashankar, B., Sireesh, S., & Madhav, M. R. (2020). Evaluation of layer coefficient ratios for geogrid-reinforced bases of flexible pavements. *Road Materials and Pavement Design*, 1-12.
- Graziani, A., Pasquini, E., Ferrotti, G., Virgili, A., & Canestrari, F. (2014). Structural response of grid-reinforced bituminous pavements. *Materials and structures*, 47(8), 1391-1408.

- Grzybowska, W., Wojtowicz, J., and Fonferko, L. (1993). Application of geosynthetics to overlays in Krakow Region of Poland. *Proceedings Reflective Cracking in Pavements, State of the Art and Design Recommendations, Second International RILEM Conference, Krakow University of Technology/Taylor & Francis*, pp: 290–298.
- Guide–A, M. E. P. D. (2008). *Manual of Practice*. American Association of State Highway and Transportation Officials, Washington.
- Gu, F., Luo, X., Luo, R., Lytton, R. L., Hajj, E. Y., & Siddharthan, R. V. (2016). Numerical modeling of geogrid-reinforced flexible pavement and corresponding validation using large-scale tank test. *Construction and Building Materials*, 122, 214-230.
- Guler, E., Atalay, I. (2016). The Effects of geosynthetics on mitigation of rutting in flexible pavements. *Proceedings of the 6th E&E Congress, Prague, Czech Republic*. DOI: [dx.doi.org/10.14311/EE.2016.101](https://doi.org/10.14311/EE.2016.101).
- Guo, Q., Li, L., Cheng, Y., Jiao, Y., & Xu, C. (2015). Laboratory evaluation on performance of diatomite and glass fiber compound modified asphalt mixture. *Materials & Design (1980-2015)*, 66, 51-59.
- Gupta, R., Mishra, D. (2016). Analysis of geogrid-reinforced flexible pavement systems using confined stiffness approach. *3rd Pan - American Conference on Geosynthetics, GeoAmericas*.
- Hachiya, Y., Umeno, S., & Sato, K. (1997). Effect of tack coat on bonding characteristics at interface between asphalt concrete layers. *Doboku Gakkai Ronbunshu*, 1997(571), 199-209.
- Hajj, E. Y., Sebaaly, P. E., & Loria, L. (2008). *Reflective Cracking of Flexible Pavements Phase I and Phase II Final Recommendations (No. Report No. 080-07-803)*.
- Hakim, B. A. (2002). The importance of good bond between bituminous layers. In *Ninth International Conference on Asphalt Pavements International Society for Asphalt Pavements*.
- Halim, A. O., Haas, R., & Phang, W. A. (1983). Geogrid reinforcement of asphalt pavements and verification of elastic theory. *Transportation Research Record*, (949).
- Helstrom, C. L., Humphrey, D. N., & Hayden, S. A. (2006). Geogrid reinforced pavement structure in a cold region. In *Current Practices in Cold Regions Engineering (pp. 1-12)*.
- Hensley, M. J. (1980). Open-graded asphalt concrete base for the control of reflectivity. In *Association of Asphalt Paving Technologists Proceedings (Vol. 49)*.

- Hartadi Sutanto, M. (2009). Assessment of bond between asphalt layers. (Doctoral dissertation, The University of Nottingham).
- Hasiba, K. (2012). Development of a testing approach for tack coat application rate at pavement layer interfaces.
- Hojat Shamami, V., & Khiavi, A. K. (2017). Effect of temperature on geosynthetic rutting performance in asphalt pavement. *Petroleum Science and Technology*, 35(11), 1104-1109.
- Holtz, R. D. (1998). Geosynthetic. Design and Construction Guidelines. Federal Highway Administration FHWA HI-95-038. DTFH61-93-C-00120.
- Hosseini, H. R. A., Darban, A. K., & Fakhri, K. (2009). The effect of geosynthetic reinforcement on the damage propagation rate of asphalt pavements.
- Hu, X., Lei, Y., Wang, H., Jiang, P., Yang, X., & You, Z. (2017). Effect of tack coat dosage and temperature on the interface shear properties of asphalt layers bonded with emulsified asphalt binders. *Construction and Building Materials*, 141, 86-93.
- Hussein, M. G., & Meguid, M. A. (2015). Numerical modeling of soil-structure interaction with applications to geosynthetics. In *International Conference on Structural and Geotechnical Engineering*, Ain Shams University, December, Cairo, Egypt (Vol. 12).
- Hussein, M. G., & Meguid, M. A. (2016). A three-dimensional finite element approach for modeling biaxial geogrid with application to geogrid-reinforced soils. *Geotextiles and Geomembranes*, 44(3), 295-307.
- Ingrassia, L. P., Virgili, A., & Canestrari, F. (2020). Effect of geocomposite reinforcement on the performance of thin asphalt pavements: Accelerated pavement testing and laboratory analysis. *Case Studies in Construction Materials*, 12, e00342.
- Jaskula, P., & Rys, D. (2017). Effect of interlayer bonding quality of asphalt layers on pavement performance. In *IOP Conf. Ser. Mater. Sci. Eng* (Vol. 236, p. 012005).
- Jenner, C. G. J., & Uijting, B. G. J. (2004). Asphalt reinforcement for the prevention of cracking in various types of pavements: long term performance and overlay design procedure. In *Fifth International RILEM Conference on Reflective Cracking in Pavements* (pp. 459-466). RILEM Publications SARL.
- Joseph, P. E., & Haas, R. (1989). Evaluating alternative solutions to reflective cracking through asphalt overlays. *Transportation Research Record*, (1215).
- Kanitpong, K., & Bahia, H. U. (2003). Role of adhesion and thin film tackiness of asphalt binders in moisture damage of HMA (with discussion). *Journal of the Association of Asphalt Paving Technologists*, 72.

- Khodaii, A., Fallah, S., & Nejad, F. M. (2009). Effects of geosynthetics on reduction of reflection cracking in asphalt overlays. *Geotextiles and Geomembranes*, 27(1), 1-8.
- Kim, K. W., Doh, Y. S., & Lim, S. (1999). Mode I reflection cracking resistance of strengthened asphalt concretes. *Construction and Building Materials*, 13(5), 243-251.
- Kim, J., & Buttlar, W. G. (2002). Analysis of reflective crack control system involving reinforcing grid over base-isolating interlayer mixture. *Journal of Transportation Engineering*, 128(4), 375-384.
- Kim, H., Sokolov, K., Poulidakos, L. D., & Partl, M. N. (2009). Fatigue evaluation of carbon FRP-reinforced porous asphalt composite system using a model mobile load simulator. *Transportation Research Record: Journal of the Transportation Research Board*, 2116, 108-117.
- Kim, S. S., Sargand, S., & Wargo, A. (2009). A simple test procedure for evaluating low temperature crack resistance of asphalt concrete (No. FHWA/OH-2009/5). Ohio Research Institute for Transportation and the Environment.
- Kim, R., Tayebali, A.A., Guddati, M.N., Karshenas, A., Cho, S. (2015). Surface layer bond stresses and strength. North Carolina Department of Transportation, Final Report HWY-2013-04.
- Khan, K. M. (2010). Evaluating rutting potential of SMA, Superpave and Marshall mixes using wheel tracker tests. *Kuwait Journal of Science & Engineering*, 37(2B), 17-23.
- Khay M. and Giraud H. (2004). Voies de circulation et fondations: Derniers développements. 5th Rencontres Géosynthétiques Francophones.
- Khedr, S. A., & Breakah, T. M. (2011). Rutting parameters for asphalt concrete for different aggregate structures. *International Journal of Pavement Engineering*, 12(1), 13-23.
- Khodaii, A., Fallah, S., & Nejad, F. M. (2009). Effects of geosynthetics on reduction of reflection cracking in asphalt overlays. *Geotextiles and Geomembranes*, 27(1), 1-8.
- Kretov, V. A., & Gorelysheva, L. A. (2000). Influence of thin interrupting layers to development of reflected cracks. In *Reflective Cracking in Pavements-Research in Practice*. Proceedings of the 4th International RILEM, OTTAWA, CANADA.
- Kumar V, V., & Saride, S. (2017). Use of digital image correlation for the evaluation of flexural fatigue behavior of asphalt beams with geosynthetic interlayers. *Transportation Research Record*, 2631(1), 55-64.
- Kumar, V., Saride, S., & Peddinti, P. R. (2017). Interfacial shear properties of geosynthetic interlayered asphalt overlays. In *Geotechnical Frontiers 2017* (pp. 442-451).

- Kwon, J., Kim, M., & Tutumluer, E. (2005). Interface modeling for mechanistic analysis of geogrid reinforced flexible pavements. In *Advances in pavement engineering* (pp. 1-15).
- Laurinavičius, A., Oginskas, R., & Žilionienė, D. (2006). Research and evaluation of Lithuanian asphalt concrete road pavements reinforced by geosynthetics. *The Baltic Journal of Road and Bridge Engineering*, 1(1), 21-28.
- Laurinavičius, A., & Oginskas, R. (2006). Experimental research on the development of rutting in asphalt concrete pavements reinforced with geosynthetic materials. *Journal of civil engineering and management*, 12(4), 311-317.
- Lee, S. J. (2008). Mechanical performance and crack retardation study of a fiberglass-grid-reinforced asphalt concrete system. *Canadian Journal of Civil Engineering*, 35(10), 1042-1049.
- Lee, J., Kim, Y. R., & Lee, J. (2015). Rutting performance evaluation of asphalt mix with different types of geosynthetics using MMLS3. *International Journal of Pavement Engineering*, 16(10), 894-905.
- Li, X., & Marasteanu, M. (2004). Evaluation of the low temperature fracture resistance of asphalt mixtures using the semi circular bend test. In *Association of Asphalt Paving Technologists-Proceedings of the Technology Sessions, AAPT 2004* (pp. 401-426).
- Li, P., Liu, J., Samueloff, M., & Jones, D. (2014). Performance of paving fabric reinforced asphalt mixture. In *Climatic Effects on Pavement and Geotechnical Infrastructure* (pp. 126-138).
- Liao, J., & Sargand, S. (2010). Viscoelastic FE modeling and verification of a US 30 perpetual pavement test section. *Road materials and pavement design*, 11(4), 993-1008.
- Ling, H. I., & Liu, Z. (2001). Performance of geosynthetic-reinforced asphalt pavements. *Journal of Geotechnical and Geoenvironmental Engineering*, 127(2), 177-184.
- Ling, H. I., & Liu, H. (2003). Finite element studies of asphalt concrete pavement reinforced with geogrid. *Journal of engineering mechanics*, 129(7), 801-811.
- Ling, J., Wei, F., Gao, J., Zhang, J., Tian, Y., & Li, Y. (2019). New test method for measuring reflective cracking in hot-mix asphalt overlay pavements. *Transportation Research Record*, 2673(6), 327-336.
- Liu, H. L., Ng, C. W., & Fei, K. (2007). Performance of a geogrid-reinforced and pile-supported highway embankment over soft clay: case study. *Journal of Geotechnical and Geoenvironmental Engineering*, 133(12), 1483-1493.

- Liu, G., Lu, W., Lou, Y., Pan, W., & Wang, Z. (2018). Interlayer shear strength of Roller compacted concrete (RCC) with various interlayer treatments. *Construction and Building Materials*, 166, 647-656.
- Loui, T., M.Satyakumar. (2013). Study on Influence of Coir Geotextile and Bitumen Content on Shear Resistance of Bituminous Overlays. *International Journal of Scientific & Engineering Research*, Vol. 4, Issue 8, ISSN 2229-5518.
- Lytton, R. L. (1989). Use of geotextiles for reinforcement and strain relief in asphalt concrete. *Geotextiles and Geomembranes*, 8(3), 217-237.
- Mandal, T., Yin, H., & Ji, R. (2018). Correlating laboratory and full-scale reflective cracking tests for airfield pavements. *Construction and Building Materials*, 169, 47-58.
- Marasteanu, M. O., Li, X., Clyne, T. R., Voller, V. R., Timm, D. H., Newcomb, D. H. (2004). Low temperature cracking of asphalt concrete pavements. MN/RC-2004-23. Submitted by University of Minnesota to Minnesota Department of Transportation.
- Marasteanu, M., Zofka, A., Turos, M., Li, X., Velasquez, R., Li, X., McGraw, J. (2007). Investigation of low temperature cracking in asphalt pavements. National pooled fund study (report MN/RC2007-43). St. Paul, MN: Minnesota Department of Transportation.
- Marasteanu, M., Moon, K.H., Teshale, E. Z., Falchetto, A. C., Turos, M., Buttlar, W., Buss, A. (2012). Investigation of low temperature cracking in asphalt pavements. National pooled fund study phase II (report no. MN/RC 2012-23). St. Paul, MN: Minnesota Department of Transportation.
- Marienfeld, M., Baker, T. (1999). Paving fabric interlayer system as a pavement moisture barrier. Transportation Research Board, Washington, D.C. Retrieved from <http://worldcat.org/issn/00978515>.
- Martin, J. S., Cooley Jr, L. A., & Hainin, M. R. (2003, February). Production and construction issues for moisture sensitivity of hot-mix asphalt pavements. In *Transportation Research Board National Seminar*. San Diego, California (pp. 209-222).
- Masad, E., Tashman, L., Little, D., & Zbib, H. (2005). Viscoplastic modeling of asphalt mixes with the effects of anisotropy, damage and aggregate characteristics. *Mechanics of Materials*, 37(12), 1242-1256.
- Mashaan, N. S., Ali, A. H., Karim, M. R., & Abdelaziz, M. (2014). A review on using crumb rubber in reinforcement of asphalt pavement. *The Scientific World Journal*, 2014.

- Mahoney, J., & Zinke, S. (2008). Asphalt pavement analyzer equipment acquisition (No. CT-2248-F-07-8). Connecticut Advanced Pavement Laboratory.
- Medved, S. P., Žlender, B., & Lenart, S. (2018). Parametric study of geocell reinforced pavement. *Građevinar*, 70(06.), 497-508.
- Ministry des Trasnports du Québec. (2018). Recueil des méthodes d'essai LC. Retrieved from <https://www3.publicationsduquebec.gouv.qc.ca>. Accessed 12 Dec 2018.
- Mirzapour Mounes, S., Karim, M. R., Khodaii, A., & Almasi, M. H. (2014). Improving rutting resistance of pavement structures using geosynthetics: An overview. *The scientific world journal*, 2014.
- Moayedi, H., Kazemian, S., Prasad, A., & Huat, B. B. (2009). Effect of geogrid reinforcement location in paved road improvement. *Electronic Journal of Geotechnical Engineering*, 14, 1-11.
- Moghadas Nejad, F., Noory, A., Toolabi, S., & Fallah, S. (2015). Effect of using geosynthetics on reflective crack prevention. *International Journal of Pavement Engineering*, 16(6), 477-487.
- Moghadas Nejad, F., Asadi, S. Fallah, S., Vadood, M. (2016). Statistical-experimental study of geosynthetics performance on reflection cracking phenomenon. *Geotextiles and Geomembranes*. 44(2), 178-187.
- Mohammad, L. N., Bae, A., Elseifi, M. A., Button, J. W., & Scherocman, J. A. (2009). Interface shear strength characteristics of emulsified tack coats. *Journal of the Association of Asphalt Paving Technologists*, 78.
- Mohammad, L. N., Bae, A., Elseifi, M. A., Button, J., & Scherocman, J. A. (2009). Evaluation of bond strength of tack coat materials in field: Development of pull-off test device and methodology. *Transportation research record*, 2126(1), 1-11.
- Molenaar, A. 1993. Evaluation of Pavement Structure with Emphasis on Reflective Cracking in Pavements. State of the art and design recommendations. In *Proceedings of the 2nd International RILEM Conference*. Taylor & Francis, 21–48.
- Molenaar, J.M.M., Molenaar, A. A. A., 2000. Fracture Toughness of Asphalt in the Semi-Circular Bend Test. In *Proceedings of the 2nd Eurasphalt and Eurobitume Congress: 509-517 Barcelona*. Spain.
- Moreno-Navarro, F., Sol-Sánchez, M., Rubio-Gámez, M. C., & Segarra-Martínez, M. (2014). The use of additives for the improvement of the mechanical behavior of high modulus asphalt mixes. *Construction and Building Materials*, 70, 65-70.

- Monismith, C. L., Secor, G. A., & Secor, K. E. (1965). Temperature induced stresses and deformations in asphalt concrete. In Association of Asphalt Paving Technologists Proceedings (Vol. 34).
- Montestruque, G., Rodrigues, R., Nods, M., & Elsing, A. (2004). Stop of reflective crack propagation with the use of PET geogrid as asphalt overlay reinforcement. In 5th International RILEM Conference on Cracking in Pavements-Mitigation, Risk Assessment and Prevention. Edited by Petit C., Al-Qadi IL et Millien A (pp. 231-238).
- Moraes, R., Velasquez, R., & Bahia, H. U. (2011). Measuring the effect of moisture on asphalt-aggregate bond with the bitumen bond strength test. *Transportation Research Record*, 2209(1), 70-81.
- Moses, O. (2011). Mechanical behaviour of stress absorbing membrane interlayers. (PhD Dissertation, University of Nottingham).
- Mounes, S. M., Karim, M. R., Mahrez, A., & Khodaii, A. (2011). An overview on the use of geosynthetics in pavement structures. *Scientific Research and Essays*, 6(11), 2234-22418.
- Mounes, S. M., Karim, M. R., Khodaii, A., & Almasi, M. H. (2014). Improving rutting resistance of pavement structures using geosynthetics: An overview. *The scientific world journal*, 2014.
- Mounes, S. M., Karim, M. R., Khodaii, A., & Almasi, M. H. (2016). Evaluation of permanent deformation of geogrid reinforced asphalt concrete using dynamic creep test. *Geotextiles and Geomembranes*, 44(1), 109-116.
- Mukhtar, M. T., & Dempsey, B. J. (1996). Interlayer stress absorbing composite (ISAC) for mitigating reflection cracking in asphalt concrete overlays (No. UILU-ENG-96-2006).
- Muraya, P. M., Molenaar, A. A. A., & van de Ven, M. F. C. (2009). Contribution of the bituminous mortar and stone skeleton to the resistance to permanent deformation in asphalt mixtures. *Journal of Testing and Evaluation*, 37(5), 424-430.
- Nageswaran, C. P. D. (2016). Adhesion of aggregate-binder systems (Doctoral dissertation, Delft University of Technology).
- Nguyen, H.M., Pouget, S., Di Benedetto, H., Sauzéat, C. (2009). Time-temperature superposition principle for bituminous mixtures. *European Journal of Environmental and Civil Engineering*, 13(9), 1095-1107.

- Nguyen, Q. T., Di Benedetto, H., & Sauzéat, C. (2012). Fatigue cracking in bituminous mixture using four point bending test. In 7th RILEM International Conference on Cracking in Pavements (pp. 665-674). Springer, Dordrecht.
- Nguyen, M. L., Blanc, J., Kerzrého, J. P., & Horny, P. (2013). Review of glass fibre grid use for pavement reinforcement and APT experiments at IFSTTAR. *Road Materials and Pavement Design*, 14(sup1), 287-308.
- Nithin, S., Rajagopal, K., & Veeraragavan, A. (2015). State-of-the art summary of geosynthetic interlayer systems for retarding the reflective cracking. *Indian Geotechnical Journal*, 45(4), 472-487.
- Noori, M., Tatari, O., Nam, B., Golestani, B., & Greene, J. (2014). A stochastic optimization approach for the selection of reflective cracking mitigation techniques. *Transportation research part A: policy and practice*, 69, 367-378.
- Noory, A., Nejad, F. M., & Khodaii, A. (2018). Effective parameters on interface failure in a geocomposite reinforced multilayered asphalt system. *Road Materials and Pavement Design*, 19(6), 1458-1475.
- Noory, A., Moghadas Nejad, F., and Khodaii, A. (2019). Evaluation of the Effective Parameters on Shear Resistance of Interface in a Geocomposite Reinforced Pavement. *International Journal of Pavement Engineering*, (20:9), 1106-1117, DOI: 10.1080/10298436.2017.1394094.
- Nsengiyumva, G., Kim, Y. R., & You, T. (2015). Development of a Semicircular Bend (SCB) Test Method for Performance Testing of Nebraska Asphalt Mixtures. Retrieved from <https://digitalcommons.unl.edu/cgi/viewcontent.cgi?article=1171&context=ndor>.
- Olard, F., & Di Benedetto, H. (2003). General "2S2P1D" model and relation between the linear viscoelastic behaviours of bituminous binders and mixes. *Road materials and pavement design*, 4(2), 185-224.
- Olidis, C., & Hein, D. (2004, September). Guide for the mechanistic-empirical design of new and rehabilitated pavement structures materials characterization: Is your agency ready. In 2004 Annual Conference of the Transportation Association of Canada.
- Orešković, M., Trifunović, S., Mladenović, G., & Bohuš, Š. (2019). Fatigue Resistance of a Grid-Reinforced Asphalt Concrete using Four Point Bending Beam Test. In *Bituminous Mixtures and Pavements VII: Proceedings of the 7th International Conference on Bituminous Mixtures and Pavements* (pp. 589-594). CRC Press/Balkema.
- Packham, D. E. (2005). In *Handbook of adhesion second edition* (p. 358). John Wiley & Sons: West Sussex, England.

- Pais, J. (2013). The reflective cracking in flexible pavements. *Romanian Journal of Transport Infrastructure*, 2(1), 63-87.
- Palmeira, E. M., & Antunes, L. G. (2010). Large scale tests on geosynthetic reinforced unpaved roads subjected to surface maintenance. *Geotextiles and Geomembranes*, 28(6), 547-558.
- Palacios C., Chehab G. R., Chaignon F. and Thompson M. (2008). Evaluation of fibre reinforced bituminous interlayers for pavement preservation. In *Proceedings of the 6th International RILEM Conference, Chicago, U.S.A.* 721-729.
- Panda, M., Sutradhar, B., Giri, J., & Chattaraj, U. (2013). An experimental study on assessment of pavement interlayer bond strength. *International Journal of Transportation Science and Technology*, 2(2), 141-147.
- Pasquini, E., Bocci, M., Ferrotti, G., & Canestrari, F. (2013). Laboratory characterisation and field validation of geogrid-reinforced asphalt pavements. *Road Materials and Pavement Design*, 14(1), 17-35.
- Pasquini, E., Bocci, M., & Canestrari, F. (2014). Laboratory characterisation of optimised geocomposites for asphalt pavement reinforcement. *Geosynthetics International*, 21(1), 24-36.
- Pasquini, E., Pasetto, M., & Canestrari, F. (2015). Geocomposites against reflective cracking in asphalt pavements: Laboratory simulation of a field application. *Road Materials and Pavement Design*, 16(4), 815-835.
- Paulino, G. H., Song, S. H., & Buttlar, W. G. (2004, May). Cohesive zone modeling of fracture in asphalt concrete. In *Proceedings of the 5th International RILEM Conference—Cracking in Pavements: Mitigation, Risk Assessment, and Preservation* (pp. 63-70). Limoges, France.
- Penman, J., & Hook, K. D. (2008). The use of geogrids to retard reflective cracking on airport runways, taxiways and aprons. In *RILEM International Conference on Cracking in Pavements* (6th: 2008: Chicago, Ill.).
- Perkins, S. W., & Ismeik, M. (1997). A synthesis and evaluation of geosynthetic-reinforced base layers in flexible pavements-part i. *Geosynthetics International*, 4(6), 549-604.
- Perkins, S. W. (1999). Mechanical response of geosynthetic-reinforced flexible pavements. *Geosynthetics International*, 6(5), 347-382.
- Perkins, S. W. (2000). Constitutive modeling of geosynthetics. *Geotextiles and Geomembranes*, 18(5), 273-292.

- Perkins, S. W. (2001). Numerical modeling of geosynthetic reinforced flexible pavements (No. FHWA/MT-01-003/99160-2). Montana. Dept. of Transportation. Research Programs.
- Perkins, S. W., & Edens, M. Q. (2003). Finite element modeling of a geosynthetic pullout test. *Geotechnical & Geological Engineering*, 21(4), 357-375.
- Perkins, S. W., Christopher, B. R., Cuelho, E. L., Eiksund, G. R., Hoff, I., Schwartz, C. W., ... & Watn, A. (2004). Development of design methods for geosynthetic reinforced flexible pavements. US Department of Transportation, Federal Highway Administration, Washington, DC, FHWA Report Reference Number DTFH61-01-X-00068, 263p.
- Perng, J. D. (1989). Analysis of crack propagation in asphalt concrete using a cohesive crack model (Doctoral dissertation, The Ohio State University).
- Perraton, D., Touhara, R., Di Benedetto, H., & Carter, A. (2015). Ability of the classical fatigue criterion to be associated with macro-crack growth. *Materials and Structures*, 48(8), 2383-2395.
- Pezzaniti, D., Beecham, S., & Kandasamy, J. (2009, June). Influence of clogging on the effective life of permeable pavements. In *Proceedings of the Institution of Civil Engineers-Water Management* (Vol. 162, No. 3, pp. 211-220). Thomas Telford Ltd.
- Pirmohammad, S., & Kiani, A. (2016). Study on fracture behavior of HMA mixtures under mixed mode I/III loading. *Engineering Fracture Mechanics*, 153, 80-90.
- Polidora, J., Sobhan, K., & Reddy, D. V. (2019). Effects of geosynthetic inclusions on the fatigue and fracture properties of asphalt overlays. Retrieved from <https://doi:10.32075/17ECSMGE-2019-0516>.
- Ponniah, J., Haas, R. (1989). Evaluating alternative solutions to reflective cracking through asphalt overlays. *Transportation Research Record: Journal of the Transportation Research Board* 1215, 282-291.
- Pozarycki, A., & Garbowski, T. (2013). Laboratory Testing of Fatigue Crack Growth in Geosynthetically Reinforced Large Scale Asphalt Pavement Samples. *Procedia Engineering*, 57, 922-928.
- Prashanth, V., Krishna, A. M., & Dash, S. K. (2016). Pullout tests using modified direct shear test setup for measuring soil-geosynthetic interaction parameters. *International Journal of Geosynthetics and Ground Engineering*, 2(2), 10.

- Prieto, J. N., Gallego, J., & Perez, I. (2007). Application of the wheel reflective cracking test for assessing geosynthetics in anti-reflection pavement cracking systems. *Geosynthetics International*, 14(5), 287-297.
- Prowell, B. D. (2010). Validating the fatigue endurance limit for hot mix asphalt (Vol. 646). Transportation Research Board.
- Quintus, H. L. V. (2007). Techniques For Mitigation of Reflective Cracking. Auburn University, Alabama, USA. Interim Report AAPTP 05-04.
- Raab, C., Partl, M. N., & Abd El Halim, A. E. H. O. (2009). Evaluation of Interlayer Shear Bond Devices for Asphalt Pavements. *Baltic Journal of Road & Bridge Engineering (Baltic Journal of Road & Bridge Engineering)*, 4(4).
- Raab, C. (2011). Development of a framework for standardisation of interlayer bond of asphalt pavements. (Doctoral dissertation, Carleton University).
- Raab, C., Arraigada, M., Partl, M. N., & Schiffmann, F. (2017). Cracking and interlayer bonding performance of reinforced asphalt pavements. *European Journal of Environmental and Civil Engineering*, 21(sup1), 14-26.
- Rahbar-Rastegar, R., Dave, E. V., & Daniel, J. S. (2018). Fatigue and thermal cracking analysis of asphalt mixtures using continuum-damage and cohesive-zone models. *Journal of Transportation Engineering, Part B: Pavements*, 144(4), 04018040.
- Rahman, A., Ai, C., Xin, C., Gao, X., & Lu, Y. (2017). State-of-the-art review of interface bond testing devices for pavement layers: toward the standardization procedure. *Journal of adhesion science and technology*, 31(2), 109-126.
- Rathmayer, H. G. (2007). Reinforcement of pavements with steel meshes and geosynthetics. *Proceeding of Design and Construction of Pavements and Rail Tracks-Geotechnical Aspects and Processed Materials*.
- Roffe J. C., and Chaignon, F. (2002). Characterization Tests on Bond Coats: Worldwide Study, Impact, Tests, and Recommendations. In *Proceedings of the 3rd International Conference Bituminous Mixtures and Pavements, Thessaloniki, Greece*, 603-614.
- Rollins, G., Rahman, M., Scofield, L., & Kalevela, S. (1991). Paving fabrics for reducing reflective cracking (No. FHWA-AZ-8801). Arizona. Dept. of Transportation.
- Romanoschi, S. A., & Metcalf, J. B. (2001). Characterization of asphalt concrete layer interfaces. *Transportation Research Record*, 1778(1), 132-139.
- Romeo, E., Freddi, F., & Montepara, A. (2014). Mechanical behaviour of surface layer fibreglass-reinforced flexible pavements. *International Journal of Pavement Engineering*, 15(2), 95-109.

- Roodi, G. H., Morsy, A. M., & Zornberg, J. G. (2017). Experimental Evaluation of the Interaction between Geosynthetic Reinforcements and Hot Mix Asphalt. In *Airfield and Highway Pavements 2017* (pp. 428-439).
- Roque, R., Birgisson, B., Drakos, C., & Dietrich, B. (2004). Development and field evaluation of energy-based criteria for top-down cracking performance of hot mix asphalt (with discussion). *Journal of the Association of Asphalt Paving Technologists*, 73.
- Roffe J. C., & Chaignon, F. (2002). Characterization tests on bond coats: worldwide study, impact, tests, and recommendations. In *Proceedings of the 3rd International Conference Bituminous Mixtures and Pavements, Thessaloniki, 2002*. (Vol. 1).
- Safavizadeh, S. A., Wargo, A., Guddati, M., & Kim, Y. R. (2015). Investigating reflective cracking mechanisms in grid-reinforced asphalt specimens: Use of four-point bending notched beam fatigue tests and digital image correlation. *Transportation Research Record*, 2507(1), 29-38.
- Safavizadeh, S. A., & Kim, Y. R. (2017). Fatigue and fracture characterization of fiberglass grid-reinforced beam specimens using four-point bending notched beam fatigue test and digital image correlation technique. *Materials and Structures*, 50(2), 110.
- Sagnol, L., Quezada, J. C., Chazallon, C., & Stöckner, M. (2019). Effect of glass fibre grids on the bonding strength between two asphalt layers and its Contact Dynamics method modelling. *Road Materials and Pavement Design*, 20(5), 1164-1181.
- Saraf, C. L., Majidzadeh, K., & Tribbett, W. O. (1996). Effect of reinforcement on fatigue life of asphalt beams. *Transportation research record*, 1534(1), 66-71.
- Saride, S., & Kumar, V. V. (2017). Influence of geosynthetic-interlayers on the performance of asphalt overlays on pre-cracked pavements. *Geotextiles and Geomembranes*, 45(3), 184-196.
- Sauzeat, C., & Di Benedetto, H. (2015). Tridimensional linear viscoelastic behavior of bituminous materials. In *Advances in Asphalt Materials* (pp. 59-95). Woodhead Publishing.
- Scarpas, A., & De Bondt, A. H. (1996). Finite elements simulation of reflective cracking in asphaltic overlays. *HERON*, 41 (1), 1996.
- Shafabakhsh, G. H., Mirabdolazimi, S. M., & Sadeghnejad, M. (2014). Evaluation the effect of nano-TiO₂ on the rutting and fatigue behavior of asphalt mixtures. *Construction and building materials*, 54, 566-571.

- Sheng, B., & Ping, W. C. V. (2016). Evaluation of Florida asphalt mixes for crack resistance properties using the laboratory overlay test procedure (No. OMNI 034114). Florida. Dept. of Transportation.
- Sherman, G. (1982). Minimizing reflection cracking of pavement overlays. NCHRP Synthesis of Highway Practice, (92).
- Shi, D., & Wang, F. (2013). Pull-out test studies on the interface characteristics between geogrids and soils. *EJGE*, 18, 5405-5417.
- Sholar, G. A., Page, G. C., Musselman, J. A., Upshaw, P. B., & Moseley, H. L. (2004). Preliminary investigation of a test method to evaluate bond strength of bituminous tack coats (with discussion). *Journal of the Association of Asphalt Paving Technologists*, 73.
- Shukla, S. K., & Yin, J. H. (2004). Functions and installation of paving geosynthetics. In *Proceedings of the 3rd Asian regional conference on geosynthetics*, Seoul (pp. 314-321).
- Singh, M., Kumar, P., & Anupam, A. K. (2016). Effect of type of aggregate on permanent deformation of bituminous concrete mixes. *Road Materials and Pavement Design*, 17(2), 417-433.
- Siriwardane, H., Gondle, R., & Kutuk, B. (2010). Analysis of flexible pavements reinforced with geogrids. *Geotechnical and Geological Engineering*, 28(3), 287-297.
- Soares, J. B., Colares de Freitas, F. A., & Allen, D. H. (2003). Crack modeling of asphaltic mixtures considering heterogeneity of the material. *Transportation Research Record*, 1832, 113-120.
- Sobhan, K., Crooks, T., Tandon, V., & Mattingly, S. (2004). Laboratory simulation of the growth and propagation of reflection cracks in geogrid reinforced asphalt overlays. In *5th International RILEM Conference on Cracking in Pavements-Mitigation, Risk Assessment and Prevention*. Edited by Petit C., Al-Qadi IL et Millien A (pp. 589-596).
- Sobhan, K., Genduso, M., & Tandon, V. (2005). Effects of geosynthetic reinforcement on the propagation of reflection cracking and accumulation of permanent deformation in asphalt overlays. In *Proceedings of the 3rd LACCEI International Latin American and Caribbean Conference for Engineering and Technology (LACCET'05) Advances in Engineering and Technology: A Global Perspective*.
- Solatiyan, E., Bueche, N., & Carter, A. (2020a). A review on mechanical behavior and design considerations for reinforced-rehabilitated bituminous pavements. *Construction and Building Materials*, 257, 119483.

- Solatiyan, E., Bueche, N., Vaillancourt, M., & Carter, A. (2020b). Permeability and mechanical property measurements of reinforced asphalt overlay with paving fabrics using novel approaches. *Materials and Structures*, 53(1), 1-15.
- Steen, E. R. (2004). Stress relieving function of paving fabrics when used in new road construction. In Proc., 5th International RILEM Conference, Edited by C. Petit, IL Al-Qadi, and A. Millien, Limoges, France (pp. 105-112).
- Stempihar, J. (2013). Development of the C* Fracture Test for Asphalt Concrete Mixtures. (PhD Dissertation, Arizona State University).
- Sudarsanan, N., Karpurapu, R., & Amrithalingam, V. (2018). An investigation on the interface bond strength of geosynthetic-reinforced asphalt concrete using Leutner shear test. *Construction and Building Materials*, 186, 423-437.
- Sudarsanan, N., Arulrajah, A., Karpurapu, R., & Amrithalingam, V. (2020). Fatigue Performance of Geosynthetic-Reinforced Asphalt Concrete Beams. *Journal of Materials in Civil Engineering*, 32(8), 04020206.
- Sutanto, M. H. (2009). Assessment of bond between asphalt layers. (Doctoral dissertation, The University of Nottingham).
- Taherkhani, H., & Jalali, M. (2017). Investigating the performance of geosynthetic-reinforced asphaltic pavement under various axle loads using finite-element method. *Road Materials and Pavement Design*, 18(5), 1200-1217.
- Tang, X., Palomino, A. M., & Stoffels, S. M. (2016). Permanent deformation behaviour of reinforced flexible pavements built on soft soil subgrade. *Road Materials and Pavement Design*, 17(2), 311-327.
- Tang, S. (2014). Evaluate the fracture and fatigue resistances of hot mix asphalt containing high percentage reclaimed asphalt pavement (RAP) materials at low and intermediate temperatures. PhD Thesis. Iowa State University.
- Tapsoba, N., Sauzéat, C., & Benedetto, H. D. (2013). Analysis of fatigue test for bituminous mixtures. *Journal of Materials in Civil Engineering*, 25(6), 701-710.
- Tarrer, A. R., & Wagh, V. (1991). The effect of the physical and chemical characteristics of the aggregate on bonding (No. SHRP-A/UIR-91-507). Washington, DC: Strategic Highway Research Program, National Research Council.
- Tashman, L., Nam, K., & Papagiannakis, A. T. (2006). Evaluation of the influence of tack coat construction factors on the bond strength between pavement layers (No. WA-RD 645.1). Olympia: Washington State Department of Transportation.

- Tayfur, S., Ozen, H., & Aksoy, A. (2007). Investigation of rutting performance of asphalt mixtures containing polymer modifiers. *Construction and Building Materials*, 21(2), 328-337.
- Tensar International Corporation (2015). United Kingdom. Online brochures printed March 2015, <http://www.tensarcorp.com>.
- Thi Bui, Q. A. (2018). A literature review of key factors influencing interlayer shear strength of multilayer asphalt pavement. *International Journal of Civil Engineering and Technology (IJCIET)* 9(3), 29–35.
- Thom, N. H. (2000). A simplified computer model for grid reinforced asphalt overlays. In *Proceedings of the 4th International RILEM Conference on Reflective Cracking in Pavements* (pp. 37-46).
- Tschegg, E. K., Kroyer, G., Tan, D. M., Stanzl-Tschegg, S. E., & Litzka, J. (1995). Investigation of bonding between asphalt layers on road construction. *Journal of Transportation Engineering*, 121(4), 309-316.
- Tapsoba, N., Sauzéat, C., & Benedetto, H. D. (2013). Analysis of fatigue test for bituminous mixtures. *Journal of Materials in Civil Engineering*, 25(6), 701-710.
- Thom, N. H. (2000). A simplified computer model for grid reinforced asphalt overlays. In *Proceedings of the 4th International RILEM Conference on Reflective Cracking in Pavements* (pp. 37-46).
- Vaitkus, A., Žilionienė, D., Paulauskaitė, S., Tuminienė, F., & Žiliūtė, L. (2011). Research and assessment of asphalt layers bonding. *Baltic Journal of Road & Bridge Engineering (Baltic Journal of Road & Bridge Engineering)*, 6(3).
- Vanelstraete A, de Bondt AH. (1997). Crack prevention and use of overlay systems. In: Vanelstraete A, Franken L (eds) *Prevention of reflective cracking in pavements*. RILEM Report,(18), 43- 60.
- Vanelstraete, A., Francken, L. (1997). *Prevention of reflective cracking in pavements: state-of-the-art report of RILEM Technical Committee 157 PRC, Systems to Prevent Reflective Cracking in Pavements*, E & FN Spon, London, Britain, 1997.
- Vanelstraete, A., Leonard, D., & Veys, J. (2000). Structural design of roads with steel reinforcing nettings. In *Proceedings of the 4th International RILEM Conference, OTTAWA, CANADA*.
- Van Deusen, D., Johanneck, L., Geib, J., Garrity, J., Hanson, C., & Dave, E. V. (2015). DCT low temperature fracture testing pilot project. Report No. MN/RC, 20.

- Vervaecke, F., Maeck, J., & Vanelstraete, A. (2008). On site validation and long term performance of anti-cracking interfaces. In RILEM International Conference on Cracking in Pavements (6th: 2008: Chicago, Ill.).
- Vespa, J. W. (2005). An evaluation of interlayer stress absorbing composite (ISAC) reflective crack relief system (No. FHWA/IL/PRR 150). Illinois. Dept. of Transportation. Bureau of Materials and Physical Research.
- Virgili, A., Canestrari, F., Grilli, A., & Santagata, F. A. (2009). Repeated load test on bituminous systems reinforced by geosynthetics. *Geotextiles and Geomembranes*, 27(3), 187-195.
- Von Quintus, H. L., Mallela, J., & Lytton, R. L. (2010). Techniques for mitigation of reflective cracks. In 2010 FAA Worldwide Airport Technology Transfer Conference Federal Aviation Administration American Association of Airport Executives.
- Wagnoner, M. P., Buttlar, W., & Paulino, G. H. (2005). Disk-shaped compact tension test for asphalt concrete fracture. *Experimental mechanics*, 45(3), 270-277.
- Wagoner, M. P., Buttlar, W. G., Paulino, G. H., & Blankenship, P. (2005). Investigation of the fracture resistance of hot-mix asphalt concrete using a disk-shaped compact tension test. *Transportation Research Record*, 1929(1), 183-192.
- Walubita, L. F., Nyamuhokya, T. P., Komba, J. J., Tanvir, H. A., Souliman, M. I., & Naik, B. (2018). Comparative assessment of the interlayer shear-bond strength of geogrid reinforcements in hot-mix asphalt. *Construction and Building Materials*, 191, 726-735.
- Wang, W., Hu, K., Feng, S., Li, G., & Höeg, K. (2020). Shear behavior of hydraulic asphalt concrete at different temperatures and strain rates. *Construction and Building Materials*, 230, 117022.
- Wasage, T. L. J., Ong, G. P., Fwa, T. F., & Tan, S. A. (2004). Laboratory evaluation of rutting resistance of geosynthetics reinforced asphalt pavement. *Journal of the Institution of Engineers*, 44(2), 29-44.
- West, R. C., Zhang, J., & Moore, J. (2005). Evaluation of bond strength between pavement layers (No. NCAT Report 05-08). Auburn University. National Center for Asphalt Technology.
- White, T. D. (2002). Contributions of pavement structural layers to rutting of hot mix asphalt pavements (Vol. 468). Transportation Research Board.
- White, G. (2017). State of the art: interface shear resistance of asphalt surface layers. *International Journal of Pavement Engineering*, 18(10), 887-901.

- Williams, R. C., Buss, A., Chen, C. (2015). Reflective crack mitigation guide for flexible pavements. Retrieved from <http://lib.dr.iastate.edu/intranstechtransfer>.
- Wu, Z., Mohammad, L. N., Wang, L. B., & Mull, M. A. (2005). Fracture resistance characterization of superpave mixtures using the semi-circular bending test. *Journal of ASTM International*, 2(3), 1-15.
- Wu, Z., Zhang, Z., Morvant, M., Paul, H., & Temple, B. (2008). Accelerated pavement testing on thin asphalt pavements with various base and subbase layers. In *Transportation and Development Innovative Best Practices 2008* (pp. 523-527).
- Wu, S., Chen, H., Zhang, J., & Zhang, Z. (2017). Effects of interlayer bonding conditions between semi-rigid base layer and asphalt layer on mechanical responses of asphalt pavement structure. *International Journal of Pavement Research and Technology*, 10(3), 274-281.
- Xia, C., Lv, S., You, L., Chen, D., Li, Y., & Zheng, J. (2019). Unified strength model of asphalt mixture under various loading modes. *Materials*, 12(6), 889.
- Xu, T., & Huang, X. (2012). Investigation into causes of in-place rutting in asphalt pavement. *Construction and Building Materials*, 28(1), 525-530.
- Yang, J., Shi, X., Wan, J., Qian, G., Pan, W., & Yang, Y. (2006). Evaluation of rutting resistance of double-layered asphalt mixes. *Road materials and pavement design*, 7(4), 533-542.
- Yang, X., & Han, J. (2013). Analytical model for resilient modulus and permanent deformation of geosynthetic-reinforced unbound granular material. *Journal of Geotechnical and Geoenvironmental Engineering*, 139(9), 1443-1453.
- Ye, H., Wang, X., Fang, N., Su, Z., & Sun, X. (2019). Interlayer Working Conditions Classification and Treatment Measures of Airport Asphalt Pavement Overlay. *Journal of Advanced Transportation*, 2019.
- Yeo, Y. S., Nikraz, H., & Jitsangiam, P. (2012). Tube suction test to measure moisture susceptibility of Australian pavements. *Engineering Journal*, 16(4), 159-168.
- Yu, B., Lu, Q., & Yang, J. (2013). Evaluation of anti-reflective cracking measures by laboratory test. *International Journal of Pavement Engineering*, 14(6), 553-560.
- Zamora-Barraza, D., Calzada-Peréz, M., Castro-Fresno, D., & Vega-Zamanillo, A. (2010). New procedure for measuring adherence between a geosynthetic material and a bituminous mixture. *Geotextiles and Geomembranes*, 28(5), 483-489.

- Zamora-Barraza, D., Calzada-Pérez, M. A., Castro-Fresno, D., & Vega-Zamanillo, A. (2011). Evaluation of anti-reflective cracking systems using geosynthetics in the interlayer zone. *Geotextiles and Geomembranes*, 29(2), 130-136.
- Zhang, J., & Hurta, G. (2008). Comparison of geotextile and geogrid reinforcement on unpaved road. In *GeoCongress 2008: Geosustainability and Geohazard Mitigation* (pp. 530-537).
- Zhang, L., Zhao, M., Shi, C., & Zhao, H. (2010). Bearing capacity of geocell reinforcement in embankment engineering. *Geotextiles and Geomembranes*, 28(5), 475-482.
- Zhengqi, Z., & Dengliang, Z. (2000). Evaluation of Geonet reinforcement in resisting reflective cracking of asphalt pavement. In *International RILEM Conference on Reflective Cracking in Pavements*, 4th, 2000, Ottawa, Ontario, Canada.
- Zhesheng, G. E., & Xiaoming, H. U. A. N. G. (2003). Prediction of asphalt mixtures fatigue properties using damage mechanics. *Journal of Traffic and Transportation Engineering*, 3(1), 40-42.
- Zhou, F., Im, S., Hu, S., Newcomb, D., & Scullion, T. (2017). Selection and preliminary evaluation of laboratory cracking tests for routine asphalt mix designs. *Road Materials and Pavement Design*, 18(sup1), 62-86.
- Zhu, X. K., & Joyce, J. A. (2012). Review of fracture toughness (G, K, J, CTOD, CTOA) testing and standardization. *Engineering Fracture Mechanics*, 85, 1-46.
- Zhu, Y., Dave, E. V., Rahbar-Rastegar, R., Daniel, J. S., & Zofka, A. (2017). Comprehensive evaluation of low-temperature fracture indices for asphalt mixtures. *Road Materials and Pavement Design*, 18(sup4), 467-490.
- Zielnski, P. 2008. Fatigue investigations of asphalt concrete beams reinforced with geosynthetics interlayer. In *Proceedings of the 6th RILEM international conference on cracking in pavements*, Chicago, pp. 751–759.
- Zofka, A., & Braham, A. (2009). Comparison of low-temperature field performance and laboratory testing of 10 test sections in the Midwestern United States. *Transportation research record*, 2127(1), 107-114.
- Zofka, A., Bernier, A., Josen, R., & Maliszewski, M. (2015). Advanced shear tester for solid and layered samples. *Introduction to Unmanned Aircraft Systems*, 397.
- Zofka, A., Maliszewski, M., & Maliszewska, D. (2017). Glass and carbon geogrid reinforcement of asphalt mixtures. *Road Materials and Pavement Design*, 18(sup1), 471-490.

- Zofka, A., & Maliszewski, M. (2019). Practical overlay design method for geogrid reinforcement of asphalt layers. *Road Materials and Pavement Design*, 20(sup1), S163-S182.
- Zornberg, J. G., & Gupta, R. (2010). Geosynthetics in pavements: North American contributions. In *Theme Speaker Lecture, Proceedings of the 9th International Conference on Geosynthetics, Guarujá, Brazil, May (Vol. 1, pp. 379-400)*.
- Zornberg, J. G. (2011). Advances in the use of geosynthetics in pavement design. In *Second National Conference on Geosynthetics (pp. 3-21)*.
- Zornberg, J. G., Azevedo, M., Sikkema, M., & Odgers, B. (2017). Geosynthetics with enhanced lateral drainage capabilities in roadway systems. *Transportation Geotechnics*, 12, 85-100.